UNIVERSITÄT
BERN

Graduate School for Cellular and Biomedical Sciences

University of Bern

The interplay of lipids and respiratory enzymes in synthetic ATP producing systems

PhD Thesis submitted by

Sabina Deutschmann

from **Villnachern AG**

for the degree of

PhD in Biochemistry and Molecular Biology

Supervisor

Prof. Dr. Christoph von Ballmoos

Department of Chemistry, Biochemistry and Pharmaceutical Sciences

Faculty of Science of the University of Bern

Co-advisor

Prof. Dr. Martin Lochner

Institute of Biochemistry and Molecular Medicine

Faculty of Medicine of the University of Bern

Accepted by the Faculty of Medicine, the Faculty of Science and the Vetsuisse Faculty of the University of Bern at the request of the Graduate School for Cellular and Biomedical Sciences

Bern, Dean of the Faculty of Medicine

Bern, Dean of the Faculty of Science

Bern, Dean of the Vetsuisse Faculty Bern

Acknowledgements

Without the great support of many people, this work would not have been possible. First of all, I would like to thank Christoph von Ballmoos for giving me the opportunity to be part of your group and to do my PhD thesis in your lab. It was seven years ago, when I started my master thesis in your lab, and it had been one of the best choices of my life. I was very happy when you then gave me the PhD position two years later. I could experience a great time in your group and I learned so many things from you. Thank you so much for all your excellent support during this time, for all your help, for many interesting and important discussions, for your exhaustless patience and for taking me as I am. You always believed in me, at least this is how I felt, and you had always an open ear for me. Thank you for being such a great boss!

I want to thank the whole von Ballmoos group for the great atmosphere in the lab and on the numerous hiking, skiing or curling trips. I would like to thank very much Lukas Rimle, my former bachelor and master student. I'd think it's not exaggerated to say I got very inspired by your thirst for knowledge. I am so grateful for all you have done for me. Not only you helped me with my measurements from time to time, when I was very busy, but I also could approach you whenever I had uncertainties. Thank you for all the interesting and great conversations and discussions, especially but not exclusively concerning our paper, for reading a lot of my texts, for all your help, and for much more! Simply said, thank you for everything. Many thanks also to Yannick Bärtschi for being my second bachelor and master student. You became the new cloning and Western Blot professional in our group. Thank you so much for your great work, you are the hope to finish my main project. And thank you for being open-minded and for contributing to the nice atmosphere in the lab. Many thanks to Micha Marti for your great effort during your bachelor thesis that I could supervise. You worked very precisely and I really appreciated your good work, especially the big ATP synthase batch you purified at that time, which I used for a lot of experiments. I am also very grateful to have had the opportunity to supervise, together with Lukas, our former apprentice Tim Marti. It was a great time and I could learn a lot. Thank you very much for all your work you have done during the six month you were in our lab, for all the enzymes you purified and all the liters of buffers and media you prepared.

I would like to thank all the other current and former members of the synthetic group for all the interesting discussions and useful inputs. Thank you, Ana Nikolov, for the many funny and sometimes impossible conversations we had (e.g. about the magic number of nine), for your enormous and catching imagination, for laughing with me until tears about things nobody else would understand, for trying to explain me the difference of Serbian phonemes, for being a helpful "supervisor", and for all the lovely post-its I came across sticking to my bench. I would like to thank Stefan "Stoni" Moning for being always

cheerful and smiling and for many good conversations and tips concerning Spy-coupling and MBPx purification; Meike Wieser, for many interesting and nice discussions; Axel Meyrat, my supervisor during my master thesis for introducing me into the lab and this interesting field of membrane proteins and for many funny talks; and the legend of our group, Andrea Amati, for being such a good bench neighbor, for all the funny and interesting discussions, for your help when we had to teach practical courses, for always knowing some short-cuts and for a lot of good and useful advises.

I also would like to express my thanks to the former PhD students in our lab. Thank you, Olivier Biner and Thomas Schick, for many interesting conversations, useful tips and for the planning and organization of a lot of adventurous group events such as a sailing trip or fonclettes. Many thanks to Simone Graf for all your help, especially for helping me to orient myself at the University of Stockholm during our bioenergetics course, without which I would have been completely lost, I think.

I would like to thank Nicolas Dolder for being such a nice office neighbor. You really helped me a lot with many useful conversations and all your advices, not only but also concerning writing. Thank you for being our KOPAS and lab police, and for always keeping order in our lab. I enjoyed our trip to the Harden conference in Bonn, and especially the funny return trip with a lot of funny and interesting conversations. I am especially very grateful for your priceless help concerning calculations of distinct lipid populations. Thank you, Roman Mahler, for interesting talks, but especially for all your help concerning IT problems. You were always immediately there when I had problems with my computer or when I had to install any program, sometimes even trying for hours to fix the problem. I would like to thank Philipp Müller for always taking the initiative and organizing many cool group events, for always helping when I needed help, and for always having some interesting topics of conversation during lunch.

Many thanks to the current master students Ana-Marija Stanic and Stefan Täuber, and to all the former master students in our group. Thank you, Stephan Berger for all your help, e.g. when ordering homogenizers from Wish, to Sarah Krummenacher, Tobias Blatter, Martin Schori, Aymar Ganguin, Yannic Müller and Eveline Jäger.

Thank you Abbas Abou Hamdan, our current Post Doc, for all the interesting conversations, for your useful advises and all your help, not only but also when we had to teach practical students. Thanks also to our former Post Doc Linda Näsvik Öjemyr for being there during my master thesis and for many useful tips. Thank you also for the PreScission protease batch you purified which I used for many cleavage experiments.

I would like to thank Sandra Schär, our former lab technician, for a lot of interesting conversations, for all your help, and for the numerous batches of bo_3 oxidase and ATP synthase you purified for general use, especially also the bo_3-SpyTag that I used for countless coupling experiments. Many thanks to our

current lab technician Leticia Herrán Villalaín for your great work, for all you helped me at the end of my work in the lab, for a lot of batches of expressed and purified enzymes, and for many interesting conversations. Thank you Lorine Gaudin for all your work you have done during your apprentice in our lab.

Finally, I would like to thank all my friends and family, who were always there for me and strengthened my back. I am very grateful to my parents (Rainer and Regula) with all my heart, for your constant support, for always believing in me, for always caring, for being patient with me and for taking me as I am. And thank you so much, my siblings Katja, Silvan and Fabiola, for being my best friends, for supporting me at any time, and for always having an open door, an open ear and great advises for me. I would not be who and where I am today without all of you. Thank you all so much!

Content

1 Abstract

All organisms require energy to maintain vital macroscopic and microscopic processes. Primary energy supplied in form of light or as nutrients has to be converted to the universal energy currency ATP before it can be used by the cells. The majority of ATP is produced at energy-converting membranes where a series of respiratory enzyme complexes couple electron transport reactions to the generation of an electrochemical proton gradient across the membrane. Similar to power generation at a hydroelectric power turbine through water pressure, the electrochemical proton gradient energizes the production of ATP by driving rotation of the molecular turbine of the ATP synthase. While the structures and mechanisms of most respiratory enzymes and the ATP synthase are well understood, relatively little is known how these respiratory complexes interact with each other, including the influence of the environment on the complexes and their interactions. Here, we used a bottom-up approach, in which the individual enzymes are purified and reinserted into a lipid bilayer to investigate the functional interplay of these enzymes. In the simplest scenario, the terminal respiratory bo_3 oxidase and the ATP synthase from *E. coli* are coreconstituted into liposomes to form a minimal respiratory chain system, where proton pumping by bo_3 oxidase is initiated by adding its reduced substrate ubiquinol Q_1, and ATP synthesis is monitored in real-time under steady-state conditions. Nilsson et al. recently found a strong influence of the lipid composition on the ATP synthesis rate in this system [1] where the stepwise insertion of negatively charged lipids into zwitterionic liposomes dramatically reduced ATP synthesis. The data indicate lipid-dependent changes in the lateral distance between the two enzymes. In this PhD thesis, we aimed to test this hypothesis by reversibly coupling bo_3 oxidase and ATP synthase, reconstituting the complex subsequently into liposomes of varying lipid composition and comparing coupled ATP synthesis rates of the coupled complex with rates of freely floating enzymes. We describe three different approaches for coupling of these two large complexes and the different challenges. While perfect stoichiometric coupling of the two enzymes has not yet been achieved here, the results are promising and are the basis for current experiments.

Instead of using the artificial DTT/Q_1 electron donor system, we have expanded the minimal respiratory chain by the monotopic complex I analogue NDH-2 to supply the system with reduced quinol Q_8, thereby generating a more natural alternative. If this alternative system was subjected to a lipid screening, we observed an inverted lipid dependency than with the Q_1 system, with a strong requirement of negatively charged lipids for coupled ATP synthesis. We were able to pinpoint this effect to an increased NADH:ubiquinone oxidoreductase activity in presence of anionic liposomes in experiments with solubilized NDH-2. We identified negatively charged liposomes to be essential for proper NDH-2 activity, indicating a charge-mediated binding of NDH-2 to the membrane.

The inverted lipid dependency of the two systems created doubt that a lipid-dependent lateral difference of the proteins is the only reason for the observed lipid effect. We thus wanted to analyze the effect of the lipid composition on the orientation of the *bo₃* oxidase. To this end, we established a novel method to determine the relative orientation of membrane proteins in liposomes that is independent of protein function. Instead, the membrane protein is site-specifically labeled with a fluorophore that is quenched stepwise after reconstitution into liposomes with membrane-impermeable quencher. A strongly lipid-dependent orientation of *bo₃* oxidase in liposomes with lower fraction of desired inside-out orientation in liposomes carrying a net negative charge compared to uncharged liposomes was indeed observed, in good agreement with the reduced ATP synthesis activity in negatively charged liposomes described above. Furthermore, we show that the fraction of inside-out orientation could be increased when reconstitution was carried out in presence of salt, suggesting an electrostatic-mediated insertion of *bo₃* oxidase into liposomes.

To suppress this unwanted effect on orientation, we aimed to achieve unidirectional inside-out orientation of *bo₃* oxidase. Based on the observation that the large head group of ATP synthase is unable to cross the membrane during reconstitution, a large soluble protein (~100 kDa) was coupled to *bo₃* oxidase using the SpyTag/SpyCatcher methodology to guide its insertion in the favored inside-out orientation. We present the successful procedure to produce the desired product keeping its native functionality and preliminary experiments with ATP synthase look very promising and are the basis for ongoing trials of unidirectional *bo₃* oxidase reconstitution.

2 Introduction

2.1 Membranes

Cells are the structural and functional units of all life, from the simplest bacterium to the most complex multicellular organism. They are surrounded by membranes which are the external boundaries separating the intracellular ingredients from the environment and in this way protecting the cell from foreign particles. Membranes enable cells to keep biomolecules or ions at relevant concentrations by unidirectional uptake from the surrounding. While bacteria have either one (gram-positive bacteria) or two (gram-negative bacteria) cell membranes, eukaryotic cells have one outer cell membrane and additionally intracellular membranes surrounding compartments like nucleus, Golgi apparatus, endosomal reticulum, mitochondria or chloroplasts. The main components of biological membranes are lipids, forming a two-dimensional lipid bilayer, and membrane proteins (MPs), that are harbored by the lipid bilayer and can protrude the lipid bilayer either on one or on both sides. When including MP parts extruding from the membrane, the thickness of a membrane is 5-8 nm [2], where the lipid bilayer itself is around 4 nm thick [3]. Membranes are flexible and able to break and reseal which allows for fusion of or fission into two sealed compartments without loss of interior molecules. This property is important e.g. in cell growth and cell movement as well as endocytosis and exocytosis. Short scale movements such as rotation of lipids, as well as membrane bending and thickness fluctuations render membranes highly dynamic. Lipid exchange and lipid flip-flop on the other hand are much slower [4]. Membranes are the site of many important cellular processes such as signaling, energy conversion or metabolism [5]. Their two-dimensional character render membranes ideal structures for the spatial organization and control of biochemical reactions due to a highly increased probability of intermolecular collisions compared to in three-dimensional space [2,5].

According to the Fluid Mosaic Model proposed by Singer and Nicolson [6], membranes act as a two-dimensional fluid lipid bilayer harboring a mosaic of integral membrane proteins, where lipids and membrane proteins can freely diffuse laterally in the membrane. As an enhancement of the model, laterally structured microdomains have later been observed. These so-called lipid rafts are less fluid and slightly thicker than the rest of the membrane and can be described as liquid-ordered domains drifting on an ocean of a more fluid lipid bilayer [2]. Although the biological function of lipid rafts remains to be defined, they are proposed to play important roles in signal transduction and membrane protein trafficking [7], e.g. by enhancing the probability of contacts between receptors and signaling proteins present in the same lipid raft [2].

An important feature of membranes is their selective permeability, meaning that they are permeable to small nonpolar but impermeable to most polar and charged molecules [2]. The permeability of membranes differs greatly between organelles. While e.g. the inner mitochondrial membrane has restricted permeability even to most ions and small molecules, the outer mitochondrial membrane harbors many pores which allow the passage of ions and bigger molecules up to 6 kDa [8], and the nuclear pore complex in the nuclear envelope even enables diffusion of molecules up to 40 kDa [9]. Moreover, membranes harbor many different membrane proteins that enable the selective transport of polar molecules or ions, either to import essential molecules such as nutrients or to actively pump ions across the membrane against their gradient. By the means of the latter, an electrochemical ion gradient is established over the membrane, which, according to the chemiosmotic theory of Mitchell [10], enables membranes to store energy, what is the basis of ATP synthesis via oxidative phosphorylation (see below).

The membrane composition differs a lot with the type of membrane, not only among different organisms but also among different tissues within the same organism, and even among different membranes of the same tissue. The complex lipid composition is specific for each type of membrane and adapted to the cell's function [11]. The asymmetric distribution of lipids across the inner and outer leaflet of the membrane (also due to low flip-flop movements) reveals that even the lipid composition of the two leaflets varies in the same membrane [4]. Further, the protein fraction of membranes can vary greatly between 30 % in human myelin sheath (where the membrane acts as electrical insulation and does not need many proteins) and 75 % e.g. in *Escherichia coli* (where a lot of enzyme-catalyzed processes take place) [2].

2.2 Lipids and detergents

2.2.1 Lipids

Lipids are biological molecules with the common property of being insoluble in water and with a broad variety of functions and chemistry [2]. While fats and oils are the principal chemical forms to store energy, other lipids act as enzyme cofactors, hydrophobic anchors for proteins, hormones or intracellular messengers, or they are structural elements for biological membranes [2]. The latter membrane lipids are mainly composed of glycerophospholipids, sphingolipids and sterols [11]. They are polar amphiphilic molecules, meaning that they have a hydrophilic head group and a hydrophobic tail. When resuspending those lipids in aqueous solutions, they usually spontaneously form a lipid bilayer where the hydrophobic tails of the two leaflets interact with each other in the middle of the membrane while the hydrophilic head groups interact with the surrounding water [12].

Sterols and sphingolipids do not exist in bacteria and for this reason are not further discussed here. In glycerophospholipids, two fatty acids are attached via ester linkage to two carbon atoms of a glycerol, of which the third carbon binds to a highly polar or charged head group via phosphodiester bond [2] (Figure 1A). Glycerophospholipids have a high chemical diversity arising from different combinations of the two fatty acids (Figure 1B) and the head group (Figure 1C) [11]. The head group can be as simple as a single phosphate (in phosphatidic acid PA), or it is composed of a hydrophilic group attached to the phosphate such as ethanolamine (in phosphatidylethanolamine PE), choline (in phosphatidylcholine PC), or glycerol (in phosphatidylglycerol PG). Depending on the hydrophilic moiety, the lipids are either net negatively charged or uncharged. A special phospholipid is cardiolipin (CL, Figure 1D) which essentially is built up of a PG attached to a PA molecule [13] and therefore contains four fatty acids. CL is predominantly found in membranes where oxidative phosphorylation takes place, as the bacterial plasma membrane and the inner mitochondrial membrane [14]. Fatty acids of glycerophospholipids can vary in chain length, number and position of double bonds, and hydroxylation [11]. Bacteria have fatty acids with 12 to 18 carbons, while eukaryotic fatty acids consist of up to 26 carbons [15]. Furthermore, fatty acids

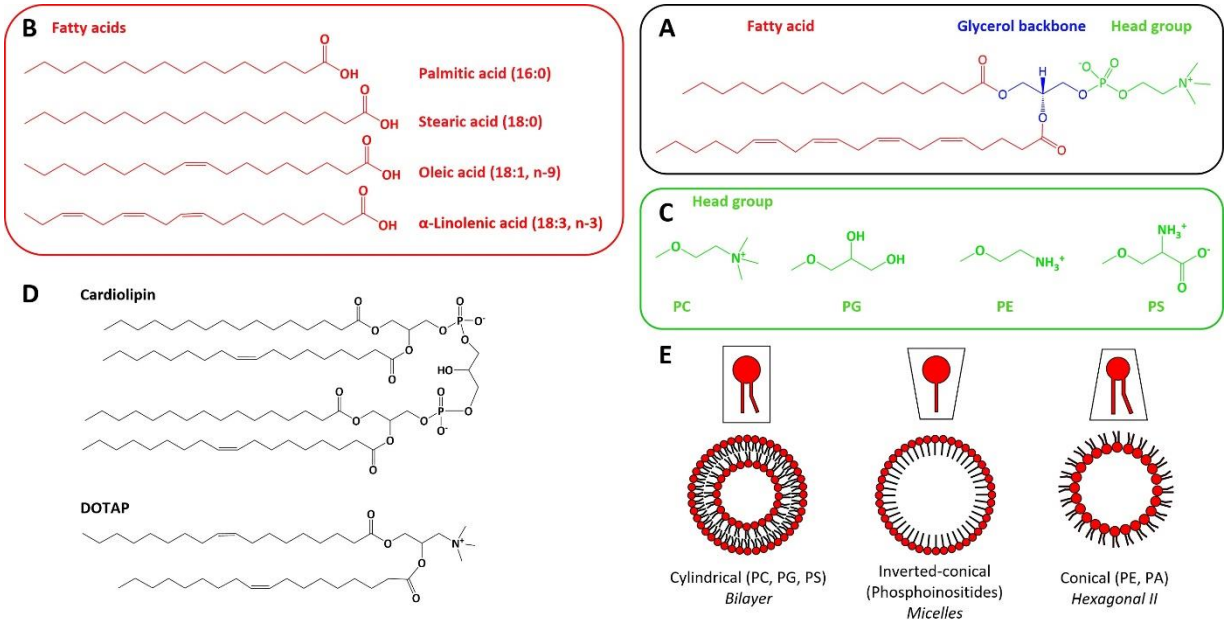

Figure 1 Chemical diversity of membrane lipids. A) General chemical structure of glycerophospholipids. A hydrophilic head group (green) and two hydrophobic fatty acid chains (red) are linked via a glycerol backbone (blue). **B)** Fatty acids differ in length, degree of saturation and position of the double bonds (in XX:Y, n-Z, XX indicates the number of carbon atoms, Y the number of double bonds and Z the position of the first double bond from the omega end). **C)** Head groups of phosphatidylcholine (PC), -glycerol (PG), -ethanolamine (PE) and -serine (PS). The net charge of lipids depends on the head group and is -1 for PG and PS and 0 for PC and PE, respectively. **D)** Structures of the special negatively charged cardiolipin (CL) and the synthetic positively charged lipid DOTAP. **E)** The geometry of lipids is either cylindrical, conical or inverted-conical and defines whether the lipids form a bilayer, hexagonal II structures or micelles in aqueous solution.

can be either saturated (no double bonds) or unsaturated (one or several double bonds). Both the chain length and the degree of saturation affect the physicochemical properties of the membrane. While long and saturated fatty acids lead to thicker and less fluid membranes due to tight packing of the hydrophobic tails and strong lipid-lipid interactions, unsaturated lipids prevent tight packing due to acyl-chain kinks [11] which increases the fluidity of the membrane. Additionally, changes in lipid composition affect the activity of MPs as well as non-membrane proteins that recognize specific lipids [11].

The bacterial membrane of *E. coli* is composed of around 75 % PE, 20 % PG and 5 % CL with minor amounts of PA, phosphatidylserine (PS) and others [15] and carries therefore a negative net charge. Bacteria have developed mechanisms to adapt membrane properties such as viscosity to match environmental conditions by adjusting the lipid composition. They do so by regulating the enzymes responsible for the formation and modulation of lipid head groups and fatty acids [16]. For example, *E. coli* incorporates more unsaturated and shorter fatty acids when it grows at lower temperatures to maintain membrane fluidity, while more long and saturated fatty acids are inserted at higher growth temperature [17].

Depending on the head-to-chain size ratio, the lipid geometry can be either cylindrical (e. g. PC, PG, PS), conical (e. g. PE, PA; these lipids are non-bilayer forming lipids meaning that it is not possible to produce pure lipid bilayers thereof) or inverted-conical (e. g. lyso-glycerophospholipids containing only one fatty acid, or phosphoinositides) [2,11,18] and co-determines the physical properties of membranes. It affects membrane spontaneous curvature and therefore is crucial for fusion/fission events [11]. Furthermore, the lipid geometry defines the type of lipid aggregates to be formed upon mixing in water. There are three types of lipid aggregates (Figure 1E): I) micelles are built from inverted-conical lipids and have a spherical shape where the hydrophobic fatty acid chains define the water-free core, being surrounded and shielded by the head groups; II) bilayers are formed as described above by cylindrical lipids and usually back-fold on themselves to reduce contact between hydrophobic edges and water forming hollow spheres called vesicles; III) and hexagonal II structures are formed by conical lipids and are inverted tubules where the hydrophilic head groups form an aqueous channel in the center surrounded by the hydrophobic chains [2,18,19].

2.2.2 Detergents

Detergents are organic molecules with a high diversity of structures. They are either extracted from plants (e.g. digitonin) or synthetically produced (e.g. DDM; Figure 2), and they are indispensable for the isolation and purification of MPs. Similar to lipids, they consist of a polar or charged head and a hydrophobic tail. In aqueous solutions, detergents form micelles which are spherical aggregates of a defined size and number of monomers (aggregation number), specific for each detergent species. As in micelles of inverted-conical lipids, the hydrophobic tail of detergents points to the core of the micelle and is

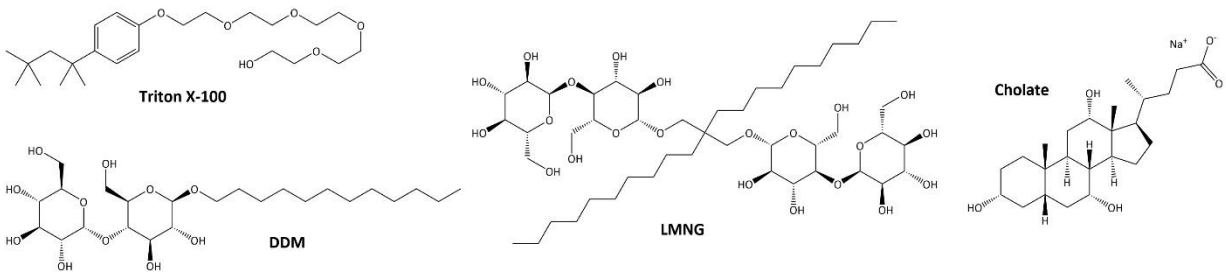

Figure 2 Structures of different detergents. Detergents are amphiphilic molecules with a hydrophilic head and a hydrophobic tail. They are indispensable for the isolation and purification of membrane proteins as they interact with the hydrophobic part of the protein, enabling its solubilization.

surrounded by the hydrophilic head. The property to form micelles is what makes detergents essential for MP solubilization. The hydrophobic parts of MPs, naturally interacting with the fatty acids of lipids, are covered by hydrophobic detergent tails while only the hydrophilic MP parts stick out of the micelles. Micelles exist only in a distinct range of temperature and detergent concentration. The minimal concentration at which micelles are formed is called the critical micellar concentration (CMC) and is characteristic for each detergent. [20] However, the CMC can vary with different conditions (pH, ionic strength, temperature, or the presence of lipids, proteins or other detergents) [21]. For the solubilization of MPs, usually high detergent concentrations are needed, while the detergent concentration is typically reduced for further purification steps but must not undershoot CMC. [20]

Detergents can be either anionic, cationic, nonionic or zwitterionic. Ionic detergents are typically harsher (i.e. more protein-denaturing) than nonionic and zwitterionic ones. Additionally, detergents exhibiting a large head group and a long tail usually are milder than short-chain detergents (which tend to result in MP denaturing or disruption of MP complexes) [22]. Unfortunately, the ideal detergent as well as the ideal concentration for solubilization has to be determined for each MP since there are no general detergents suitable for all MPs, resulting in laborious trial-and-error processes. Thereby, it is important to consider also downstream processes as detergents can interfere with measurements. As an example, detergents with an aromatic ring are not compatible with protein concentration determination measurements via UV absorption as they absorb UV light at 280 nm. [20]

Interestingly, some detergents are able to selectively solubilize certain membrane types. Triton X-100 for example only solubilizes bacterial inner membrane but not the outer membrane [23], and Digitonin selectively solubilizes the eukaryotic plasma membrane but not the mitochondrial membrane [24].

2.3 Membrane proteins

Membrane proteins (MPs) can be classified into three groups: integral, peripheral and amphitropic MPs. Integral MPs are firmly integrated into the lipid bilayer by hydrophobic forces and can only be

extracted by the use of detergents, organic solvents or other molecules disrupting the membrane by hydrophobic interactions [2,25]. They are either polytopic transmembrane proteins (TM) meaning they span both membrane leaflets, or monotopic when they are associated only with one leaflet [26]. Structural elements of most transmembrane proteins are hydrophobic α-helical bundles or β-barrels [25]. Further, so-called annular lipids (lipids bound to the transmembrane region of a MP) [2] can be essential for MP activity and for free diffusion of the MP in the lipid bilayer. Typically, annular lipids are removed during treatment with harsh detergents while mild detergents do not remove them. Integral MPs are represented e.g. by ion channels or respiratory complexes I-IV. Peripheral MPs are less firmly associated with the membrane than integral MPs and interact with the membrane through electrostatic interactions as well as hydrogen bonds with lipid head groups or hydrophilic domains of integral MPs. They can be detached from biological membranes by treatments breaking electrostatic interactions or hydrogen bonds such as increasing ionic strength or changing the pH [2]. The respiratory enzyme NDH-2 (see below) represents a peripheral membrane protein. Amphitropic proteins can be both cytosolic and membrane bound resulting from regulated reversible association with the membrane. They either non-covalently interact with lipids or membrane proteins, or they exhibit one or more covalently attached lipids [2]. The process of binding to lipids regulates their function [27]. As an example, the activity of the amphitropic protein CTP:phosphocholine cytidylyltransferase (CCT), which catalyzes a rate-limiting step in the synthesis of PC, is highly increased in the membrane-bound state compared to the soluble state [28].

Typically, it is significant to know the MP's structure to obtain a better understanding of its function. 30-40 % of proteins of most genomes are estimated to be MPs [26,29]. However, although the number of published MP structures increased in the past years [30,31], only approximately 3 % of all published protein structures in the protein data bank are MPs [31,32]. This most likely is predicated on the difficulties to overexpress and purify MPs in decent amounts for structure determination in a way they are functionally active [33]. Additionally, MPs are purified with the use of detergents, which sometimes tend to be quite harsh leading to incorrectly folded or inactive MPs. In other words, it is most often challenging to obtain purified MPs that retain their activity and are at the same time useful for structure determination. The availability of MP structures is further important for the development of new drugs since MPs are prominent drug targets [26,34] (they are target of more than 60 % of drugs on the market [25]).

2.3.1 The respiratory chain

2.3.1.1 The mitochondrial respiratory chain

All life relies on the continuous supply with external energy either in the form of light or nutrients. This energy is converted into the universal energy carrier ATP in three main steps. Nutrients such as fats, carbohydrates or amino acids are oxidized first to acetyl-coenzyme A and then, in a second step, to CO_2,

and the energy released in these reactions is stored in form of reduction equivalents such as NADH or succinate. In the last step, electrons are transferred in a series of redox reactions from NADH to oxygen to produce water. In this electron transport chain (ETC) called respiratory chain, respiratory enzyme complexes use the energy of energetically 'downhill' electron transfer reactions to pump protons across the membrane, so-called proton-coupled electron transfer [35]. Transport of protons across the membrane is electrogenic and thus not only leads to a difference in pH on either side of the membrane (ΔpH), but also to a transmembrane charge difference (ΔΨ). The so-generated electrochemical proton gradient is termed proton motive force (*pmf*) Δ*p* and consists of two components: I) a chemical proton gradient resulting from the separation of protons by the membrane (ΔpH), and II) an electric potential generated by the separation of charge (ΔΨ) [35]. The *pmf* in turn drives the synthesis of ATP by the ATP synthase.

The eukaryotic respiratory chain is located in the inner mitochondrial membrane and is composed of four complexes CI-CIV (Figure 3) as well as the two electron carriers cytochrome *c* and ubiquinone. In the first step, CI couples the electron transfer from NADH to the hydrophobic and membrane-embedded ubiquinone to the transport of four protons across the membrane. CII reduces ubiquinone while oxidation of succinate to fumarate, and, unlike CI, does not translocate protons across the membrane. The ubiquinol coming from CI and CII is then re-oxidized by CIII which transfers the two electrons from ubiquinol to two molecules of cytochrome *c*, which is located in the intermembrane space. In the final step, electrons are transferred from cytochrome *c* to the final electron acceptor oxygen by CIV, accompanied by proton transport to the intermembrane space and reduction of oxygen to water. In total, for every two electrons from NADH, 10 protons are pumped across the membrane generating a *pmf* that is used by the ATP synthase (and other mitochondrial transporters). [2]

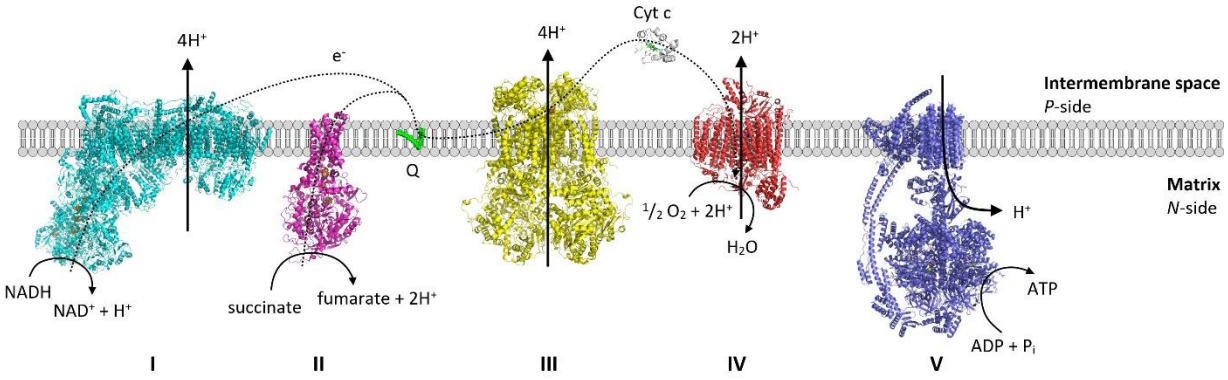

Figure 3 Mitochondrial respiratory chain consisting of complexes I-IV and the ATP synthase (V). Electrons are transferred from NADH and succinate via ubiquinone Q and cytochrome c through complexes I-IV to the final electron acceptor oxygen. The free energy from these electron transport processes is converted to an electrochemical proton gradient termed proton motive force (*pmf*) by proton pumping of complexes I, III and IV, which drives the ATP synthase to synthesize ATP.

2.3.1.2 The respiratory chain from *E. coli*

The four complexes in the inner mitochondrial membrane constitute the prototypical respiratory chain that is typically found in textbooks. While the basic concept, oxidation of reduction equivalents forming a *pmf*, is the same in prokaryotes, the prokaryotic respiratory chain is much more versatile and diverse [36]. *E. coli* is a gram-negative bacterium that possesses two membranes with the ETC located at the inner bacterial membrane and consisting of two consecutive redox steps which are linked by quinones (Figure 4). In the first step, at least 15 different dehydrogenases oxidize ten different electron donor substrates (e. g. NADH, succinate or hydrogen), thereby reducing quinone. The latter is re-oxidized in the second step by different terminal reductases which transfer the electrons to at least six different electron acceptors (O_2, nitrate, nitrite, fumarate, trimethylamine N-oxide, or DMSO). *E. coli* lacks the intermediate step of CIII/cytochrome *c* found in mitochondria and electrons from the quinol pool are directly used for the reduction of terminal electron acceptors. Most dehydrogenases can work together with most terminal reductases building a branched respiratory chain. The complexity is even increased by the use of three different quinones, namely ubiquinone (UQ-8 [37]), menaquinone (MK-8 [37]) or demethylmenaquinone (DMK-8 [37]). [38] Thereby, ubiquinone is the main quinone under aerobic conditions while menaquinone and demethylmenaquinone are used mainly at lower oxygen concentrations [39]. The diversity of its respiratory chain allows *E. coli* to adapt to varying conditions such as the supply of nutrients or oxygen.

While NDH-1 and bo_3 oxidase are able to pump protons across the membrane, most dehydrogenases and terminal reductases generate a *pmf* by a redox loop mechanism. Thereby, electrons are transferred in a first half-loop from the electron donor (on the *P*-side of the membrane) through the membrane to quinone, which consumes protons from the other side of the membrane (*N*-side), by a first enzyme.

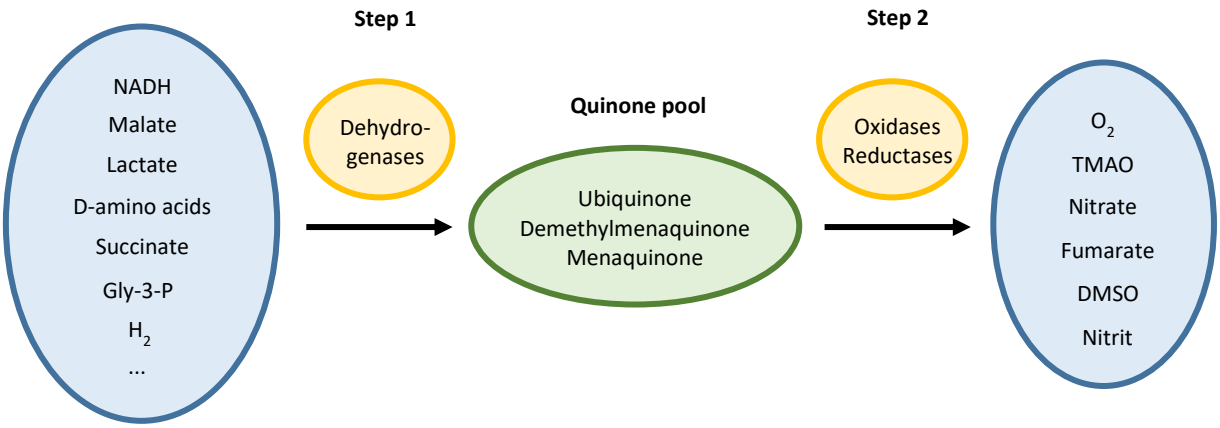

Figure 4 The respiratory chain of *E. coli*. In a first step, a total of 10 different substrates are oxidized by different dehydrogenases, which transfer electrons to a quinone pool. Different oxidases and reductases re-oxidize the quinone pool by the reduction of several final electron acceptors. [26]

Quinol then crosses the membrane to be re-oxidized by another enzyme in the second half-loop, releasing protons to the more positive side of the membrane (*P*-side). [38] Another group of enzymes (e.g. NDH-2, see below) does not contribute directly to the *pmf* generation but is required for the supply or consumption of quinone/quinol to allow the second respiratory enzyme to work and to contribute to the *pmf*. Thereby, it is important that at least one of the two enzymes of an ETC is contributing to the *pmf*. In *E. coli*, the combination of non-coupling dehydrogenases with non-coupling terminal reductases is avoided by transcriptionally regulated expression of suitable enzymes. [38,40]

2.3.1.3 NDH-2

One of the most important primary dehydrogenases of the *E. coli* respiratory chain is NDH-1 [38]. Being a homolog of mitochondrial complex I, it catalyzes the electron transfer from NADH to quinone and couples this reaction to proton pumping which renders it the only proton-pumping dehydrogenase of the respiratory chain of *E. coli*. NDH-1 is mainly expressed under anaerobic conditions, while it is present in lower concentrations at higher oxygen levels [40]. Under aerobic conditions, NADH dehydrogenase II (NDH-2) is the major NADH dehydrogenase in *E. coli*. [38] NDH-2 catalyzes the same reaction as NDH-1, however, does not pump protons and thus does not make any direct contribution to the *pmf*. Although the proton pumping NDH-1 conserves more energy than NDH-2, the latter might be essential because it is not inhibited via a negative feedback loop by a high *pmf*. Thus, NDH-2 enables higher metabolic flux resulting in higher rates of ATP synthesis [41,42]. Furthermore, it regenerates NAD^+, allowing glycolysis at high *pmf* and preventing the bacteria from switching to fermentation [43].

NDH-2 (Figure 5) is a monotopic single-subunit enzyme with a molecular weight around 50 kDa located at the cytosolic side of the inner bacterial membrane of *E. coli* [44] as well as other prokaryotes and is even found in archaea, yeast, fungi and plants [45]. It was shown to be essential in several bacterial pathogens. This, and its absence in animals, renders NDH-2 a potential drug target against human pathogens and parasites [41]. It catalyzes electron transfer from NADH mainly to quinone via a non-covalently bound FAD cofactor [41]. The NDH-2 crystal structures of four organisms have been solved in the past ten years: Ndi1 from *Saccharomyces cerevisiae* [46,47], bacterial NDH-2 from *Caldalkalibacillus thermarum* [41,48] and

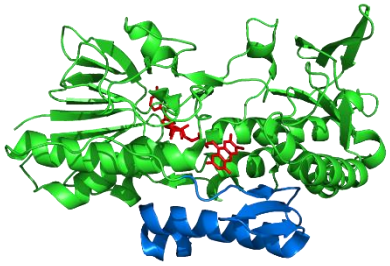

Figure 5 Structure of the monotopic, single-subunit NDH-2 from *C. thermarum*. C-terminal region is depicted in blue and non-covalently bound FAD is shown in red sticks. (PDB 6BDO [48])

Staphylococcus aureus [49], and NDH2 from *Plasmodium falciparum* [50]. In all structures, two Rossmann folds (see [51]) non-covalently bind the cofactor FAD and the substrate NADH, and a third C-terminal domain is responsible for membrane anchoring and quinone binding. The catalytic mechanism of NDH-2 from *C. thermarum* was published in 2017 by Blaza et al. [52]. It indicates that the two substrates bind at distinct binding sites and that the reaction follows a ternary-complex mechanism during enzyme turnover with NADH and menadione, meaning that after being oxidized, NAD^+ binds tightly to the reduced FAD and is not released before FAD is re-oxidized by menadione [52]. Knowledge about the structure and mechanism of NDH-2 helps to develop new therapeutic drugs targeting NDH-2.

An open question is how NDH-2 binds to the membrane. Initially, it was suggested that NDH-2 binds via two transmembrane helices located at the C-terminus of the enzyme [53]. However, this was proven wrong by Villegas et al. [44]: Treatment of NDH-2 containing membranes with either high ionic strength or alkaline buffers (conditions known to selectively extract peripheral membrane proteins) resulted in NDH-2 being present in the supernatant, excluding transmembrane binding of NDH-2. In further experiments, Villegas et al. tested a hypothesis brought forward after bioinformatics analysis [54] that the C-terminal region of NDH-2 is responsible for membrane anchorage. Therefore, they expressed four truncated NDH-2 mutants lacking 13, 28, 43 or 57 C-terminal amino acids, respectively, and could show by SDS-PAGE that, while wildtype NDH-2 and the first two truncation mutants (13, 28 amino acids, respectively) were present in the membrane fraction, the other two mutants were located mainly in the cytosolic fraction [44], thus supporting the hypothesis. Similar results were obtained by Feng et al. [46] and Heikal et al. [41] with truncated mutants of Ndi1 and the *C. thermarum* NDH-2, respectively. Furthermore, the amino acid sequence supports the hypothesis of the C-terminal region being involved in membrane binding. The C-terminal domains of NDH-2 enzymes discussed here are mainly composed of hydrophobic and positively charged amino acids. Membrane binding of NDH-2 is hypothetically achieved by I) electrostatic interactions between the positively charged amino acids in the C-terminus of NDH-2 and negatively charged lipid head groups of the membrane, and II) hydrophobic interactions between the hydrophobic amino acids mainly of the C-terminal domain of NDH-2 and the fatty acids of the membrane. Experimental proof of this hypothesis however is still pending.

2.3.1.4 *bo₃* oxidase

Cytochrome *bo₃* ubiquinol oxidase, or short *bo₃* oxidase, is the main terminal oxidase of the respiratory chain of *E. coli* expressed under aerobic conditions. It belongs to the superfamily of heme-copper oxidases [55,56] and couples the reduction of oxygen to water with proton pumping. *bo₃* oxidase is composed of four subunits I-IV (Figure 6A and B) with a total molecular mass of around 140 kDa, where subunit I contains the catalytic site. Subunits I-III are homologues of the three mitochondrially encoded subunits I-III of the *aa₃*-type cytochrome c oxidase [57]. The catalytic redox center (Figure 6C) in subunit I consists

of a low-spin *b* heme and a binuclear center which is formed by a high-spin o_3 heme and a copper ion (Cu_B). As a substrate, bo_3 oxidase uses ubiquinol Q_8 [58] from which electrons are transferred via the heme *b* to the binuclear center, where they are used to reduce molecular oxygen to water [59,60]. Thereby, bo_3 oxidase contributes to the *pmf* via two mechanisms: I) the protons and electrons used for the reduction of oxygen are taken from opposite sides of the membrane resulting in a net transfer of one positive charge from the negative (*N*) to the positive (*P*) side of the membrane [60], and II) by additional proton pumping from the *N*-side to the *P*-side of the membrane [60].

The structure of bo_3 oxidase was first solved in 2000 by Abramson et al. (PDB 1FFT) [59] at a resolution of 3.5 Å (Figure 6A). It has a similar overall structure as aa_3-type cytochrome *c* oxidase from *P. denitrificans* [61]. Although 25 % of the complex could not be resolved and no ubiquinone was present in this X-ray structure, Abramson et al. identified 25 transmembrane helices and were capable of modeling a ubiquinone molecule into a proposed binding site which is similar to ubiquinone binding sites of other membrane proteins [59]. Not until 20 years later, Su et al. published a second structure of bo_3 oxidase (Figure 6B, PDB 6WTI) using a new methodology called 'Build and Retrieve' (see [62]) to determine cryo-EM structures at near-atomic resolution [62]. They subjected a heterogeneous sample of Ni-affinity purified HpnN from *B. pseudomallei*, which had been expressed in *E. coli*, to cryo-EM and found the most abundant protein to be bo_3 oxidase (followed by HpnN). By this means, Su et al. solved the structure of bo_3 oxidase

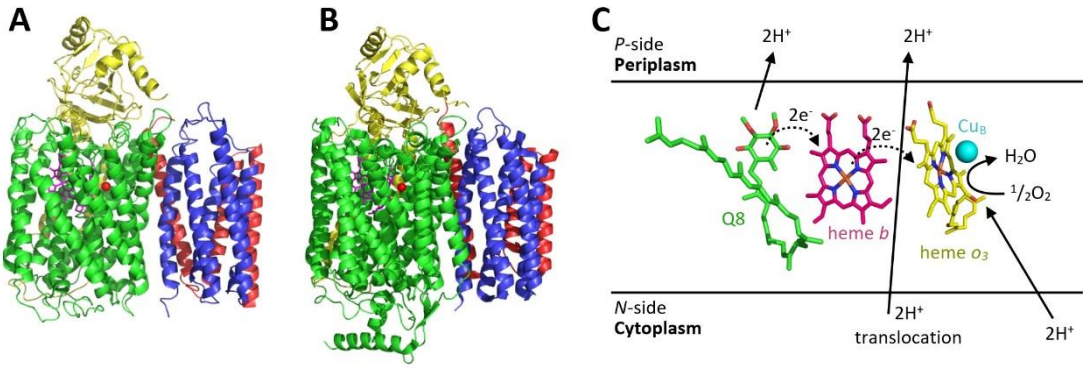

Figure 6 bo_3 oxidase from *E. coli*. A) First structure of *E. coli* bo_3 oxidase solved by Abramson et al. (PDB 1FFT) [59]. **B)** Recently published structure of bo_3 oxidase exhibiting cytoplasmic swelling in subunit I (PDB 6WTI) [62]. All four subunits I (green), II (yellow), III (blue) and IV (red) are shown in cartoon and hemes *b* and o_3 and the Cu_B ion are shown in magenta sticks and red spheres, respectively (**A** and **B**). **C**) Electron and proton transfer in the reaction center of bo_3 oxidase. Electrons are transferred from quinol Q_8 via heme *b* to the binuclear reaction center composed of heme o_3 and Cu_B, where they reduce oxygen to water. The energy released by this reaction is used to pump protons across the membrane from the *N*-side to the *P*-side. Additionally, protons are released from quinol to the *P*-side, while protons for the reduction of oxygen are taken up from the *N*-side. By this means, bo_3 oxidase generates a *pmf*.

at 2.20 Å which consisted of 23 transmembrane helices where the distribution for subunits I, II, III and IV was 13, 2, 5 and 3 transmembrane helices, respectively. Further, the structure clearly depicts heme *b*, heme o_3, Cu_B and even bound ubiquinol. Up to now, it is still under debate if bo_3 oxidase contains rather one or two ubiquinol binding sites [63–65]. The new structure from Su et al. however strongly indicates that ubiquinol has only one binding site in bo_3 oxidase which coincides with the high-affinity binding site proposed earlier [62]. Another striking difference in the two structures of Abramson and Su is found in subunit I. The structure of Su et al. shows a swelling of the cytosolic part of subunit I clearly protruding into the aqueous solution which was absent in the first structure from Abramson et al. but had been present in the recently published structure of cytochrome aa_3-600 menaquinol oxidase from *Bacillus subtilis* [66]. The new high-resolution structure of Su et al. will facilitate the investigation of bo_3 oxidase and the design of new mutants.

2.3.1.5 The ATP synthase

The F_1F_0 ATP synthase is a universally conserved nanomachine responsible for the synthesis of the majority of ATP produced in living cells [67]. It is found in energy-transducing membranes of bacteria, mitochondria or chloroplasts [68] and is closely related to the vacuolar (V-type, acidifying intracellular compartments [2]) and archaeal (A-type) ATPase [69]. Normally, the ATP synthase catalyzes ATP production from ADP and P_i using *pmf* as an energy source. However, in some bacteria under anaerobic conditions, when the *pmf* is low, the enzyme works in reverse and the hydrolysis of ATP is used to pump protons against their electrochemical gradient to generate a *pmf*. Like this, the ATP synthase enables ATP generated by substrate level phosphorylation to be used to establish a *pmf* which in turn is essential for many cellular functions such as chemotaxis or membrane transport processes [69].

The ATP synthase is composed of two major domains (Figure 7A), the water-soluble F_1 part and the membrane-embedded F_0 part which are connected via a central and a peripheral stalk. The mushroom-shaped F_1 domain consists of subunits $\alpha_3\beta_3\gamma\delta\varepsilon$ and has a total mass of around 380 kDa. It harbors the ADP/ATP binding site and, by a rotary mechanism, catalyzes ATP synthesis and hydrolysis [67]. Similar to the segments of an orange, the six $\alpha_3\beta_3$ subunits are arranged alternately around the central stalk subunits γ and ε, while each β subunit contains a catalytic ATP/ADP binding site. The rest of subunits γ and ε interact with the F_0 domain. Like this, as the central stalk, subunit γ attaches the F_1 head group to the F_0 part. The bacterial F_0 domain is responsible for ion translocation across the membrane and is usually composed of subunits $ab_2c_{8\text{-}15}$ [69–71] (where the c subunits form a cylindrical ring and the number of c subunits depends on the organism but is constant in a given organism [67]; e.g. *E. coli* has a c_{10} ring [72,73]). In the forward synthesis direction, ion translocation along the electrochemical ion gradient drives the rotation of the c ring against subunits a and b_2, where b_2 (together with subunit δ) acts as a peripheral stalk connecting subunit a with the $\alpha_3\beta_3$ head group. Altogether, the *pmf*-driven rotation of the rotor (c

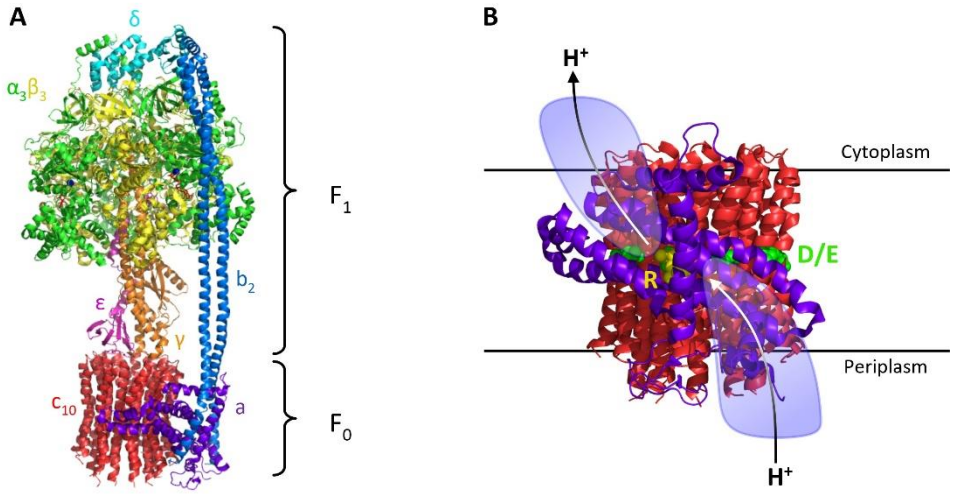

Figure 7 The ATP synthase from *E. coli* A) Structure of F_1F_0 ATP synthase from *E. coli* composed of a water-soluble cytosolic F_1 part and a membrane-bound F_0 part. A *pmf* drives the c ring to turn against subunit a. This rotation is transferred to subunit γ which induces conformational changes in the $\alpha_3\beta_3$ head group leading to the synthesis of ATP from ADP and phosphate. **B)** The F_0 part contains two half-channels in subunit a (transparent blue), separated by a highly conserved arginine (yellow) in subunit a. Protons access the conserved glutamate/aspartate in subunit c from the periplasmic side via a first half-channel and release after one rotation around the c ring to the cytoplasmic side via a second half-channel. (PDB 6OQU [72])

ring and subunits γ and ε) against the stator (subunits $\alpha_3\beta_3\delta ab_2$) induces conformational changes in the catalytical $\alpha_3\beta_3$ head, like this catalyzing ATP synthesis. Contrarily, ATP hydrolysis in the F_1 domain induces rotator revolution in the opposite direction, driving ion transport across the membrane through F_0 against the electrochemical gradient, thereby generating a *pmf*. Depending on the organism, the total subunit composition can vary, e.g. mammalian ATP synthases essentially having additional subunits in the stalk region. [67,69,70]

While the structures of most ATP synthase subunits have been partially solved decades ago, subunit a remained unresolved for a long time, mainly because it dissociates from the ATP synthase when it is exposed extendedly to detergent [74]. In earlier models, the arrangement of α-helices in subunit a was expected to be transmembrane what is common for α-helices of any other known membrane protein. It was thus a huge surprise in 2015 when the first structure was published showing horizontal α-helices for subunit a that run almost perpendicular to the transmembrane helices of the c ring [75]. In the meanwhile, structures of subunit a have been solved for a number of organisms and for several types of ATP synthases (F-type, V-type) [70,76,77]. All those structures had in common two membrane-intrinsic nearly horizontal helices interacting with the c ring, making them a conserved feature of ATP synthases [74]. In 2020, the structure of the *E. coli* ATP synthase was solved including subunit a [72]. It exhibited the same

membrane-intrinsic α-helices, and further showed that the N-terminus of subunit a is found on the periplasmic side of the membrane while the C-terminus points to the cytoplasm.

With the new subunit a structures, the model of proton translocation through the F_0 part was developed (Figure 7B). Protons access a highly conserved glutamate (or aspartate; D61 in *E. coli*) in the ion binding site of the c subunit via a half-channel in subunit a from the lumenal or periplasmic side of the membrane. On the other hand, protons release from the glutamate via a second half-channel in subunit a to the mitochondrial matrix or bacterial cytoplasm. Both half-channels span half the membrane, are lined by polar and charged residues, and are separated by a highly conserved and essential arginine in subunit a (R210 in *E. coli*), which prevents proton leakage between the two channels. The current model for torque generation in the F_0 part envisages that protons access the c ring glutamate (or aspartate) via the first half-channel and neutralize its negative charge, enabling the uncharged side chain to partition into the hydrophobic membrane. Movement of the c ring in counterclockwise direction (when looking from the matrix or bacterial cytoplasm) renders the glutamate (or aspartate) of the adjacent c subunit accessible to the first half-channel, where another protonation reaction happens. Like this, a protonated subunit rotates all around the c ring until it encounters the second half-channel, where the proton is released by the high pH of the mitochondrial matrix or bacterial cytoplasm. [72,74,75,78] The anew deprotonated glutamate (or aspartate) is not able to partition back into the membrane due to its negative charge. Instead, it passes the arginine and accesses again the first half-channel to become reprotonated. The relative location of the two half-channels, the conserved arginine as well as the direction of the *pmf* allow rotation of the c ring only in one direction. [75]

2.3.1.6 Supercomplexes

In the past 20 years, it was recognized that mitochondrial respiratory complexes are organized in higher order structures called supercomplexes which are composed of various stoichiometries of complexes I, III and IV (such as the respirasome $I_1III_2IV_1$) [73] and possibly complex II [79], whereas the ATP synthase has not been found to be part of supercomplexes so far. Supercomplexes were proposed to stabilize the individual respiratory complexes, to regulate the ETC activity or to reduce the production of reactive oxygen species (ROS) by reducing electron leakage. However, in spite of numerous studies, the physiological role as well as the mechanism of assembly of supercomplexes remain unclear [39,73,79]. Supercomplexes were not only found in mitochondria but also in bacteria such as *Paracoccus denitirificans* [80] or *Rhodobacter spheroides* [81]. A strong enrichment of quinone in supercomplexes of *P. denitrificans* has been observed, suggested to promote electron transfer, which raises the question of the role of quinone distribution for supercomplexes, a highly debated topic [82]. Furthermore, cardiolipin, which is essential for catalytic activities and influences the dynamics of supercomplexes in eukaryotes, has been shown to be enriched at the poles of rod-shaped bacteria [83]. The role of this uneven distribution for

respiratory chain supramolecular complexes in prokaryotes remains another key question [82]. *E. coli* was shown to organize its respiratory complexes in subdomains rather than supercomplexes [39], where multiple copies of equal complexes co-localize but different complexes do not [84]. Furthermore, *pmf* generating enzymes and *pmf* sinks (ATP synthase or flagellar motor) were found at different sites in the membrane [84]. The lack of supercomplexes in *E. coli* was suggested to arise from the need of *E. coli* to quickly adopt to changing environmental conditions, which would be strongly impeded if respiratory complexes would be organized in stoichiometrically defined supercomplexes [84].

2.4 Membrane protein reconstitution in a nutshell

Section 2.4 is a reprint of our 2020 review [85]:

In the seminal reconstitution experiment of Racker and Stoeckenius (described in [85]), native purple bacteria were mixed with cholate-extracted mitochondrial particles (containing enriched F_1F_0 ATP synthase) with asolectin lipids that had been sonicated and solubilized by the bile salt sodium cholate. This mixture was then dialyzed to remove excess detergent allowing the formation of proteoliposomes capable of light-driven ATP synthesis.[86] Almost 50 years later, close variants of this very method are still powerful protocols to reconstitute MPs. Over the years, several other approaches to functionally reconstitute purified MPs into liposomes were developed. Some employ organic solvents, or mechanical means such as sonication, freeze-thawing, or French-press.[87,88] However, the most common methods are based on the use of detergents discussed in the next paragraphs. For an overview of different reconstitution techniques consider the pioneering reviews[87] and[89], for more recent perspectives refer to.[21,90–92]

Generally, the process of detergent-mediated reconstitution can be divided into two main steps. First, a purified and detergent-solubilized MP is mixed with lipids. Second, the detergent is removed from the mixture, leading to the incorporation of the MP into liposomes. In the first step, the lipids are added to the solubilized MP either as fully solubilized mixed detergent-lipid micelles, or as preformed, detergent-destabilized vesicles (for the latter see Figure 8). Detergent removal in the second step is achieved by various methods based on the critical micelle concentration (CMC) of the employed detergent.[87] For small sized micelles (< 25 kDa, high CMC; e.g. sodium cholate, octyl glucoside), rapid dilution, dialysis with an appropriately sized membrane or size exclusion chromatography can be used. For detergents forming large micelles (typically very low CMC), adsorption to polystyrene beads or complex formation with various cyclodextrins is used.[91,93–95] Especially the use of cyclodextrins holds promise as different ring sizes are available that offer some specificity for certain detergents,[93] e.g. allowing the selective removal of one detergent from a detergent mixture. While the exact mechanism of reconstitution by

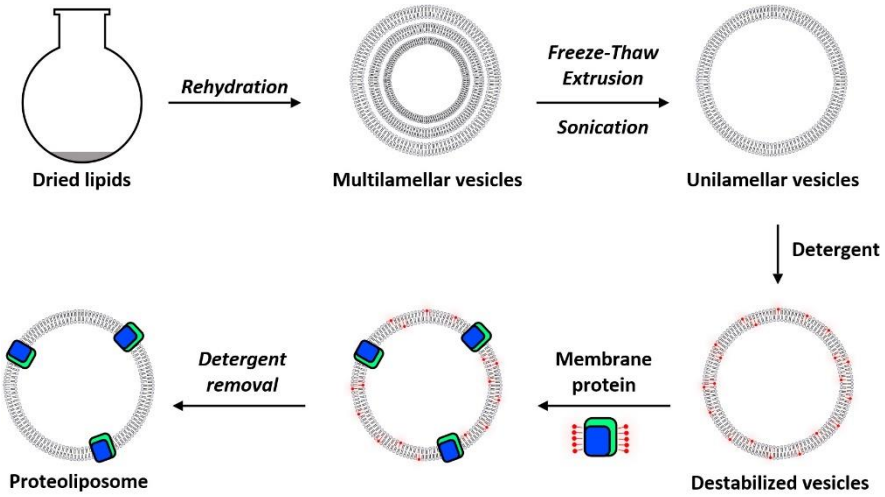

Figure 8 Typical detergent-mediated reconstitution process. Lipids are resuspended in chloroform and mixed in a desired ratio in a round bottom flask followed by evaporation of chloroform to get a dried lipid film. The latter is resuspended in buffer, achieving a suspension of multilamellar vesicles. To get unilamellar vesicles, the mixture is subjected to a series of freeze-thaw cycles followed by extrusion through a polycarbonate filter, or, alternatively, sonication. Detergent is then added in order to destabilize the lipid bilayer, enabling the insertion of detergent-solubilized membrane proteins. Finally, the detergent is removed by one of several methods such as e.g. gel filtration, rapid dilution or adsorption to polystyrene beads, resulting in tight proteoliposomes.

detergent removal is still not fully understood,[90,96] there is agreement that at a critical detergent concentration (which depends on a variety of factors), solubilized MPs cannot be kept in a soluble state any further and either precipitate or spontaneously integrate into the present phospholipid membrane.[90,92] The efficiency of the reconstitution process (fraction of the solubilized MP that incorporates into liposomes) depends on various factors, as e.g. the MP of interest itself, the type of detergent used, the initial detergent concentration, the composition of the lipid membrane, the choice of buffer and ionic strength and importantly, the method and rate of detergent removal.[87,90]

A special role is assigned to the lipid composition in proteoliposomes. Critical aspects for a good lipid mixture are easy liposome formation, preservation of enzyme activity and tightness of the liposomes towards leakage of protons or other ions. For many MPs, a (rather crude) lecithin (phosphatidylcholine (PC)) extract of soybean has been successfully applied. In this extract, next to PC, phosphatidylethanolamine (PE), and the negative lipid phosphatidyl inositol (PI) are the other main components. Although both PC and PI are not found in bacteria, the extract has been successfully used for many prokaryotic MPs. In addition, natural extracts from bacteria, e.g. from *Escherichia coli* or mixtures from synthetic lipids are used. Tsai and Miller[97] have convincingly shown that mixtures of synthetic lipids are much tighter towards proton leakage compared to a polar extract of *E. coli* lipids. Although being outside of the scope of this review, it is noteworthy that the correct lipid composition can have a direct impact on the protein activity as briefly described in the following few examples. Non-bilayer lipids such as PE

Table 1: Non-exhaustive list of different studies with a focus on coreconstitution of MPs or orientation of MPs. For the latter, studies are further distinguished between simply investigating orientation under one or several different conditions and actively influencing orientation by different means. Studies are grouped according to the investigated MP and the origin of the MP and the studied parameter is indicated. A short summary of the study is provided in the comments row.

Membrane Protein	Organism	Study	Comments	References
aa_3*CcO*	*Rhodobacter sphaeroides*	Coreconstitution	Coreconstitution of aa_3*CcO* with F_1F_0 ATP synthase (*E. coli*) or spinach ATP synthase.	[104]
		Investigating orientation	70 - 80 % CcO was found with soluble domain of subunit II carrying the cytochrome *c*-binding site towards the outside of the liposomes. Functional unidirectionality can be imposed over orientation of the MP in the liposomal membrane by providing cytochrome *c* and electrons only on one side of the membrane.	[105]
	Paracoccus denitrificans	Influencing orientation	MP was immobilized on Ni-NTA-functionalized silica nanoparticles for orientated encapsulation into liposomes (bead on outside of proteoliposome).	[106,107]
ArcD2	*Lactococcus lactis*	Coreconstitution	Coreconstitution with OpuA and soluble proteins ArcA, B and C (*L. lactis*)	[108]
bacteriorhodopsin	*Halobacterium salinarum*	Coreconstitution	Coreconstitution with ATP synthase from bovine heart mitochondria.	[86]
		Investigating orientation	Only slight preference for inside-out was detected.	[109]
			Orientation in proteoliposomes was shown to depend on lipid composition of the liposomes, pH value, ionic strength, & membrane curvature (in order of decreasing influence on orientation).	[110]
Ca^{2+}-P-ATPase	rabbit sarcoplasmic reticulum	Investigating orientation	Unidirectional orientation with 80% - 100% of the cytoplasmic domain facing outwards was observed, depending on the rate of detergent removal	[111]
cytochrome bo_3 ubiquinol oxidase	*E. coli*	Coreconstitution	coreconstitution of bo_3 oxidase with F_1F_0 ATP synthase (*E. coli*) via charge-mediated fusion of liposomes to GUVs	[112,113]
			coreconstitution of bo_3 oxidase with F_1F_0 ATP synthase (*E. coli*) or spinach ATP synthase	[104]
			coreconstitution of bo_3 oxidase with F_1F_0 ATP synthase (*E. coli*) via SNARE-mediated fusion	[114]
		Investigating orientation	72 - 77 % to pump protons out of liposomes	[115,116]
			Unidirectional orientation is reported using a reconstitution method based on Rigaud *et al.*[87] However, no biochemical proof of unidirectionality is provided.	[117]
cytochrome *b*-563/*c*-554 (Q*bc*)	*Synechococcus 6716*	Coreconstitution	Coreconstitution with H^+-ATP synthase from *Synechococcus 6716.*	[118]
F_1F_0 ATP synthase	*E. coli*	Coreconstitution	Refer to cytochrome bo_3 ubiquinol oxidase. Further coreconstitutions with Na^+/H^+ antiporters (*Thermus thermophilus* NapA and human NHA2),rat VGLUT2 as well as mitochondrial complex I from *Bos Taurus* together with alternative oxidase from *Trypanosoma brucei brucei*.	[119–122]
		Investigating orientation	> 97 % of F_1 facing outwards was shown.	[123]
LacS	*Streptococcus thermophilus*	Investigating orientation	Different detergents & detergent concentrations were evaluated as well as different rates of detergent removal. Unidi-	[124,125]

			rectional inside-out orientation is reported for reconstitution with Triton X-100 and random orientation for reconstitution with n-Dodecyl β-D-maltoside.	
large-conductance calcium- and voltage-activated potassium channel (BK)	*Homo sapiens*	Investigating orientation	70% inside-out orientation of MP is reported.	[126]
mechanosensitive channel of small conductance (MscS)	*Bacterial* (no further statement made)	Investigating orientation	Unidirectional incorporation is reported based solely on electrophysiological results; no physical evidence is provided. Two ion channel reconstitution methods based on dehydration/rehydration of liposomes in presence of MP were tested.	[127]
Na^+/K^+-P-ATPase	*Electrophorus electricus* or *Squalus acanthias*	Investigating orientation	Functional unidirectionality was imposed over orientation of MP in membrane by selective inhibition of one of the two orientation populations with ouabain (exterior) or vanadate ions (interior).	[128,129]
	dark red outer medulla of kidney of adult New Zealand white rabbits	Investigating orientation	Different protein-to-lipid ratios, different phospholipids and methods of detergent removal were investigated.	[130]
proteorhodopsin	uncultured Gammaproteobacterium EBAC31A08	Coreconstitution	Coreconstitution with *Spinacia oleracea* PSII and *Bacillus pseudofirmus* ATP synthase	[131]
		Influencing orientation	Interaction of MP with the surface of the liposomes was shown to dictate orientation. The surface charge of liposomes was modulated to prearrange orientation.	[132,133]
			MP was immobilized on Ni-NTA-functionalized silicate beads for orientated reconstitution (bead on outside of proteoliposome).	[134]
			Fusion domains were reported to guide the orientated insertion of proteorhodopsin into liposomes.	[135]
various (Ca^{2+}-P-ATPase, H^+-F-ATPase, LacS)	various	Investigating orientation	More uniform orientation of MPs was observed in the reconstituted liposomal bilayer when reconstituted into preformed, detergent-destabilized liposomes.	[125,136–139]
voltage-dependent K^+ channel (K_VAP)	*Aeropyrum pernix*	Influencing orientation	Ni-NTA-functionalized beads were used as membrane organization centers during bilayer reconstitution (bead in proteoliposome; bSUM).	[140]
YidC	*Escherichia Coli*	Coreconstitution	Coreconstitution with LacY and SecYEG as a fusion construct	[141,142]

were shown to stimulate the activity of secondary transporters (e.g. Lyp1 of *Saccheromyces cerevisiae)*.[98] Furthermore, the head groups of lipids, especially of anionic lipids, are responsible for the topology and the regulation of conformational dynamics of transporters by interacting with the transport proteins.[99–103] The importance of negatively charged lipids, especially cardiolipin, for the activity and stability of bacterial and mitochondrial respiratory (super)complexes has also been described.[14,143,144]

The impact of lipids on the reconstitution process has been studied for some proteins, e.g. Na^+/K^+-ATPase.[130,145–148] De Lima Santos *et al*.[130] proposed that the lipids surrounding the MP, as well as the physical state of the lipid environment as e.g. its fluidity, have a stabilizing effect on MPs. Longer saturated fatty acyl chains decreased membrane fluidity leading to activity loss of the MP. Thus, phospholipid mixtures that contribute to membrane fluidity (higher fractions of short-chain or unsaturated fatty

acyl chains) can reduce activity loss.[130,145,147,149] Further excellent studies, in which many of these parameters have been described, were published for bacteriorhodopsin and ATP synthase by Paternostre and colleagues, as well as for LacS by Knol and colleagues (see Table 1 and references therein as well as Lichtenberg *et al.*).[150] These studies show that the lipid composition can affect both the reconstitution yield and the orientation of the protein in the membrane (see below). A final complication is the natural asymmetry of lipid composition in the two leaflets of the bilayer as observed in eukaryotes and prokaryotes[151–153] and first protocols for the generation of asymmetric liposomes have been described.[154,155]

In contrast with natural membranes, proteoliposomes contain much fewer proteins (< 5% of lipid weight), as higher amounts of protein often negatively affect the reconstitution process. An interesting approach to tackle this problem is the GreCon method, in which the solubilized protein is placed onto a sucrose density gradient with increasing concentrations of cyclodextrin and detergent destabilized liposomes. During centrifugation, the detergent is gradually replaced by lipids, yielding liposomes with very high protein content, even triggering 2D-cristallization.[156] In the density gradient, proteoliposomes and empty liposomes migrate differently and are visible as opaque bands allowing their facile separation. Such proteoliposomes have been successfully used for electron tomography imaging using large membrane complexes,[157] but have not yet been tested for transport measurements. In recent years, peptides mimicking the properties of nanodiscs,[158] i.e. embedding the MP in small lipid bilayer discs surrounded by a scaffold protein, have been described.[159–161] While these have the advantage over traditional nanodiscs that their size can be modulated by varying the peptide to lipid ratio, they share the common drawback that they cannot be used to extract protein from native membranes, making the prior use of detergent necessary. A MP extraction method not requiring any detergent is based on the use of styrene maleic acid (SMA) lipid particles (SMALPs), which has been successfully employed to purify[162,163] and also functionally reconstitute MPs into lipid bilayers.[164–168] Recent examples are the purification and reconstitution of cytochrome *c* oxidase from *Saccharomyces cerevisiae*[167] and of a plant sodium/proton antiporter.[168] Although not without downside (the solubilization properties of SMAs are pH-dependent),[169] these novel molecules are valuable gadgets in the toolbox of MP biochemists.

2.5 Coreconstitution of membrane proteins

Section 2.5 is a reprint of our 2020 review [85]:

The incorporation of different MPs into the same liposomal membrane is called coreconstitution and is desirable for several reasons. The small interior volume of liposomes leads to quick accumulation or depletion of the transported substrate, which does not allow for long steady-state measurements and

thus complicates quantitative interpretation of the data. For instance, if a membrane potential is required for the transport process, often a potassium/valinomycin diffusion potential is used that quickly exhausts due to the rapid change of the internal K^+ concentration. Furthermore, as our understanding of biological processes increases, the interplay of different proteins at the molecular level becomes an important field of research. An impressive example of cooperating enzymes are the members of the respiratory chain which have been shown to form different supercomplexes in mitochondria.[79,170] Functional measurements comparing kinetics and efficiencies between individual complexes or multiple complexes arranged in a supercomplex are necessary to understand the functional relevance of such supramolecular arrangements.[171,172]

There are relatively few reports on the coreconstitution of more than one type of MP in the same liposomal membrane. Most work has been published on the coreconstitution of ATP synthase together with proton pumps such as bacteriorhodopsin, cytochrome bo_3 ubiquinol oxidase and cytochrome *c* oxidase, which energize the liposomal membrane with an electrochemical potential. Such systems have been recently extended by the addition of peripheral MPs. Biner *et al.*[121] added trypanosomal alternative oxidase to proteoliposomes containing coreconstituted ATP synthase from *E. coli* and mitochondrial complex I to generate a minimal respiratory chain. Furthermore, ATP synthase has been used as a constant generator of proton motive force for several proton dependent secondary transporters, such as Na^+/H^+ antiporter[119,122] and glutamate transporter.[120] An alternative way to regenerate ATP from ADP and phosphate was recently shown in a synthetic metabolic network consisting of coreconstituted ArcD and OpuA as well as soluble proteins ArcA, B and C entrapped in the vesicle lumen. In this complex network, ArcA – D couple the breakdown of arginine to the regeneration of ATP which is then used by OpuA for glycine betaine transport which regulates the internal osmotic balance of the vesicles.[108] Non-transport related processes can also be studied by coreconstitution such as the chaperone activity of the MP YidC on the folding of LacY.[141] Further examples of coreconstitutions are given in Table 1. In all these examples, both types of integral MPs have been reconstituted in parallel. However, given the individual requirements of every MP for optimal reconstitution and orientation, it has to be assumed that these coreconstitutions were far from being optimal.[86,104,118]

One way to resolve this problem is to split the coreconstitution into two steps. First, either protein of interest is reconstituted under optimal conditions individually, followed by fusion of the two populations. Successful functional coreconstitution of two MPs by fusion was first reported using a minimal SNARE machinery that fused liposome populations containing either F_1F_0 ATP synthase or bo_3 oxidase.[114] The same enzymes have also been successfully coreconstituted using fusion of oppositely charged proteoliposome populations.[112,113] However, the latter method requires the use of non-natural positively charged lipids, limiting the free choice of the lipid composition. Alternative techniques which

have been used for "pure" liposome fusion are coiled-coil forming peptides[173] as well as complementary DNA strands.[174,175] However these methods have not yet been tested with MP containing liposomes.[176]

From the above considerations on coreconstitution experiments, it is obvious that the relative number of MPs reconstituted (stoichiometry) and the distribution of orientation of these MPs is of high importance for quantitative interpretations. Given the various parameters influencing reconstitution efficiency and orientation (see below), this seems an almost insuperable obstacle. A ray of hope was provided by Raschle *et al.* with a method that ensures a 1:1 reconstitution stoichiometry of MPs. Using maleimide chemistry, complementary DNA molecules were attached to a unique cysteine of individual VDAC populations[177]. Upon DNA hybridization, the two populations form a stable complex that can be purified and reconstituted. This technique should be applicable to any MP and using DNA linkers of appropriate lengths might not only ensure the correct stoichiometry, but also correct relative orientation of the reconstituted proteins. Alternatively, proteins can be genetically linked by creating a fusion construct that can be cleaved via proteases, as was used in the coreconstitution of SecYEG and YidC in a 1:1 stoichiometry.[142]

2.6 The importance of the lipid composition on coupled *bo₃*-ATP synthesis activity

The respiratory complexes have been studied in detail and many mechanistic details have been elucidated by a variety of biochemical and biophysical methods [59,62,67,178,179]. However, functional interactions between different primary proton pumping complexes as well as between primary proton pumps and the ATP synthase remain unelucidated. The latter might be of particular interest to understand how protons pumped by the respiratory complexes reach the ATP synthase to drive ATP synthesis. In text books, typically a large ΔpH between the two bulks on either side of the membrane of mitochondria or bacteria is illustrated as part of the *pmf* in order to explain the driving force of ATP synthesis. However, the actual ΔpH in the cristae membranes (the mitochondrial invaginations harboring the respiratory complexes and the ATP synthase) of yeast cells has been shown to be too small (ΔpH = 0.1) to support ATP synthesis by the ATP synthase [180]. Furthermore, alkaliphilic organisms exhibit an inverted ΔpH due to their highly alkaliphilic environment (pH 10-13) which renders the total *pmf* too low to drive ATP synthesis [181]. As a possible explanation to overcome these problems, a phenomenon called lateral proton transfer along the membrane has been suggested where proton equilibration with the bulk solution after being ejected by a proton pump is kinetically delayed. Protons are instead hypothesized to be transferred laterally along the membrane surface [180,182–186]. This scenario would enhance the possibility of a proton to reach a proton consumer, such as the ATP synthase, and would thus enable ATP

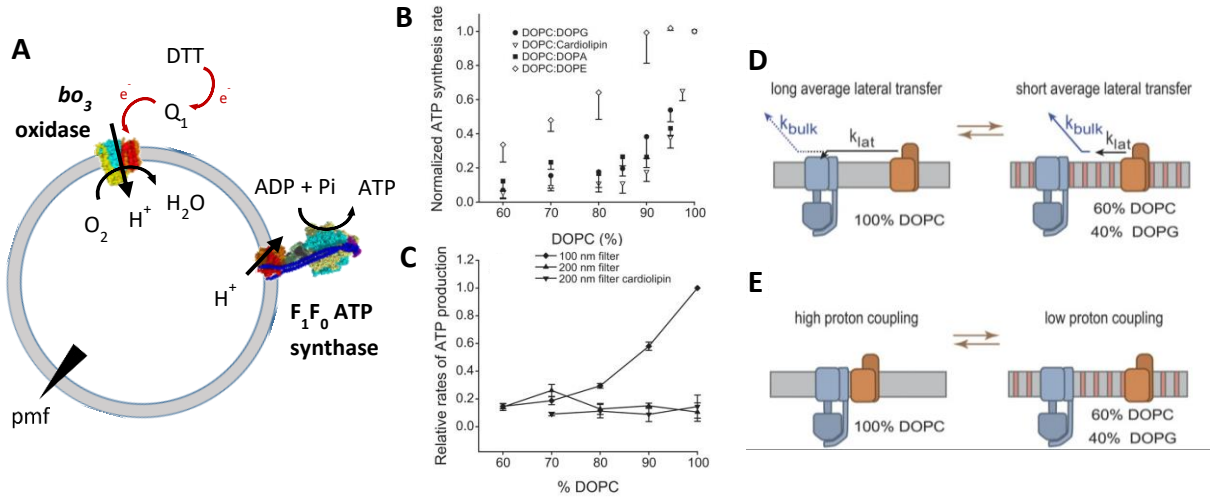

Figure 9 Influence of lipid composition on coupled *bo₃*-ATP synthesis activity. A) Scheme of coupled *bo₃*-ATP synthesis activity. Upon addition of DTT and quinone Q_1, *bo₃* oxidase pumps protons into liposomes, generating a *pmf* which is used by the ATP synthase to produce ATP. **B)** Nilsson et al. [1] observed a drastic decrease in *bo₃*-ATP synthesis activity when negatively charged lipids (DOPG, cardiolipin, DOPA) or another zwitterionic lipid (DOPE) are inserted into DOPC liposomes. **C)** The lipid dependency is vanished in larger liposomes (i.e. with lower enzyme density). Nilsson et al. hypothesize that either the lateral proton transfer rate (**D**) or the lateral enzyme distance (**E**) is changed by the lipid composition. (Figures B-E are taken from [1])

synthesis at low or inverted ΔpH. Two mechanisms for this phenomenon are currently debated. In the first proposal (the proton hopping mechanism), the phospholipid head groups are supposed to retain protons at the surface as transient buffer molecules [187,188], while in the second, protons are kept in a structured water layer between the membrane surface and the bulk solution which delays their equilibration with the bulk [189–191].

A few years ago, our group has established a minimal system of respiratory chain, *bo₃* oxidase and ATP synthase both from *E. coli* coreconstituted into liposomes [1,192,193] (Figure 9A). Upon addition of an electron donor (DTT/Q_1) to the system, *bo₃* oxidase pumps protons into liposomes generating a *pmf* which leads to ATP synthesis by the ATP synthase. In 2016, Nilsson et al. investigated the influence of the lipid composition on this so-called coupled *bo₃*-ATP synthesis activity [1] (Figure 9B). As a standard lipid composition, they used liposomes of 100 % DOPC and the observed ATP synthesis activity was 100 %. They added increasing fractions of negatively charged lipids (DOPG, DOPA, CL) to zwitterionic DOPC liposomes and observed a strong decrease in coupled *bo₃*-ATP synthesis activity. In contrast, the effect of the addition of another zwitterionic lipid (DOPE) was less pronounced. Interestingly, this lipid dependency was only observed at high protein per liposome density (Figure 9C). The authors excluded a number of trivial lipid-dependent effects: I) a lipid-dependent activity of the individual enzymes; II) lipid-dependent quinol diffusion; III) lipid-dependent proton permeability of the membrane. Additionally, on the basis of their findings that the lipid dependency vanished at an enzyme density below a certain

threshold, the authors suggested a lipid-independent reconstitution efficiency and lipid-independent protein orientation. The lipid composition thus seems to affect the rate of proton exchange between the two enzymes. To explain their findings, the authors proposed two hypotheses: Either I) the lateral distance between *bo₃* oxidase and ATP synthase is changed by differing lipid composition (Figure 9E), or II) the rate of lateral proton transfer along the membrane surface is altered (Figure 9D). In both cases, the probability of a proton to reach the ATP synthase is affected by the lipid composition. With their experiments, Nilsson et al. could not discriminate between the two hypotheses. In a follow-up study, Sjöholm et al. performed fluorescence correlation spectroscopy (FCS) and fluorescence cross-correlation spectroscopy (FCCS) experiments with fluorescently labeled *bo₃* oxidase and ATP synthase and compared the data with activity measurements [193]. They could show a link between lateral enzyme distance and coupled *bo₃*-ATP synthesis activity, which would support the first hypothesis of [1]. These findings indicate a mechanism for cells to regulate the ATP synthesis rate by changing the lateral enzyme distance rather than changing the activity of the enzymes themselves [193].

2.7 SpyTag/SpyCatcher

Peptide tags have become indispensable in the world of biochemists. The fact that they are easily integrable into proteins by genetic tools but also their minimally disruptive properties make them important for protein purification, detection or immobilization [194–197]. A drawback of peptide tags, however, is their binding with low affinity. An elegant and powerful system to covalently connect two polypeptide chains *in vivo* or *in vitro* was developed by Zakeri et al. [197]. They split the collagen adhesion domain CnaB2 from the fibronectin binding protein FbaB found in *Streptococcus pyogenes* into a 13 amino acid peptide tag and a 138 amino acid protein partner which they termed SpyTag and SpyCatcher, respectively (Figure 10A). Both SpyTag and SpyCatcher are genetically introduced as fusion partner of the proteins of interest. By simply mixing the two partners together, the unprotonated Lys31 in SpyCatcher nucleophilically attacks the carbonyl group of Asp117 in SpyTag to form an irreversible isopeptide bond (the ε amino group of Lys31 reacts with the side chain of Asp117), catalyzed by SpyCatcher-Glu77 [198] (Figure 10B), as it takes place in the original protein CnaB2. The reaction was shown to be highly specific and high yielding and its robustness to diverse pH, buffer, temperature and detergent conditions renders it suitable to many *in vivo* and *in vitro* applications such as live cell imaging or cell lysate pull-downs. Beneficially, SpyTag was reactive when fused to either terminus or internally of a protein.

Although the amide bond formation of SpyTag and SpyCatcher is fast, its reaction rate (1.4×10^3 M^{-1} s^{-1}) [199] is far from the ideal where protein-protein interactions take place at the diffusion limit ($>10^5$-10^6

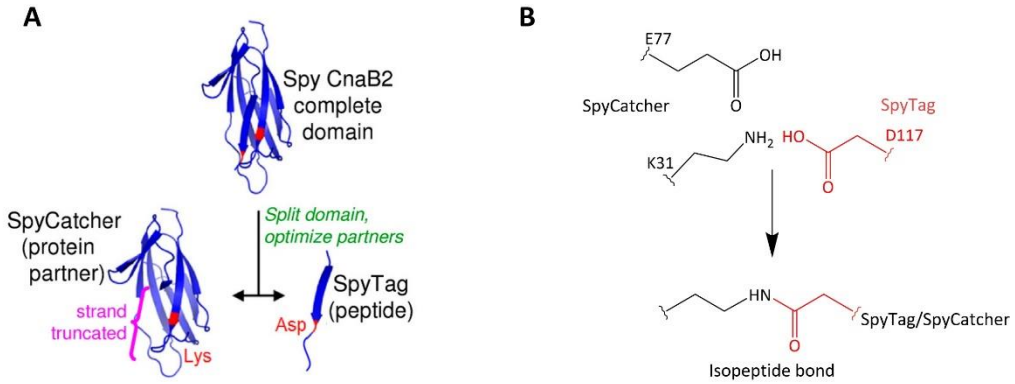

Figure 10 SpyTag/SpyCatcher system. A) CnaB2 from *Streptococcus pyogenes* was split to gain SpyCatcher protein and SpyTag peptide (Figure from [197]). **B)** Isopeptide bond formation between Lys31 of SpyCatcher and Asp117 of SpyTag, promoted by SpyCatcher Glu77, is spontaneous and irreversible.

M^{-1} s^{-1}) [200]. By phage display selection, Keeble et al. improved the reaction rate more than 12-fold, generating the SpyTag002/SpyCatcher002 pair [201] and by further optimization of the two partners, they developed the third-generation SpyTag003/SpyCatcher003 variants [199]. Mainly structural stabilization and increasing of surface polarity of SpyCatcher but also the introduction of positive charge on the SpyTag's N-terminus increased the reaction rate of the 003 pair by a factor of nearly 400 compared to SpyTag/SpyCatcher [199]. With a rate constant of 5.5 x 10^5 M^{-1} s^{-1}, the isopeptide formation of SpyTag003/SpyCatcher003 is now in the onset range of diffusion-controlled protein-protein interactions [200]. Important features of the new SpyTag003/SpyCatcher003 generation are further its lack of side reactions, its specificity in a series of cellular systems and the absence of cysteines in both Tag and Catcher [199], enabling specific chemical modification of site-specifically introduced cysteines on the protein of interest. Moreover, the third generation SpyTag003/SpyCatcher003 are backwards compatible with earlier versions.

Usually, SpyTag-containing proteins have been purified via a His-tag. The His-tag, however, most often is redundant after purification and for many applications has to be cleaved off afterwards which in turn is time-consuming and reduces the yield. To overcome this problem, Khairil Anuar et al. remodeled SpyCatcher to SpyDock which is still binding SpyTag but is no longer able to covalently catch it [202], enabling protein purification via SpyTag. This was reached by the introduction of negative charge and reduced flexibility in SpyCatcher002, and especially by mutating the catalytically active Glu77 to Ala77. An additionally introduced Cys at position Ser49 enabled the site-specific linkage of SpyDock to sepharose beads to give maximum purification yield. Although elution has to be carried out at 2.5 M imidazole, proteins tested so far revealed little aggregation and were still active. The authors moreover showed that both SpyTag and SpyTag002 were suitable for purification via SpyDock and that the SpyTag could be at any site of the protein. With this so-called Spy&Go purification, the purity of proteins could be increased from 66.4 % to 98.9 % in contrast to His-tag purification [202]. Similarly, SpyDock-coupled

beads can be used to remove unreacted SpyTagged proteins from a SpyTag/SpyCatcher coupling reaction [202].

2.8 The problem of protein orientation

Section 2.8 is a reprint of our 2020 review [85]:

In cells, insertion of MPs in membranes is thought to happen co-translationally and the final orientation of the protein is fixed during insertion and remains static (see [203] for a recent discussion on the topic). Unfortunately, this is not the case during MP reconstitution into liposomes as no translational machinery or chaperones are present that help to insert MPs into the liposomal bilayer.[110,204]

The relative orientation of the inserted MP strongly affects functional studies. As liposomes typically contain many copies of the MP in a random orientation, hundreds of different proteoliposome populations are formed during a single reconstitution process, causing a strong heterogeneity in the experimental system (see Figure 11B). In some cases, functional unidirectionality can be imposed over random orientation of the MPs by using substrates which are unable to penetrate the membrane (e.g. ATP, NADH, cytochrome *c*), but in others, the substrate binding site is located in the hydrophobic part of the membrane and, hence, both populations are stimulated (e.g. quinone-coupled enzymes). Alternatively, membrane-impermeable inhibitors can be used, which selectively inhibit one enzyme population.[139] In a worst-case scenario, the reconstitution method yields unidirectional insertion, but in the non-preferred orientation (e.g. substrate binding site on the inside), complicating functional experiments. The orientation of MPs is not only important for primary ion pumps but has to be considered as well for secondary transport proteins. While these can often catalyze transport of their substrates in both directions, the affinities for the substrate might be different on either side of the membrane, a situation that severely complicates the quantitative interpretation of experimental results. The difficulties imposed by uncontrolled orientation are even more pronounced if the coupled activity of two or more MPs coreconstituted in the same liposomal membrane is investigated (see Table 1). The orientation of reconstituted MPs is difficult to predict and even harder to influence, and it seems to be essentially unique for each protein and specific set of reconstitution technique.[90] Over the past decades, however, several studies have accumulated knowledge on protein orientation (see Table 1). Many reports describe the use of bacteriorhodopsin or proteorhodopsin, which are good models for monomeric MPs with no soluble domain, but inadequate as models for large multi-subunit MPs or MPs harboring large soluble domains. A prerequisite for the investigation of MP orientation in liposomal membranes is a reliable assay to determine the ratio of the two possible populations. If feasible, orientation can be assessed via a functional assay that is able to discriminate the relative contribution of both populations.

As an example, the orientation of respiratory complex I in liposomes can be determined by measuring NADH:hexaammineruthenium oxidoreductase activity that can be spectroscopically followed at 340 nm. If NADH, which is membrane-impermeable, is added to liposomes, only the population with the NADH binding site oriented towards the outside will contribute to the activity. Upon solubilization of the proteoliposomes with detergent, all complex I molecules will contribute to the activity. Setting both activities in relation allows for estimation of the orientation of complex I in the liposomes.[205] However, care has to be taken in such approaches, as detergents often affect turnover activities of enzymes. Furthermore, if the measured activity is independent of the presence of the membrane, non-incorporated enzyme also contributes to the activity. A different method that has been used to determine orientation of proteo-/bacteriorhodopsin, is the use of proteases which will only digest MP domains accessible from the outside of the liposomes due to their inability to cross the lipid bilayer. The cleavage pattern can then be analyzed by SDS-PAGE, Western blot or mass spectrometry.[133,206,207] However, this cannot be considered as a general approach, since cleavage patterns are expected to become increasingly complex with larger proteins, and proteolysis might be incomplete. A special case is the F_1F_0 ATP synthase, in which those hydrophilic F_1 head groups that are located on the outside of the liposomes can be specifically stripped off using defined buffer conditions.[123] Yet another approach, often used for secondary antiporters, is based on the selective labelling of cysteine residues from the outside by a membrane impermeable thiol-reactive compound. This is followed by complete labelling with membrane permeable biotin-maleimide that can later be detected by Western-blot analysis.[125,208,209] Further attempts to determine orientation of MPs reconstituted into liposomes can be found in Table 1.

Over the years, it has been found that numerous parameters can affect enzyme orientation during reconstitution. De Lima Santos *et al.*[130] report that at a slow detergent removal rate, liposome formation precedes protein incorporation into liposomes (leading to a more unidirectional incorporation of the MP), while liposome formation and protein incorporation happen simultaneously with fast detergent removal (resulting in a random orientation of MPs). Knol *et al.*[125] found a similar behavior for LacS, including further differences depending on the detergent used for reconstitution. If unidirectional orientation is not desirable, repetitive freeze/thaw cycles were shown to randomize orientation.[94] In general, experiments have shown that orientation seems to be more uniform when the MPs are reconstituted into preformed, partially detergent-solubilized liposomes.[96,137,138,211] A rationale behind this observation is that the most hydrophilic domain will be least efficient in crossing the bilayer, and the protein will insert with its most hydrophobic side first.[96] However, experiments with cytochrome *c* oxidases show that the hydrophilic extramembraneous cytochrome *c*-binding domain (~ 25 kDa) of subunit II is not sufficient to promote more asymmetry than a 70:30 ratio.[105] F_1F_0 ATP synthase, on the other hand,

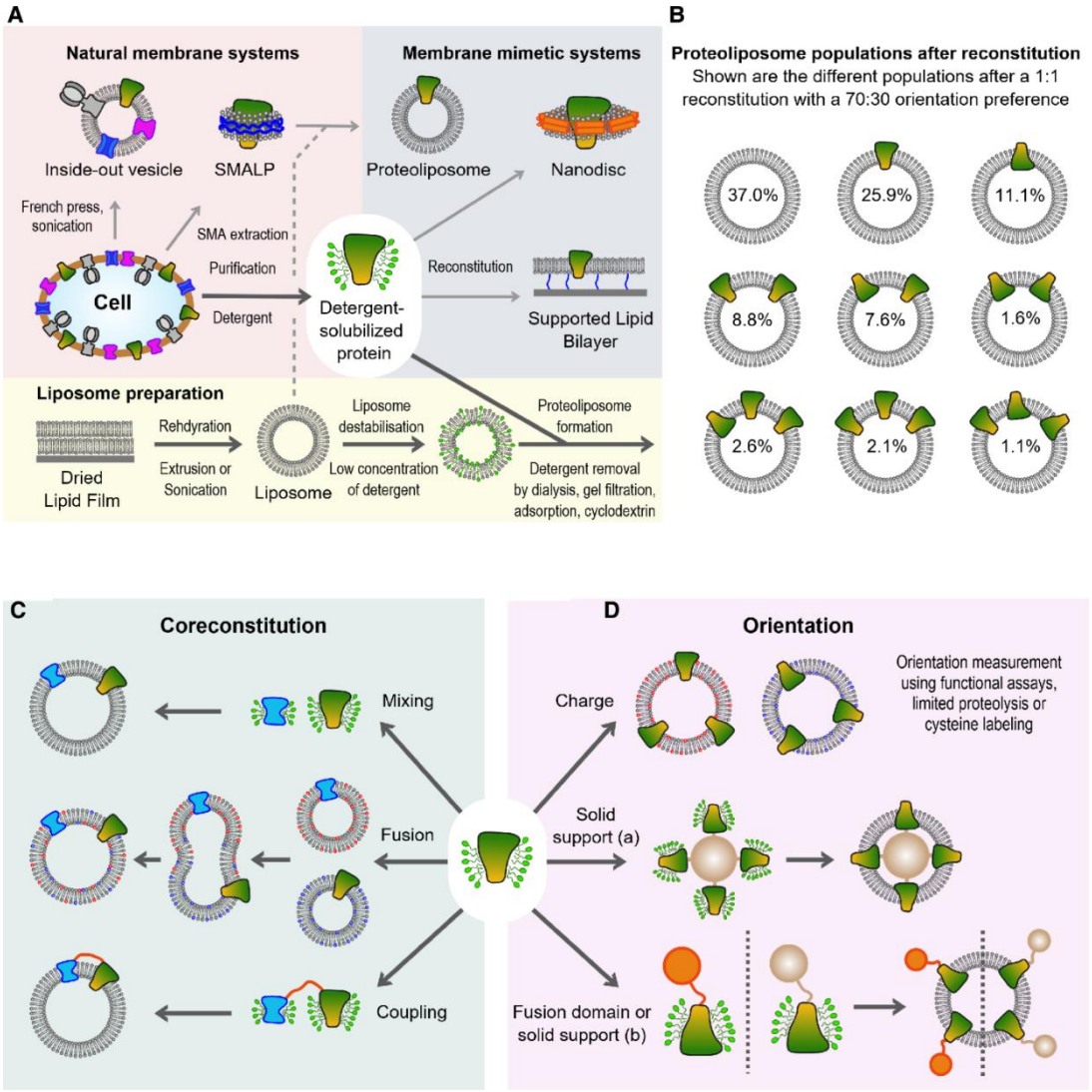

Figure 11 The ins and outs of membrane protein reconstitution A) The general procedure for the formation of proteoliposomes is shown as well as a few alternative approaches for the *in vitro* study of membrane protein (MP) function. In a first step, MPs are extracted and purified from the native cell environment using detergents. In parallel, liposomes are formed by rehydration of a dried lipid film and subsequent extrusion or sonication of the vesicles. These liposomes are partially solubilized by the addition of detergents and mixed with the detergent-solubilized MP to form proteoliposomes after removal of the detergent by a variety of methods. Detergent-free extraction of MPs from the cell can be achieved by generating inside-out vesicles[210] or using styrene-maleic acid (SMA) copolymers to generate SMALPs. The latter can be used for the detergent-free reconstitution of MPs into liposomes.[162–168] If a closed compartment is not needed, detergent-solubilized MPs can also be reconstituted into planer supported lipid bilayers or nanodiscs.[92] **B)** The calculated distribution of proteoliposome populations after reconstitution with a 1:1 liposome to protein stoichiometry and a 70% green-side out preference in orientation. Values were calculated assuming a Poisson distribution for reconstitution and a binomial distribution for orientation. Only populations >1% are shown. **C)** Coreconstitution of more than one membrane protein. Shown are coreconstitutions by a combined incubation of both MPs with liposomes, via fusion of different proteoliposome populations (e.g. charge-mediated fusion, red lipids = negatively charged, blue lipids = positively charged),[112,113] or via

covalent/transient coupling of the MPs prior to reconstitution.[177] **D)** Methods for the guided orientation during reconstitutions. Shown are examples of charge-controlled insertion,[132,133] by coupling the MP to a solid support (a) that will be encapsulated by the liposome[140] or by attaching a fusion domain[135] or coupling to a solid support (b)[106,107] that will be excluded from the vesicle interior. (Figure prepared by Nicolas Dolder)

with its soluble 350 kDa F_1 head group, has been reported to incorporate >95% with its head piece towards the outside with a similar reconstitution protocol.[123] In proteins such as bR and pR, where no large soluble domain is present, the interaction of the surface charge of the proteins and liposomes seems to play a role.[132,133] Tunuguntla *et al.* hold the asymmetry of charge distribution of pR, i.e. an overall positive charge at the C-terminus and a negative charge at the N-terminus, responsible for the lipid-charge dependent orientation of pR in liposomes. Through the use of either positively or negatively charged lipids in their liposomes, the N- or the C-terminus could be attracted towards the liposomal membrane, respectively, promoting a unidirectional orientation of pR.[133] In one of the very few attempts to actively influence orientation, Ritzmann *et al.*[135] recently showed that fusion domains can guide orientated insertion of pR into liposomes. By genetic engineering, GFP and mCherry were added to the C-terminus or to the N-terminus as fusion domains, respectively. The resulting fusion proteins pumped protons across the liposomal membrane in opposite directions upon reconstitution. This elegant method is unique in the sense that both orientations can be chosen by attaching a fusion domain on either end of the protein and is a promising approach for small proteins with no soluble domain. Whether the addition of a GFP is sufficient to orient larger MPs remains to be determined. Other approaches for guided orientation employed Ni-NTA-functionalized beads to immobilize His-tagged MPs prior to reconstitution,[106,107,140] a method also used to form planar bilayers for AFM studies.[212,213] The liposomal membrane was formed *de novo* between the immobilized MPs either around the bead-support,[140] or the beads were suggested to force unidirectional orientation because they were too big to be incorporated into the newly formed liposomes.[106,107] However, a more thorough characterization of these methods, e.g. regarding membrane leakiness, is required. Taken together, despite identification of several parameters that influence orientation of a MP in liposomes, there is still no general method to reconstitute MPs independently of all these parameters. The rather unpredictable effect of the lipid composition on the yield and on the orientation displays a major problem, as the effect of different lipid compositions on protein activity is a frequent aspect of research. A general method for guided orientation of MPs independent of the lipid composition is highly desirable. Approaches, in which orientation is guided by steric constraints might display a promising tool that has to be further developed in the future.[106,107,135,140] Robust and easy to implement methods for the quantitative determination of incorporation yield and relative protein orientation are required to compare established and develop new reconstitution protocols, e.g. only a small subset of detergents have been used in reconstitution.

3 Aims of the thesis

To investigate membrane proteins, they are typically overexpressed, isolated and reconstituted into a membrane-mimetic system such as liposomes. The relative orientation of a membrane protein thereby is critical for its function and therefore knowledge of orientation is requested for quantitative analysis of functional assays. Current orientation determination methods typically rely on functional measurements that are specific for a certain type of membrane protein, or they rely on time-consuming and laborious assays, but so far, no simple and generally applicable method has been reported. In a first part of this thesis, we established a novel method to estimate the relative orientation of membrane proteins in liposomes.

As a first application of this method, we measured the orientation of the terminal respiratory bo_3 oxidase from *E. coli* in liposomes of different lipid composition to get more insight into the way bo_3 oxidase inserts into the lipid bilayer during reconstitution. This is relevant as a few years ago, bo_3 oxidase co-reconstituted with the *E. coli* ATP synthase showed a very strong lipid dependency with the reasons not fully understood. The hypothesis put forward by the authors is based on a lipid-dependent proton transfer between bo_3 oxidase and ATP synthase. In a second part of this thesis, we aimed to understand this phenomenon better, including the dependence of protein orientation by the liposome composition. In addition, we aimed to reversibly but tightly couple bo_3 oxidase and ATP synthase to be able to fix the lateral distance to measure ATP synthesis activity with proteins coupled or freely floating in the bilayer of the liposome. Three different approaches are proposed: I) Coupling via oligonucleotides site-specifically attached to the individual enzymes; II) Expression and purification of a hybrid enzyme where one subunit of each complex is fused and separated via a linker containing a protease cleavage site; and III) Coupling via SpyTag/SpyCatcher [197] fused to one subunit of bo_3 oxidase and ATP synthase, respectively.

Finally, we explored ways to extend the minimal respiratory system using the monotopic respiratory enzyme NDH-2 as well as natural bo_3 oxidase substrate ubiquinone Q_8 to induce proton pumping by bo_3 oxidase and consequently ATP synthesis. We further intended to investigate the importance of the lipid composition on this extended system as well as to shed light on the binding mechanism of NDH-2 to the lipid bilayer by using different NDH-2 mutants.

4 Results

4.1 Rapid Estimation of Membrane Protein Orientation in Liposomes

4.1.1 List of contributions

Title	Rapid Estimation of Membrane Protein Orientation in Liposomes
Journal	ChemBioChem
Status	Published, 11.11.21
Authors	Sabina Deutschmann*, Lukas Rimle*, Christoph von Ballmoos * contributed equally
Contributions	The project was supervised by Christoph von Ballmoos. Experiments were designed, analyzed and results were interpreted together with Christoph von Ballmoos. Design and construction of cysteine mutants were done by Sabina Deutschmann. The overall principle of the assay was established by Lukas Rimle during his master thesis supervised by Sabina Deutschmann. Further elaboration, i.e. liposome flotation assay, was developed by Sabina Deutschmann. Measurements for the publication were done by Sabina Deutschmann and Lukas Rimle. Writing of the draft was done by Lukas Rimle, Sabina Deutschmann and Christoph von Ballmoos.

4.1.2 Abstract

The topological organization of proteins embedded in biological membranes is crucial for the tight interplay between these enzymes and their accessibility to substrates in order to fulfil enzymatic activity. The orientation of a membrane protein reconstituted in artificial membranes depends on many parameters and is hardly predictable. Here, we present a convenient approach to assess this important property independent of the enzymatic activity of the reconstituted protein. Based on cysteine-specific chemical modification of a target membrane protein with a cyanine fluorophore and a corresponding membrane-impermeable fluorescence quencher, the novel strategy allows rapid evaluation of the distribution of the two orientations after reconstitution. The assay has been tested for the respiratory complexes bo_3 oxidase and ATP synthase of *Escherichia coli* and the results agree well with other orientation determination approaches. Given the simple procedure, the proposed method is a powerful tool for optimization of reconstitution conditions or quantitative orientation information prior to functional measurements.

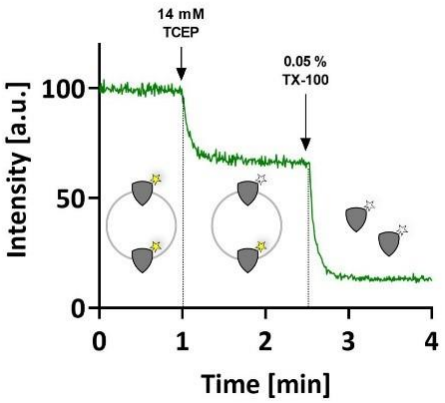

4.1.3 Introduction

Biological membranes are two-dimensional barriers that separate cellular compartments with potentially different chemical properties. These membranes are packed with proteins that organize and mediate communication and molecule transport between the two sides of the membrane. A membrane protein (MP) can span the membrane in two possible orientations – right-side out as found in the intact cell or inside-out as found e.g. in inverted membrane vesicles. The orientation of a MP has direct consequences for the access to substrates and ligands and is therefore critical for its functionality. In cells, insertion is co-translational and mediated by the translation machinery,[203] and usually unidirectional. Insertion of MPs into artificial membranes such as liposomes, however, occurs in the absence of any auxiliary enzymes leading to more random orientation. The topological organization in liposomes is specific for each MP and depends strongly on the reconstitution method and conditions,[90] and it is hardly predictable. Highly unidirectional reconstitution has rarely been described, while a preference for one orientation is often observed.[85,109,115,123,206,214] Knowledge of the orientation distribution of the protein is highly desirable to design proteoliposome experiments and their quantitative analysis. In the past, relative orientation of MPs has been measured with functional assays if the substrate is membrane-impermeable, and enzyme activity is readily determined (e.g. ATPase activity,[121] NADH-dehydrogenase I activity[205]). If this is not possible (e.g. light-driven enzymes, membrane-permeable substrates, elaborate functional assays or non-enzymatic MPs), alternative methods have been applied.

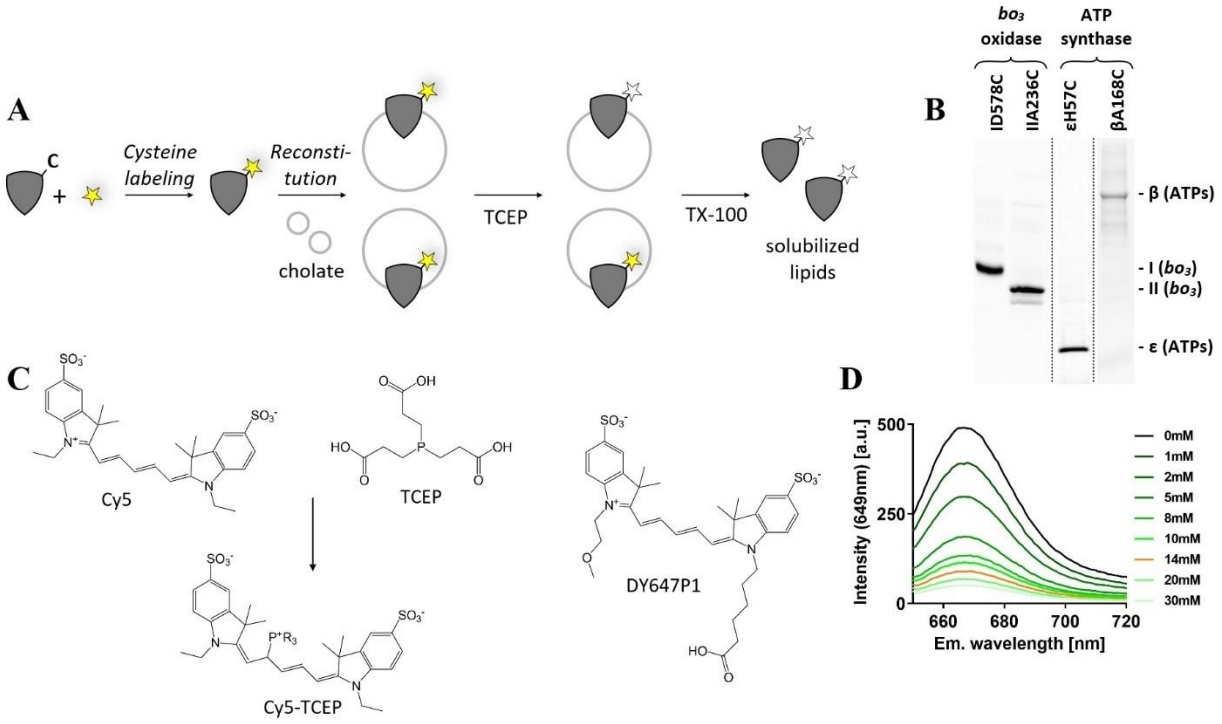

Figure 4.1.1 A) Scheme of the TCEP-based orientation determination assay. A single-cysteine MP is labeled with DY647P1 via maleimide chemistry and reconstituted into liposomes partially solubilized with cholate. The two possible orientation populations are sequentially quenched. In a first step, outwards oriented dye is quenched by TCEP addition, while residual fluorophores are quenched upon solubilization of liposomes by Triton X-100 in a second step. **B)** Fluorescence image of SDS-PAGE from different single-cysteine *bo₃* oxidase-DY647P1 and ATP synthase-DY647P1 mutants. *bo₃* oxidase subunits I and II as well as ATP synthase subunits β and ε are indicated on the right side. **C)** Chemical structures of cyanine dye Cy5 and quencher TCEP as well as Cy5-TCEP adduct, and DY647P1. **D)** Emission scan (λex = 639 nm) of TCEP titration to 100 nM DY647P1-labeled *bo₃* oxidase in 250 mM Tris-HCl pH 8.5 containing 0.05% Triton X-100.

Functionally independent methods include side-selective protease digestion of reconstituted MPs and subsequent analysis via SDS-PAGE[133,206] or site-specific biotinylation of cysteine residues followed by Western-Blot analysis.[215] Both methods are rather time-consuming and proteolysis approaches are likely to be limited to small proteins as band pattern complexity increases for larger proteins (for recent review on the topic, see Ref.[85]).

In the present work, we set out to establish a straightforward and rapid assay to measure MP orientation in liposomes independent of function and applicable to a wide variety of MPs (Figure 4.1.1A). The assay is based on the recent observation that certain cyanine fluorophores (e.g. Cy5 or DY647P1) can be rapidly and selectively quenched by the membrane-impermeable chemical Tris(2-carboxyethyl)phosphine (TCEP), a widely used reductant.[216] We have selectively labeled single-cysteine mutants of the *E. coli* multi-subunit respiratory enzymes *bo₃* oxidase and ATP synthase with the fluorescent dye DY647P1 based on maleimide chemistry. The labeled protein was reconstituted into liposomes and

fluorescence of DY647P1 was monitored before and after addition of TCEP to determine the amount of fluorophore accessible to the quencher. Finally, liposomes were solubilized, allowing TCEP to quench the remainder of fluorophores, and orientation was calculated as the ratio of initial to total quench.

4.1.4 Results

Protein labeling and setup of experiment

The motivation to develop such an assay is our interest in terminal quinol oxidases, such as bo_3 and bd oxidase of *E. coli*. They react with membrane-embedded ubiquinol and reduce molecular oxygen to water, coupled to proton pumping. Thereby, they establish a directed proton motive force (*pmf*) across biological membranes, fueling ATP synthesis by the F_1F_0 ATP synthase or many other *pmf*-driven processes such as nutrient uptake by secondary transport proteins. As ubiquinol binding happens in the transmembrane part of the enzyme,[217] both populations are activated in the presence of ubiquinol and cancel each other's *pmf* out, complicating quantitative interpretation of proton transport or ATP synthesis measurements. The recent observation of Vaughan et al. that Cy5, but not Cy2 or Cy3, is rapidly quenched by TCEP (Figure 4.1.1C) via 1,4-addition at the γ-carbon of the polymethine bridge[216] prompted us to exploit this property. The overall scheme of the experiment is depicted in Figure 4.1.1A. Purified bo_3 oxidase labeled with Cy5 on a single-cysteine mutant is reconstituted into liposomes, yielding proteoliposomes with an unknown orientation distribution of bo_3 oxidase. Addition of a sufficiently high TCEP concentration quenches selectively fluorophores located on the outside of the liposomes, as TCEP cannot readily cross membranes.[218] Further addition of a minimal but sufficient amount of detergent destabilizes the liposomes, allowing TCEP to reach the remainder of the fluorophores located on the inside. Several closely related dyes to Cy5 are commercially available and due to its slightly higher solubility and lower price, we have settled for DY647P1 (Figure 4.1.1C) in our experiments.

Consistent with,[216] efficient quenching was reached with the deprotonated phosphorus form of TCEP (pKa = 7.66[219]) and experiments were thus performed in high buffer at pH 8.5.

The eight natural cysteines in bo_3 oxidase (except C25 on subunit II, which is palmitoylated[220]) were replaced by alanine using molecular biology techniques and a single cysteine was introduced either at position D578 in subunit I (*N*-side of bo_3; see Figure 4.1.2A) or at position A236 in subunit II (*P*-side of bo_3). Care was taken to choose sites at the distance from the membrane with good aqueous accessibility. Cysteines were selectively labeled via maleimide derivatization[221] and specificity of the labeling towards the respective subunits was confirmed using SDS-PAGE and fluorescence detection (Figure 4.1.1B). The lack of a fluorescent band for subunit II in the ID578C sample shows the inaccessibility of the remaining C25 for DY647P1 labeling due to palmitoylation.

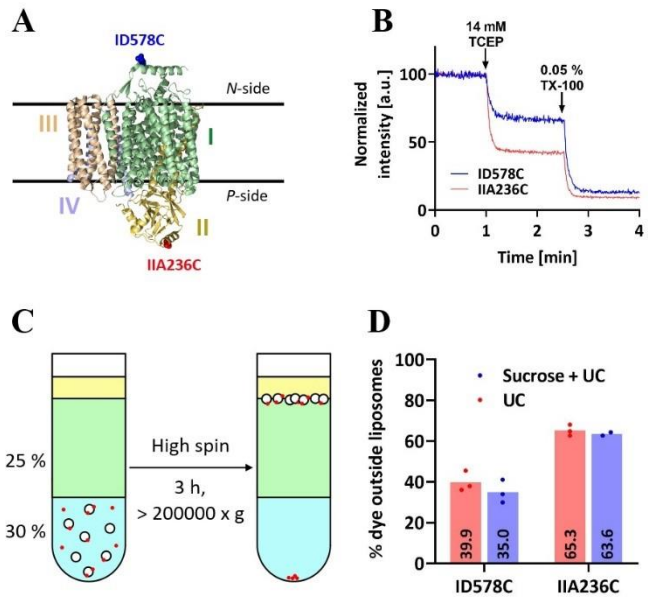

Figure 4.1.2 A) Cartoon representation of *E. coli* bo_3 oxidase structure (PDB 6WTI) with subunit I (pale green), II (yellow), III (pale orange), IV (light blue). Residues ID578C and IIA236C used for single cysteine labeling are depicted in blue and red spheres, respectively. **B)** Raw data of a typical TCEP-based orientation measurement. After monitoring a baseline, TCEP is added, yielding a rapid drop in fluorescence, indicating quenching of the accessible fluorophores by TCEP. A second quench is obtained after addition of detergent to solubilize liposomes, rendering all fluorophores accessible to TCEP quenching. **C)** Principle of liposome flotation assay to separate non- reconstituted MPs from proteoliposomes. Reconstituted liposomes are mixed with a final concentration of 30% sucrose (blue) and layered in an ultracentrifugation tube with 25% sucrose solution (green) and finally with buffer (yellow). After centrifugation (3 h, >200,000×g) in a fixed-angle rotor, liposomes floating in the interface of the two top layers are collected while non-reconstituted or aggregated MP is pelleted. **D)** Percentage of dye oriented to the outside of liposomes of bo_3 oxidase mutants ID578C and IIA236C after reconstitution followed by ultracentrifugation (UC) or liposome flotation assay (Sucrose + UC), respectively. Inside-out and right-side out oriented bo_3 oxidase populations are determined by ID578C and IIA236C, respectively.

To find an optimal TCEP concentration for our quenching experiments, DY647P1-labeled bo_3 oxidase solubilized in detergent solution was titrated with TCEP up to 30 mM. For the remainder of the experiments, 14 mM was used which resulted in >85% quenching (Figure 4.1.1D). Linear dilution effects by addition of aqueous quencher and detergent solutions were considered during data evaluation.

Orientation measurement of bo_3 oxidase

Raw data from a typical TCEP-based orientation determination measurement is depicted in Figure 4.1.2B. Liposomes (10-100 µL) containing ID578C-labeled bo_3 oxidase were suspended in measurement buffer (1.4 mL) and a fluorescence baseline was recorded (corresponding to 100 % fluorescence: Figure 4.1.2B blue line). After ~1 min, 14 mM TCEP was added from a 1 M stock solution and a rapid fluorescence decrease to ~70 % was observed. Addition of 0.05 % Triton X-100, allowing TCEP to access and

quench dyes located on the inside of liposomes, decreased fluorescence to 5-10% of the starting value. Orientation, or rather distribution of the two enzyme populations, was calculated from the ratio of the first to the total quench (Figure S4.1.1). Similar results were obtained if liposomes were solubilized with 0.05 % DDM instead of Triton X-100, indicating that the second quench can be induced also by other detergents. The experiment displayed in Figure 4.1.2B yields a ~40 % inside-out orientation of *bo₃* oxidase, well in agreement with estimations made from single molecule studies (~70 % right-side out[115]).

To validate our method, we repeated the experiment with *bo₃* oxidase labeled at position IIA236 on subunit II, being on the opposite side of the membrane than ID578 (Figure 4.1.2A). Convincingly, the results are inverted, and the first quench was now larger than observed with ID578 mutant (Figure 4.1.2B red line), yielding a ~65 % orientation right-side out. Theoretically, the relative values of the first quench of the two experiments should add up to 100 %. Data from three independent measurements however yielded a slightly higher value of 105-110 % (Figure 4.1.2D, red bars), which indicates an overestimation of the first quench. A possible reason for an overestimation is non-reconstituted MP, either aggregated or soluble, that will contribute to the first quench. We have addressed this problem using an additional liposome purification step termed liposome flotation assay (Figure 4.1.2C). Here, the liposome suspension is deposited on a two-step sucrose gradient and centrifuged for 3 h. Non-incorporated or aggregated proteins have a higher density and will be pelleted on the bottom of the tube, while the lighter proteoliposome fraction floats on top of the upper sucrose layer.[222,223] The results from these experiments indeed affected the orientation ratio in the expected direction and the total sum was now close to 100 % (Figure 4.1.2D, blue bars; for more detail see Figure S4.1.2).

Recently, Yue et al.[224] and Huang et al.[225] have used a related approach to verify calculations that predict peptide insertion into membranes. Peptides were labeled using TAMRA and fluorescence quenching was titrated by tryptophan addition to the solution. Using the Stern-Volmer equation describing the quenching behavior, the relative orientation of the peptides in the membrane was calculated.

We have adapted this approach and titrated liposomes containing reconstituted *bo₃* oxidase (labeled with DY647P1 either at ID578 or IIA236) with different amounts of TCEP (Figure 4.1.3A). Although quenching of DY647P1 by TCEP is based on a covalent bond formation, the concentration dependent quenching followed the Stern-Volmer relationship (Supplementary Figure S4.1.3A). We therefore applied the same equation as Yue et al.[224] used for tryptophan-TAMRA quenching. The apparent Stern-Volmer quenching constant for the different enzymes was determined in the absence of liposomes but in presence of 0.05 % Triton X-100 (Equation (1), see Experimental Section; Figure S4.1.3A). In a second step, TCEP was titrated to reconstituted liposomes and the data was fitted with Equation (2) (see Experimental Section; Figure 4.1.3A, S4.1.3B), allowing calculation of *bo₃* oxidase orientation in liposomes.

As shown in Figure 4.1.3B, the values obtained with the rapid method above (red bars) correlated well with the more laborious titration experiments (blue bars).

Orientation measurement of ATP synthase

The ATP synthase is a highly conserved enzyme that uses the *pmf* generated by terminal oxidases such as *bo₃* oxidase to catalyze ATP synthesis from ADP and phosphate by its rotational mechanism. The enzyme harbors a relatively small membrane part (F_0) and a large mushroom-like extra-membrane part (F_1 part, consisting of $\alpha_3\beta_3\gamma\varepsilon\delta$ and harboring ADP/ATP binding site; Figure 4.1.3C). To determine the orientation of reconstituted ATP synthase, its reversible reaction of ATP hydrolysis is exploited typically in an ATP regenerating assay.[121,226,227] As ATP is not membrane-permeable, its addition only leads to

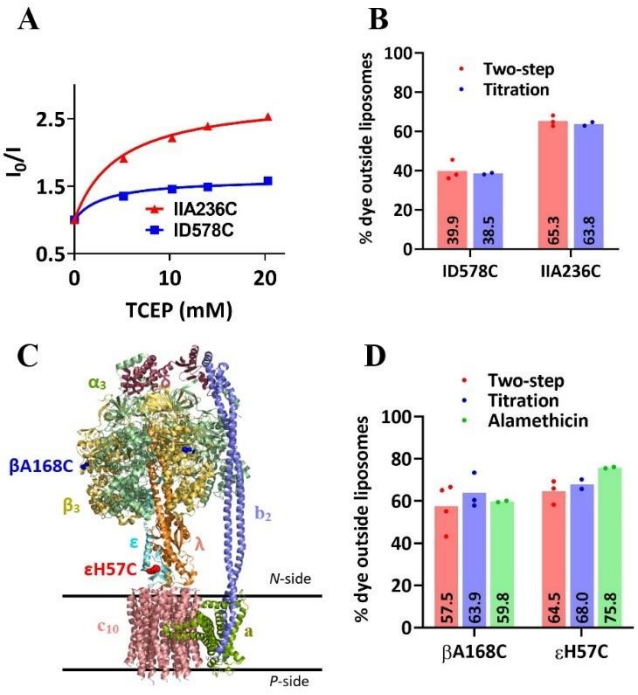

Figure 4.1.3 A) Fluorescence quenching titration assay [224,225]. TCEP was titrated to liposomes reconstituted with DY647P1-labeled *bo₃* oxidase mutants ID578C and IIA236C for orientation determination by fitting the data to Equation (2) (see Experimental Section). The apparent Stern-Volmer constant was measured for both mutants in detergent solution (see Figure S4.1.3B). **B)** Comparison of two step and titration quenching method. *bo₃* oxidase orientation was determined either by the here presented TCEP-based method (Two-step) or by fluorescence titration (Titration)[224,225] for both ID578C and IIA236C mutants (see text for details). **C)** Overall structure of the *E. coli* ATP synthase (PDB 6OQU). βA168 and εH57 are shown in blue and red spheres, respectively, and the membrane is depicted by lines. **D)** Orientation of *E. coli* ATP synthase was determined by the here presented TCEP-based method (Two-step), by fluorescence quenching titration (Titration)[224,225] or by a function-based alamethicin assay (see Figure S4.1.4) [121] for both mutants βA168C and εH57C. For the fluorescence quenching titration assay, the Stern-Volmer constant was measured for both mutants in detergent and the data were fitted with Equation (2) (see Experimental Section; Figure S4.1.3).

ATP hydrolysis from the enzymes with F_1 heads oriented towards the outside. After addition of alamethicin, a membrane pore-forming agent,[228] ATP can also access the internally located ATP binding sites and total ATP hydrolysis can be determined (Figure S4.1.4). To compare this activity-based method with the two fluorescence-based methods, two single-cysteine variants in the F_1 part were constructed. Single cysteines either located in subunit β at position A168 or at position H57 of subunit ε were labeled with DY647P1 using maleimide chemistry as described above. In contrast to labeling at subunit ε, labeling at subunit β was poor, despite the presence of three cysteine copies per enzyme (see discussion). Figure 4.1.3D shows that the three different assays yielded similar results for each mutant. Interestingly, however, a significant discrepancy of the orientation distribution between the two mutants was observed that is discussed in detail below.

4.1.5 Discussion

Reconstitution of purified MPs is a powerful technique to investigate the function and reaction mechanism of an enzyme, and is widely used for respiratory enzymes, primary and secondary transporters, and receptors. The best-known reconstitution technique was established by Rigaud[136] and many other colleagues and is based on formation of a ternary complex of preformed liposomes, detergent and MP. After an appropriate incubation time, the detergent is removed by one of several established techniques. Here, we have employed sodium cholate as a detergent and have destabilized preformed liposomes before the MP was added. The small cholate micelles were then removed by a Zetadex-25 gel filtration column. Liposome reconstitution is accompanied by an unpredictable distribution of the two possible enzyme orientations after the ternary complex has been formed and the detergent is removed. For a variety of reasons, it is interesting to determine the relative protein orientation, but no general and convenient methods exist.[85] Here, we took advantage of the membrane-impermeability of TCEP to quench Cy5 related fluorophores site-specifically attached to MPs to distinguish the inside-out from right-side out oriented population by quenching the fluorescence of the two populations sequentially.

Care has to be taken that labeling of the MP occurs specifically and that uncontrolled labeling is suppressed. We have chosen maleimide-based labeling of single-cysteine variants of the enzymes that occurs specifically with reasonable reaction rates. Further strategies are N-terminal amine labeling (at lower pH) or fusion of SNAP or HALO Tag to the protein of interest. Alternatively, fast and specific labeling can be achieved by bioorthogonal reactions if an unnatural, click-chemistry competent amino acid is introduced in the protein using amber tRNA suppression methods (e. g. amino acids containing alkine, azide, trans-cyclooctene handle).[229] Complete labeling of the enzyme population is not necessary, but a sufficient fluorescence signal is desirable for reliable orientation determination. If downstream experiments are planned with the same liposomes, the labeled protein should be tested for

activity (all mutants tested here retained protein function). We suggest a location of the cysteine at the protein surface to ensure good accessibility to the aqueous environment, allowing rapid labeling and efficient quenching by TCEP. While the *bo₃* oxidase mutants ID578C and IIA236C showed similar labeling efficiencies, ATP synthase mutant βA168C was significantly less labeled than εH57C. For optimal results, several single-cysteine variants of the protein of interest should be tested. The protocol described here was not tested with fluorophores attached to protein residues close to the membrane surface, but we would not recommend such constructs. Although not described for Cy5, fluorophores typically react highly sensitively to their local environment, and accessibility of a negatively charged compound as TCEP might also be affected by the charged (negative or zwitterionic) surface of a lipid bilayer.

Fluorescence of DY647P1 was measured at excitation and emission wavelengths 649 nm and 672 nm, respectively. In an effort to minimize light scattering effects, we blueshifted the excitation to 580 nm, while keeping emission at 672 nm, yielding a lower starting fluorescence that required more liposomes per measurement. No difference of orientation values was observed between the two settings and we therefore suggest to use λex = 649 nm to minimize sample volume.

TCEP quenching is most efficient if the solution pH is above the phosphorous pKa of TCEP (7.66[219]) and membrane impermeability is warranted by the three deprotonated carboxylic acid side chains. If one or more of the acids is esterified, the pKa decreases to <5 for the triply esterified version, however at the expense of membrane permeability.[218] Measurement conditions of pH 8.5, however, are unproblematic and liposome integrity is not affected. High buffer capacity was used to avoid any changes on pH after addition of the acidic TCEP stock solution. In our experiments, we settled for 14 mM TCEP, showing >85 % quenching and allowing a rapid experimental procedure.

We have verified the working principle of our method using two *bo₃* oxidase mutants that are labeled on opposite sides of the membrane. In these, the first quench reflects thus either the fraction of inside-out or the fraction of right-side out oriented MPs. In theory, the sum of the two experiments should add up to 100 %, but it was found to be slightly above.

A likely explanation is that incorporation of protein into liposomes is not complete and that a remainder is dissolved or suspended as protein or protein-lipid aggregates. The fluorescence of these non-incorporated proteins will be quenched after addition of TCEP (first quench), leading to an overestimation of the outwards oriented fluorophore population. These aggregates are neither removed during reconstitution nor during the following ultracentrifuge collection. Non-continuous density gradients have been used to separate liposomes from non-incorporated protein or even differentiate between empty liposomes and liposomes containing protein, but these require centrifugation times >12 hours. A more

rapid approach is the liposome flotation assay,[222,223] in which proteoliposomes are mixed with a 30 % sucrose solution and layered with an equal volume of 25 % sucrose and a thin buffer layer and subjected to ultracentrifugation for three hours. The liposome fraction devoid of non-incorporated protein migrates to the top of the gradient and can be conveniently collected and used for orientation measurements or activity measurements. We found that the procedure indeed decreases the first quench in all our measurements and is therefore recommended for more exact results. However, a solid estimation of MP orientation is also possible without this additional step, providing the method to be a fast and easy assay to estimate the orientation of MPs prior to other experiments or for reconstitution optimization.

We further compared our rapid two-step method with the results obtained by a fluorescence quenching titration assay[224,225] and found very similar results. In the latter, it is not necessary to solubilize the liposomes and the fraction of outwards oriented fluorophore is calculated using the Stern-Volmer equation. The method, however, relies on the Stern-Volmer constant that must be determined prior to orientation determination in the absence of liposomes. Finally, we tested our method with reconstitution of the *E. coli* ATP synthase and compared it with another method based on enzyme activity. Here, membrane-impermeable ATP is added to liposomes and ATP hydrolysis is first assessed on the outside, before pore-forming alamethicin is added to allow ATP to reach also the catalytic sites of the inwardly-oriented ATP synthases. It is preferred to not use detergents in functional assays, as these often affect turnover number of enzymes (typically increasing) by uncoupling them.[85,121,230] Results of this function-based assay supported the accuracy of our novel method.

We were surprised to see the relatively random orientation of the *E. coli* ATP synthase (60 to 75 % with the F_1 head towards the outside). In an earlier work, our group found an almost unidirectional orientation of >90 % with the same enzyme using Western Blotting, and a recent publication reports around 75±20 %.[121] While the enzyme used in these experiments was always the *E. coli* ATP synthase, the purification protocols and the reconstitution conditions were not identical. In the experiments with highest level of orientation, purified protein was reconstituted into liposomes of high density (30 mg/mL), while here and in the recent report, only 10 mg/mL or 5 mg/mL were used, respectively. It is beyond the scope of the present manuscript to discuss the possible implications in detail, but such differences in liposome concentration can lead to different levels of liposome solubilization and thus a different kinetics of protein insertion into liposomes can be envisioned as discussed in impressive detail for lacS.[214] We also attribute the observed difference in orientation with the ATP synthase labeled either at βA168C or εH57C to similar phenomena. Not only were they purified using two different purification protocols (see Experimental Section), but the former was also less efficiently labeled, yielding a larger

enzyme volume used for reconstitution for βA168C than for εH57C. This increases also the detergent concentration during reconstitution and likely affects the properties of ternary complex and the kinetics of detergent removal, two important properties that influence orientation.[85,136,214,231] These findings underline the importance and usefulness of a rapid assay that assesses the influence of several parameters during reconstitution, independent of the protein's function, which is often sensitive to experimental parameters (e.g. lipid composition, detergent used, kinetics of detergent removal).

In conclusion, we provide methodology and testing of a robust and straightforward estimation of MP orientation after reconstitution into liposomes. Although it is generally applicable, it must be optimized for every single protein by finding an appropriate position for labeling. However, once this is done, the method is rapid and powerful, and determination of orientation can be performed before every measurement. To increase the accuracy of the determination, we suggest performing a liposome flotation assay to remove non-incorporated protein. This additional procedure will further allow to determine the efficiency of the reconstitution process by comparing total fluorescence before and after the flotation assay. Here, it is important to critically monitor the exact volumes of the different fractions and correct for dilution effects during the procedure. This is not critical for the determination of the orientation, however, since a ratiometric value is obtained that is independent of the liposome yield in the flotation assay.

4.1.6 Experimental section

Expression of ATP Synthase

ATP synthase variants βA168C and εH57C were constructed from cysteine-free plasmid pFV2[232] using standard molecular biology techniques and constitutively expressed in *E. coli* DK8 cells (lacking the whole ATP operon). Cells were grown in LB medium containing 100 µg/ml ampicillin and 1 mM $MgCl_2$ from precultures for at least 4-5 h in a LEX48 system (epiphyte3) at 38 °C.

Purification of ATP synthase variant βA168C

Cells were harvested by centrifugation and broken by 3 passes through MAXIMATOR (HPL6 High-Pressure Homogenizer, Maximator AG) at 1200 bar at 2 °C in Buffer A (50 mM HEPES pH 8, 100 mM NaCl, 5 % glycerol) containing DNase I (spatula tip) and protease inhibitors PMSF (0.1 mM) and Pefabloc (spatula tip; Biomol). After removal of cell debris (centrifugation at 5000 x *g* for 0.5 h, 4 °C), membranes were pelleted by ultracentrifugation (175'000 x *g*, 1.5 h, 4 °C) and resuspended in 10 mM Tris-HCl pH 7.5 (1 ml per g of wet cells). For solubilization, homogenized membranes were diluted with 2 x solubilization buffer S (50 mM Hepes pH 7.5, 100 mM KCl, 250 mM sucrose, 20 mM imidazole, 40 mM 6-aminohexanoic acid, 15 mM P-aminobenzamidin, 5 mM $MgSO_4$,0.1 mM Na_2-EDTA, 0.2 mM DTT, 0.8 %

soy bean type_II asolectin, 1.5 % *n*-octyl β-D-glucopyranoside, 0.5 % sodium deoxycholate, 0.5 % sodium cholate, 2.5 % glycerol) in a ratio of 1:1 and incubated at 4 °C for 1.5 h while stirring. Non-solubilized material was removed by ultracentrifugation (200'000 *x g*, 30 min, 4 °C) and the supernatant was looped on a prepacked 5 ml HisTrap column (GE Healthcare) equilibrated with buffer S at 4 °C for 2 h. The column was washed with 4 column volumes (cv) of buffer S containing 40 mM imidazole and 2 cv of buffer S containing 90 mM imidazole. Purified protein was eluted with buffer S containing 250 mM imidazole and fractions containing ATP synthase were identified by ATP regenerating assay [226] and pooled. The pooled fraction was divided into aliquots, frozen in liquid nitrogen and stored at -80° C.

Purification of ATP synthase variant εH57C

Cells were harvested and membranes were prepared as described above in Buffer B (50 mM MOPS/NaOH pH 8, 100 mM NaCl, 5 mM $MgCl_2$, 5% glycerol). Pelleted membranes (2 ml per g of wet cells) were resuspended in Buffer C (50 mM MOPS/NaOH pH 8, 100 mM NaCl, 5 mM $MgCl_2$, 30 g/l sucrose, 10% glycerol). For solubilization, LMNG (Anatrace) was added to a final concentration of 2 % from a 5 % stock solution. After the suspension was stirred for 30 min at room temperature and 30 min at 4 °C in presence of 1 mM PMSF, 5 ml of Buffer C was added per g of membranes and non-solubilized material was removed by ultracentrifugation (200'000 x *g*, 0.5 h, 4 °C). The supernatant was loaded onto a prepacked 5 ml HisTrap column (GE Healthcare) in presence of 10 mM imidazole via loop loading for 2 h at 4 °C. Bound protein was eluted via gradient elution from 20 mM to 400 mM imidazole in Buffer C containing 0.005 % LMNG. Fractions containing ATP synthase were identified by ATP regenerating assay [226] , pooled and concentrated with a 100 kDa MWCO Amicon Ultra-15 filter (Merck Millipore). The pooled fraction was divided into aliquots, frozen in liquid nitrogen and stored at -80 °C.

Purification of cytochrome bo_3 oxidase variants

bo_3 oxidase mutants were expressed in *E. coli* strain C43Δcyo [233] cells containing the appropriate plasmid based on pETcyo [234] encoding for the entire *cyo* operon. Cells were grown either in M63 minimal medium (3 g/l KH_2PO_4, 7 g/l K_2HPO_4, 0.5 mg/l $FeSO_4$, 100 µg/ml ampicillin, 1 mM $MgSO_4$, 100 mg/l thiamine, 10 uM $CuSO_4$, 0.2 % glucose, 0.2 % NH_4Cl) containing 100-200 µg/ml ampicillin in a LEX48 system at 38 °C. Expression was induced at an OD_{600} of 0.5-1 with 1 mM IPTG (Santa Cruz) followed by an additional incubation at 38 °C for at least 4-5 h. Cells were harvested by centrifugation, resuspended in Buffer D (50 mM Hepes pH 8.3, 5 mM $MgCl_2$) containing DNase I and protease inhibitors PMSF (1 mM) and Pefabloc (spatula tip; Biomol) and lysed by 3-4 passes through MAXIMATOR (HPL6 High-Pressure Homogenizer, Maximator AG) at 2 °C. After cell debris was removed by centrifugation (8'000 x *g*, 0.5 h, 4 °C), membranes were harvested by ultracentrifugation (200'000 x *g*, 1 h, 4 °C) and resuspended in Buffer E (50 mM K_2HPO_4, pH 8.3) containing 5 mM imidazole. Solubilization was performed with 1 %

DDM (Glycon Biochemicals GmbH) for 2 h at 4 °C, followed by ultracentrifugation (200'000 x *g*, 45 min, 4 °C). Solubilized protein was loaded on prepacked 5 ml HisTrap columns (GE Healthcare), washed with buffer E containing 0.05% DDM and 35 mM imidazole and eluted with the same buffer containing 100 mM imidazole. Fractions containing bo_3 oxidase were pooled and concentrated with a 100 kDa MWCO Amicon Ultra-15 filter (Merck Millipore). The pooled fraction was divided into aliquots, frozen in liquid nitrogen and stored at -80° C.

Site-specific labelling with DY647P1-maleimide

Labeling was essentially performed as described.[221] Purified protein (20-40 µM for bo_3 oxidase mutants and 2-5 µM for ATP synthase mutants) was diluted in a ratio of 1:5 with maleimide reaction buffer (20 mM Hepes pH 6.5, 100 mM KOAc, and either 0.05 % DDM (bo_3 oxidase) or 0.005 % LMNG (ATP synthase)) to adjust the pH. Cysteines were reduced by the addition of 0.4 mM TCEP and the samples were incubated overnight at 4 °C (end-over-end rotation) with a 10-fold excess of DY647P1-maleimide (Dyomics GmbH). Excess dye was removed by gel filtration using CentriPure P10 column (emp Biotech GmbH) and three cycles of diluting and concentrating with an Amicon Ultra-15 filter (Merck Millipore).

Liposome preparation

Lipids were dissolved in chloroform and mixed in a PC/DOPG (LIPOID E PC S; LIPOID PG 18:1/18:1) ratio of 60/40 % (w/w). Chloroform was evaporated overnight in a desiccator and lipids resuspended in liposome buffer L (50 mM MOPS-BTP, pH 6.75) at a concentration of 40 mg/ml. The liposomes were made unilamellar by 7 cycles of freezing (liquid nitrogen), thawing (at 29.4 °C) and 10 s vortexing. Liposomes were aliquoted, frozen in liquid nitrogen and stored at -80°C. Directly before use, an aliquot was thawed at 29.4 °C, diluted with buffer L to 10 mg/ml and extruded 21 times through a Whatman polycarbonate membrane (Sigma Aldrich) with a 100 nm pore size.

Reconstitution of membrane proteins

Reconstitution of ATP synthase or bo_3 oxidase was performed as described by von Ballmoos et al.[104]. Briefly, liposomes were partially solubilized by 0.4 % sodium cholate (from a 30 % stock solution) before enzymes were added. We used varying amounts of protein to adjust for fluorescence signal (3-5 proteins per 100 nm liposome; lipid:protein ratios (w/w) were = 120-140 for bo_3 oxidase and 25-100 for ATP synthase). The mixture was incubated for 30 min at 4 °C with occasional flicking of the tube, followed by removal of the detergent by gel filtration (CentriPure P10, emp Biotech GmbH). Equilibration and elution usually were done with Reconstitution buffer (100 mM MOPS pH 7.5, 25 mM K_2SO_4 1 mM $MgCl_2$). Liposomes were either pelleted by ultracentrifugation (Ti 70.1 rotor, 200'000 x *g*, 1 h, 4 °C) or subjected to a liposome flotation assay (see below).

Liposome flotation assay

Non-reconstituted enzyme was separated from the liposome mixture by a sucrose gradient after reconstitution as described[222,223] with minor adaptations. Briefly, 1.2 ml of P10 eluate after reconstitution was mixed homogenously with 1.6 ml 60 % sucrose (dissolved in Reconstitution buffer) and 400 µl Reconstitution buffer to get a final concentration of 30 % sucrose. In a Beckman Type 70.1 Ti rotor tube, the mixture was then carefully layered first with 4 ml 25 % sucrose and then with 800 µl Reconstitution buffer. All solutions were precooled to 4° C to improve layering experience. Sucrose gradients were centrifuged in the fixed-angle Beckman Type 70.1 Ti rotor at 200'000 x *g* for 3 h at 4 °C, setting acceleration and deceleration (coast) to the minimum. The liposome layer was removed from the sucrose gradient (~1 ml) and liposomes were pelleted by ultracentrifugation at 200'000 x *g* for 45 min at 4 °C to remove sucrose. Pelleted liposomes were resuspended in 200 µl Reconstitution buffer.

Orientation Determination by TCEP-Based Assay

For the TCEP-based orientation determination assay, 10-100 µl liposomes was diluted in 1.4 ml 250 mM Tris-HCl, pH 8.5 and fluorescence of DY647P1 was monitored (excitation 649 nm or 580 nm, emission 672 nm) on a Cary Eclipse Fluorescence Spectrometer (Agilent Technologies). After the baseline was stable (~1 min), 14 mM TCEP was added from a 1 M stock solution, leading to a first quenching plateau. After ~2.5 min, 0.05 % Triton X-100 from a 20 % stock solution was added and fluorescence monitored until the signal was stable (~5 min). The orientation was determined by calculating the ratio between the first and the total quench. Dilution effects from TCEP and Triton X-100 adding were considered during calculation, assuming a linear decrease of fluorescence proportional to dilution of fluorophore.

Fluorescence quenching titration assay

Fluorescence quenching titration experiments were performed as described in Yue et al [224]. First, ~100 nM labelled bo_3 oxidase or ATP synthase solubilized in 250 mM Tris-HCl, pH 8.5, 0.05 % Triton was mixed with increasing TCEP concentrations (0 mM-20 mM) and fluorescence quenching was monitored as described above. The apparent Stern-Volmer constant (K_{sv}) was obtained from fitting the obtained fluorescence ratios to the Stern-Volmer equation (Equation (1)) (Prism software, GraphPad).

$$\frac{Io}{I} = 1 + Ksv\,[TCEP] \text{ (Equation 1)}$$

As described in Yue et al. [224], the percentage of outside oriented dye (x) in liposomes can be determined with various fluorescence ratios obtained with increasing TCEP concentration using the previously calculated K_{sv} according to the following formula:

$$\frac{Io}{I} = \frac{1+Ksv*[TCEP]}{(1-x)*(1+Ksv*[TCEP])+x}$$ (Equation 2)

Alamethicin assay

ATP hydrolysis based orientation measurements were performed according to Biner et al.[121] In brief, ATP hydrolysis of proteoliposomes was measured with ATP regenerating system that couples ATP re-generation to NADH oxidation[226] in presence of 100 nM valinomycin and 2 µM FCCP to prohibit the buildup of an inhibitory *pmf*. ATP was added (2.5 mM) from a 250 mM stock solution and NADH oxidation was followed spectrometrically at 340 nm. After a few minutes, the pore-forming substance Alamethicin from *T. viride* (20 ug/ml; 5 mg/ml stock solution in DMSO) was added and NADH oxidation was monitored. The orientation was calculated by dividing the NADH oxidation slope before and after Alamethicin addition (Figure S4.1.4). A linear range of at least 1 minute was chosen to calculate the slope of ATP hydrolysis.

4.1.7 Acknowledgements

We thank Stefan Moning for his help in testing optimal fluorescence measurements settings and we are grateful to Dr. Andrea Amati for helpful discussions regarding this project. Work in the lab of Christoph von Ballmoos was supported by grants from the Swiss National Science Foundation (No. 176154) and the Uni Bern Forschungsstiftung. Open access funding provided by University of Bern.

Keywords: fluorescence quenching • liposomes • membrane proteins • orientation determination • site-specific modification of proteins

4.1.8 Conflict of interest

The authors declare no conflict of interest.

4.1.9 Supplementary

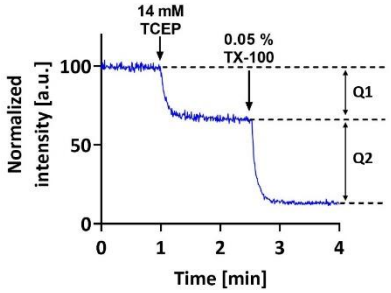

$$Dye\ outside\ [\%] = \frac{Q1}{Q1 + Q2} * 100$$

Figure S4.1.1 TCEP-based approach to determine MP orientation in liposomes. Fluorescence of DY647P1 was monitored (649 nm, 672 nm) until a stable baseline was reached. First quench (Q1) was initiated with adding 14 mM of membrane-impermeable TCEP corresponding to outside-oriented fluorophores. After reaching a plateau, maximal quench (Q2) was induced with adding 0.05 % TX-100, allowing TCEP to quench residual fluorophores. The fraction of dye outside liposomes (corresponding to inside-out or right-side out orientation, depending on the dye's location on the MP) was calculated according to the formula shown on the right side.

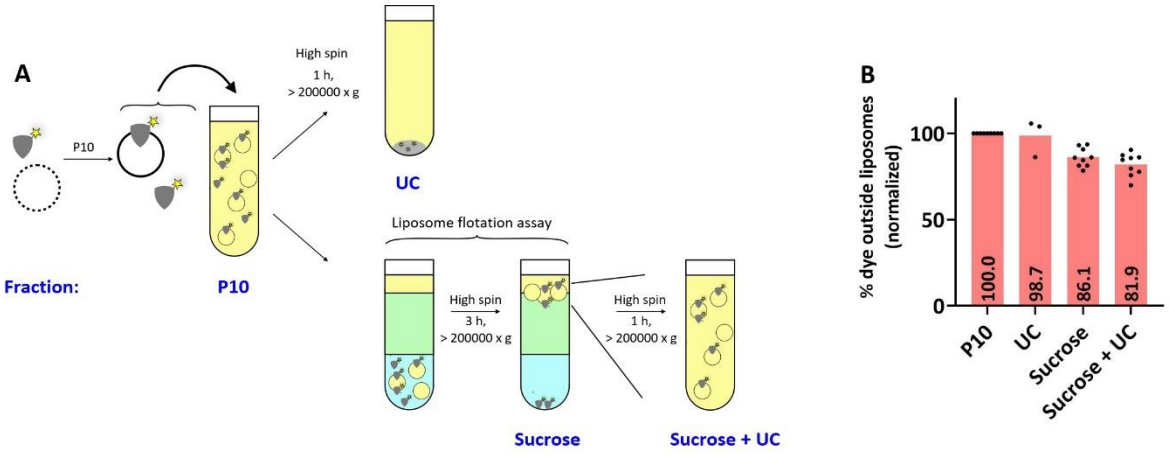

Figure S4.1.2 A) Workflow of detergent-mediated reconstitution of labeled MPs. Detergent-destabilized liposomes were mixed with labeled target MP and incubated for 0.5 h at 4 °C, followed by P10 size exclusion chromatography to remove detergent (P10). Proteoliposomes were either pelleted by ultracentrifugation and resuspended (UC), or mixed with 60 % sucrose in a ratio of 1:1 (lightblue). The mixture was layered with 25 % sucrose solution (green) and buffer (yellow) and proteoliposomes were separated from unreconstituted MPs by ultracentrifugation for 3 h in a liposome flotation assay. Liposomes floating on top of the sucrose gradient (Sucrose) were pelleted afterwards by an additional ultracentrifugation step and subsequently resuspended for measurements (Sucrose + UC). **B)** Orientation of *bo₃* oxidase determined with TCEP-based assay using samples of the afore-mentioned workflow. For the bar plot, measurements of several experimental setups (e.g. different lipid composition, different *bo₃* oxidase mutants) were combined and values were normalized to orientation of *bo₃* oxidase determined after P10.

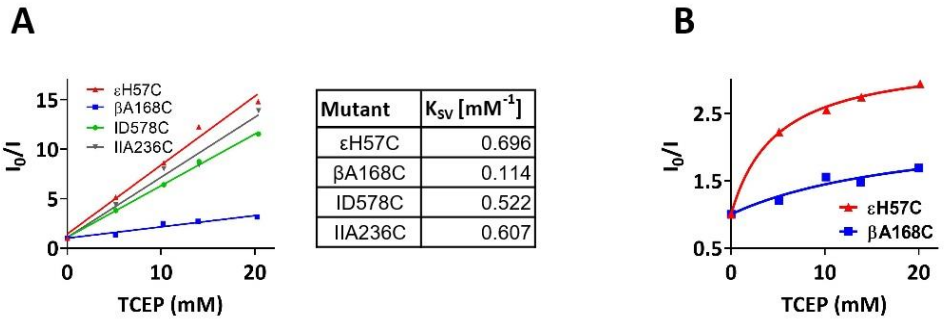

Mutant	K_{SV} [mM^{-1}]
εH57C	0.696
βA168C	0.114
ID578C	0.522
IIA236C	0.607

Figure S4.1.3 Fluorescence quenching titration assay according to [224,225]**. A)** Apparent Stern-Volmer constant was determined for every mutant in detergent-containing buffer with increasing TCEP concentration and fitted in a linear regression. **B)** Proteoliposomes harboring ATP synthase mutants were titrated with TCEP and orientation was determined by fitting the values to Equation (2) (see Experimental Section).

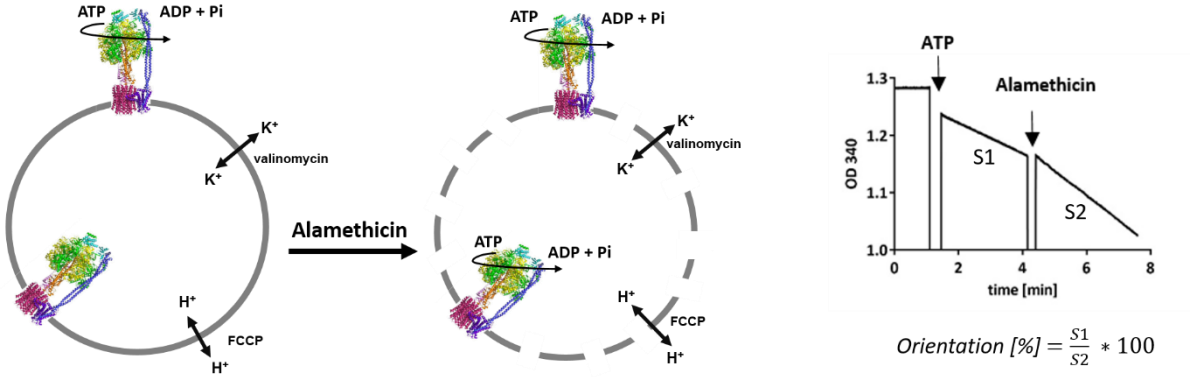

Figure S4.1.4 Alamethicin assay [121] **to determine ATP synthase orientation.** ATP hydrolysis was measured with an ATP regenerating assay [226] detecting absorption at 340 nm. ATP synthase with the F_1 headpiece outside of liposomes were activated by addition of membrane-impermeable substrate ATP, leading to slope S1. Addition of pore-forming substance alamethicin resulted in activation of the second ATP synthase population with the head piece inside of liposomes (slope S2). The orientation was then calculated by taking the ratio of slopes before and after alamethicin addition.

4.2 Impact of the lipid composition on *in vitro* mimicking respiratory chain systems

4.2.1 List of contributions

Title	Impact of the lipid composition on *in vitro* mimicking respiratory chain systems
Status	Manuscript/Draft
Authors	Sabina Deutschmann, Olivier Biner, Martin Schori, Lukas Rimle, Christoph von Ballmoos
Contributions	The project was supervised by Christoph von Ballmoos. Experiments were designed, analyzed and results were interpreted together with Christoph von Ballmoos. Experiments in Figure 1 were performed by Olivier Biner with contributions to Figure 1D by Sabina Deutschmann. Experiments in Figure 2C were performed by Martin Schori and Sabina Deutschmann. The homology model in Figure 2A was done by Christoph von Ballmoos. Cloning, expression and Western Blot experiments of NDH-2 mutants were performed by Martin Schori. Experiments in Figure 3C and 5 were performed by Lukas Rimle and Sabina Deutschmann. Experiments in Figure 4 and 6 were performed by Sabina Deutschmann. Calculations of liposome fractions were done by Nicolas Dolder. Writing of the draft was done by Sabina Deutschmann and Christoph von Ballmoos.

4.2.2 Abstract

Mimetic respiratory chain systems are powerful tools to investigate interactions between different respiratory complexes and how these interactions are influenced by their environment. One such system is the coreconstitution of the terminal cytochrome *bo₃* oxidase and the ATP synthase from *E. coli* in liposomes, where *bo₃* oxidase provides a proton motive force that drives ATP synthesis by the ATP synthase. Here, we extend this system and use either complex II or NDH-2 as electron entry points allowing to use the natural ubiquinone Q_8. We find a strong requirement for negatively charged lipids for the NDH-2 dependent system that is in contrast to earlier results without NDH-2 that are also reproduced here. First, we show that NDH-2 requires negatively charged lipids for activity and second, we identify the relative orientation of *bo₃* oxidase in liposomes as a contributing parameter of the strong lipid dependency. The fraction of desired inside-out oriented *bo₃* oxidase (inside pumping) in overall negatively charged liposomes was significantly decreased compared to neutral or positively charged liposomes, consequently resulting in decreased proton motive force generation and decreased ATP synthesis rates. Reconstitution in the presence of varying salt concentration indicate an electrostatic-mediated insertion of *bo*$_3$ oxidase into the lipid bilayer. To enable a uniform insertion, independent of the lipid composition, of *bo*$_3$ into liposomes, we present our efforts to actively orient *bo*$_3$ oxidase by coupling a large soluble unit to the cytosolic side of the enzyme that should favor inside-out insertion.

4.2.3 Introduction

Biological life relies on the continuous supply of energy to fulfill a great diversity of tasks such as biosynthesis of macromolecules, transport processes, or signal transduction [36]. Energy is ultimately gained either from reduced energy-rich substrates or from light, and the majority is converted into the universal energy currency adenosine triphosphate (ATP). The majority of ATP is produced at energy converting biological membranes, where a series of respiratory complexes in mitochondria or aerobic bacteria couple electron transfer reactions to the transport of protons across the membrane, thus generating a transmembrane electrochemical proton gradient termed proton motive force (*pmf*) which serves to drive ATP synthesis by the ATP synthase and many other transmembrane transport processes. While the highly conserved respiratory chain of eukaryotes is located in mitochondria and consists of four enzyme complexes, bacterial electron transfer chains show astonishing diversity and flexibility [36]. The respiratory chain from *E. coli*, e.g., consists of two consecutive redox steps – oxidation of electron donor substrates and reduction of terminal electron acceptors – which are linked by the electron mediator quinone [38]. In the past decades, respiratory complexes have been extensively studied [59,62,67,179], while functional interactions between the individual complexes and especially with the ATP synthase remain obscure. An interesting question concerns the importance of the membrane lipid environment on such interactions. Cardiolipin, e.g., which is specifically found in energy-converting membranes, was shown

to be essential for oxidative phosphorylation, associating with several respiratory complexes [235] and modulating their activities [82]. It has further been implicated in the stability of mitochondrial supercomplexes and the oligomerization of prokaryotic respiratory complexes [82]. An elegant approach to study protein-lipid interactions is to overexpress and purify the individual complexes and coreconstitute them subsequently into membrane-mimetic systems such as liposomes, in a bottom-up approach. Minimal respiratory systems have been established in liposomes by this means, where one or more respiratory complexes (*pmf* generators) has been coreconstituted with the F_1F_0 ATP synthase (*pmf* consumer) [1,104,121]. One example is the coreconstitution of the terminal bo_3 oxidase with the ATP synthase from *E. coli* [1,104]. The primary proton pump bo_3 oxidase reduces molecular oxygen to water using membrane-bound ubiquinol as electron donor. Thereby, a total of 8 H^+ are transported per reduced O_2 from the *N*-side to the *P*-side of the membrane, establishing a *pmf*. The ATP synthase on the other hand is a highly conserved enzyme responsible for the synthesis of the majority of ATP produced in cells. It consists of a water-soluble F_1 part containing the ATP/ADP binding sites, and a membrane-embedded F_0 part responsible for proton translocation. The *pmf* drives rotation of a rotatory part in F_0 against a stator part that is transmitted into the active sites via a rotating central shaft resulting in ATP synthesis. In the coreconstituted system of bo_3 oxidase and ATP synthase, proton pumping by bo_3 oxidase is initiated by addition of water-soluble quinol Q_1 in combination with an electron source (DTT) and the ATP synthesis rate can be monitored under steady state conditions [1,192,236]. Applying this system, Nilsson et al. investigated the influence of the lipid composition on coupled ATP synthesis activity in liposomes of varying lipid composition and found a strong effect of negatively charged lipids (DOPG, DOPA, cardiolipin (CL)) present in DOPC liposomes, strongly decreasing coupled ATP synthesis rates compared to pure uncharged liposomes (DOPC) [1]. As a direct impact of individual enzyme activities was excluded by a series of control experiments, the authors suggested that the altered lipid composition affects the proton exchange between the two enzymes. In the past, a so-called lateral proton transfer along the membrane surface has been proposed, where equilibration of protons with the bulk solution is kinetically delayed and protons ejected by primary proton pumps are first transferred laterally along the membrane [182–191]. The phenomenon is dependent on proton diffusion and enzyme distance and the findings of Nilsson et al. thus indicate that the different lipid compositions either influence the proton transfer rate or the lateral distance between bo_3 oxidase and ATP synthase [1]. The latter was supported by fluorescence correlation spectroscopy (FCS) and fluorescence cross-correlation spectroscopy (FCCS) experiments [193] one year later. While Nilsson et al. could exclude a number of trivial lipid-dependent effects, they were not able to determine the effect of the lipids on the relative orientation of the two enzymes in liposomes, especially the orientation of bo_3 oxidase [1]. Importantly, the relative orientation of bo_3 oxidase is expected to have a strong effect on the observed ATP synthesis. As both bo_3 populations are

activated by the membrane-embedded quinol, the "wrongly oriented" population counteracts *pmf* formation of the "correctly oriented". The ATP synthase has been shown to insert almost exclusively in an inside-out orientation in preformed liposomes treated with non-solubilizing concentrations of detergent [123]. In a single-molecule study, it has been shown that bo_3 oxidase orients more randomly in crude soybean lipids, with around 70 % in a right-side out orientation, which would provide a net *pmf* to the wrong side, incapable of supporting ATP synthesis [115,116]. Furthermore, the effect of coreconstitution on the relative orientation has not been discussed or investigated so far. This is mainly due to the lack of a fast and activity-independent assay to determine the orientation of membrane proteins in liposomes. Recently, we have established an assay to measure the orientation of membrane proteins in liposomes based on fluorescently labeled membrane protein mutants and a membrane-impermeable quencher (see Chapter 4.1). This assay is generally applicable and independent on the enzyme activity.

Here, we expanded the minimal respiratory system using NDH-2 from *E. coli* and its substrate NADH to induce coupled ATP synthesis by coreconstituted bo_3 oxidase and ATP synthase using full-length ubiquinone Q_8 as a more natural alternative to the commonly used DTT/Q_1 and investigated the influence of the lipid composition on this system. We found negatively charged lipids to be essential for NDH-2/NADH induced coupled ATP synthesis, indicating an inversed lipid dependency compared to the DTT/Q_1 induced coupled activity (observed by [1]). Experiments with purified NDH-2 indicate that negatively charged lipids are essential for efficient quinone reduction. Next, we investigated lipid dependency of bo_3 oxidase orientation in liposomes with the novel fluorescence-based orientation determination method. We found a substantial lipid effect, in which negatively charged lipids shift the orientation distribution towards the less favorable right-side out orientation. Finally, we show our efforts to influence bo_3 oxidase orientation towards the inside-out orientation by site-specific coupling of a large soluble unit to guide bo_3 oxidase insertion in the desired orientation.

4.2.4 Results

Three-component artificial E. coli respiratory chain

In our earlier attempts with liposomes containing coreconstituted bo_3 oxidase and ATP synthase, electrons required for bo_3 activity were added from the outside by addition of DTT and water-soluble ubiquinone analogue Q_1. To lift our system to the next level, we aimed to use the natural ubiquinone Q_8 from *E. coli*. In contrast to short chain quinones, however, Q_8 does not react with DTT and has to be reduced very harshly (e.g. sodium borohydrate) which is incompatible with biological systems. In *E. coli* the quinone pool is reduced by a series of dehydrogenases, e.g. complex I, II or NDH-2. In a first set of experiments, we aimed to mimic the natural scenario with the purified enzymes of fumarate reductase or the non-proton pumping NADH dehydrogenase NDH-2. Lipids dissolved in chloroform were mixed

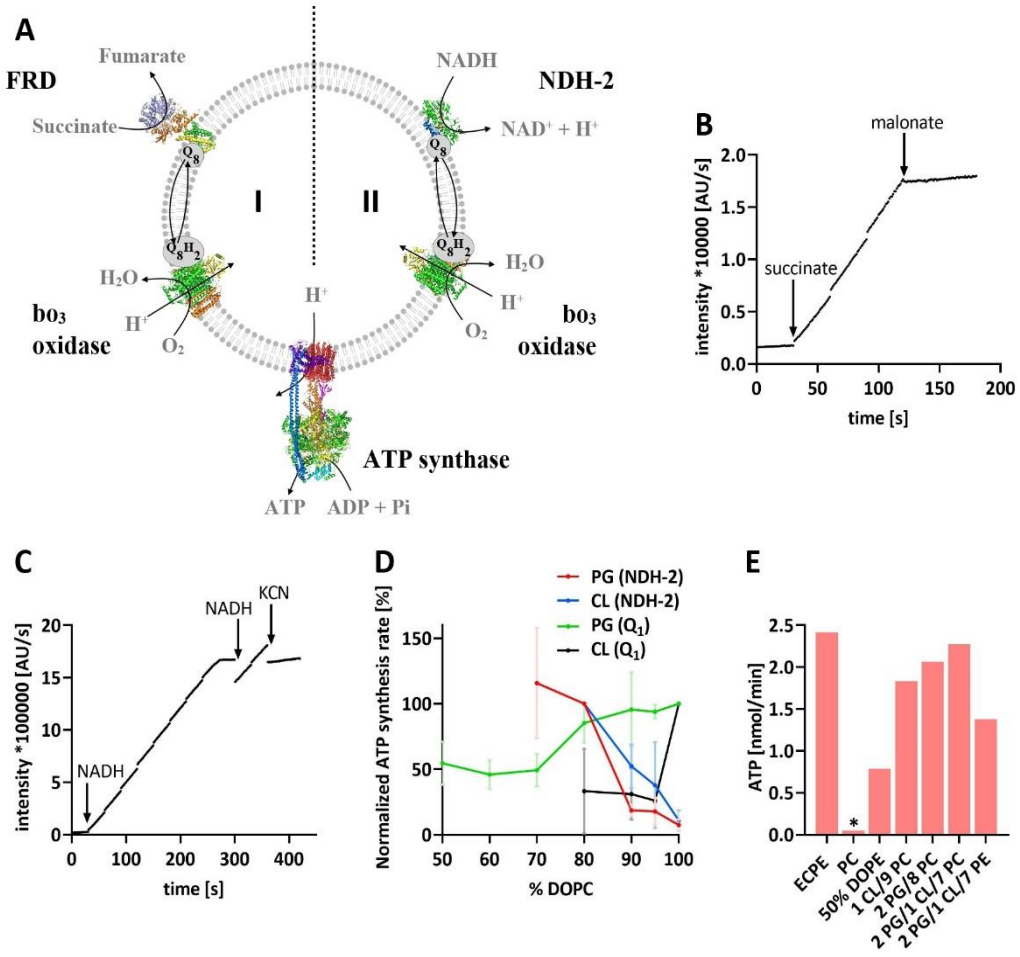

Figure 4.2.1 A) Bottom-up approaches of artificial respiratory chain of *E. coli*. For approach I, FRD, *bo₃* oxidase and ATP synthase are coreconstituted into liposomes containing e-mediator ubiquinol Q_8. Addition of succinate leads to Q_8 reduction by FRD, followed by re-oxidation of Q_8 and simultaneous proton translocation through *bo₃* oxidase. The so-generated *pmf* is used by F_1F_0 ATP synthase to produce ATP which in turn is detected via luminescence. In an alternative approach II, Q_8 is reduced upon NADH addition by the peripheral membrane protein NDH-2, which can be added to proteoliposomes during measurements. **B)** Approach I. ATP synthesis was initiated by adding 1 mM succinate and inhibited by 400 µM of FRD inhibitor malonate. **C)** Approach II. To start ATP synthesis, NDH-2 and 200 µM NADH were added and ATP production was monitored until NADH was fully oxidized. Addition of extra NADH reactivated ATP synthesis until 50 mM KCN addition, which inhibits *bo₃* oxidase. **D)** Coupled ATP synthesis rate initiated either by NDH-2/NADH or Q_1/DTT [1,192] in DOPC liposomes containing varying amounts of DOPG or cardiolipin. For Q_1/DTT induced ATP synthesis, 20 µM Q_1 and 4 mM DTT were used to start the reaction, while NDH-2/NADH induced ATP synthesis was measured as described in (**C**). Rates were normalized to either 100 % DOPC (Q_1/DTT induced) or to 80 % DOPC (NDH-2/NADH induced). **E)** NDH-2/NADH induced coupled ATP synthesis activity in different liposomes. 500 nM NDH-2 were added to proteoliposomes containing *bo₃* oxidase, ATP synthase and Q_8 and ATP synthesis was initiated by 200 µM NADH. ECPE: *E. coli* polar extract. (**B**, **C** and **E** measured by Olivier Biner)

with Q_8, and the solvent was evaporated before liposome formation by buffer rehydration.

First, in addition to *bo*$_3$ oxidase and ATP synthase, also purified FRD was added during the reconstitution process (Figure 4.2.1A, approach I). FRD catalyzes oxidation of succinate to fumarate coupled to quinone reduction in the membrane. The reaction was started by addition of succinate and ATP synthesis was followed *in situ* using luciferin/luciferase. As depicted in Figure 4.2.1B, ATP synthesis was detected immediately after succinate addition, indicating FRD-catalyzed quinone reduction, re-oxidation of quinol with simultaneous *pmf* generation through proton translocation by *bo*$_3$ oxidase, and finally ATP synthesis by ATP synthase[237]. The reaction was inhibited by FRD complex II inhibitor malonate. Titration of succinate dependence is found in Figure S4.2.1.

Next, we replaced FRD with the monotopic NADH dehydrogenase NDH-2 (Figure 4.2.1A, approach II). The advantage of the peripheral membrane protein NDH-2 (Figure 4.2.2A) is that it can be added to liposomes during measurements and has not to be present in the reconstitution mixture. In this scenario, NDH-2 is added from a stock solution to liposomes containing *bo*$_3$ oxidase and ATP synthase and the reaction is started by addition of NADH. High rates of steady state ATP synthesis was measured until NADH was fully oxidized and could be regained after further addition of NADH (Figure 4.2.1C). The reaction could be inhibited by KCN, a *bo*$_3$ oxidase inhibitor. Titration of the relevant parameters quinone Q_8, NADH and added NDH-2 are shown in Fig. S4.2.1. In comparison to the FRD liposomes, much higher ATP synthesis rates were obtained, although the amount of *bo*$_3$ oxidase and ATP synthase were similar in the two experiments. This can be explained by a faster quinone reduction rate of NDH-2 than FRD (higher turnover number and number of NDH-2 than FRD per liposome).

Next, we tested the influence of the lipid composition on the latter experimental system and we found that high ATP synthesis rates were only observed in liposomes containing negatively charged lipids (DOPG, CL, *E. coli* polar extract ECPE; Figure 4.2.1D (red and blue), 4.2.1E), but not in liposomes containing only zwitterionic DOPE or DOPC lipids. While the rate in DOPC/PE = 1:1 was drastically reduced, essentially no synthesis was observed in pure DOPC liposomes. This is in stark contrast to results obtained earlier, when ATP synthesis is induced by DTT/Q_1. We therefore used the same liposomes as above and followed ATP synthesis also in the presence of DTT/Q_1. Indeed, the dependency pattern was inverted, with highest activities found in pure DOPC liposomes and reduced rates in liposomes containing negatively charged lipids (Figure 4.2.1D, green and black). The lipid dependency was somewhat less pronounced than published [1], but the overall trend was identical with a clearly reduced activity in liposomes containing the negatively charged lipids DOPG or CL.

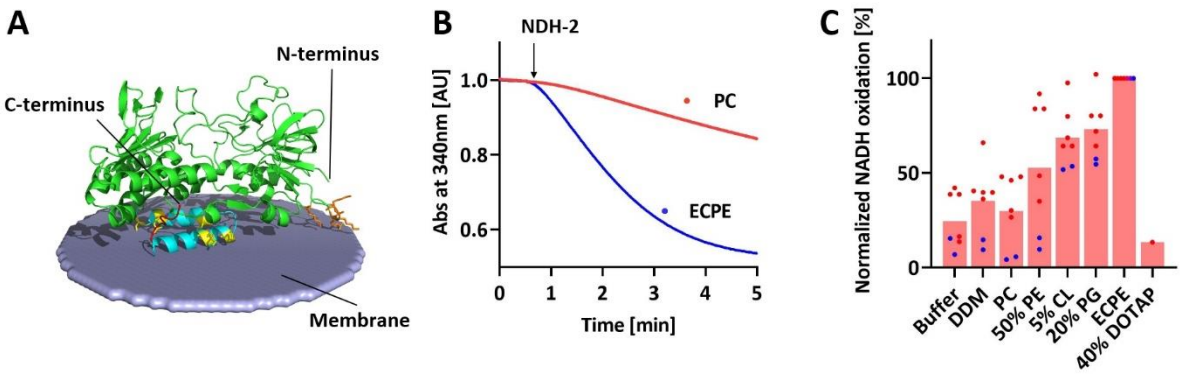

Figure 4.2.2 A) Homology model of *E. coli* peripheral membrane protein NDH-2. Positively charged amino acids in the C-terminal domain are colored yellow, and positively charged amino acids in the N-terminal domain are colored orange. The C-terminus is depicted in red. The membrane is indicated in purple. **B)** NADH:quinone oxidoreductase activity measurement of NDH-2. Absorption of NADH is monitored at 340 nm. After reaching a baseline of buffer (20 mM Hepes pH 7.4, 200 mM NaCl, 20 mM KCl) containing 100 µM NADH, 1 mg/ml liposomes and 100 µM Q_2, NADH oxidation is initiated by the addition of NDH-2. **C)** Lipid-dependent NDH-2 activity. NADH oxidation activity of NDH-2 was measured in presence or in absence (buffer or 0.05 % DDM) of different liposomes (1 mg/ml). The maximal slope was depicted as a bar plot. CL: cardiolipin; ECPE: *E. coli* polar extract. Blue dots represent measurements performed (by Martin Schori) with an NDH-2 batch provided by the lab of Martin Högbom (Stockholm) while red dots were measured with homemade NDH-2.

A straight-forward explanation of this observation is the requirement of negatively charged lipids for NDH-2 activity. It has been proposed that NDH-2 interacts via an amphipathic helix with the membrane surface, but its effect on activity has not been described to our knowledge. We therefore spectroscopically measured NADH oxidation activity of NDH-2 in presence of liposomes with different lipid compositions (Figure 4.2.2). Short chain ubiquinone Q_2 was used as electron acceptor and *bo*$_3$ was added to keep the quinone pool oxidized. As seen in Figure 4.2.2B, NADH oxidation is observed as a decrease in absorption at 340 nm that is proportional to NADH:ubiquinone Q_2 oxidoreductase activity of NDH-2. First, we titrated empty liposomes (up to 1 mg/ml) made from ECPE to a solution containing 3.3 nM NDH-2 and found a strong activation of NADH oxidation activity, which was saturated at >0.1 mg/ml liposomes (Figure S4.2.2A). Next, we measured the same activity in the presence of different liposomes (1 mg/ml) and our results show that NADH:ubiquinone oxidoreductase activity is indeed lipid-dependent (Figure 4.2.2C) with higher activity in presence of net negatively charged liposomes (ECPE, DOPG, CL) than in presence of uncharged DOPC or positively charged DOTAP liposomes, or in absence of any liposomes (buffer or DDM). We observed this effect for all purified NDH-2 batches, however, it was most prominent in one batch which was purified in the lab of Martin Högbom from the University of Stockholm (Figure 4.2.2C, blue dots). The differences might arise from different levels of co-purified

lipids. In the absence of quinone, only slow NADH oxidation is observed that can be attributed to NADH:O_2 oxidoreductase activity, i.e. formation of superoxide [238].

bo_3 oxidase orientation

Although the effect of negatively charged liposomes was less drastic than initially described (see discussion for possible explanations), the negative impact was highly reproducible. This is surprising, as natural membranes are negatively charged and cardiolipin has even been proposed to be crucial for oxidative phosphorylation [235]. In a second part of this work, we therefore committed ourselves to resolve the observed lipid dependency of DTT/Q_1 induced ATP synthesis activity. A possible explanation that could not be investigated in the previous work was a lipid-dependent orientation of the *pmf*-generating *bo_3* oxidase. As both populations are activated by membrane-embedded quinone, already a slight shift in the orientation distribution could have a pronounced effect on *pmf* size and thus ATP synthesis rate. With the method established in our lab and described in Chapter 4.1, we investigated *bo_3* oxidase orientation in liposomes of different lipid composition. Briefly, a single cysteine introduced either at position D578 on subunit I, position A21 on subunit III (*N*-side of protein; Figure 4.2.3A), or

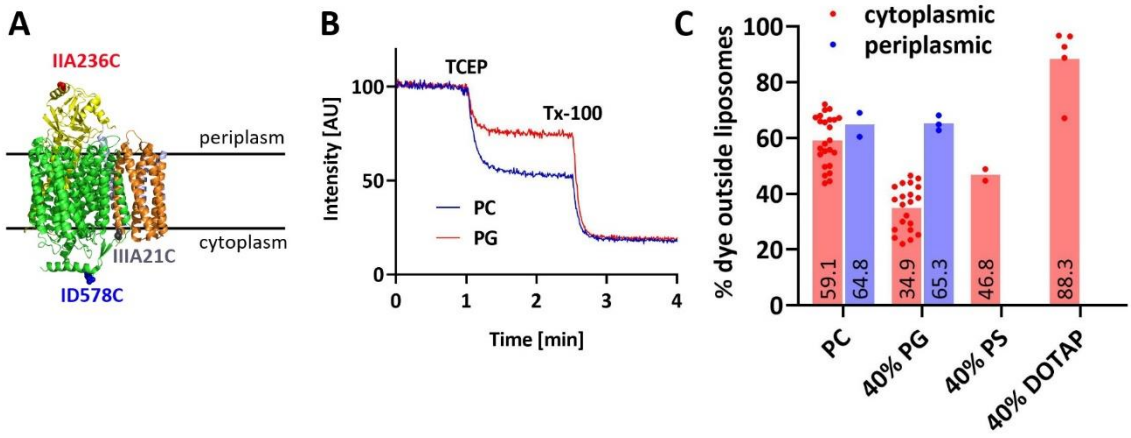

Figure 4.2.3 A) Structure of *bo_3* oxidase. Single-cysteine mutants used for orientation determination are depicted in spheres. Cysteines were located either at periplasmic side (IIA236C) or at cytoplasmic side (ID578C or IIIA21C). **B)** TCEP-based orientation determination of *bo_3* oxidase. Site-specifically DY647P1-labeled *bo_3* oxidase mutants are reconstituted in liposomes. To determine the orientation, fluorescence was monitored and fluorophores located on the outside of liposomes are quenched in a first step by 14 mM TCEP. Full quench was achieved in a second step after adding 0.05 % Triton X-100. To calculate the orientation, the first quench was set in relation to the full quench (see also Chapter 4.1). Liposomes were composed of either only PC or 6:4 PC:PG. **C)** *bo_3* oxidase orientation in different liposomes. *bo_3* oxidase was reconstituted in liposomes (10 mg/ml) partially solubilized by 0.4 % sodium cholate. After removal of sodium cholate by gel filtration, liposomes were pelleted by ultracentrifugation and orientation was determined via TCEP-based assay. Liposomes were composed of pure PC, or of 60 % PC and either 40 % PG, 40 % PS or 40 % DOTAP.

position A236 on subunit II (*P*-side of protein) in an otherwise cysless bo_3 oxidase was labeled with fluorophore DY647P1 via maleimide chemistry. Labeling specificity was controlled via SDS-PAGE and fluorescence detection (Figure S4.2.4). The three labeled enzymes were then reconstituted individually into liposomes, where the label is present either inside or outside the liposome, depending on the orientation of the enzyme. For orientation determination, the fluorescence of DY647P1 was monitored and DY647P1 present on the outside of liposomes was rapidly quenched by membrane-impermeable TCEP (Figure 4.2.3B). After reaching a plateau, full quench was induced by solubilization of liposomes with Triton X-100, rendering also dyes initially present on the inside of liposomes accessible to TCEP quench. We could determine the fraction of dye present on the outside of liposomes by setting the first quench in relation to the full quench. A representative raw trace is shown in Figure 4.2.3B for an experiment with ID578C-labeled bo_3 oxidase reconstituted in pure PC or 6:4 PC:DOPG liposomes, indicating a pronounced difference in orientation. In detail, we measured either the fraction of inside-out (with ID578C or IIIA21C) or right-way out (with IIA236C) oriented bo_3 oxidase, respectively, where inside-out is the desired orientation for coupled ATP synthesis. The results of all measurements are summarized in Figure 4.2.3C, every point indicating a separate reconstitution experiment. While the orientation of bo_3 oxidase in pure PC liposomes is around 60 % inside-out, only 35 % inside-out orientation is found in liposomes containing 40 % DOPG lipids. The effect of negatively charged lipids was corroborated in liposomes containing other negatively charged lipids (47 % in PC/PS (3:2) liposomes, Figure 4.2.3C; 42 % and 38 % in PC/CL (9:1) and PC/CL (4:1) liposomes, respectively, (n=1)). Impressively, we could revert

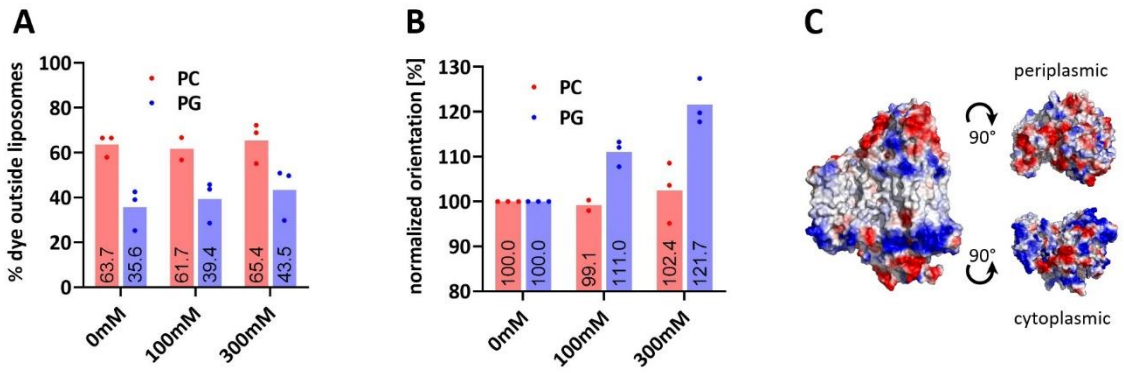

Figure 4.2.4 A) and **B)** Orientation of bo_3 oxidase after reconstitution in presence or in absence of salt. DY647P1-labeled bo_3 oxidase-IIIA21C was reconstituted in absence or in presence of 100 mM/300 mM NaCl either in pure PC liposomes (PC) or in 4:6 PG/PC (PG). Orientation was determined via TCEP-based assay and depicted in bar plots either as fraction of inside-out orientation (**A**) or normalized to the orientation in absence of salt (**B**). **B)** Surface charge distribution of bo_3 oxidase with side view (left) and top and bottom view (right), respectively. Positively charged and negatively charged areas are colored in blue and red, respectively. (Drawn with PyMOL with PDB 6WTI)

the effect using positively charged (non-natural) lipids (PC:DOTAP=3:2) that yielded proteoliposomes with 88 % bo_3 enzymes in the inside-out orientation (Figure 4.2.3C).

These data strongly point towards an important role of electrostatic interactions during the reconstitution of bo_3 oxidase into liposomes. We reasoned that high amount of salt concentrations might weaken this interactions and influence the orientation distribution. We thus reconstituted bo_3 oxidase in presence of salt (100 mM and 300 mM NaCl) and determined the orientation. As depicted in Figure 4.2.4, an increased fraction of inside-out orientation in negatively charged liposomes (DOPG) was indeed observed in the presence of increasing amounts of NaCl, while no salt effect was observed in zwitterionic PC liposomes. An electrostatic effect on orientation can be rationalized based on the surface charge distribution in the bo_3 oxidase structure. As depicted in Figure 4.2.4C, the cytoplasmic facing surface is more positively charged than the periplasmic facing side. An electrostatic interaction between the cytoplasmic surface and the negatively charged liposome surface might guide bo_3 oxidase to enter with that side of the protein into the partially solubilized liposome first, leading to a preferentially right-side out orientation as observed in our experiments.

Next, we repeated the orientation measurements in the presence of ATP synthase that has been shown to preferentially orient in the inside-out orientation with its large F_1 moiety on the outside of the liposomes [123]. Although no direct interaction between bo_3 oxidase and ATP synthase has been described, we wondered if the presence of preferentially inside-out reconstituted ATP synthase might affect the

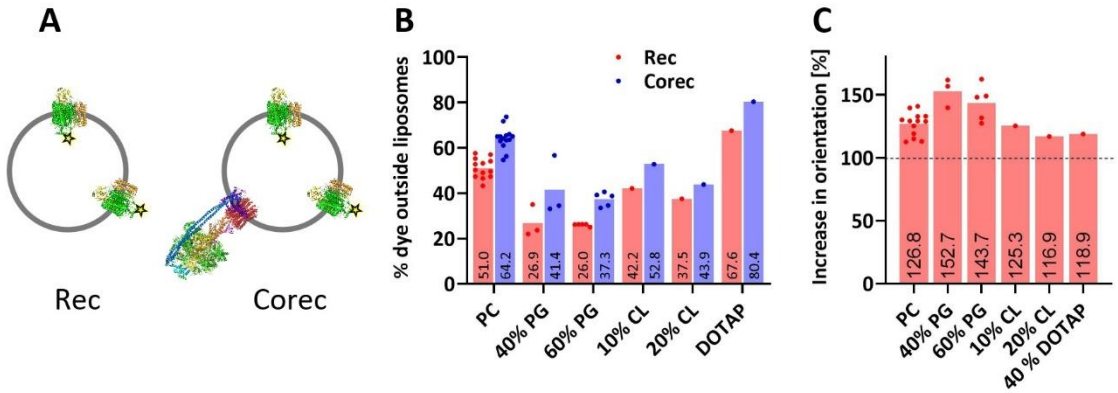

Figure 4.2.5 A) Schematic representation of reconstituted and coreconstituted enzymes. bo_3 oxidase from *E. coli* was labeled with DY647P1 at the cytoplasmic side of the enzyme and either reconstituted into liposomes of different lipid composition (Rec) or coreconstituted into the same liposomes together with the ATP synthase from *E. coli*. The orientation of bo_3 oxidase was then determined with the TCEP-based orientation determination assay. **B)** and **C)** Orientation of bo_3 oxidase in liposomes composed of PC with varying amounts of negatively charged (PG, CL) or positively charged (DOTAP) lipids. Orientation is depicted as fraction of inside-out orientation (**B**) or as relative increase in orientation (inside-out) when bo_3 oxidase was coreconstituted with ATP synthase compared to when it was reconstituted alone ($\left(\frac{\text{Orientation (corec)}}{\text{Orientation (rec)}} * 100\right)$ (**C**).

orientation of *bo₃* oxidase. As depicted in Figure 4.2.5, we indeed observed that the fraction of inside-out orientation of *bo₃* oxidase was significantly increased if *bo₃* oxidase was coreconstituted with the ATP synthase from *E. coli* compared to when it was reconstituted alone. The same effect was observed for all lipid mixtures that we tested (pure PC, 40 % PG, 10/20 % CL, 40 % DOTAP), but was most prominent in liposomes containing PG lipids.

Towards uniform bo₃ orientation during reconstitution

The data presented above clearly show that the lipid composition affects the orientation of *bo*$_3$ oxidase during reconstitution. The findings show that when liposomes carry a net negative charge less *bo*$_3$ oxidase molecules are oriented in the inside-out orientation, which is required for acidification of the liposomal lumen and thus ATP synthesis, and are in line with the observations made earlier [1]. Obviously, these findings complicate the understanding of how lipids influence the proton transfer between *bo*$_3$ oxidase and ATP synthase. In the following, we show our efforts to suppress this unwanted side-effect by a maximizing uniform orientation of *bo*$_3$ oxidase in the inside-out topology. The basic idea of the approach is based on the reconstitution method developed by Rigaud and Levy [87]. Preformed liposomes are only partially solubilized with sodium cholate, i.e. they are not losing their spherical shape, before detergent-solubilized protein is added that forms a ternary complex with the mixed lipid-detergent micelles. Subsequent removal of detergent by gel filtration, dialysis or polystyrene beads renders proteoliposomes. Using this method, a general trend can be observed that membrane proteins with a large soluble domain enter the membrane preferentially with this domain on the outside of the liposomes. Reports of such proteins, e.g. ATP synthase, complex I, membrane transhydrogenase, show uniform orientations >75 % [121,123,239]. We have recently successfully oriented the small membrane protein proteorhodopsin (~25 kDa) by coupling a large soluble protein (~60 kDa) to either the N- or the C-terminus that are located on opposite sides of the protein. Coupling was achieved by *in vitro* coupling using SpyTag/SpyCatcher technology [197,199]. Technically, the 13 amino acid SpyTag was either fused to the N- or the C-terminus of proteorhodopsin. The soluble domain, maltose binding protein fused to SpyCatcher, was expressed and purified separately. The two proteins were then mixed in order to allow coupling and the coupled product purified via gel filtration. With this approach, we showed that depending on the site of coupling, light-driven proton transport occurred in opposite direction, supporting a guided orientation ([240], manuscript in preparation). Here, we used the same strategy with the *bo*$_3$ oxidase by coupling an even larger soluble domain (2x MBP (MBPx) + SpyCatcher003 = 95 kDa) to the cytoplasmic side of the protein that should orient the protein in its inside-out orientation. First attempts with SpyTag fused to the C-terminus of subunit I (the only C-terminus on the cytoplasmic side) showed poor coupling efficiency and we therefore employed a purified single-cysteine mutant of *bo₃* oxidase (ID578C), which was labeled with a SpyTag003 peptide, equipped with an N-terminal maleimide (Figure

4.2.6A). In parallel, MBPx-SpyCatcher003 fusion protein was expressed and purified, and then coupled with *bo*$_3$-SpyTag003 by incubation. If maleimide labeling was incomplete, SpyTag003 labeled of *bo*$_3$ oxidase was purified using Spy&Go purification [202], before it was mixed with MBPx-SpyCatcher003 for coupling. Coupling efficiency was then ~90 % according to SDS-PAGE analysis (Figure 4.2.6B). The purified coupling product *bo*$_3$-MBPx was then coreconstituted with ATP synthase in pure PC liposomes as well as in liposomes containing 40 % DOPG. As a control, we coreconstituted the uncoupled single-cysteine *bo*$_3$ oxidase-SpyTag003 variant with ATP synthase. The four liposome preparations were then subjected to DTT/Q_1 driven ATP synthesis experiments and ATP synthesis was followed by the luciferase system. The results depicted in Figure 4.2.6C show that >2 x higher ATP synthesis rates were observed

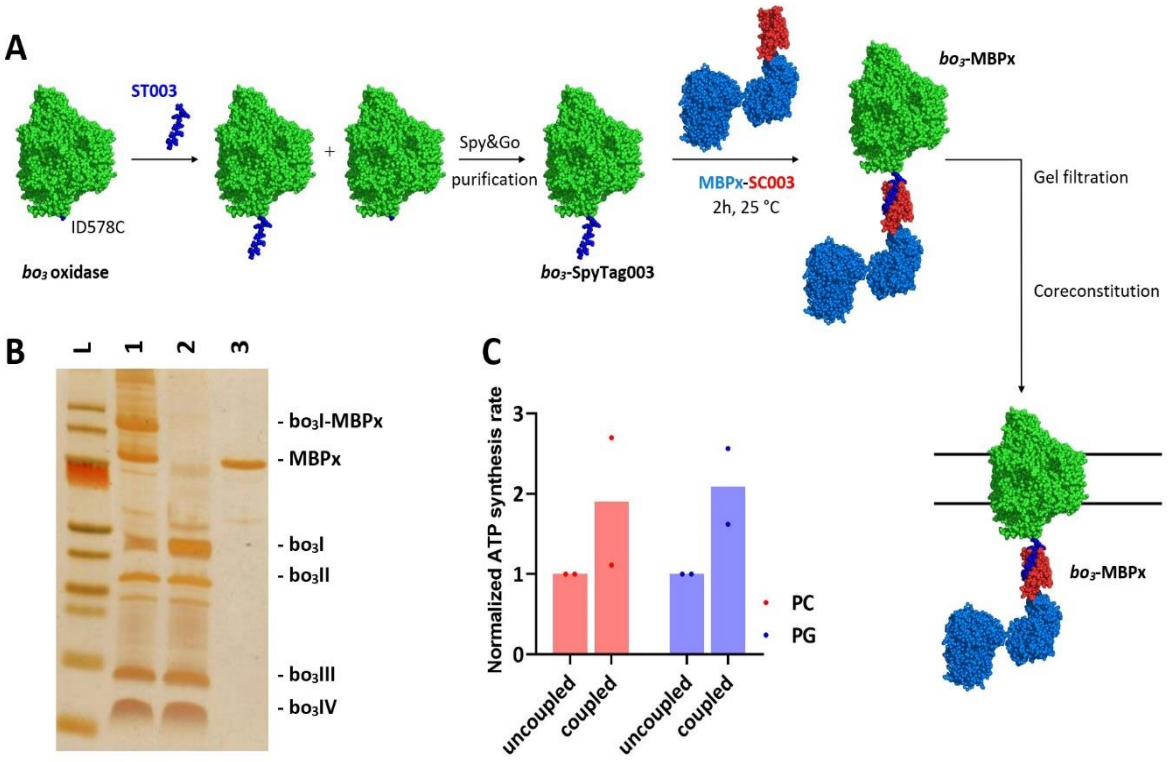

Figure 4.2.6 A) Coupling of *bo*$_3$ oxidase with MBPx via SpyTag003/SpyCatcher003. Single-cysteine mutant *bo*$_3$-ID578C was labeled with SpyTag003 peptide via maleimide chemistry. Unlabeled *bo*$_3$ oxidase was then removed in a Spy&Go purification step using SpyDock coupled to SulfoLink® Coupling Resin (ThermoFisher) before *bo*$_3$-SpyTag003 was coupled with MBPx-SC003 by incubation for 3 h at 25 °C, 1200 rpm. *bo*$_3$-MBPx was then purified via gel filtration and coreconstituted with ATP synthase for coupled ATP synthesis activity measurements. **B)** Silver-stained SDS-PAGE (9 %) of *bo*$_3$-MBPx coupling. With 1: *bo*$_3$-MBPx; 2: *bo*$_3$-ID578C-SpyTag003; 3: MBPx-SpyCatcher003; L: PageRuler™ Prestained Protein Ladder, 10 to 180 kDa (Thermo Scientific). **C)** Coupled ATP synthesis activity with *bo*$_3$ and *bo*$_3$-MBPx. ATP synthase was coreconstituted with either *bo*$_3$-SpyTag003 (uncoupled) or with *bo*$_3$-MBPx (coupled) and coupled ATP synthesis activity was measured via luminescence. Therefore, the reaction was initiated with 4 mM DTT and 100 µM Q_2. ATP synthesis rates were normalized to rates obtained with uncoupled *bo*$_3$-SpyTag003. Activity was measured in pure PC liposomes or in PC liposomes containing 40 % PG.

in experiments with *bo₃*-MBPx compared to uncoupled *bo₃* in both PC liposomes and PG-containing liposomes, indicating that the relative amount of inside-out orientation was increased in both preparations. The threefold difference between ATP synthesis rates between PC and PG containing lipids observed with the uncoupled *bo₃* oxidase, however, remained unchanged in the preparations with *bo₃*-MBPx protein. Same amounts of the two *bo₃* oxidase preparations (coupled and uncoupled) were used in reconstitution experiments and their oxygen consumption rates were identical (130±10 e^-/s/*bo₃*).

4.2.5 Discussion

Mimetic respiratory chain systems are important building blocks for the bottom-up construction of artificial cells. A few years ago, our group developed a robust system, in which the *E. coli* enzymes *bo₃* oxidase and ATP synthase are coreconstituted, enabling steady-state ATP synthesis by addition of DTT as electron source. Nilsson et al [1] found that the rate of ATP synthesis depends strongly on the lipid composition of the liposomes. Here, we found the same trend (maximal rate observed in pure PC lipids and up to 50 % decreased coupled ATP synthesis activity in presence of negatively charged lipids) although less pronounced than in [1] (up to 90 % decreased ATP synthesis activity). Since we did the overall same procedure using similar protocols, the difference in effect is not fully clear. First, the ATP synthase was purified in a buffer with a complex composition, called Magic buffer, that was originally described by Ishmukhametov et al. [232]. One component of Magic buffer is crude soy bean lipids that has been suggested to stabilize extracted ATP synthase. These lipids, however, also might influence the lipid-dependent changes in coupled ATP synthesis activity by contributing to the overall lipid composition. The lipid concentration in Magic buffer was 8 mg/ml, thus contributing up to 20 % to the total lipid composition during reconstitution. However, when we decreased the lipid content in Magic buffer to 3 mg/ml, we could not see differences in lipid effects. Since the overall purification procedure of both *bo₃* oxidase and ATP synthase were the same as in [1], with only minor changes, we exclude the purification of the enzymes being responsible for the weaker lipid effect observed in our lab.

A further reason for a changed lipid effect could be based on differences in the reconstitution procedure, e.g. when more detergent is used leading to more complete solubilization of liposomes during reconstitution, which has been shown to influence membrane protein orientation [214,241]. However, our protocols applied were identical to [1] (with 0.4 % cholate, 5 enzymes each per liposome, 10 mg/ml liposomes). Finally, the purity or the quality of the lipids used might influence the effect. While Nilsson et al. [1] used Avanti lipids, we have used lipids from different companies (Avanti, Lipoid), but could not detect differences between the different preparations, and we are thus unable to currently understand the observed differences in lipid effect.

Mimicking respiratory system with complex II or NDH-2

The use of DTT and water-soluble quinone Q_1 enables *in vitro* steady-state ATP synthesis by coreconstituted *bo₃* oxidase and ATP synthase. This electron donor/mediator pair, however, reflects not the physiological substrates. *E. coli* rather uses membrane-soluble ubiquinone Q_8 that is reduced by different dehydrogenases [38]. We therefore improved the minimal respiratory system of coreconstituted *bo₃* oxidase and ATP synthase by using membrane-soluble Q_8 and two different *E. coli* quinone-reducing enzymes (FRD or NDH-2), resulting in a complete aerobic respiratory chain from *E. coli*, composed of three enzymes.

In a first approach, we were able to successfully coreconstitute three enzymes (FRD, *bo₃* oxidase, ATP synthase) in one reconstitution step into liposomes containing Q_8, and to initiate ATP synthesis by adding succinate to those proteoliposomes that was blocked after addition of FRD inhibitor malonate. In a second approach, FRD was replaced by NDH-2, which under aerobic conditions is the major NADH dehydrogenase expressed in *E. coli* [38]. NDH-2 is a peripheral membrane protein and can be added directly to proteoliposomes containing *bo₃* oxidase, ATP synthase and Q_8, and in the presence of NADH initiated steady-state ATP synthesis. The apparent K_M values for succinate, Q_8 and NADH were titrated and found comparable with literature values [192,242,243] (Figure S4.2.1), indicating that the synthetic respiratory systems reflects the physiological situation well.

The NDH-2 system yielded higher ATP synthesis rates, comparable to the ones found with DDT/Q_1 and we therefore compared the lipid dependency profile of these two systems, as the initial experiments were done in *E. coli* polar lipid extract. Interestingly, essentially no ATP was synthesized in net uncharged liposomes, if NADH/NDH-2 was used as an electron source, while increasing ATP synthesis rates were observed in liposomes containing increasing amounts of negatively charged lipids. Since in both systems, *bo₃* oxidase is the only proton pump and the basic concept is equal, the difference indicates either lipid-dependent changes in Q_8 diffusion rates or lipid-dependent NDH-2 activity. It was shown by [1] that Q_1 diffusion, binding to *bo₃* oxidase and electron transfer was lipid-independent. However, this has not been reported for Q_8 so far. A decreased Q_8 diffusion rate in uncharged compared to in negatively charged liposomes would slow down electron transfer from NDH-2 to *bo₃* oxidase leading to a decreased *pmf* that could explain our findings. However, this has to be tested. Alternatively, the lipid effect rises from altered quinone reduction through NDH-2. We thus further investigated the influence of the lipid composition on NADH:quinone oxidoreductase activity of NDH-2 (Figure 4.2.2C), using water-soluble Q_2 (that behaves similarly to Q_1) as a substrate. We found that the lipid dependency of NADH:Q_2 oxidoreductase activity was indeed very similar to the one observed for ATP synthesis activity, with higher activity in presence of anionic compared to uncharged or cationic liposomes. The highest activity was observed in presence of negatively charged ECPE liposomes, which is an extract of polar

lipids from *E. coli* and therefore mimics the physiological environment of NDH-2. ECPE liposome titration to the assay revealed that only small amounts of liposomes already largely increased NADH oxidation activity of NDH-2 (Figure S4.2.2A). We also titrated Q_2 to NDH-2 in NADH:Q_2 oxidoreductase measurements and observed a ~30 fold higher K_m when the reaction happened in presence of ECPE liposomes than in buffer, while v_{max} was 5 fold increased (Figure S4.2.2B). These results together indicate that NDH-2 activity is increased if bound to liposomes and only poorly active in solution. The increased K_m of Q_2 in the presence of liposomes suggests the two following aspects: First, the quinone binding site of NDH-2 is in close contact with the membrane part (likely embedded) that requires that Q_2 can predominantly reach it via the membrane, but not via the aqueous solution. Second, the increased K_m value might be explained by the ubiquinone's property to form micelles at low concentrations (14 µM [244]) thus stabilizing the aqueous form and delaying the entry of Q_2 into the liposomes. The effect should be less drastic with Q_1 that has a much higher CMC than Q_2, but this was not yet tested.

While the lipid-dependent effect is similar in both NDH-2 activity and *bo*$_3$ oxidase/ATP synthase activity, it is more pronounced in the latter. In coupled ATP synthesis, we could not detect activity in DOPC liposomes, while a substantial amount of NADH oxidation activity was observed with the same liposomes. A likely reason for this difference is the different quinones used. The very hydrophobic Q_8 is present only in the lipid bilayer, while the more hydrophilic Q_2 is found both in solution and in the lipid bilayer. Thus, NDH-2 could be activated also in a non-membrane bound state in presence of Q_2, but it is only reducing Q_8 and inducing ATP synthesis when it is bound to *bo*$_3$ oxidase/ATP synthase-containing liposomes. Despite this promiscuous activity in the absence of a membrane, the data support that membrane binding itself stimulates NADH:ubiquonone oxidoreductase activity and that this binding and increase in activity is strongly enhanced if the membrane carries a net negative charge.

NDH-2 binding to the membrane is proposed to happen via the C-terminal amphipathic helix which was shown to be essential for membrane-localization and its deletion resulted in water-soluble NDH-2 [41,44,46]. This alpha-helical domain, consists both of positively charged and hydrophobic residues, but lacks negatively charged amino acids, yielding a net positive charge. Since positively charged amphipathic domains are known to mediate binding to anionic membranes [54], the cationic amino acids in the C-terminal domain of NDH-2 could be responsible for NDH-2 membrane binding. It could be hypothesized that NDH-2 is localized at the membrane through electrostatic interactions between positively charged amino acids and negatively charged lipid head groups and that membrane-binding is supported by hydrophobic interactions between hydrophobic amino acids of the C-terminal domain and fatty acids of lipids. We wanted to experimentally verify this hypothesis and designed mutants with altered C-terminal domains. Since no structure is available for NDH-2 from *E. coli*, a 3D homology model (Figure 4.2.2A) based on the structure of NDH-2 from *Caldalkalibacillus thermarum* (which has a sequence

identity with *E. coli* NDH-2 of 23 % and also a net positively charged C-terminal domain; PDB 6BDO) was built. In a first mutant, we replaced the C-terminal positively charged amino acids with glutamine (R391Q, R394Q, R402Q, H409Q and K413Q; mutant "charges to Q"). The same mutations were present in the second mutant "charges to Q truncated" which had an additional deletion of the 10 C-terminal amino acids. Finally, in mutant "N-term charges to A" a number of positively charged amino acids at the N-terminus of NDH-2, which were suggested to support NDH-2 localization at the membrane [54], were replaced by alanine (K27A, RKK(30-32)AAA). The mutants were expressed in *E. coli* cells and membranes were prepared and collected by ultracentrifugation. Pellet and supernatant were analyzed by Western Blot (anti His-tag) to track localization of the mutant protein (Figure S4.2.3). Interestingly, only the wildtype NDH-2 was found mainly in the membrane fraction, while all three mutants were in the cytosolic fraction, indicating that they were no longer able to bind to the membrane. This is an indication that positively charged amino acids both at the N- and C-terminus are essential for membrane localization of NDH-2. Unfortunately, we were unable to purify the mutants in sufficient quantity and purity to repeat the lipid dependency experiments as described for the wildtype (NADH:quinone oxidoreductase and NDH-2 induced ATP synthesis activity). Further purification trials thus will be required in future.

The orientation of bo_3 oxidase and ATP synthase

The original observation by Nilsson et al. [1] that negatively charged lipids decrease respiratory coupled ATP synthesis in liposomes was strongly counter-intuitive. The lipid composition of *E. coli* consists of roughly 75 % PE, 20 % PG and 5 % cardiolipin [15]. Thus, highest coupled activity was expected in negatively charged rather than in uncharged liposomes, as the former mimic the natural environment of the enzymes much better. The question thus arises if the effect has rather an unnatural source created during our *in vitro* measurements. Nilsson et al. [1] could exclude a number of trivial lipid-dependent effects such as lipid-dependent overall enzyme activity, quinol diffusion or proton leaks. As a matter of fact, ATP synthesis activity driven by a synthetic *pmf* was higher in the presence of negatively charged lipids. They also argued that the lipid dependency is unlikely due to changes in the orientation of the two enzymes, without experimentally determining the orientation, though. From single enzyme measurements, the orientation of bo_3 oxidase in liposomes has been estimated earlier to be around 70 % right-side out (measured in liposomes of ECPE [115,116] and soybean lipid extracts [115]), but no data from other lipid compositions exist. We therefore developed the method described in Chapter 4.1 and used it to determine the orientation of bo_3 oxidase in liposomes with different lipid compositions (Figure 4.2.3C). While we could confirm an inside-out orientation of bo_3 oxidase of around 35-45 % in liposomes containing negatively charged lipids DOPG, CL and DOPS (which is in good agreement with the above-mentioned literature values of 70 % right-side out), the fraction of inside-out oriented bo_3 oxidase was

significantly increased to 50-60 % in uncharged PC liposomes and even higher in liposomes containing positively charged DOTAP lipids. Insertion of purified membrane proteins into liposomes is a complex process and the interaction of the protein with the lipid bilayer prior to insertion is expected to be a critical step [225]. Thus, our data strongly indicate an electrostatic interaction between the protein and the membrane that influences the process. This hypothesis is supported by the surface charge distribution of bo_3 oxidase (Figure 4.2.4C) showing an overall positively charged and negatively charged surface at its cytoplasmic and periplasmic side of the membrane, respectively. During reconstitution of *bo₃* oxidase into negatively charged liposomes, the positively charged cytoplasmic part of *bo₃* oxidase is supposed to be attracted by the negatively charged lipid bilayer via electrostatic interactions more frequently than the negatively charged periplasmic part, increasing its chance to be inserted into the membrane and resulting in a higher fraction of *bo₃* oxidase in a right-side out orientation (and thus a lower fraction of inside-out orientation). In our experiments with increasing salt concentrations, these electrostatic interactions were weakened, leading to an increased fraction of inside-out oriented *bo₃* oxidase in PG liposomes, while salt did not have an effect on the orientation in PC liposomes (Figure 4.2.4A and B). Charge-mediated insertion into liposomes had also been reported for other enzymes in the past [225,245,246] and seems to be a general phenomenon.

Interestingly, preliminary experiments show also an effect of the presence of ATP synthase on bo_3 oxidase orientation during reconstitution. We found that the presence of ATP synthase, which is expected to be mainly inside-out (see also Chapter 4.1), increases the fraction of inside-out oriented bo_3 oxidase in both PC and PG-containing liposomes, but stronger in the latter. We want to emphasize that the data is preliminary and incomplete, but all performed experiments so far support the initial observation.

Effect of bo₃ oxidase orientation on coupled ATP synthesis activity

Orientation of a membrane protein reconstituted in liposomes directly affects its functionality if the substrate is not membrane permeable and only one population is activated. In case of the ATP synthase, the membrane-impermeable substrates ADP and phosphate only activate the inside-out population of ATP synthase with its catalytically active F_1 part located on the outside of liposomes. Thus, the right-side out oriented ATP synthase population remains silent in functional experiments, but of course affects the number of functionally active enzymes. On the other hand, the membrane-soluble quinol acting as a substrate for bo_3 oxidase activates both orientation populations [115,192]. As mentioned above, bo_3 oxidase reduces molecular oxygen to water which is coupled to proton pumping from the *N*-side to the *P*-side of the membrane and generating a directed *pmf*. In liposomes with mixed orientations, the activities of the two populations thus compete with each other and the final *pmf* is the sum of both activities. The presence of "wrongly" oriented right-side out *bo₃* oxidases are therefore a more complex problem than right-side out oriented ATP synthases.

Ideally for our purposes of respiratory ATP synthesis, liposomes contain unidirectionally inside-out oriented *bo*$_3$ oxidase and ATP synthase, where *bo*$_3$ oxidase pumps protons into liposomes that are exported by the ATP synthase during ATP synthesis, allowing an endless proton cycle. Thus, each *bo*$_3$ oxidase being present in a right-side out orientation leads to a decrease in coupled ATP synthesis activity. If the "natural" orientation of *bo*$_3$ oxidase in liposomes is close to 50:50, already slightly increased fractions of right-side out oriented *bo*$_3$ oxidase results in a substantial decrease in *pmf* and finally in coupled ATP synthesis rate. The higher right-side out orientation of *bo*$_3$ oxidase measured in PG-containing (~65% right-side out) compared to pure PC liposomes (~50 % right-side out) is thus a very relevant finding in explaining the decreased coupled ATP synthesis activity observed in those liposomes [1].

In PC liposomes, we have determined that the majority of *bo*$_3$ oxidases pumps to the inside (~65%), enabling ATP synthesis. However, this is not the case in PG-containing liposomes, where the majority of *bo*$_3$ oxidase is present in a right-side out orientation, yielding a net outside pumping of protons. Nevertheless, ATP synthesis, although decreased, is also observed in these vesicles. How is that even possible if net proton transport is to the outside? We will discuss this problem with the example of liposomes containing 40 % PG, however, it is also valid for other negatively charged liposomes.

I) An unexpected, but potentially important finding was the significantly increased fraction of inside-out oriented *bo*$_3$ oxidase if coreconstituted with ATP synthase. The reason for this finding is unknown so far but deserves further investigation. We hypothesize that the increased *bo*$_3$ oxidase orientation is either due to interactions between *bo*$_3$ oxidase and ATP synthase during reconstitution where the high inside-out orientation of the large ATP synthase forces the small *bo*$_3$ oxidase in the same orientation, or that reconstituted ATP synthase locally changes the environment in the lipid bilayer guiding the *bo*$_3$ oxidase to insert in the inside-out orientation. The mitochondrial ATP synthase dimer has been shown to bend the lipid bilayer by 90 ° inducing cristae formation in mitochondria, while also the ATP synthase monomer bends the membrane (45 °) [247–249]. If a similar bending property is assumed for the *E. coli* ATP synthase, its presence in the membrane could influence *bo*$_3$ oxidase insertion. Such an interplay is not unlikely, as respiratory membranes (IMM or cytoplasmic membranes of bacteria) are extremely packed with proteins (up to 3:1 protein/lipid (w/w)) and a correct relative orientation of the two enzymes is likely energetically favorable. In PG liposomes, inside-out orientation of *bo*$_3$ oxidase up to 45-55 % were measured when reconstituted with ATP synthase, making ATP synthesis much more likely.

II) The number of enzymes and their distribution in liposomes has also to be considered. Typically, a theoretical number of 5 *bo*$_3$ oxidase and 5 ATP synthase per liposome was used, which means that with a *bo*$_3$ oxidase orientation of 40 % inside-out and a constant number of liposomes, the net pumping direction would be outwards (3 pump out, 2 pump in) and thus no ATP could be produced by ATP syn-

thase. However, proteins are not homogeneously distributed into liposomes, but rather follow a Poisson distribution [250]. The non-unidirectional orientation of the enzymes and the fact that both bo_3 oxidase orientations are active and pump competitively in or out of the liposomes, respectively, enhances the complexity. In a simplified model, we calculated the fraction of vesicles able to generate an inside-positive *pmf* (which is needed for ATP synthesis), as well as the amount of protons per liposome that are net inwards pumped per second into this fraction of liposomes assuming a theoretical number of 100 protons pumped per bo_3 oxidase per second (see Supplementary for calculations). Orientation of ATP synthase was neglected. According to our calculations, assuming a 40 % inside-out bo_3 oxidase orientation, indeed ~25 % of liposomes exhibit net inwards pumping (liposomes with more bo_3 oxidases inside-out than right-side out) with an average net inwards pumping of ~45 protons per liposome in this fraction (where 500 protons per liposome is the theoretical maximum in case of unidirectional inside-out orientation of bo_3 oxidase). This indicates that although less than 50 % of bo_3 oxidase is oriented in the desired orientation, still a relatively high fraction of liposomes is theoretically able to synthesize ATP.

III) Generally and especially in textbooks, it is assumed that proton transfer from bo_3 oxidase to the ATP synthase occurs via bulk solution. However, a long standing hypothesis has been postulated already in the 1960 that protons might be transferred via lateral proton transfer in case the lateral enzyme distance is below a certain threshold [1,182–191]. In this scenario, proton equilibration with the bulk solution is kinetically delayed and protons instead are transferred along the membrane surface, until they are picked up by an ATP synthase or released from the membrane to the bulk. This hypothesis is also important in the discussion how alkaliphilic bacteria are able to synthesize ATP under unfavorable energetic conditions of a large inverted ΔpH [251,252]. In our scenario, this hypothesis would kinetically uncouple the two different bo_3 populations and ATP synthesis is possible from the fraction of enzymes that pump to the inside, irrespective of the presence of a majority of outwards pumping enzymes in the same liposome.

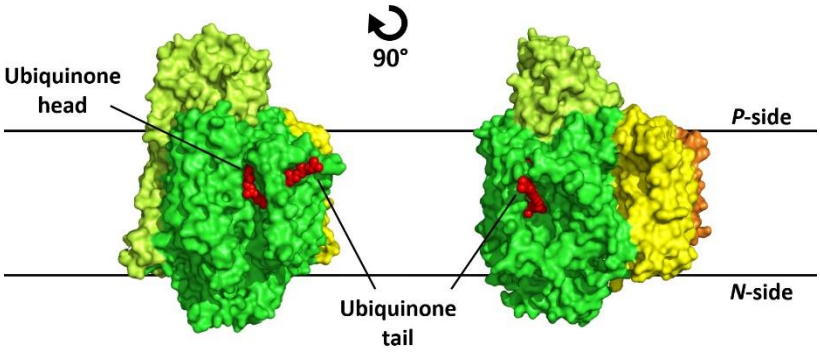

Figure 4.2.7 *E. coli bo₃* oxidase represented in surface with ubiquinone Q_8 (red) bound in a groove in subunit I (green). Structure was drawn with PyMOL (PDB 6WTI).

IV) Finally and rather trivial, it cannot be excluded that for unknown reasons, the inside-out oriented population of bo_3 oxidase is more active than the one of right-side out oriented. Such an asymmetric activity pattern would allow the generation of a net *pmf* that energizes ATP synthesis. A potential asymmetry might arise from the fact, that quinol is only formed on the outside of the liposome (as DTT is not membrane permeable and Q_1 thus has to travel in and out of the liposomes to the binding site). Very recent cryo-EM structures [62,217] show that the quinone binding site is located close to the *P*-side of the membrane (Figure 4.2.7) , rendering the binding sites of the outwards-pumping population closer to the reduced quinol pool in the environment. On the other hand, access to the binding site seems to occur via a groove formed by several transmembrane helices with an entry site close to the *N*-side of the membrane [217]. If entry of quinol into this access groove is limiting, the inwards-pumping population might be favored.

Although it is likely that the lipid effects observed by [1] are affected from the described differences in *bo₃* oxidase orientation (further discussed below), not all experiments can be explained by this means. First, we also measured the orientation of *bo₃* oxidase in liposomes containing 60 % PC and 40 % PE (both zwitterionic lipids) and observed a similar orientation as in pure PC liposomes in agreement with electrostatic interactions being important during reconstitution. However, *bo₃* oxidase orientation is thus not responsible for the 65 % decrease in coupled ATP synthesis activity in these liposomes measured by [1] and indicates other effects leading to the drop in activity, such as changes in lateral proton transfer rates as discussed in [1]. Second, without measuring it, Nilsson et al. assumed a constant *bo₃* oxidase orientation in different liposomes mainly due to the following observation. If the same number of proteins were reconstituted in 200 nm instead of 100 nm liposomes, the enzyme density was decreased 4-times which led to a markedly decreased overall ATP synthesis activity which was found to be independent of the lipid composition. They hypothesize that in 200 nm vesicles, the distance between *bo₃* oxidase and ATP synthase is now too large to allow direct lateral proton transfer between them and that protons rather exclusively are transferred via bulk solution. To support this hypothesis, they had to assume that enzyme orientation was neither affected by liposome size nor lipid composition. Our data, however, are in contrast to this assumption and *bo₃* oxidase orientation is indeed affected by lipid composition. In the following, we thus want to discuss several options for the lipid-independent coupled ATP synthesis activity observed [1] in 200 nm vesicles.

I) In the current project, we only measured the effect of lipids on *bo₃* oxidase orientation in 100 nm liposomes. It is possible that *bo₃* oxidase orientation is less lipid-dependent in 200 nm liposomes. An increase in liposome size leads to changes in membrane bending stress. As Huang et al showed [225], decreased membrane bending stress in larger liposomes results in impeded insertion of bacteriorhodopsin (bR) into liposomes. Although they could not observe significant changes in orientation of bR

when increasing liposome diameter from 50 nm to 100 nm liposomes, they stated that more experiments are required to elucidate effects of the membrane curvature on membrane protein orientation. Further, bR is a small single-subunit enzyme with only 7 transmembrane helices (TMHs) and might not be a good model enzyme to compare with the multi-subunit *bo₃* oxidase with its 23 TMHs [62] that is more likely to be affected.

II) It is possible that the reconstitution efficiency and relative distribution of enzymes is altered by the liposome size (as mentioned above [225]). If the change in reconstitution efficiency e.g. is more pronounced in PC than in PG liposomes (i.e. worse reconstitution in PC than in PG in larger liposomes), the benefit of PC liposomes due to increased inside-out orientation of *bo₃* oxidase might be canceled out.

However, Nilsson et al also show that if the number of proteins per vesicle is increased in 200 nm liposomes (up to 42 enzymes per 200 nm vesicle), the lipid dependency, although weaker was recovered. This recovery effect makes indeed a strong case for an important role of enzyme density and thus enzyme distance, as the two reasons discussed above (membrane curvature, reconstitution efficiency) should not influence these results. It thus seems that the observed lipid dependency in coupled ATP synthesis activity observed by [1] is a combined result of at least two effects.

Similarly to above (see also Supplementary), we have calculated the number of protons being pumped inside liposomes with a net inwards pumping (liposomes containing more inside-out than right-side out oriented *bo₃* oxidases) when the orientation of *bo₃* oxidase is 75 % (PC liposomes) and 53 % (PG liposomes), respectively, as an indication for the statistical possibility for ATP synthesis in these liposomes. While in average 262 protons/liposome are pumped into PC liposomes, 103 protons/liposome are pumped in liposomes containing 40 % PG. Thus, a 2.5 fold higher ATP production would be expected in PC than in PG liposomes. Although, as mentioned above, our calculations are highly simplified, they indicate a decrease in ATP synthesis rates in PG liposomes due to decreased *bo₃* oxidase orientation. However, it is much less than the 10 fold decrease in ATP synthesis activity observed by Nilsson et al., which indicates that enzyme orientation might not be the only influence but it is rather a combination of different effects.

In a follow-up study of [1] by the same authors, Sjöholm et al. provided further evidence for a functional link between lateral enzyme distance and coupled ATP synthesis activity [193]. They performed fluorescence correlation spectroscopy (FCS) and fluorescence cross-correlation spectroscopy (FCCS) experiments using fluorescently labeled *bo*₃ oxidase and ATP synthase and found no indication for a specific interaction between the two enzymes, when hydrophilic dyes were used. However, if hydrophobic dyes were used, an inadvertent cross-correlation was observed that was assigned to an unspecific hydrophobic interaction of the two dyes in the aqueous environment. Interestingly, liposomes with these

proteins showed a higher ATP synthesis activity than those with hydrophilic dyes, thus coupling lateral distance and ATP synthesis activity. Taken together, these and our data indicate that the lipid-dependent ATP synthesis rates observed are caused by a combination of effects, in which both lipid-dependent alterations of the lateral enzyme distance of *bo₃* oxidase and ATP synthase as well as *bo₃* oxidase (and maybe ATP synthase) orientation play an important role. A further effect could be a lipid-dependent change in the lateral proton transfer rate, as it has been observed for protonation kinetics of lipid-coupled fluorescein [253].

A better picture of the lipid effect on coupled ATP synthesis activity could be obtained if one or both observed factors (lateral enzyme distance or *bo₃* oxidase orientation) can be eliminated. Within this thesis, we therefore also intended to orient *bo₃* oxidase lipid-independently in liposomes (see below), and to fix the lateral distance between *bo₃* oxidase and ATP synthase by reversible coupling (see Chapter 4.3).

Actively influencing bo₃ oxidase orientation

As a paradigm for unidirectional and lipid-independent protein orientation, ATP synthase was chosen, which prior to the start of this work, was shown to orient >90 % in the inside-out orientation in liposomes made from soybean extract with a ~30 % negative charged. We later found that ATP synthase orientation also depends on the detergent concentration used (see Chapter 4.1), but values >75 % can be expected. The high inside-out oriented fraction is assumed to originate from the presence of the very large peripheral and water-soluble F_1 part of the ATP synthase that is unlikely to penetrate the liposomal membrane during reconstitution [214,241]. However, it is critical to mention that this rationale can only be applied to reconstitution techniques in which the liposomes are not fully solubilized as described by Levy and Rigaud [87]. We therefore envisaged to guide inside-out orientation of *bo₃* oxidase in a similar fashion by attaching a large soluble unit to the cytosolic part of the enzyme which similarly to the F_1 part of the ATP synthase should not cross the lipid bilayer. In our lab, we have successfully developed the system for the smaller light-driven proton pump proteorhodopsin. Using the SpyTag/SpyCatcher system, we coupled a highly water-soluble protein consisting of two copies of the maltose binding protein (MBPx) and a SpyCatcher protein (~95 kDa in total) to *bo₃* oxidase (see Figure 4.2.6A) and coreconstituted the coupling product into liposomes together with ATP synthase. Preliminary measurements indicate a twofold increase in ATP synthesis activity if the coupled *bo₃*-MBPx was coreconstituted with ATP synthase compared to the uncoupled *bo₃* oxidase. The *bo₃* oxidase constructs were also assayed for oxygen consumption activities but no difference was observed between the uncoupled and MBPx-coupled *bo₃* oxidase. The ATP synthesis rate was increased in both PC and PG liposomes and the difference between the two samples remained (3 times higher activity in PC than PG-containing liposomes). Unfortunately, no orientation measurements were done so far because of time

reasons. Efficient coupling of *bo₃* to MBPx was a difficult process. As we were unable to find a good localization for a SpyTag with the primary sequence of *bo₃* oxidase, we used a single cysteine mutant and coupled SpyTag via maleimide chemistry. With the cysteine already taken for SpyTagging, we could not label the protein with DY647P1 and measure orientation as described in Chapter 4.1. In the future, we aim to label MBPx with DY647P1, which will facilitate the experiments. Although MBPx likely helps to orient *bo₃* in the inside-out orientation, the 3x higher ATP synthesis rates in PC than in PG liposomes with coupled *bo₃*-MBPx indicate that the orientation is still not equal in the two samples. MBPx-SpyCatcher003 has ~100 kDa and thus is slightly smaller than *bo₃* oxidase and not sufficiently large to affect orientation efficiently. It thus might be interesting to use even larger soluble units than MBPx such as the soluble $\alpha_3\beta_3\gamma\varepsilon$ subunits from the ATP synthase that form the F_1 head. If fusion of a SpyCatcher subunit (~20 kDa) is successful to one of the subunits, a powerful handle with a molecular weight of 330 kDa could be used (Figure S4.2.5). Furthermore, reconstitution should be done in high salt conditions to reduce electrostatic interactions during the reconstitution process.

In conclusion, we investigated the influence of the lipid composition on artificial *E. coli* respiratory chain in liposomes and found it to be an extremely difficult and challenging topic. The lipid composition has been shown to be crucial for membrane protein structure and function in many cases [11,18,254]. We demonstrated coreconstitution of a three-component respiratory chain from *E. coli* using either FRD or NDH-2 to initiate coupled ATP synthesis by *bo₃* oxidase and ATP synthase and showed that negatively charged lipids are required for the latter system. This was confirmed in NADH:Q_2 oxidoreductase measurements with isolated NDH-2, indicating charge-mediated docking of NDH-2 to liposomes, corroborated with several NDH-2 mutants in which important cationic amino acids in the C-terminal domain were replaced. Moreover, we measured the orientation of *bo₃* oxidase in liposomes and observed increasing fractions of *bo₃* oxidase being present in the undesired right-side out orientation in liposomes with increasing fraction of anionic lipids. We identified this lipid-dependent *bo₃* oxidase orientation to be very likely one of the components contributing to lipid dependency in coupled ATP synthesis activity observed by Nilsson et al. [1]. Finally, initial successful trials are presented to guide unidirectional orientation of *bo₃* oxidase in the desired inside-out orientation by coupling it to a large soluble unit MBPx.

4.2.6 Material and methods

All chemicals, if not otherwise stated, were purchased from Sigma-Aldrich.

Expression and purification of bo₃ oxidase mutants

Single-cysteine *bo₃* oxidase mutants (ID578C, IIA236C, IIIA21C) were constructed from plasmid pETcyoII [234], encoding for the entire *cyo* operon. Wildtype and mutant *bo₃* oxidase was expressed in *E. coli* strain C43Δcyo [233] cells. Cells were grown either in M63 minimal medium (3 g/l KH_2PO_4, 7 g/l K_2HPO_4, 0.5 mg/l

$FeSO_4$, 100 µg/ml ampicillin, 1 mM $MgSO_4$, 100 mg/l thiamine, 10 µM $CuSO_4$, 0.2 % glucose, 0.2 % NH_4Cl) or in petcyo medium (0.5 % yeast extract, 1 % peptone from meat, 1 % NaCl, 0.5 % glycerol, 2 mM $MgSO_4$, 30 µM $FeSO_4$, 10 µM $CuSO_4$) containing 100-200 µg/ml ampicillin in a LEX48 system at 38 °C. Expression was induced at an OD_{600} of 0.5-1 with 1 mM IPTG (Santa Cruz) followed by an additional incubation at 38 °C for at least 4-5 h. Cells were harvested by centrifugation, resuspended in Buffer D (50 mM Hepes pH 8.3, 5 mM $MgCl_2$) containing DNase I and protease inhibitors PMSF (1 mM) and Pefabloc (spatula tip; Biomol) and lysed by 3-4 passes through MAXIMATOR (HPL6 High-Pressure Homogenizer, Maximator AG) at 2 °C. After cell debris was removed by centrifugation (8'000 x *g*, 0.5 h, 4 °C), membranes were harvested by ultracentrifugation (200'000 x *g*, 1 h, 4 °C) and resuspended in Buffer E (50 mM K_2HPO_4, pH 8.3) containing 5 mM imidazole. Solubilization was performed with 1 % DDM (Glycon Biochemicals GmbH) for 2 h at 4 °C (typically with additional PMSF), followed by ultracentrifugation (200'000 x *g*, 45 min, 4 °C). Solubilized protein was loaded on prepacked 5 ml HisTrap columns (GE Healthcare), washed with buffer E containing 0.05% DDM and 35 mM imidazole and eluted with the same buffer containing 100 mM imidazole. Fractions containing bo_3 oxidase were pooled and concentrated with a 100 kDa MWCO Amicon Ultra-15 filter (Merck Millipore). The pooled fraction was divided into aliquots, frozen in LN_2 and stored at -80° C.

Expression of ATP synthase mutants

Single-cysteine ATP synthase variants were constructed from cysteine-free plasmid pFV2 [232] using standard molecular biology techniques and constitutively expressed in *E. coli* DK8 cells (lacking the whole ATP operon). Cells were grown in LB medium containing 100 µg/ml ampicillin and 1 mM $MgCl_2$ from precultures for at least 4-5 h in a LEX48 system (epiphyte3) at 38 °C. ATP synthase was either purified with Magic Buffer (Buffer S) or with buffer containing LMNG (see below). ATP synthase purified in Magic buffer was used for most experiments, while ATP synthase in LMNG was used for experiments in Figure 4.2.6.

Purification of ATP synthase in Magic buffer

Cells were harvested by centrifugation and broken by 3 passes through MAXIMATOR (HPL6 High-Pressure Homogenizer, Maximator AG) at 1200 bar at 2 °C in Buffer A (50 mM HEPES pH 8, 100 mM NaCl, 5 % glycerol) containing DNase I (spatula tip) and protease inhibitors PMSF (0.1 mM) and Pefabloc (spatula tip; Biomol). After removal of cell debris (centrifugation at 5000 x *g* for 0.5 h, 4 °C), membranes were pelleted by ultracentrifugation (175'000 x *g*, 1.5 h, 4 °C) and resuspended in 10 mM Tris-HCl pH 7.5 (1 ml per g of wet cells). For solubilization, homogenized membranes were diluted with 2 x solubilization buffer S (50 mM Hepes pH 7.5, 100 mM KCl, 250 mM sucrose, 20 mM imidazole, 40 mM 6-aminohexanoic acid, 15 mM P-aminobenzamidine, 5 mM $MgSO_4$, 0.1 mM Na_2-EDTA, 0.2 mM DTT, 0.8 %

soy bean type II asolectin, 1.5 % *n*-octyl β-D-glucopyranoside, 0.5 % sodium deoxycholate, 0.5 % sodium cholate, 2.5 % glycerol; Magic buffer) in a ratio of 1:1 and incubated at 4 °C for 1.5 h while stirring. Non-solubilized material was removed by ultracentrifugation (200'000 *x g*, 30 min, 4 °C) and the supernatant was looped on a prepacked 5 ml HisTrap column (GE Healthcare) equilibrated with buffer S at 4 °C for 2 h. The column was washed with 5 column volumes (cv) of buffer S containing 40 mM imidazole and 3 cv of buffer S containing 90 mM imidazole. Purified protein was eluted with buffer S containing 250 mM imidazole and fractions containing ATP synthase were identified by ATP regenerating assay [226] and pooled. The pooled fraction was divided into aliquots without concentrating, frozen in LN_2 and stored at -80° C.

Purification of ATP synthase in LMNG

Cells were harvested and membranes were prepared as described above in Buffer B (50 mM MOPS/NaOH pH 8, 100 mM NaCl, 5 mM $MgCl_2$, 5 % glycerol). Pelleted membranes were resuspended (2 ml per g of wet cells) in Buffer C (50 mM MOPS/NaOH pH 8, 100 mM NaCl, 5 mM $MgCl_2$, 30 g/l sucrose, 10 % glycerol). For solubilization, LMNG (Anatrace) was added to a final concentration of 2 % from a 5 % stock solution (in water). After the suspension was stirred for 30 min at room temperature and 30 min at 4 °C in presence of 1 mM PMSF, 5 ml of Buffer C was added per g of membranes and non-solubilized material was removed by ultracentrifugation (200'000 x *g*, 0.5 h, 4 °C). The supernatant was loaded onto a prepacked 5 ml HisTrap column (GE Healthcare) in presence of 10 mM imidazole via loop-loading for 2 h at 4 °C. Bound protein was eluted via gradient elution from 20 mM to 400 mM imidazole in Buffer C containing 0.005 % LMNG. Fractions containing ATP synthase were identified by ATP regenerating assay [226], pooled and concentrated with a 100 kDa MWCO Amicon Ultra-15 filter (Merck Millipore). The pooled fraction was divided into aliquots, frozen in LN_2 and stored at -80 °C.

Expression and purification of NDH-2

NDH-2 was expressed in BL21Δcyo(DE3) or BL21(DE3)pLysS using the plasmid pETNDH-2_N5 (gift from Robert Gennis from the University of Illinois). Cells were grown in LB medium containing 100 µg/ml ampicillin and 1 mM $MgSO_4$ either in a shaker or in a LEX48 system at 37 °C until OD_{600} reached 0.6, followed by induction with 0.5-1 mM IPTG. NDH-2 was expressed for an additional 4 h at 37 °C and cells were harvested by centrifugation and resuspended in Buffer F (10 mM Hepes pH 7.4, 100 mM NaCl, 10 mM KCl) containing 20 % glycerol, 2 mM $MgCl_2$, 1 mM PMSF and a spatula tip of Pefabloc (Biomol) and DNaseI. Cells were broken by 3 passes through MAXIMATOR (HPL6 High-Pressure Homogenizer, Maximator AG) at 1500-2000 bar at 2 °C and unbroken cells were removed by centrifugation (8000 x *g*, 30 min, 4 °C) before membranes were pelleted by ultracentrifugation (175'000 x *g*, 1 h, 4 °C). Membranes

were resuspended in Buffer F (2 ml per g of wet cells) containing 1 mM PMSF and a spatula tip of Pefabloc. For solubilization, 2 % DDM (Glycon Biochemicals GmbH) was added from a 20 % stock solution and the sample was diluted with Buffer F to a final DDM concentration of 1 %. After incubation for 1 h at 4 °C while stirring, non-solubilized material was removed by ultracentrifugation (175'000 x g, 1 h, 4 °C) and 10 mM imidazole was added to supernatant. The supernatant was then bound either onto a prepacked 5 ml HisTrap column (GE Healthcare) or Ni-NTA beads equilibrated with Buffer F containing 0.05 % DDM and 10 mM imidazole. Bound protein was eluted either via gradient elution in Buffer F containing 0.05 % DDM from 5 mM to 300 mM imidazole, or washed first with 10 cv Buffer F containing 0.05 % DDM and 20 mM imidazole followed by same buffer containing 50 mM imidazole and eluted with 5 cv of the same buffer containing 200 mM imidazole. Yellow or peak fractions were pooled and concentrated with a 100 kDa MWCO Amicon Ultra-15 filter (Merck Millipore). The pooled fraction was divided into aliquots, frozen in LN_2 and stored at -80 °C.

Expression and purification of Fumarate reductase

Fumarate reductase from *E. coli* was overexpressed and purified as described [114]. (Done by Olivier Biner)

Expression and purification of MBPx-SpyCatcher003

pET21-MBPx-SpyCatcher003-3xFLAG was constructed from pET21-MBPx-SpyCatcher-3xFLAG (from Dr. Andrea Amati [240]) and SpyCatcher003 insert (ordered at Gene Universal) using standard molecular biology techniques. It contains an N-terminal 6xHis-Thrombin site-3xFLAG-tag sequence and was expressed in *E. coli* BL21 pLysS. Cells were grown in LB medium containing 100 µg/ml ampicillin at 38 °C in a LEX48 system (epiphyte3) until reaching OD_{600} of 1. After induction with 1 mM IPTG (Santa Cruz), MBPx-SpyCatcher003 was expressed overnight at 27 °C.

MBPx-SpyCatcher003 was purified via affinity chromatography as described [199] with some changes. In brief, cells were harvested by centrifugation and resuspended in Ni-NTA buffer (50 mM TrisHCl pH 7.8, 300 mM NaCl) containing DNase I, PMSF and Pefabloc (Biomol). Cells were broken by MAXIMATOR (3 passes, 1500-2000 bar, 2 °C; HPL6 High-Pressure Homogenizer, Maximator AG) and insoluble material was removed by centrifugation (8000 x *g*, 0.5 h, 4 °C). The supernatant containing His-tagged MBPx-SpyCatcher003 was loaded on PureCube 100 Ni-NTA Agarose beads (Cube Biotech) in presence of 5 mM imidazole via batch-binding by stirring for 2 h at 4°C. Unspecifically bound proteins were washed off by 15 cv Ni-NTA buffer containing 40 mM imidazole and purified MBPx-SpyCatcher003 was eluted with 5-7 cv Ni-NTA buffer containing 250 mM imidazole. Fractions containing protein were identified by OD_{280}, pooled and concentrated using an Amicon Ultra-15 filter (Merck Millipore) with a 50 kDa MWCO.

For further purification, MBPx-SpyCatcher003 was applied to thrombin (Lee Biosolutions) digestion to remove the His-tag (overnight incubation at 4 °C). The reaction was stopped by the addition of 0.2 mM PMSF and thrombin was removed by passing the sample through a HiTrap Heparin column (GE Healthcare). The flow-through was then passed through a prepacked HisTrap column (GE Healthcare) to remove free His-tag and concentrated with an Amicon Ultra-15 filter (Merck Millipore) with a 50 kDa MWCO.

Site-specific labeling with DY647P1-maleimide

Labeling was performed as described [221,255]. In brief, purified single-cysteine mutants were diluted with maleimide reaction buffer (20 mM Hepes pH 6.5, 100 mM KOAc, 0.05 % DDM) in a ratio of 1:5 to adjust the pH. The cysteines were reduced with 0.4 mM TCEP and the samples were incubated with a 10-fold excess of DY647P1-maleimide (Dyomics GmbH) over the protein overnight at 4 °C (end-over-tail rotation). Excess dye was removed by gel filtration (CentriPure P10 or P50, emp Biotech GmbH) using maleimide reaction buffer for equilibration and elution and three cycles of diluting and concentrating with a 100 kDa Amicon Ultra-15 filter (Merck Millipore).

Site-specific labeling with SpyTag003-peptide-maleimide

For *bo₃*-SpyTag003, single-cysteine ID578C *bo₃* oxidase mutant was labeled with SpyTag003-peptide-maleimide. Therefore, Ni-NTA purified *bo₃* oxidase with a concentration of 50-60 µM was incubated with a 20-fold excess of TCEP over the protein for 1.5 h at 23 °C, 300 rpm and TCEP was removed by gel filtration using CentriPure P5 column (emp Biotech GmbH) equilibrated with 100 mM Hepes pH 7.4 containing 0.05 % DDM.

SpyTag003-peptide containing an N-terminal maleimide (GenScript) was dissolved in 50 mM Hepes pH 6.1 at a concentration of 10 mM. A 20-fold excess of SpyTag003-peptide over protein was added to the pre-reduced *bo₃* oxidase mutant and the reaction was incubated for 2 h at 23 °C, 300 rpm. Excess SpyTag003-peptide was removed by gel filtration using CentriPure P5 column (emp Biotech GmbH) equilibrated with 100 mM Hepes pH 7.4 containing 0.05 % DDM and by three cycles of diluting and concentrating with an Amicon Ultra-15 filter of 100 kDa MWCO (Merck Millipore).

The efficiency of peptide labeling was monitored by coupling with MBPx-SpyCatcher003 and subsequent SDS-PAGE analysis. In samples with low coupling efficiency, labeled *bo₃* oxidase molecules were separated by unlabeled ones via SpyDock purification as described [202] with some changes. In brief, SpyDock was expressed and purified as described [202] by our lab technician Leticia Herrán Villalaín and coupled to SulfoLink™ Coupling Resin (ThermoFisher Scientific) according to [202]. SulfoLink-SpyDock beads were then equilibrated with TP buffer (25 mM orthophosphoric acid, 0.05 % DDM, pH 7 adjusted with Tris base). *bo₃*-SpyTag003 was diluted with TP buffer in a ratio of 1:1 and bound via batch-binding

to SulfoLink-SpyDock for 1 h at 4 °C. Via gravity flow, beads were washed first with 150 cv of TP buffer and then with 100 cv of TP buffer containing 500 mM imidazole. *bo₃*-SpyTag003 was eluted with 3 cv of TP buffer pH 8 containing 5 M imidazole. Imidazole was removed immediately after elution via gel filtration using CentriPure P10 column (emp Biotech GmbH) and one cycle of diluting/concentrating with Amicon Ultra-15 filter of 100 kDa MWCO (Merck Millipore).

SpyTag/SpyCatcher coupling

For the coupling of *bo₃* oxidase-SpyTag003 with MBPx-SpyCatcher003, the enzymes were mixed with a 2x molar excess of MBPx-SpyCatcher003 and 0.05 % DDM was added. Coupling reaction was incubated for 2 h at 25 °C, 1200 rpm. Coupling products were frozen as aliquots in LN_2 and stored at -80 °C.

Liposome preparation

Lipids used were purchased from Avanti Polar Lipids (18:1 Cardiolipin; *E. coli* Extract Polar; 18:1 (Δ9-Cis) PC (DOPC); 18:1 (Δ9-Cis) PE (DOPE); 18:1 TAP (DOTAP)) or from Lipoid (LIPOID E PC S; LIPOID PG 18:1/18:1; LIPOID E PE). Lipids were dissolved in chloroform and mixed in appropriate ratios. If necessary, 2 mol% Q_8 (dissolved in chloroform) was mixed with lipids. Chloroform was evaporated in a desiccator overnight and lipids were resuspended either in Buffer L1A (20 mM Hepes pH 7.5, 2.5 mM $MgCl_2$, 50 g/l sucrose) or L1B (50 mM MOPS-BTP pH 6.75) at a concentration of 5-10 mg/ml for coupled ATP synthesis measurements, in Buffer L2 (20 mM Hepes pH 7.4, 200 mM NaCl, 20 mM KCl) at a concentration of 5-10 mg/ml for NADH oxidation measurements with NDH-2, or in Buffer L1B (50 mM MOPS-BTP pH 6.75) at a concentration of 40 mg/ml for orientation measurements. To get unilamellar liposomes, the suspension was subjected to 7 cycles of freezing (liquid nitrogen) and thawing (at 29.4 °C), each cycle followed by vortexing for some seconds. Liposomes were divided into aliquots, frozen in LN_2 and stored at -80 °C.

Liposomes used for coupled ATP synthesis measurements were thawed directly before use and extruded 21 times through a Whatman polycarbonate membrane (Little Chalfont or Sigma Aldrich) with a 100 nm pore size.

Liposomes used for NADH:ubiquinone oxidoreductase measurements of NDH-2 were thawed directly before use and sonicated with a tip sonicator (5 min, pulse on 30 s, pulse off 30 s, amplitude 40 %).

Liposomes used for orientation measurements were thawed directly before use, diluted with Buffer L1B to 10 mg/ml and extruded 21 times through a Whatman polycarbonate membrane (Sigma Aldrich) with a 100 nm pore size.

Reconstitution/Coreconstitution of membrane proteins

Reconstitution of the individual enzymes ATP synthase or *bo₃* oxidase was performed similarly to coreconstitution of the two enzymes as described by von Ballmoos et al. [104]. Briefly, liposomes were partially

solubilized with 0.4 % sodium cholate using a 30 % stock solution, before the enzymes were added. For coupled ATP synthesis measurements, we used 5 enzymes per liposome each, while for orientation measurements, varying amounts of fluorescently labeled protein were used (3-5 enzymes per liposome) to adjust for fluorescence signal. The mixture was incubated for 0.5 h at 4 °C (let stand) or at room temperature (300 rpm), followed by gel filtration (CentriPure P10 column, emp Biotech GmbH) to remove detergent. Equilibration and elution were done either with Buffer R1 (20 mM Hepes, pH 7.5, 2.5 mM $MgCl_2$, 25 g/l sucrose) for coupled ATP synthesis measurements or with Buffer R2 (100 mM MOPS pH 7.5, 25 mM K_2SO_4 1 mM $MgCl_2$) for orientation measurements. Depending on the downstream application, the liposomes were either pelleted by ultracentrifugation (Type 70.1 Ti rotor, 200'000 x *g*, 1 h, 4 °C) or directly used for measurements.

For coreconstitution of *bo₃* oxidase, ATP synthase and FRD, 250 µl 5 mg/ml liposomes were partially solubilized with 0.6 % cholate and mixed with the three enzymes, before the detergent was removed by gel filtration (CentriPure P10 column, emp Biotech GmbH) after 30 min. (Done by Olivier Biner)

Coupled ATP synthesis activity measurements

Coupled ATP synthesis activity was measured as described [1]. Briefly, proteoliposomes were mixed with 500 µl measuring buffer M (20 mM Tris-PO_4 pH 7.5, 5 mM $MgCl_2$, 4 mM DTT, 80 µM ADP, 0.2 mg/ml ATP Bioluminescence Assay Kit CLS II (Roche)). After measuring a baseline with GloMax® 20/20 Luminometer (Promega) for 30 s, the reaction was started with 20 µM Q_1 and luminescence was measured for 90 s. The reaction was stopped with the addition of at least 50 µM KCN. A known amount of ATP was added and ATP synthesis rates [pmol ATP/s] were calculated by subtraction of baseline slope and normalization with ATP addition.

For NDH-2/NADH induced or FRD-induced coupled ATP synthesis activity measurements, proteoliposomes containing Q_8 were mixed with buffer M lacking DTT and baseline luminescence was detected. The reaction was started by adding either 200 µM NADH and 300-500 nM NDH-2 or 1 mM succinate, respectively. FRD was inhibited with 400 µM malonate.

NADH oxidation measurements with NDH-2

NADH:Q_2 oxidoreductase activity of NDH-2 was measured spectroscopically at 430 nm with a Cary 60 UV-Vis Spectrophotometer (Agilent Technologies). Absorption of 1 ml Buffer L2 (20 mM Hepes pH 7.4, 200 mM NaCl, 20 mM KCl) containing 100 µM NADH, 100 µM Q_2 (homemade, Sandra Schär), 1 mg/ml liposomes and 3.2-32 nM wildtype *bo₃* oxidase was measured until reaching a stable baseline, before NADH oxidation was initiated by addition of 0.8-80 nM NDH-2. NDH-2 activity was determined with the slope after NDH-2 addition and depicted as relative activity normalized to activity in presence of ECPE liposomes.

Orientation determination

For the TCEP-based orientation determination assay, site-specifically DY647P1-labeled single-cysteine mutants were reconstituted into liposomes as described above. After ultracentrifugation, liposomes were resuspended in Buffer R2 (typically ½ of volume of liposomes used for reconstitution) and 10-100 µl were diluted in 1.4 ml 250 mM TrisHCl pH 8.5. Fluorescence of DY647P1 was monitored (excitation 649 nm, emission 672 nm; slits 5 nm/10 nm) on a Cary Eclipse Fluorescence Spectrometer (Agilent Technologies). After reaching a stable baseline (1 min), a first quenching plateau was induced by addition of 14 mM tris(2-carboxyethyl)phosphine (TCEP). After 2.5 min, liposomes were solubilized by adding 0.05 % Triton X-100 (20 % stock solution) leading to a total quench, and fluorescence was monitored until the signal was stable (5min). The orientation was calculated as the ratio between the first and the total quench.

4.2.7 Supplementary

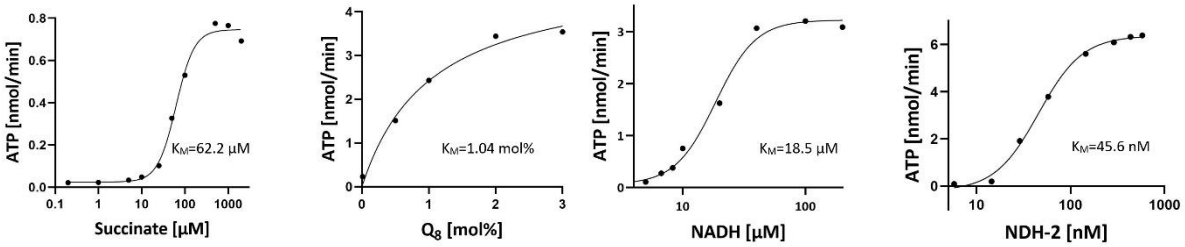

Figure S4.2.1 Titrations of synthetic respiratory chain components. *bo*$_3$ oxidase, ATP synthase and FRD were coreconstituted into 5 mg/ml ECPE liposomes (100 nm), while NDH-2 was added to liposomes during measurements. One component was titrated at a time, while the others were kept in excess (500 nM NDH-2; 200 µM NADH; 1 mM succinate; 2 mol% Q_8). Values were fitted in GraphPad Prism (Michaelis-Menten (Q_8); Sigmoidal, 4PL, X is concentration (Succinate, NADH, NDH-2)). K_M values are indicated. (Experiments done by Olivier Biner)

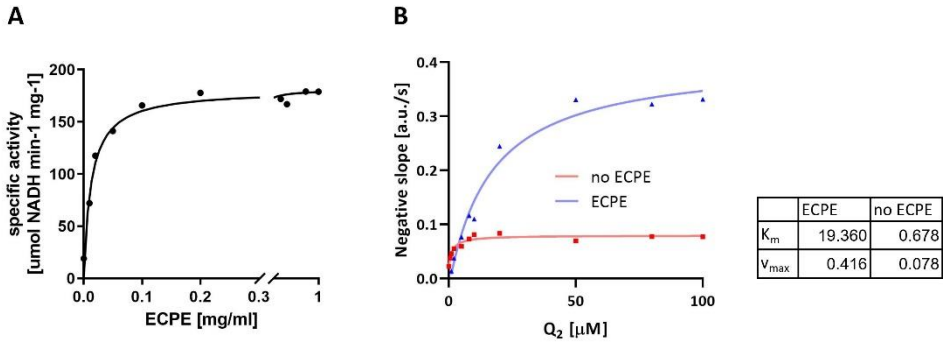

	ECPE	no ECPE
K_m	19.360	0.678
v_{max}	0.416	0.078

Figure S4.2.2 Titration experiments of NADH:Q_2 oxidoreductase activity of NDH-2. A) ECPE liposomes were titrated to NADH oxidation measurements. (Done by Martin Schori) **B)** Quinone Q_2 was titrated to NADH oxidation measurements in presence and in absence of 1 mg/ml ECPE liposomes. For both (**A**) and (**B**), NADH absorption was measured at 340 nm and NADH oxidation was initiated by adding NDH-2. Negative slopes were fitted by Michaelis-Menten equation in GraphPad Prism.

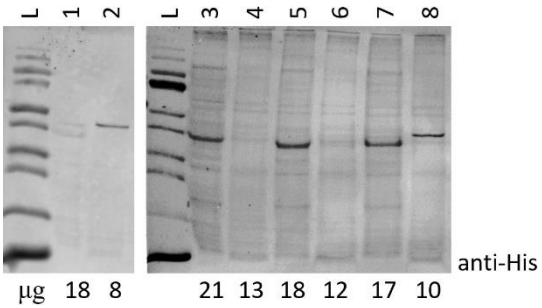

Figure S4.2.3 Western Blot against His-tag from test expressions of NHD-2 wildtype and mutants. 1 µl of membrane vesicles and cytosolic fraction after cell breakage were loaded on a 12 % gel and blotted on a PVDF membrane probing for His-tag. Total protein amount was determined with a Pierce™ BCA Protein Assay Kit (Thermo Scientific) and is indicated below the blot. (Experiments done by Martin Schori)

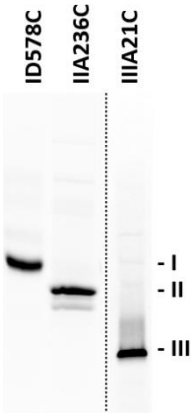

Figure S4.2.4 Fluorescence image of SDS-PAGE from single-cysteine *bo₃* oxidase-DY647P1 mutants ID578C, IIA236C and IIIA21C. *bo₃* oxidase subunits I, II or III are indicated on the right side of the gel. (IIIA21C done by Lukas Rimle)

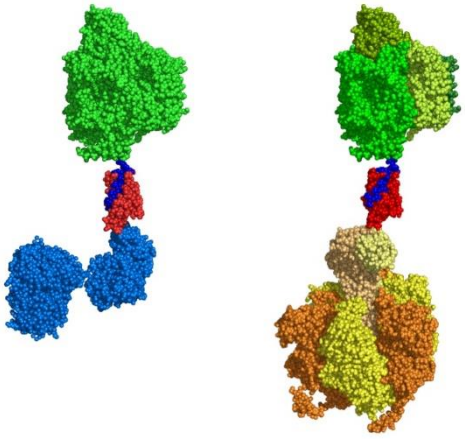

Figure S4.2.5 Structural representation of *bo₃* oxidase (green) coupled to either MBPx (lightblue, left) or $\alpha_3\beta_3\gamma\varepsilon$ from the F_1F_0 ATP synthase (yellow/orange, right) via SpyTag (blue)/SpyCatcher (red). MBPx/$\alpha_3\beta_3\gamma\varepsilon$ can be coupled covalently via SpyTag/SpyCatcher to a single-cysteine of *bo₃* oxidase.

Calculation of liposome fractions with net inwards pumping of protons:

Fractions of liposomes with net inwards pumping activity were calculated in Microsoft Excel. In a matrix, the probability of a certain liposome (characterized by the total number of reconstituted proteins and the fraction of the (desired) inside-out orientation populations) to occur is calculated by Formula 1:

$$= IFERROR((POISSON.DIST(a, b, FALSE) * BINOM.DIST(c, a, d, FALSE)),0)$$

with:

- a: Number of proteins reconstituted in a distinct liposome
- b: Mean number of proteins per liposome
- c: Number of inside-out oriented proteins in a distinct liposome
- d: Orientation of the membrane protein

In Figure S4.2.6, each cell of the table calculated with Formula 1 represents a liposome with a distinct number of reconstituted proteins of which a specific number of proteins is present in the desired inside-out orientation. Exemplarily, the cells with 0, 1, 2 and 3 proteins/liposome are represented in Figure S4.2.7. To calculate the percentage of liposomes that exhibit net inside proton-pumping, all cells harboring more inside-out oriented than right-side out oriented proteins (yellow cells in Figure S4.2.6) were summed up (resulting in blue cells; distribution see in Figure S4.2.7).

Number of proteins per liposome

Number of inside-out oriented proteins	0	1	2	3	4	5	6	7	8	9	10	11	12	13	14	15	16	17	18	19	20
0	0.007	0.02	0.03	0.03	0.023	0.014	0.007	0.003	0.001	4E-04	1E-04	3E-05	7E-06	2E-06	4E-07	7E-08	1E-08	2E-09	4E-10	6E-11	1E-11
1	0	0.013	0.04	0.061	0.061	0.045	0.027	0.014	0.006	0.002	7E-04	2E-04	6E-05	1E-05	3E-06	7E-07	1E-07	3E-08	5E-09	8E-10	1E-10
2	0	0	0.013	0.04	0.061	0.061	0.045	0.027	0.014	0.006	0.002	7E-04	2E-04	6E-05	1E-05	3E-06	7E-07	1E-07	3E-08	5E-09	8E-10
3	0	0	0	0.009	0.027	0.04	0.04	0.03	0.018	0.009	0.004	0.001	5E-04	1E-04	4E-05	1E-05	2E-06	5E-07	1E-07	2E-08	3E-09
4	0	0	0	0	0.004	0.013	0.02	0.02	0.015	0.009	0.005	0.002	7E-04	2E-04	7E-05	2E-05	5E-06	1E-06	2E-07	5E-08	9E-09
5	0	0	0	0	0	0.002	0.005	0.008	0.008	0.006	0.004	0.002	8E-04	3E-04	1E-04	3E-05	8E-06	2E-06	5E-07	1E-07	2E-08
6	0	0	0	0	0	0	6E-04	0.002	0.003	0.003	0.002	0.001	6E-04	3E-04	1E-04	3E-05	1E-05	3E-06	7E-07	2E-07	3E-08
7	0	0	0	0	0	0	0	2E-04	5E-04	8E-04	8E-04	6E-04	3E-04	2E-04	7E-05	3E-05	9E-06	3E-06	8E-07	2E-07	4E-08
8	0	0	0	0	0	0	0	0	4E-05	1E-04	2E-04	2E-04	1E-04	9E-05	4E-05	2E-05	7E-06	2E-06	7E-07	2E-07	5E-08
9	0	0	0	0	0	0	0	0	0	1E-05	3E-05	4E-05	4E-05	3E-05	2E-05	1E-05	4E-06	2E-06	5E-07	2E-07	4E-08
10	0	0	0	0	0	0	0	0	0	0	2E-06	6E-06	9E-06	9E-06	6E-06	4E-06	2E-06	8E-07	3E-07	1E-07	3E-08
11	0	0	0	0	0	0	0	0	0	0	0	3E-07	1E-06	2E-06	2E-06	1E-06	7E-07	4E-07	2E-07	6E-08	2E-08
12	0	0	0	0	0	0	0	0	0	0	0	0	6E-08	2E-07	3E-07	3E-07	2E-07	1E-07	6E-08	3E-08	9E-09
13	0	0	0	0	0	0	0	0	0	0	0	0	0	9E-09	3E-08	4E-08	4E-08	3E-08	2E-08	9E-09	4E-09
14	0	0	0	0	0	0	0	0	0	0	0	0	0	0	1E-09	4E-09	6E-09	6E-09	4E-09	3E-09	1E-09
15	0	0	0	0	0	0	0	0	0	0	0	0	0	0	0	2E-10	5E-10	8E-10	8E-10	6E-10	3E-10
16	0	0	0	0	0	0	0	0	0	0	0	0	0	0	0	0	2E-11	6E-11	9E-11	9E-11	7E-11
17	0	0	0	0	0	0	0	0	0	0	0	0	0	0	0	0	0	2E-12	7E-12	1E-11	1E-11
18	0	0	0	0	0	0	0	0	0	0	0	0	0	0	0	0	0	0	3E-13	8E-13	1E-12
19	0	0	0	0	0	0	0	0	0	0	0	0	0	0	0	0	0	0	0	3E-14	9E-14
20	0	0	0	0	0	0	0	0	0	0	0	0	0	0	0	0	0	0	0	0	3E-15
	0.007	0.034	0.084	0.14	0.175	0.175	0.146	0.104	0.065	0.036	0.018	0.008	0.003	0.001	5E-04	2E-04	5E-05	1E-05	4E-06	1E-06	3E-07
	0	0.013	0.013	0.049	0.031	0.056	0.026	0.03	0.011	0.01	0.003	0.002	5E-04	3E-04	7E-05	3E-05	7E-06	3E-06	5E-07	2E-07	3E-08

Figure S4.2.6 Table of probabilities of a distinct liposome to occur calculated with Formula 1. Each cell represents a liposome with a given number of reconstituted proteins and a given number of proteins in the desired inside-out orientation. The probability to have a distinct number of proteins/liposome (red cells) were calculated by summing up the cells of the appropriate column. To calculate the fraction of liposomes exhibiting net inside pumping (blue cells), the probabilities of the yellow cells (harboring more inside-out oriented than right-side out oriented proteins) were summed up. Calculations in this example were made with a mean number of 5 proteins/liposome and an inside-out orientation of *bo₃* oxidase of 40 %.

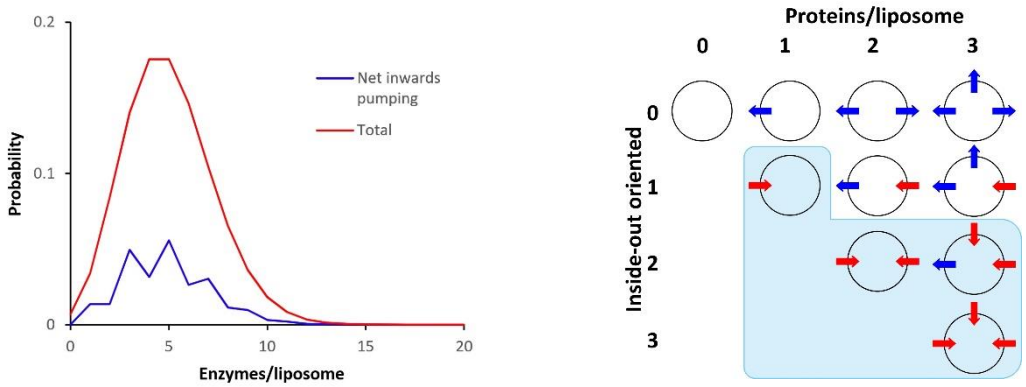

Figure S4.2.7 Probability of liposomes. Left: The probability of liposomes containing a specific number of enzymes (red cells in Figure S4.2.6) was plotted against the number of proteins/liposome (Total). Similarly, the probability of liposomes exhibiting net inwards pumping (blue cells in Figure S4.2.6) was plotted (Net inwards pumping). Calculations in this example were made with a mean number of 5 proteins/liposome and an inside-out orientation of *bo₃* oxidase of 40 %. Right: Representation of possible liposomes exhibiting a distinct number of proteins per liposome with a specific number of inside-out oriented proteins exemplarily with 0, 1, 2 or 3 proteins/liposome. The lightblue shadow marks the liposomes with net inside proton pumping (more inside-out than right-side out oriented proteins).

In a second table, we calculated the number of totally inside pumped protons for each of those yellow cells by assuming a pumping activity of 100 protons/*bo₃* oxidase with Formula 2:

$$= (Number\ of\ insideout\ oriented - Number\ of\ rightside\ out\ oriented) * 100$$

We then multiplied this number with the table in Figure S4.2.6 and again summed up all cells to calculate the average number of protons that are net pumped inside liposomes. In the specific example in Figure S4.2.6 and S4.2.7 (of 5 proteins/liposome and an inside-out orientation of 40 %), 24.7 % of all liposomes exhibit net inside-pumping with an average of 45.5 protons/liposome pumped inside this fraction of liposomes.

4.3 Investigating the importance of lateral enzyme distance on proton coupling of *bo₃* oxidase and ATP synthase

4.3.1 List of contributions

Title	Investigating the importance of lateral enzyme distance on proton coupling of *bo₃* oxidase and ATP synthase
Status	Experimental
Authors	Sabina Deutschmann, Christoph von Ballmoos
Contributions	The project was supervised by Christoph von Ballmoos. Experiments were designed, analyzed and results were interpreted by Christoph von Ballmoos and Sabina Deutschmann. Experiments were performed by Sabina Deutschmann. Cloning, expression and purification of *bo₃*-IST was performed by Sandra Schär. Cloning, expression and purification of ATPs-aSCHA was performed by Micha Marti during his bachelor thesis supervised by Sabina Deutschmann.

4.3.2 Introduction

Our group has established a bottom-up minimal respiratory system through the coreconstitution of the *E. coli* respiratory enzymes *bo₃* oxidase and ATP synthase into liposomes. There, proton pumping by *bo₃* oxidase is initiated by the addition of an electron donor (DTT/Q_1) leading to the generation of a *pmf*, which fuels ATP synthesis by the ATP synthase. In 2016, Nilsson et al. investigated the influence of the lipid composition on this system [1]. They coreconstituted the two enzymes into liposomes of varying lipid compositions and unexpectedly observed a massively decreased ATP synthesis rate in liposomes carrying a net negative charge (DOPG, cardiolipin (CL), DOPA) compared to uncharged liposomes (DOPC). The effect was not observed, though, if the enzyme density was decreased by increasing the liposome size. In the article, the results are discussed in connection to the phenomenon of lateral proton transfer along the membrane which had been proposed and intensively investigated in the past [182–184,186,188,189,256–259], in which protons ejected by proton pumps (e.g. *bo₃* oxidase) do not immediately equilibrate with the bulk, but are initially restricted to transfer along the membrane surface where they can be consumed by proton acceptors such as the ATP synthase. The probability of such transfer is controlled by the proton diffusion rate and the distance between producer (*bo₃* oxidase) and consumer (ATP synthase). The authors [1] thus conclude that the lipid composition either influences the lateral proton transfer rate or the lateral distance between *bo₃* oxidase and ATP synthase. In a follow-up study, Sjöholm et al. found a link between lateral enzyme distance and ATP synthesis rates with fluorescence correlation spectroscopy (FCS) and fluorescence cross-correlation spectroscopy (FCCS) experiments [193]. They conclude that negatively charged lipids increase the average lateral distance between *bo₃* oxidase and ATP synthase, thus decreasing the probability of protons to be directly transferred from *bo₃* oxidase to ATP synthase via the membrane resulting in decreased ATP synthesis rates.

In this project, we aimed to test this hypothesis experimentally by physically, but reversibly, coupling *bo₃* oxidase and ATP synthase in a stoichiometric ratio to fix the lateral distance between the two enzymes. Next, the coupled complex is reconstituted into liposomes with varying lipid composition and respiratory ATP synthesis with DTT/Q_1 is measured before and after cleaving the two enzymes. This strategy has the advantage that the results can be displayed in a ratiometric manner, e.g. before cleavage:after cleavage for every lipid composition. Consequently, several factors such as reconstitution efficiency or relative orientation of the enzymes in liposomes are excluded. Over the course of this PhD, we used three different approaches to couple *bo₃* oxidase and ATP synthase with varying success: I) Coupling via oligonucleotides that are coupled to single-cysteine mutants of the enzymes via maleimide chemistry where cleavage is possible via DNase treatment; II) Construction, expression and purification of a *bo₃* oxidase-ATP synthase fusion enzyme containing a protease cleavage site in the linker between

the two fused subunits; III) Coupling via SpyTag/SpyCatcher [197,199] fused to *bo₃* oxidase and ATP synthase, respectively, with linkers containing protease cleavage sites. In this chapter, the effort of the three approaches are explained and discussed.

4.3.3 Results and discussion

Coupling via oligonucleotides

In a first approach, we were inspired by a protocol from Raschle et al. [177] who coupled two or three voltage-gated anion channels (VDAC) via oligonucleotides to control protein stoichiometry and composition during nanodisc reconstitution. They labeled different batches of single-cysteine VDAC mutants with short oligonucleotides and formed homodimeric or homotrimeric complexes via basepairing of complementary DNA sequences. Upon reconstitution of the purified complexes into nanodiscs and subsequent DNase digestion, they obtained reconstituted untethered membrane proteins in nanodiscs in a defined stoichiometry.

Similarly, we aimed to label *bo₃* oxidase and ATP synthase with single-stranded complementary oligonucleotides that will basepair after mixing, and to reconstitute the obtained complex into liposomes with varying lipid composition. ATP synthesis will then be measured before and after DNA cleavage via DNase digestion. Our lab has recently used an oligonucleotide-based method to entrap fluorescent dyes on the inside of liposomes [260]. First, single-cysteines were introduced at different locations into otherwise cysless *bo₃* oxidase (except IIC25, which is postranslationally palmitoylated [220] and is thus not reactive for maleimide) and ATP synthase. The mutations were based on the structures available at that time (*bo₃* oxidase: PDB 1FFT; ATP synthase: PDB 5T4Q) and expressed in *E. coli bo₃* oxidase or ATP synthase knockout strains, respectively. After affinity chromatography purification, the proteins were labeled with Cy5-maleimide to test for labeling specificity (Figure S4.3.1), before coupling with single-stranded DNA fragments. As a control, we also purified and incubated cysteine-free mutants of *bo₃* oxidase (both with unmutated IIC25 and with IIC25A) and ATP synthase with Cy5-maleimide. All single-cysteine and cysteine-free mutants were expressed in reasonable amounts and were active in oxygen turnover and ATP hydrolysis measurements, respectively, after purification. While all cysteines were available for labeling, however, the specificity was poor, and Cy5 fluorescence was also found in the cysless control mutants. For further improvement of labeling specificity, we subjected purified single-cysteine mutants to gel filtration, but the results were unsatisfactory. Therefore, we decided relatively early in the process to abandon this approach.

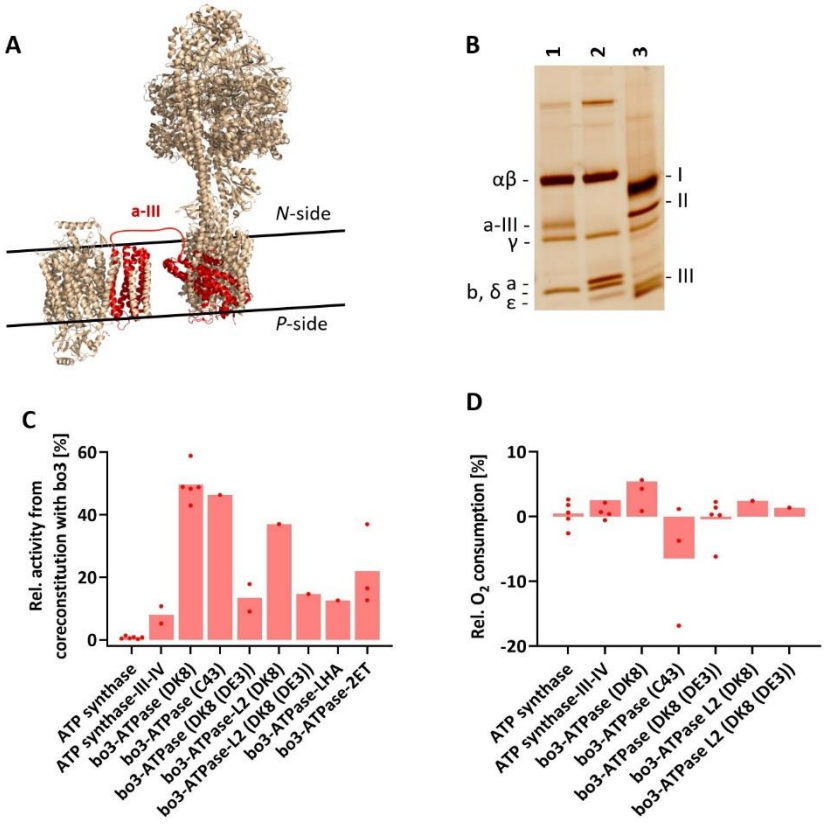

Figure 4.3.1 A) Schematic representation of *bo₃* oxidase-ATP synthase fusion enzyme. In red: Subunit III (*bo₃* oxidase) is fused C-terminally to subunit a (ATP synthase) with a 38-66 amino acid linker containing an HRV 3C PreScission protease cleavage site. The membrane is indicated as black lines. **B)** SDS-PAGE of fusion enzyme expressed in DK8 cells (silver-stained). 1: *bo₃* oxidase-ATP synthase fusion enzyme; 2: ATP synthase wildtype; *bo₃* oxidase wildtype. **C)** Coupled ATP synthesis activity of different fusion enzyme samples. Fusion enzymes or wildtype ATP synthase were reconstituted either alone or coreconstituted with wildtype *bo₃* oxidase. The activity of the reconstituted enzymes is depicted relative to the corresponding activity of the coreconstituted wildtype enzymes. **D)** Oxygen consumption activity of different fusion enzyme samples. Oxygen consumption rates were measured in buffer containing 0.1 % DDM and normalized to wildtype *bo₃* oxidase.

bo₃ oxidase-ATP synthase fusion enzyme

In the second approach, we aimed to connect *bo₃* oxidase and ATP synthase by means of a genetic fusion of the two enzymes. *E. coli* bo_3 oxidase and ATP synthase are both multi-subunit enzymes composed of 4 and 8 different subunits, respectively. As a strategy, we aimed to fuse one subunit of each complex, while the other subunits remain unchanged. The two fused subunits are connected by a linker moiety which on the one hand defines the distance between *bo₃* oxidase and ATP synthase and on the other hand contains a protease cleavage site that allows separation of the two complexes during downstream measurements. Importantly, to be accessible for protease digestion the linker needs to be present on the outside of the liposomes and thus at the *N*-side of the proteins. To avoid loss of activity, non-catalytic subunits, if possible, are preferred targets for fusion. With regard to these criteria, we

decided to fuse subunit III from *bo₃* oxidase C-terminally to subunit a from ATP synthase (Figure 4.3.1A). We therefore cloned subunit III into the pBWU13 plasmid encoding the ATP synthase subunits, with a 38 amino acid linker, containing an HRV 3C PreScission cleavage site, separating the two fused subunits a and III. It has been shown that the *bo₃* oxidase subunits III and IV assemble first [261], followed by addition of subunits I and II. To enhance *bo₃* oxidase subunit assembly in the fusion enzyme, subunit IV was cloned downstream of subunit a-III into the pBWU13 plasmid (resulting in plasmid pBWU13-III-IV; Figure S4.3.2A).

In a first attempt, we expressed the fusion enzyme in *E. coli* DK8 strain, which lacks the operon for the ATP synthase, but contains the full *bo₃* operon, using the pBWU13-III-IV plasmid. Thus, the residual *bo₃* oxidase subunits (I and II) are not overexpressed here, but were rather expected to be complemented from the genomic expression of *bo₃* oxidase subunits in DK8 cells. Membranes were detergent-extracted and subjected to Ni-NTA affinity chromatography to pull on the His-tag present on subunit β (ATP synthase) and analyzed via SDS-PAGE. All ATP synthase subunits as well as the a-III fusion subunit are well detectable. To measure ATP synthesis activity and thus the functionality of the ATP synthase part of the hybrid enzyme, we coreconstituted the fusion enzyme with wildtype *bo₃* oxidase. Rather surprisingly, the fusion enzyme exhibited high ATP synthesis activity (~80 % from wildtype ATP synthase activity (Figure S4.3.3, red bars)), indicating that fusion of the 22 kDa transmembrane subunit III to the C-terminus of subunit a was well tolerated and did not affect ATP synthase integrity and function significantly. On the other hand, subunits I, II or IV from *bo₃* oxidase are not detected on the SDS-PAGE. In good agreement, the oxygen consumption activity of the fusion enzyme was very scarce (Figure 4.3.1D). These results indicate the lack of remaining *bo₃* oxidase subunits in the fusion enzyme, especially the catalytic subunit I. This is further supported by the absence of the characteristic heme peaks in UV/Vis absorption spectra.

We therefore tried to enhance the amount of missing *bo₃* oxidase subunits in the fusion enzyme by overexpressing them in parallel from a second plasmid (pET-cyo-ΔIII; Figure S4.3.2B) in which subunit III was removed from the *bo₃* operon. The two plasmids (pBWU13-III-IV and pET-cyo-ΔIII) confer two different antibiotic resistances and were co-transformed into three different *E. coli* strains (DK8; DK8 (DE3); C43 (DE3)) to overexpress the entire fusion enzyme. The fusion enzyme (referred to as *bo₃*-ATPase) was purified similarly as ATPase-III-IV via Ni-NTA chromatography (pET-cyo-ΔIII does not carry a His-Tag). We first tested the oxygen consumption activities of the different purified products (Figure 4.3.1D). Unfortunately, they were all low and only a slight increase was observed compared to the expression without additional *bo₃* plasmid. Again, if reconstituted with wildtype *bo₃* oxidase, all constructs showed ATP synthesis activity (Figure S4.3.3, red bars), although expression in C43 cells only yielded low values. Finally, we measured coupled ATP synthesis activity of the fusion enzyme without additional

wildtype *bo₃* oxidase to estimate the amount of coupled ATP synthesis activity fueled from fusion *bo₃* oxidase activity (absolute values shown in Figure S4.3.3, blue bars; ratio of ATP synthesis from single reconstitution to coreconstitution shown in Figure 4.3.1C). While most batches showed very low values, one batch (DK8) showed 50 % of the coupled ATP synthesis activity with the fusion enzyme reconstituted alone. A second batch (C43 (DE3)) showed the same behavior, however exhibited very low absolute ATP synthesis and oxygen consumption activities and was thus not considered for downstream measurements. Both low general oxygen consumption activity and missing spectroscopic evidence for hemes in all batches indicated very poor *bo₃* oxidase assembly and absence of the catalytic subunit I. A possible explanation is a too short linker between subunit a and subunit III thus preventing efficient *bo₃* oxidase assembly. Next, the length of the linker between subunits a and III was extended from 38 to 66 amino acids in the pBWU13-III-IV plasmid and was subsequently co-expressed with pET-cyo-ΔIII in *E. coli* DK8 and DK8 (DE3) strains (named *bo₃*-ATPase-L2). However, the amount of *bo₃* oxidase subunit I and consequently *bo₃* oxidase activity could not be increased in the hybrid enzyme containing an increased linker (Figure 4.3.1D; 4.3.1C; S4.3.3, blue bars).

Although it showed low *bo₃* oxidase assembly and activity, "*bo₃* -ATPase (DK8)" (expressed in DK8 with first generation linker) was the best sample concerning relative and absolute activities of both enzymes. It showed all expected ATP synthase subunits and additionally the a-III fusion subunit, but lacked in *bo₃* oxidase subunit bands on an SDS-PAGE (Figure 4.3.1B). Importantly, it showed 50 % ATP synthesis activity if reconstituted alone compared to coreconstitution with wildtype *bo₃* oxidase. We therefore intended to use this batch for our "main experiment" mentioned above, i.e. reconstitution into different liposomes, protease cleavage and subsequent comparison of ATP synthesis rates of coupled and cleaved enzymes. Prior to that, we wanted to establish protocols for efficient protease digestion of the linker protein. To monitor cleavage, an HA-tag was inserted into the (first generation) linker between subunits a and III which enables detection of the fusion subunit before and after cleavage via Western Blot. As seen in Figure 4.3.2A, cleavage performed in solution was complete after overnight HRV 3C digestion at 5 °C.

For the "main experiment", we thus reconstituted the fusion enzyme (1 or 10 enzymes per liposome, respectively) into pure DOPC as well as 3:7 DOPG/DOPC liposomes. Half of the sample was cleaved with HRV 3C PreScission protease and the other half was incubated with buffer, but without protease and both preparations were subjected to coupled ATP synthesis measurements. As a control, we coreconstituted wildtype *bo₃* oxidase and ATP synthase and treated them the same way. From the hypothesis put forward by Nilsson et al. [1] and Sjöholm et al. [193], we would not expect large differences in coupled ATP synthesis rates of the fusion enzymes in DOPC and DOPG liposomes (since *bo₃* oxidase and ATP synthase are in close proximity). After cleavage, however, the enzymes are expected to drift apart and

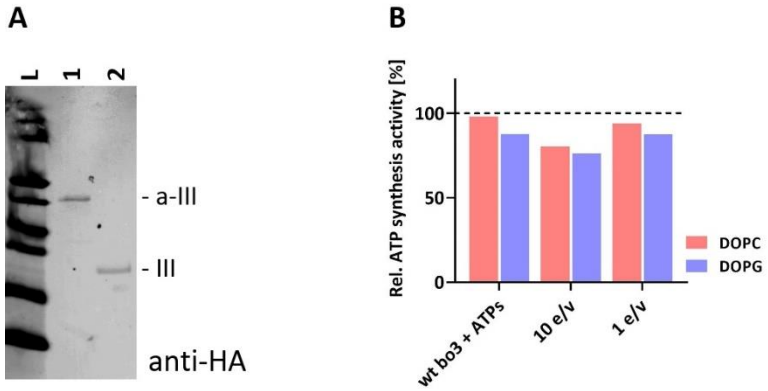

Figure 4.3.2 A) Western Blot of HRV 3C cleavage of fusion enzyme (anti HA-tag; HA-tag present in linker between subunit a and III). Cleavage was performed in Buffer H overnight at 5 °C. L: PageRuler™ Prestained Protein Ladder, 10 to 180 kDa (Thermo Scientific); 1: uncleaved *bo₃* oxidase-ATP synthase fusion protein; 2: cleaved fusion enzyme. **B)** Investigation of the influence of lateral enzyme distance on coupled ATP synthesis activity ("main experiment"). Fusion enzyme (sample *bo₃*-ATPase (DK8)) was reconstituted either into 100 % PC or in 3:7 DOPG/DOPC liposomes (10 e/v and 1 e/v; either 10 or 1 enzymes per vesicle (e/v)) and ATP synthesis initiated with DTT/Q_1 was measured with a luminometer. As a control, wildtype *bo₃* oxidase and ATP synthase (10 e/v each) were coreconstituted. The activity of the cleaved fusion enzyme is depicted relative to the activity of uncleaved fusion enzyme.

ATP synthesis is expected to drop stronger in DOPG-containing than in DOPC liposomes containing 10 enzymes. In experiments with liposomes containing only 1 enzyme (which is below the threshold of enzyme density where Nilsson et al. observed the lipid dependency [1]), the difference between the two liposome compositions is expected to be smaller. Interestingly, we observed only negligible decrease in ATP synthesis rates after cleavage and these were independent of the lipid composition and enzyme density (Figure 4.3.2B, coupled activity of cleaved enzymes normalized to activity of uncleaved complex). A similar decrease was also observed with coreconstituted wildtype *bo₃* oxidase and ATP synthase, where the lateral enzyme distance is expected to be independent of protease treatment, and is likely an artifact of the incubation procedure. Taken together, the fusion enzyme thus exhibits similar behavior as wildtype enzymes and falls short of our expectations.

Although the data indicate that the lateral distance between *bo₃* oxidase and ATP synthase is not contributing to the lipid dependency in coupled activity observed by [1], we were hesitant to over-interpret the present data due to several reasons. First, the experiment was done only once without control experiments, e.g. of the individual enzymes. Second, as mentioned above, the conditions of the fusion enzyme were far from optimal since *bo₃* oxidase subunits were missing in UV/VIS spectroscopy measurements. Third, we cannot exclude that the *bo₃* oxidase activity arises from co-purified wildtype rather than from internally fused *bo₃* oxidase. It is a well-known phenomenon that wildtype *bo₃* oxidase is co-purified during affinity purification of any membrane protein of interest via His-tag due to a naturally occurring histidine-rich sequence in subunit III [262]. However, since wildtype ATP synthase was purified

at the same day as the *bo₃*-ATPase batch used for the "main experiment", using the same protocol and buffers, and did not show *bo₃* oxidase activity (ATP synthase sample in Figure 4.3.1C and 4.3.1D), this scenario seems unlikely. The high coupled ATP synthesis activity of the "*bo₃*-ATPase (DK8)" despite very low oxygen consumption activity and lack of subunit I rather indicates that the few *bo₃* oxidase molecules are coupled to ATP synthase. However, it is possible that these few particles exhibited high activity but were protected from TEV protease cleavage (by the presence of the other *bo₃* subunits).

The expression and purification of a complex in which *bo₃* oxidase and ATP synthase are fused is very tempting as next to the fixed distance, it exhibits also a fixed *bo₃* to ATP synthase stoichiometry. However, the genetic fusion of two such large multi-subunit enzymes during expression also requires proper parallel assembly of the two enzymes, which is obviously a challenging task. A further reason for low assembly of the *bo₃* oxidase might be competition of the fusion subunit a-III with wildtype subunit III that is expressed in DK8 from the chromosomal gene. To circumvent this problem, the fusion enzyme could be expressed in a *bo₃* oxidase/ATP synthase double knockout *E. coli* strain, such as e.g. strain RA1 [263]. Unfortunately, the RA1 cells we obtained were not viable. Taken together, an approach in which the two proteins are coupled as fully folded holoenzymes is more promising. We therefore started a new approach which allowed covalent linkage after purification, however without the requirement of labeling the individual complexes.

Coupling via SpyTag/SpyCatcher

In a third approach, we combined the two previous approaches by coupling the complexes post translationally via SpyTag/SpyCatcher coupling [197,199] (Figure 4.3.3A). The Howarth lab developed a powerful system to covalently couple two polypeptide chains *in vivo* or *in vitro* [197] via pure genetic tools. They split the protein CnaB2 from *Streptococcus pyogenes* into a short peptide of 13 amino acids and a small protein partner of 12.3 kDa which they termed SpyTag and SpyCatcher, respectively. By simple incubation of the two partners together, a covalent isopeptide bond between the two partners is formed. For our experiments, we chose *bo₃* oxidase to carry the SpyTag C-terminally fused to subunit I (plasmid cloned earlier (plasmid map in Figure S4.3.5B) and purified by former lab technician Sandra Schär for another project). Since C-terminal fusion of *bo₃* oxidase subunit III to ATP synthase subunit a did not impair ATP synthase activity substantially in our second approach (see above), we also fused SpyCatcher C-terminally to subunit a (plasmid map Figure S4.3.5A) as a reaction partner. We expressed the ATP synthase-aSpyCatcher complex in *E. coli* DK8 strain and purified it via His-tag affinity chromatography. The purified protein showed all expected subunits on an SDS-PAGE with fusion subunit a-SpyCatcher (Figure 4.3.3B, lane 1). If coreconstituted with *bo₃* oxidase, it retained 50 % of wildtype ATP synthesis activity (Figure 4.3.3C). In a next step, epitope tags were inserted into both *bo₃* oxidase-ISpyTag and

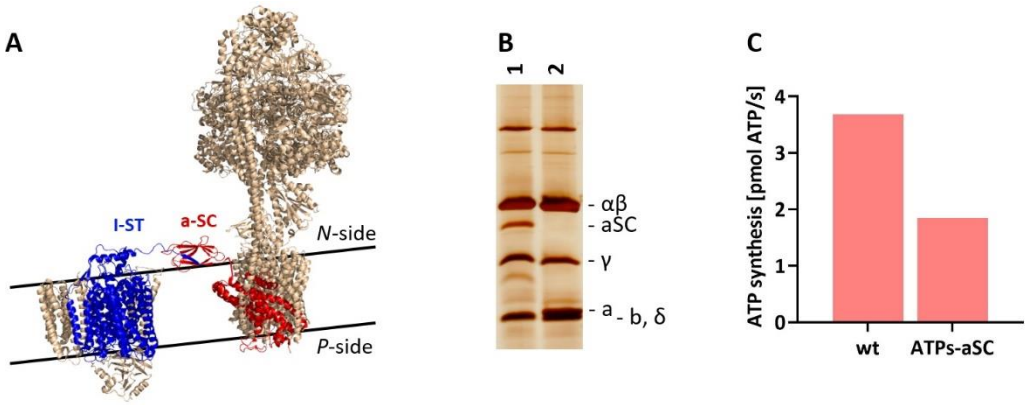

Figure 4.3.3 A) Schematic representation of *bo₃* oxidase-ATP synthase complex coupled via SpyTag/SpyCatcher. In red: SpyCatcher is fused C-terminally to subunit a (ATP synthase) with a 56 amino acid linker containing an HRV 3C PreScission and a TEV protease cleavage site. Blue: SpyTag is fused C-terminally to subunit I (*bo₃* oxidase) with a 28 amino acid linker containing an HRV 3C PreScission protease cleavage site. **B)** SDS-PAGE (silver-stained). 1: ATP synthase-aSpyCatcher; 2: ATP synthase wildtype. **C)** ATP synthesis activity. Wildtype ATP synthase (wt) and ATP synthase-aSpyCatcher were both coreconstituted with wildtype *bo₃* oxidase and coupled ATP synthesis activity initiated with DTT/Q_1 was measured via luminescence.

ATP synthase-aSpyCacher to monitor the SpyTag/SpyCatcher coupling reaction and subsequent protease cleavage via Western Blot. Using molecular biology techniques, we inserted an HA-tag C-terminally of subunit a-SpyCatcher, and a 3xFLAG-tag N-terminally of subunit I-SpyTag. SDS-PAGE analysis and activity measurements of the purified enzyme complexes indicated no impairment of the enzymes through inserted epitope tags.

Next, the two complexes were mixed and coupling was monitored. Unfortunately, coupling seems to be inhibited in presence of both epitope tags (Figure S4.3.6), while good (or complete) coupling of subunits was observed when only one of the two enzymes was carrying an epitope tag. Since detection of HA-tag resulted in much clearer bands than 3xFLAG-tag, we continued optimizing the coupling with the detection of HA-tag using *bo₃* oxidase lacking FlagTag. Interestingly, if the amount of *bo₃* oxidase was increased, the desired coupling product decreased, indicating an inhibitory effect of either *bo₃* oxidase or *bo₃* oxidase buffer ingredients. To further investigate this effect, we titrated detergent to the coupling reactions and observed an inhibitory effect of DDM (Figure S4.3.7) as well as cholate (data not shown) already in small concentrations. Although this is in contrast to observations of Zakeri et al. [197] that did not see impaired coupling in presence of detergents, there are important differences. While we coupled two membrane proteins (naturally interacting with detergents), Zakeri et al. coupled soluble proteins (SpyTag-MBP with SpyCatcher) in presence of different detergents. For further coupling reactions, the detergent concentration was therefore tried to be kept minimal (i.e. 0.05 % DDM in buffer (slightly above CMC) and keeping the volume of *bo₃* oxidase for coupling minimal).

While we were able to efficiently couple ATP synthase subunit a-SpyCatcher, we cannot estimate the coupling efficiency of *bo₃* oxidase subunit I-SpyTag by this means. We also investigated coupling capability of *bo₃* oxidase with another SpyCatcher target, MBPx-SpyCatcher003 (third generation SpyCatcher003 [199], see below) that was used to orient *bo₃* oxidase (see previous chapter). Since the coupling reaction with a single subunit protein (MBPx) yields a simpler band pattern on SDS-PAGE than with ATP synthase, analysis via Western Blot was avoided. While we observed a band of coupled subunit I-MBPx, coupling efficiency was very scarce and a high fraction of subunit I rendered uncoupled. In attempts to increase coupling efficiency, e.g. by increasing incubation time or changing detergent, it became evident that purified *bo₃*-ISpyTag consists of two populations, where one population is able to couple rapidly, while the other does not couple at all. We assume that the non-reactive population is unable to couple because the SpyTag is sterically hindered to couple or lacks for unknown reasons completely. To remove the non-reactive population, sample purification via affinity purification using Spy&Go purification [202] is an option, where the active population binds to SpyDock protein (engineered from SpyCatcher retaining affinity for SpyTag without the ability to form a covalent bond) linked to maleimide activated beads and the bound protein can be eluted with high imidazole concentrations. This strategy should drastically increase the yield of the coupling reaction between *bo₃* oxidase and ATP synthase.

For the "main experiment", a *bo₃* oxidase-ATP synthase complex with a 1:1 stoichiometry is required. Consequently, uncoupled enzymes need to be avoided, either by complete reaction of both partners or subsequent separation of the coupled complex from uncoupled enzymes. Since no complete coupling was observed, we opted for purification of the final product, however, both proteins contain a HisTag, rendering a post-coupling Ni-NTA purification not an ideal choice. Interestingly, Lukas Rimle (another PhD student in the lab) found that *bo₃* oxidase elutes in two steps (at ~60 mM and ~125 mM imidazole) with proteins hardly distinguishable on SDS-PAGE and in activity measurements. He investigated the difference of the two peaks by Western Blot analysis and mass spectrometry and found that only *bo₃* oxidase of the second peak is the desired full-length enzyme, while the first peak *bo₃* oxidase exhibits a truncated subunit II lacking a C-terminal part including the His-tag (which resulted in early elution during affinity chromatography; Figure S4.3.8A). This protein still binds reasonably well to Ni-NTA material because of its above-mentioned histidine-rich stretch in the N-terminus of subunit III acting as "natural His-tag". We thus used the material from the first peak and coupled it with ATP synthase-aSpyCatcher-HA and purified the complex via the His-tag on subunit β of the ATP synthase. As confirmed via Western Blot analysis against HA-tag, >50 % of the ATP synthase was coupled. Unexpectedly, however, Western Blot analysis against His-tag also revealed that the sample contained *bo₃* oxidase

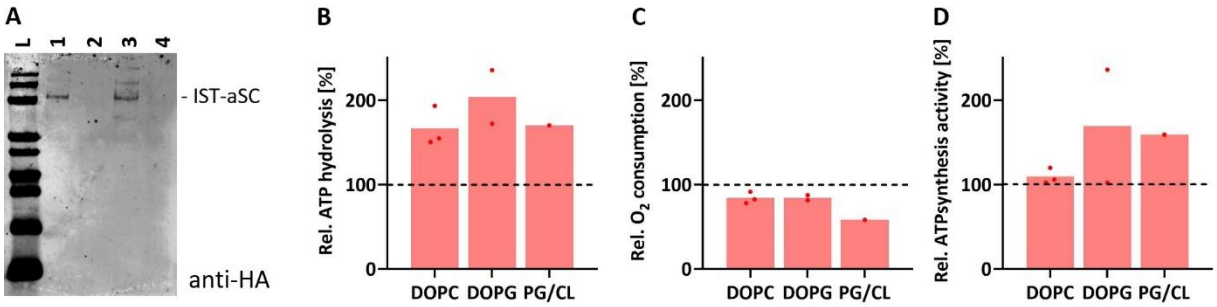

Figure 4.3.4 A) Western Blot of HRV 3C cleavage of SpyTag/SpyCatcher coupled *bo₃* oxidase-ATP synthase (anti HA-tag; HA-tag present C-terminally of SpyCatcher). Coupled *bo₃* oxidase-ATP synthase complex was reconstituted into liposomes (either 100 % DOPC or 3:7 DOPG/DOPC) and cleavage was performed in liposomes overnight at 4 °C. L: PageRuler™ Prestained Protein Ladder, 10 to 180 kDa (Thermo Scientific); 1: coupled in DOPC liposomes; 2: cleaved in DOPC liposomes; 3: coupled in DOPG liposomes; 4: cleaved in DOPG liposomes. **B-D)** Investigation of the influence of lateral enzyme distance on coupled ATP synthesis activity ("main experiment"). SpyTag/SpyCatcher coupled *bo₃* oxidase-ATP synthase was reconstituted into liposomes (100 % DOPC, 3:7 DOPC/DOPG or 1:2:7 CL/DOPG/DOPC), cleaved and ATP hydrolysis (**B**), oxygen consumption (**C**) or coupled ATP synthesis (**D**) activity was measured. Activity of cleaved enzymes is depicted relative to the activity of uncleaved enzymes. For **D**, relative increase/decrease in activity of the individual enzymes (**B**, **C**) was considered.

with a His-tag on subunit II (Figure S4.3.8B). Therefore, we cannot assume that all *bo₃* oxidase present in the purified sample is coupled to ATP synthase and we did not follow this approach further.

A radically different approach was tried when inverted membrane vesicles of cells either containing overexpressed *bo₃* oxidase-ISpyTag or ATP synthase-aSpyCatcher-HA were mixed. The rationale of this experiments is to omit the use of detergent during coupling, potentially leading to increased coupling efficiency. We analyzed coupling efficiency via Western Blot against HA-tag and tried a series of different conditions to promote membrane fusion (in presence of PEG 8000, Ca^{2+}, EDTA, Triton X-100 or lipids), however, coupling was not successful with any of the conditions.

Although coupling efficiency was not ideal, we took our best preparation that showed almost full ATP synthase coupling (with potentially excess of free *bo₃* oxidase however) and reconstituted it into liposomes (pure DOPC, 3:7 DOPG/DOPC, 1:2:7 CL/DOPG/DOPC) at a density of 5 enzymes per liposome to perform the "main experiment". Again, half of the sample was cleaved after reconstitution with HRV 3C PreScission protease (Figure 4.3.4A), which seemed to be complete, and we compared coupled ATP synthesis activity of coupled and cleaved samples. Interestingly, we observed an increase in coupled ATP synthesis activity after protease cleavage in all liposomes. To estimate the effect of cleavage on the individual activities of the enzymes, we determined the activities of the individual enzymes before and after cleavage, and a 1.5- to 2-fold increase in activity was found for ATP hydrolysis (Figure 4.3.4B), while only a small effect was seen for oxygen consumption (Figure 4.3.4C). To calculate coupled ATP

synthesis activity (Figure 4.3.4D), we considered the activities of the individual enzymes before and after cleavage and obtained no significant effect of cleavage on coupled activity in DOPC liposomes, while coupled activity was increased in net negatively charged liposomes (containing DOPG, or CL and DOPG, respectively) after cleavage. This was surprising, since we would have expected a drop in activity in negatively charged liposomes after cleavage due to increased lateral distance between *bo₃* oxidase and ATP synthase, similar to what was observed by Nilsson et al [1]. At this point, we do not want to over-interpret this data as several prerequisites for the experiment were not ideal. First, a change in the activity of the individual enzymes upon cleavage is highly unfavorable and if possible should be avoided. Even though we considered changes in activity of the individual enzymes for calculation of Figure 4.3.4D, it might not represent actual coupled activity (e.g. since we measured ATP hydrolysis instead of ATP synthesis). A prerequisite of the experiment is thus individual enzyme activities that are independent on coupling or cleavage. The significant increase in ATP synthesis and ATP hydrolysis rates after cleavage indicates that the general activity of the enzyme is affected by the presence of the SpyCatcher fusion. Since the construct contains both cleavage sites before and after the SpyCatcher part, we removed the first and hoped to eliminate the problem. The clone is ready for expression and purification, but due to time reasons has not been tested yet. Second, we need a method to monitor the amount of uncoupled *bo₃* present in the sample. As an alternative to the inhibitory FLAG-tag on subunit I, we will insert a single-cysteine on subunit I that can be labeled with a fluorophore via maleimide chemistry allowing detection of coupling efficiency of *bo₃* oxidase-ISpyTag via fluorescent scan of SDS-PAGE. However, at the moment, this is still ongoing. Due to the above-mentioned reasons, we might not be able to interpret the data in Figure 4.3.4.

Despite all our efforts, we were not able to obtain a pure coupled *bo₃* oxidase-ATP synthase complex by SpyTag/SpyCatcher so far. Currently, the master student Yannick Bärtschi continues the project using third generation SpyTag003/SpyCatcher003 [199] sequences that required new cloning, but the new constructs are expected to couple up to 400 times faster. Additionally, he inserted a single-cysteine into subunit I-SpyTag which will allow tracking of coupling efficiency of this subunit after fluorescent labeling. Preliminary experiments look promising showing better coupling efficiencies. Using LMNG as a detergent and very slow flow-rates, he is able to separate a large fraction of free *bo₃* from the complex by size exclusion chromatography.

As an alternative to SpyCatcher, Keeble et al. recently established the DogTag/DogCatcher pair by splitting the adhesin RrgA from *Streptococcus pneumoniae*, which upon incubation covalently couples via transamidation [264]. Similarly to SpyTag/SpyCatcher, the reaction is tolerant to a variety of conditions. However, DogTag is especially developed to be inserted into protein loops, where it reacts much faster than SpyTag, which characteristic is mainly explained by its β hairpin structure. This will expand the

possibilities of efficient Tag insertion into *bo₃* oxidase and might provide a good alternative to SpyTag003/SpyCatcher003.

In an alternative approach, *bo₃* oxidase-ISpyTag might be expressed without a His-tag and coupled after solubilization of membrane vesicles (however, without prior purification) with ATP synthase-aSpyCatcher, followed by His-tag purification via ATP synthase-βHis.

4.3.4 Conclusion and outlook

In this chapter, we aimed to investigate the influence of the lateral distance between *bo₃* oxidase and ATP synthase on coupled ATP synthesis activity. An indispensable prerequisite of our experiment is a stoichiometric complex of *bo₃* oxidase and ATP synthase that can be separated during the experiment. We tried to obtain this complex via three different approaches. In a first approach, the labeling specificity of single-cysteine mutants via maleimide chemistry was very low, preventing subsequent steps of maleimide-based coupling of single-stranded DNA fragments to achieve *bo₃* oxidase-ATP synthase coupling via basepairing. In the two other approaches, we tried to achieve coupling either via genetic fusion of two subunits (one from each complex) or via SpyTag/SpyCatcher coupling technology. A key problem of these two approaches was to experimentally verify the integrity and the stoichiometry of the complexes. While complications of the fusion enzyme might have arisen mainly at the assembly step of the complex during expression resulting in incomplete *bo₃* oxidase-ATP synthase complex, we had difficulties to track coupling via SpyTag/SpyCatcher due to inhibitory effects of epitope tags on the reaction. Expression of the fusion enzyme in a double knockout *E. coli* strain (lacking both *bo₃* oxidase and ATP synthase operons, e.g. RA1 strain) could circumvent the problem of bad assembly by avoiding assembly of wildtype subunits a/III competing with fusion subunit a-III.

SpyCatcher fusion to subunit a seems to inhibit ATP synthase function resulting in significant gain in activity upon protease cleavage, which renders data interpretation difficult. To circumvent this problem, the cleavage site between subunit a and SpyCatcher will be removed. In an ongoing master project in our group, the SpyTag/SpyCatcher was further exchanged by more efficient third generation SpyTag003/SpyCatcher003 pair and a single-cysteine was inserted in subunit I to be able to track coupling of *bo₃* oxidase via fluorescence.

While we knew that the project was very challenging from the start, we did not expect such difficulties in obtaining the desired results. However, we are convinced that such experiments where proteins could be coupled together to mimic the natural cellular proximity (given by the high protein:lipid ratio) would be a powerful tool to investigate interdependencies of membrane proteins and effects of lipids by circumventing the natural drawback of the “dilution” of the proteins if reconstituted into liposomes. The SpyCatcher technologies holds great promise for such experiments since the coupling partner can

be incorporated by genetic tools omitting posttranslational modifications such as cysteine labeling and enabling high complex assembly during expression.

4.3.5 Material and methods

Material

If not otherwise stated, chemicals were purchased from Sigma-Aldrich.

Cloning

Single-cysteine ATP synthase variants were constructed from cysteine-free plasmid pFV2 [232]. pBWU13-III-IV was cloned by insertion of a'-III-IV-insert ordered at Gene Universal into pBWU13. pBWU13-aSpyCatcher was constructed from pBWU13 using a SpyCatcher insert ordered at Gene Universal. ATP synthase-aSpyCatcher-HA was cloned from pBWU13-aSpyCatcher by former Bachelor student Micha Marti. Amino acid sequences of fusion subunits are found in appendix.

Single-cysteine bo_3 oxidase mutants were cloned from cysteine-free plasmid pETcyo-CL (with unmutated C25 on subunit II; provided by Christoph von Ballmoos from Postdoc in Stockholm). Mutants bo_3-IIA76C and bo_3-IIY78C were provided by Christoph von Ballmoos. pET-cyo-ΔIII (kan^r) was cloned by mutating H6 in subunit III of pETcyoIII to a stop codon. pETcyo-ISpyTag was cloned from pETcyoII by former lab technician Sandra Schär through separating the genes for subunit I and III (which in pETcyoII are overlapping) and fusion of SpyTag C-terminally to subunit I via linker. Amino acid sequences of fusion subunits are found in appendix.

Standard molecular biology techniques were used.

Expression and purification

Single-cysteine ATP synthase variants, as well as ATP synthase-aSpyCatcher(-HA) were expressed in *E. coli* strain DK8 (lacking the whole ATP operon) transformed with the appropriate plasmid and purified with solubilization buffer S as described in Chapter 4.1. bo_3 oxidase-ATP synthase fusion enzyme was expressed in *E. coli* strains DK8, DK8 (DE3) or C43 (DE3) either transformed only with pBWU13-III-IV or with pBWU13-III-IV and pET-cyo-ΔIII in LB containing $FeSO_4$ and $CuSO_4$, induced with 1 mM IPTG if required, and purified with solubilization buffer S as described in Chapter 4.1.

Single-cysteine bo_3 oxidase variants as well as bo_3-ISpyTag were expressed in *E. coli* strain C43Δcyo [233] either using a standard shaker or a LEX48 system at 37 °C as described in Chapter 4.1 and purified as described in Chapter 4.1.

Site-specific labeling with Sulfo-Cy5

Enzymes were incubated with 6x excess of TCEP in Buffer G (100 mM Tris-phosphate pH 7) for 10 min at room temperature, before 20x excess of Sulfo-Cy5-maleimide over the enzyme was added. The samples were incubated for 2 h at room temperature, concentrated with a Vivaspin 500 (Sartorius) 100 kDa MWCO and loaded on an SDS-PAGE.

Coupling

For the coupling of *bo₃* oxidase-ISpyTag with ATP synthase-aSpyCatcher, the enzymes were mixed in corec buffer H (20 mM Hepes pH 7.5, 2.5 mM $MgSO_4$, 50 g/l sucrose) in an appropriate ratio (1:1 when coreconstituted for "main experiment"). Coupling reaction was incubated either only for 2 h at 25 °C, 1200 rpm, or additionally overnight at 4 °C, 1200 rpm.

Cleavage

Cleavage of fusion enzyme or SpyTag/SpyCatcher coupled enzyme was performed either with solubilized enzyme (in Buffer H) or with enzymes reconstituted in liposomes. Enzymes were cleaved with a 5-10x weight excess of HRV 3C PreScission protease (expressed and purified by former Postdoc Linda Näsvik Öjemyr) over the complex.

Reconstitution/Coreconstitution of complexes

Reconstitution was performed as described [1]. Briefly, wildtype *bo₃* oxidase and ATP synthase, fusion enzyme or SpyTag/SpyCatcher coupled enzyme were (co)reconstituted into liposomes partially solubilized with 0.4 % cholate. Cholate was removed by gel filtration (CentriPure P10, emp Biotech GmbH) after incubation for 30 min at 4 °C. Equilibration and elution were done either with Buffer H or with Buffer I (10 mM MOPS-KOH pH 7.5, 5 mM $MgCl_2$, 100 mM KCl). After elution, liposomes were either used for protease digestion or directly used for activity measurements. Usually, 5 enzymes per liposome were reconstituted.

Liposome preparation

Liposomes were essentially prepared as described in Chapter 4.1. Dried lipids were resuspended either in Buffer H or in Buffer I at a concentration of 10 mg/ml. After 7 cycles of freeze-thawing (LN_2, 29.4 °C), liposomes were aliquoted, frozen in LN_2 and stored at -80°C. Directly before use, an aliquot was thawed at 29.4 °C and extruded 21 times through a Whatman polycarbonate membrane (Sigma Aldrich) with a 100 nm pore size. Lipids were purchased from Avanti (18:1 (Δ9-Cis) PC (DOPC), 18:1 (Δ9-Cis) PG (DOPG), 18:1 Cardiolipin).

Oxygen consumption measurement

Oxygen consumption was measured with an Oxygraph+ (Hansatech Instruments). A baseline of 1 ml Buffer N (50 mM Hepes pH 8, or 50 mM K_2HPO_4 pH 8, 0.1 % DDM if measured in solution; 50 mM K_2HPO_4

pH 8.3, 30 mM NH_4Cl if measured in liposomes) containing 2 mM DTT and solubilized or reconstituted enzyme, respectively, was measured until stable, before 20 µM quinone Q_1 was added to start the reaction. For bar plots, the slope was normalized to the slope of wildtype *bo₃* oxidase.

Regenerating ATP hydrolysis assay

ATP hydrolysis activity was determined by ATP regenerating assay [226]. Briefly, absorption at 340 nm was measured with a Cary 60 UV-Vis Spectrophotometer (Agilent Technologies). After baseline of Buffer K (50 mM Hepes pH 7.5, 100 mM K_2SO_4, 3 mM K-phosphoenol pyruvate, 0.25 mM NADH, 150 U lactate dehydrogenase, 100 U pyruvate kinase, 2 mM NaCl, 10 mM $MgCl_2$, 0.01 % Triton X-100, 2.5 mM ATP) was stable, the reaction was started by the addition of sample. For bar plots, usually negative slopes of cleaved samples were normalized to negative slopes of the appropriate uncleaved samples.

Coupled ATP synthesis activity measurements

Coupled ATP synthesis activity was measured as described [1]. Briefly, 10-50 µl liposomes were added to 500 µl measuring buffer M (20 mM Tris-PO_4 pH 7.5, 5 mM $MgCl_2$, 4 mM DTT, 80 µM ADP, 0.2 mg/ml ATP Bioluminescence Assay Kit CLS II (Roche)) and a baseline was measured with GloMax® 20/20 Luminometer (Promega) for 30 s. The reaction was started with 20 µM Q_1 and luminescence was measured for 90 s. For normalization of ATP synthesis rates, 0.4 µM ATP was added. ATP synthesis rates [pmol ATP/s] were calculated by subtraction of baseline slope and normalization with ATP addition.

Western Blot

For Western Blotting, proteins were separated by SDS-PAGE and blotted on a PVDF Transfer Membrane (ThermoFisher Scientific) at 4 °C. The membrane was blocked with blocking buffer (5 % fat-free milk, 0.05 % Tween 20 in PBS) for 2 h at room temperature before overnight incubation at 4 °C with primary antibody in the same buffer at concentrations suggested by the company. The membrane was washed with PBS containing 0.1 % Tween 20 and incubated, if necessary, with secondary antibody in the same buffer for 1 h at room temperature, followed by another washing step. The membrane was scanned by Odyssey infrared imager (LI-COR).

4.3.6 Supplementary

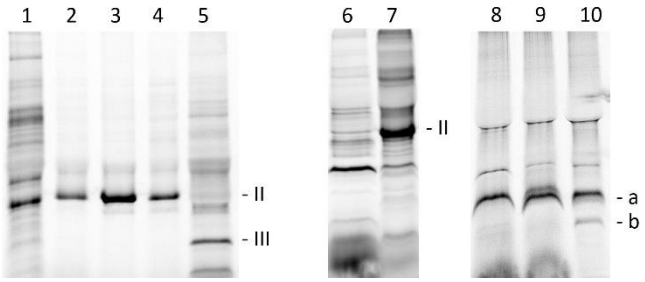

Figure S4.3.1 Fluorescent scan of SDS-PAGE with fluorescently labeled *bo₃* oxidase (1-7) and ATP synthase (8-10) mutants. Single-cysteine mutants were labeled with Sulfo-Cy5-maleimide for 2 h at RT or overnight at 4 °C before being loaded on an SDS-PAGE. Gels were scanned with a G:BOX (Syngene). 1: Cysteine-free; 2: IIA283C; 3: IIA76C; 4: IIY78C; 5: IIIA21C; 6: IIC25A; 7: IIG214C; 8: Cysteine-free; 9: aH95C; 10: bA32C. All *bo₃* oxidase mutants except IIC25A contain C25 which is postranslationally palmitoylated and thus should not be accessible for maleimide labeling.

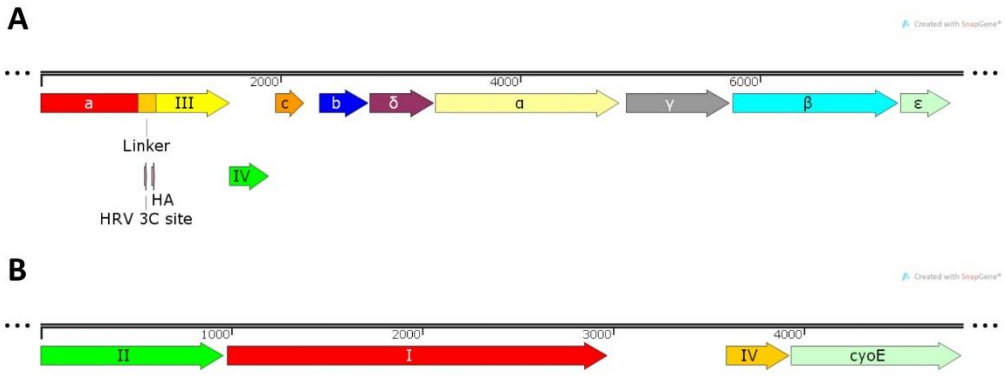

Figure S4.3.2 Plasmid map of pBWU13-III-IV-LHA (A) and pET-cyo-ΔIII (B). A) *bo₃* oxidase subunit III was fused C-terminally to subunit a of ATP synthase into pBWU13 (encoding ATP synthase operon, His-tag on subunit β, Amp^r) separated by a linker containing HRV 3C PreScission cleavage site and HA-tag. Subunit IV (*bo₃* oxidase) was additionally introduced into the plasmid. **B)** To avoid expression of subunit III, a stop codon was inserted after 6 amino acids of subunit III in pETcyoIII (His-tag would be N-terminal of subunit III, Kan^r).

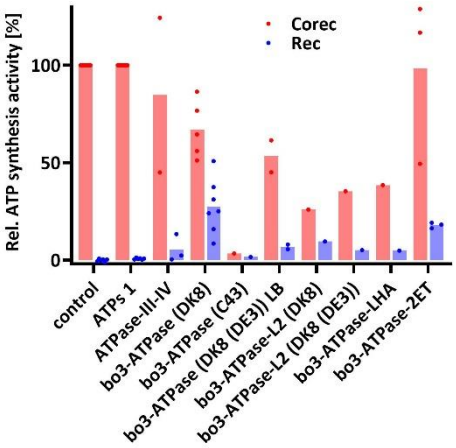

Figure S4.3.3 Coupled ATP synthesis activity of wildtype *bo₃* oxidase and ATP synthase (control) as well as different batches of *bo₃*-ATPase fusion enzymes either coreconstituted with wildtype *bo₃* oxidase (red) or reconstituted alone (blue). Rates were normalized to coreconstitution of wildtype enzymes. ATP production was detected via luminescence.

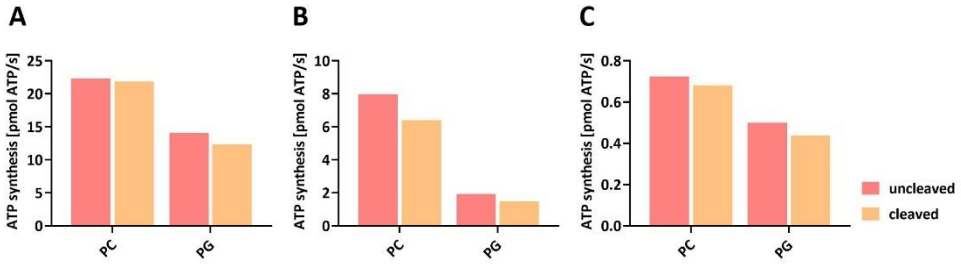

Figure S4.3.4 Coupled ATP synthesis activity with *bo₃*-ATPase fusion enzyme of Figure 4.3.2B depicted as pmol ATP synthesized per second. Wildtype *bo₃* oxidase and ATP synthase ((**A**), 10 enzymes per vesicle (e/v)) or fusion enzyme (10 e/v (**B**) or 1 e/v (**C**)) were (co)reconstituted into 100 % DOPC or 3:7 DOPG:DOPC liposomes before treating with HRV 3C PreScission protease. Coupled ATP synthesis activity of uncleaved and cleaved samples was measured via luminescence.

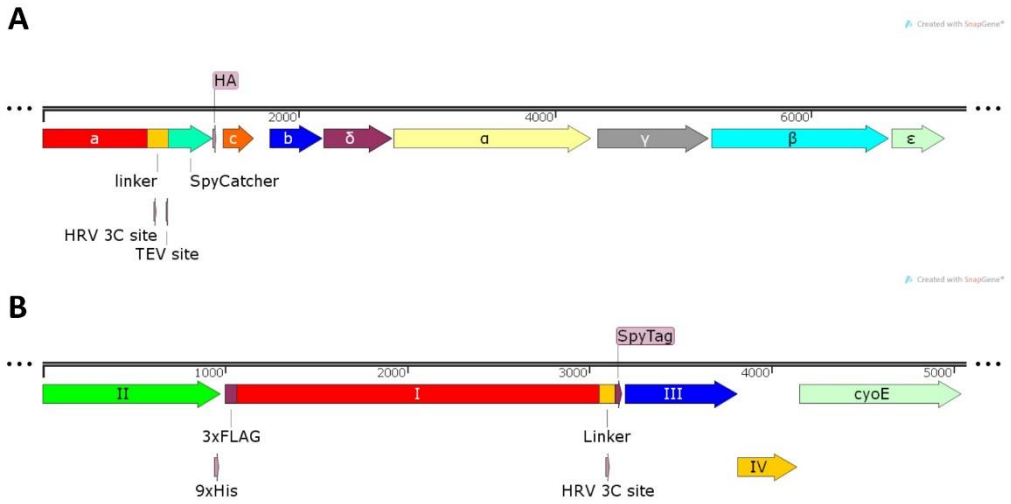

Figure S4.3.5 Plasmid map of pBWU13-aSpyCatcher-HA (A) and pETcyo-3xFLAG-ISpyTag (B). A) SpyCatcher containing a C-terminal HA-tag was fused C-terminally to subunit a of ATP synthase into pBWU13 (encoding ATP synthase operon, His-tag on subunit β, Amp^r) separated by a linker containing HRV 3C PreScission and TEV cleavage site. **B)** SpyTag was fused C-terminally to subunit I containing an N-terminal 3xFLAG-tag separated by a linker containing HRV 3C PreScission cleavage site into pETcyoII (Amp^r, cloned by former lab technician Sandra Schär).

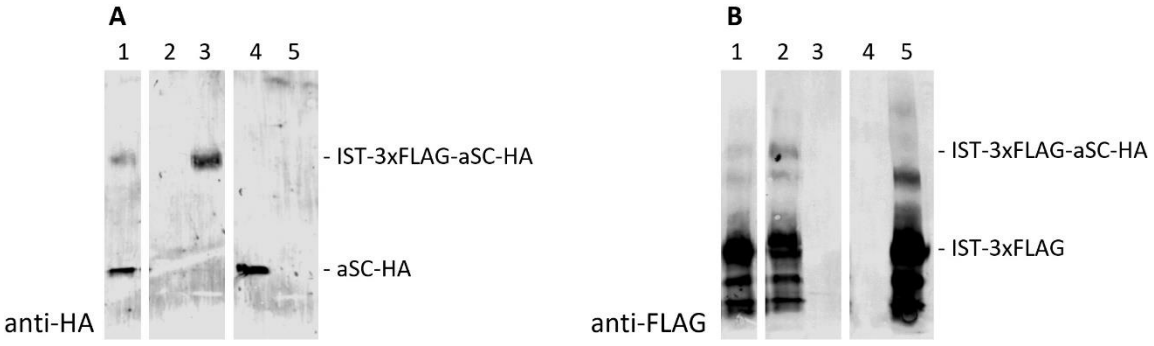

Figure S4.3.6 Western Blot analysis of SpyTag/SpyCatcher coupling. *bo₃* oxidase and ATP synthase were coupled via SpyTag/SpyCatcher by incubation for 3 h at 25 °C, 1200 rpm and coupling products were subjected to SDS-PAGE followed by Western Blot analysis. **A)** Anti HA-tag (ATP synthase subunit a-SpyCatcher-HA). **B)** Anti FLAG-tag (*bo₃* oxidase subunit I-SpyTag-3xFLAG). Coupling of: 1: ATPase-aSpyCatcher-HA and *bo₃*-3xFLAG-ISpyTag; 2: ATPase-aSpyCatcher and *bo₃*-3xFLAG-ISpyTag; 3: ATPase-aSpyCatcher-HA and *bo₃*-ISpyTag. 4: ATPase-aSpyCatcher-HA; 5: *bo₃*-3xFLAG-ISpyTag.

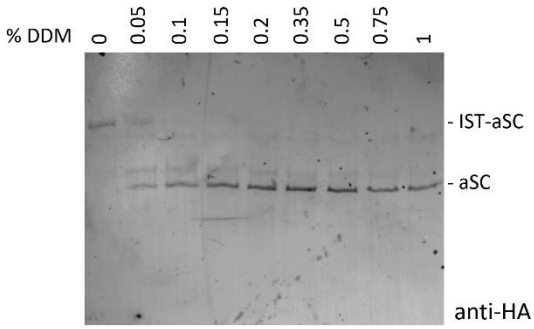

Figure S4.3.7 Western Blot analysis anti HA-tag (ATP synthase subunit a-SpyCatcher) of DDM titration to SpyTag/SpyCatcher coupling. Coupling was performed by mixing ATPase-aSpyCatcher-HA and *bo₃*-ISpyTag and incubation for 2 h at 25 °C, 1200 rpm, in presence of 0-1 % DDM. Subunits I-SpyTag and a-SpyCatcher are indicated.

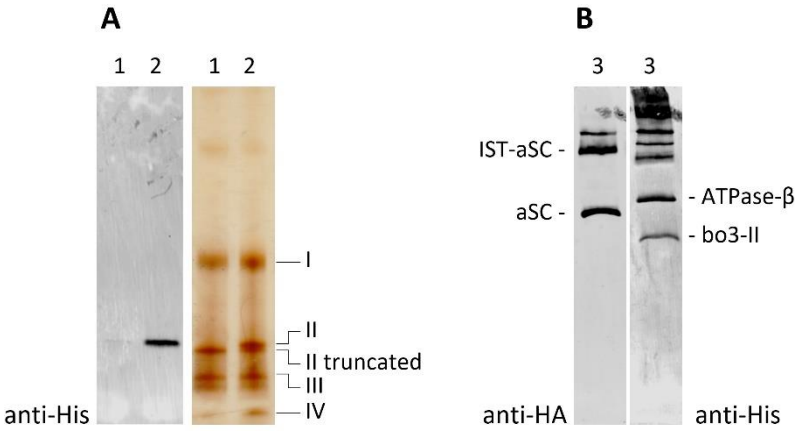

Figure S4.3.8 A) Western Blot against His-tag and silver-stained SDS-PAGE from affinity purification of *bo₃* oxidase via His-tag with peak 1 (1) containing a truncated subunit II without His-tag, and peak 2 (2) containing full-length subunit II with His-tag. **B)** Western Blot against HA-tag (left) and against His-tag (right) of coupling product after His-tag purification. After coupling of *bo₃* oxidase-ISpyTag from peak 1 with ATP synthase-aSpyCatcher-HA (containing a His-tag on subunit β), the product was loaded on Ni-beads (PureCube 100 Ni-NTA Agarose, Cube Biotech), washed with 40 mM and 90 mM imidazole, and eluted with 250 mM imidazole.

Amino acid sequences

a-III fusion subunit in pBWU13-III-IV (subunits are colored as a-linker1-HRV 3C cleavage site-III):

MASENMTPQDYIGHHLNNLQLDLRTFSLVDPQNPPATFWTINIDSMFFSVVLGLLFLVLFRSVAKKATSGVPGKFQT
AIELVIGFVNGSVKDMYHGKSKLIAPLALTIFVWVFLMNLMDLLPIDLLPYIAEHVLGLPALRVVPSADVNVTLSMALG
VFILILFYSIKMKGIGGFTKELTLQPFNHWAFIPVNLILEGVSLLSKPVSLGLRLFGNMYAGELIFILIAGLLPWWSQWIL
NVPWAIFHILIITLQAFIFMVLTIVYLSMASEEHGGGSGALEGGSVDGGSGSLEVLFQGPGSENGGSGGAAAMATDT
LTHATAHAHEHGHHDAGGTKIFGFWIYLMSDAILFSILFATYAVLVNGTAGGPTGKDIFELPFVLVETFLLLFSSITYGM
AAIAMYKNNKSQVISWLALTWLFGAGFIGMEIYEFHHLIVNGMGPDRSGFLSAFFALVGTHGLHVTSGLIWMAVL
MVQIARRGLTSTNRTRIMALSLFWHFLDVVWIAVFTVVYLMGAM

a-III fusion subunit in pBWU13-III-IV-L2 (subunits are colored as a-linker2- HRV 3C cleavage site-III):

MASENMTPQDYIGHHLNNLQLDLRTFSLVDPQNPPATFWTINIDSMFFSVVLGLLFLVLFRSVAKKATSGVPGKFQT
AIELVIGFVNGSVKDMYHGKSKLIAPLALTIFVWVFLMNLMDLLPIDLLPYIAEHVLGLPALRVVPSADVNVTLSMALG
VFILILFYSIKMKGIGGFTKELTLQPFNHWAFIPVNLILEGVSLLSKPVSLGLRLFGNMYAGELIFILIAGLLPWWSQWIL
NVPWAIFHILIITLQAFIFMVLTIVYLSMASEEHGGGSGALEGGSVDGGSGSGGSGSLEVLFQGPGGSGSGGSGSGG
SGSLEVLFQGPGSENGGSGGAAAMATDTLTHATAHAHEHGHHDAGGTKIFGFWIYLMSDAILFSILFATYAVLVNG
TAGGPTGKDIFELPFVLVETFLLLFSSITYGMAAIAMYKNNKSQVISWLALTWLFGAGFIGMEIYEFHHLIVNGMGPD
RSGFLSAFFALVGTHGLHVTSGLIWMAVLMVQIARRGLTSTNRTRIMALSLFWHFLDVVWIAVFTVVYLMGAM

a-III-HA fusion subunit in pBWU13-III-IV-HA (subunits are colored as a-linker- HRV 3C cleavage site-HA-tag-III):

MASENMTPQDYIGHHLNNLQLDLRTFSLVDPQNPPATFWTINIDSMFFSVVLGLLFLVLFRSVAKKATSGVPGKFQT
AIELVIGFVNGSVKDMYHGKSKLIAPLALTIFVWVFLMNLMDLLPIDLLPYIAEHVLGLPALRVVPSADVNVTLSMALG
VFILILFYSIKMKGIGGFTKELTLQPFNHWAFIPVNLILEGVSLLSKPVSLGLRLFGNMYAGELIFILIAGLLPWWSQWIL
NVPWAIFHILIITLQAFIFMVLTIVYLSMASEEHGGGSGALEGGSVDGGSGSLEVLFQGPGSENGGSGGAAAYPYDVP
DYAAAAMATDTLTHATAHAHEHGHHDAGGTKIFGFWIYLMSDAILFSILFATYAVLVNGTAGGPTGKDIFELPFVLV
ETFLLLFSSITYGMAAIAMYKNNKSQVISWLALTWLFGAGFIGMEIYEFHHLIVNGMGPDRSGFLSAFFALVGTHGLH
VTSGLIWMAVLMVQIARRGLTSTNRTRIMALSLFWHFLDVVWIAVFTVVYLMGAM

a-SpyCatcher fusion subunit in pBWU13-aSpyCatcher (subunits are colored as a-linker-HRV 3C cleavage sit-TEV cleavage site-SpyCatcher-(HA-tag))

MASENMTPQDYIGHHLNNLQLDLRTFSLVDPQNPPATFWTINIDSMFFSVVLGLLFLVLFRSVAKKATSGVPGKFQT
AIELVIGFVNGSVKDMYHGKSKLIAPLALTIFVWVFLMNLMDLLPIDLLPYIAEHVLGLPALRVVPSADVNVTLSMALG
VFILILFYSIKMKGIGGFTKELTLQPFNHWAFIPVNLILEGVSLLSKPVSLGLRLFGNMYAGELIFILIAGLLPWWSQWIL
NVPWAIFHILIITLQAFIFMVLTIVYLSMASEEHGGGSGALEGGSVDGGSGSLEVLFQGPGSENGGSGGAAAMSYYD
YDIPTTENLYFQGAMVDTLSGLSSEQGQSGDMTIEEDSATHIKFSKRDEDGKELAGATMELRDSSGKTISTWISDGQ
VKDFYLYPGKYTFVETAAPDGYEVATAITFTVNEQGQVTVNGKATKGDAHI(YPYDVPDYA)

I-SpyTag fusion subunit in pETcyoII-ISpyTag (subunits are colored as I-linker-HRV 3C cleavage site-SpyTag):

MFGKLSLDAVPFHEPIVMVTIAGIILGGLALVGLITYFGKWTYLWKEWLTSVDHKRLGIMYIIVAIVMLLRGFADAIM
MRSQQALASAGEAGFLPPHHYDQIFTAHGVIMIFFVAMPFVIGLMNLVVPLQIGARDVAFPFLNNLSFWFTVVGVI
LVNVSLGVGEFAQTGWLAYPPLSGIEYSPGVGVDYWIWSLQLSGIGTTLTGINFFVTILKMRAPGMTMFKMPVFTW
ASLCANVLIIASFPILTVTVALLTLDRYLGTHFFTNDMGGNMMMYINLIWAWGHPEVYILILPVFGVFSEIAATFSRKR
LFGYTSLVWATVCITVLSFIVWLHHFFTMGAGANVNAFFGITTMIIAIPTGVKIFNWLFTMYQGRIVFHSAMLWTIG
FIVTFSVGGMTGVLLAVPGADFVLHNSLFLIAHFHNVIIGGVVFGCFAGMTYWWPKAFGFKLNETWGKRAFWFWII
GFFVAFMPLYALGFMGMTRRLSQQIDPQFHTMLMIAASGAVLIALGILCLVIQMYVSIRDRDQNRDLTGDPWGGR
TLEWATSSPPPFYNFAVVPHVHERDAFWEMKEKGEAYKKPDHYEEIHMPKNSGAGIVIAAFSTIFGFAMIWHIWW
LAIVGFAGMIITWIVKSFDEDVDYYVPVAEIEKLENQHFDEITKAGLKNGNGSGSGSGSGGSLEVLFQGPGSGSGSGG
SAHIVMVDAYKPTK

I-SpyTag fusion subunit in pETcyoII-3xFLAG-ISpyTag (subunits are colored as 3xFLAG-tag-I-linker-HRV 3C cleavage site-SpyTag):

DYKDHDGDYKDHDIDYKDDDDKMFGKLSLDAVPFHEPIVMVTIAGIILGGLALVGLITYFGKWTYLWKEWLTSVDH
KRLGIMYIIVAIVMLLRGFADAIMMRSQQALASAGEAGFLPPHHYDQIFTAHGVIMIFFVAMPFVIGLMNLVVPLQI
GARDVAFPFLNNLSFWFTVVGVILVNVSLGVGEFAQTGWLAYPPLSGIEYSPGVGVDYWIWSLQLSGIGTTLTGINF
FVTILKMRAPGMTMFKMPVFTWASLCANVLIIASFPILTVTVALLTLDRYLGTHFFTNDMGGNMMMYINLIWAWG
HPEVYILILPVFGVFSEIAATFSRKRLFGYTSLVWATVCITVLSFIVWLHHFFTMGAGANVNAFFGITTMIIAIPTGVKIF
NWLFTMYQGRIVFHSAMLWTIGFIVTFSVGGMTGVLLAVPGADFVLHNSLFLIAHFHNVIIGGVVFGCFAGMTYW
WPKAFGFKLNETWGKRAFWFWIIGFFVAFMPLYALGFMGMTRRLSQQIDPQFHTMLMIAASGAVLIALGILCLVIQ
MYVSIRDRDQNRDLTGDPWGGRTLEWATSSPPPFYNFAVVPHVHERDAFWEMKEKGEAYKKPDHYEEIHMPKNS
GAGIVIAAFSTIFGFAMIWHIWWLAIVGFAGMIITWIVKSFDEDVDYYVPVAEIEKLENQHFDEITKAGLKNGNGSGS
GSGSGGSLEVLFQGPGSGSGSGGSAHIVMVDAYKPTK

5 Overall discussion, conclusions and outlook

Investigation of lipid dependency

The lipid composition of biological membranes is highly diverse and can differ enormously not only among different species but also among different tissues, organelles, and even among the two leaflets of the same lipid bilayer. The lipid composition is adapted to the function of a particular membrane conferring its unique physicochemical properties. Example properties are membrane fluidity, thickness or membrane curvature – considering also the interdependency of most of these properties [265]. Thereby, it is rather the sum of membrane properties than the specific lipid composition that define a membrane's function [265]. Cells consequently have developed a broad variety of mechanisms to maintain physicochemical membrane homeostasis, of which the molecular mechanism is largely unknown to date. There is also very little knowledge about the exact mechanisms how lipid changes are directly implicated in diseases [11]. However, the great number of diseases related to lipids (e.g. Alzheimer's disease, cystic fibrosis or cancer) impressively illustrates the importance of the lipid composition for proper membrane function and health. Only small differences in both the lipid head group and the fatty acid chain were reported to have severe effects, either by disrupting metabolic pathways resulting in a lack of desired products and subsequent accumulation of substrates or unexpected products, or by altering membrane properties [266–268]. Changes in the latter can affect membrane protein structure and function through different mechanisms, e.g. by altering membrane protein recruitment or activity through conformational changes. The general physicochemical properties of the membrane, but also direct interactions with the innermost shell of lipids, called annular lipids, are crucial for proper transmembrane protein conformation and function. [11]

During *in vitro* investigation of membrane proteins, they are typically biochemically isolated from expression cells and subsequently reconstituted into membrane mimicking systems such as liposomes, which are generally considered to be a convenient system to analyze lipid-lipid and lipid-protein interactions and due to their compartmentalization are suitable to study enzymes with a vectorial function. Although powerful, these experiments require critical quality control to discriminate between biological and artificial effects, i.e. membrane protein orientation or reconstitution efficiency. We used liposomes to investigate minimal respiratory systems composed of two or three different respiratory complexes from *E. coli*, in which bo_3 oxidase is initiated to pump protons inside liposomes and the so-generated *pmf* is used by the ATP synthase to produce ATP, which in turn can be detected via luminescence. We are especially interested in investigating the importance of the lipid composition on these particular systems. In order to better compare quantitative results of this kind of activity measurements, we addressed the relative orientation of the enzymes in liposomes, a parameter which had been neglected so far but is assumed to have major effects on the system. In this thesis (see Chapter 4.1), we have

developed a novel assay to rapidly estimate the relative orientation of membrane proteins in liposomes on the basis of site-specific fluorescent labeling of a membrane protein of interest with subsequent reconstitution and sequential quenching of the two orientation populations by a membrane-impermeable quencher. Although the method requires designing of suitable single-cysteine mutants and subsequent labeling, once this is established, the procedure displays a powerful method to estimate the orientation of membrane proteins. A major advantage of the here developed method is its independence of the membrane protein's function, enabling its use also for structural proteins. It is compatible with many downstream experiments and can easily be performed in advance.

On the basis of this method, we have identified a strong lipid-dependent orientation of bo_3 oxidase in liposomes with decreasing fraction of inside-out orientation (~35 %) in net negatively charged compared to uncharged liposomes (~60 %). As elucidated in chapter 4.2, the observed lipid dependency seems to be caused by electrostatic-mediated insertion of bo_3 oxidase into the lipid bilayer during reconstitution. Electrostatic interactions affecting orientation of a target membrane protein have been previously reported for various membrane proteins [110,245,246], indicating that charge-mediated reconstitution seems to be a general phenomenon. Unpredictable orientation of bo_3 oxidase (and other membrane proteins) affects functional measurements (e.g. the two orientation populations canceling out each other's *pmf*), illustrating impressively the potential impact of non-biological effects on *in vitro* measurements. In order to obtain quantitative results with such proteins, the orientation either has to be rigorously determined in advance (what however does not consequently rule out complicated data analysis) or reconstitution protocols yielding uniform orientation have to be established.

Several approaches have been described to unidirectionally orient membrane proteins in liposomes in literature. Exemplarily, it was possible to increase insertion of proteorhodopsin in the desired orientation when changing the lipid composition [133], however, this method is not suitable if the impact of different lipid compositions is at the core of the investigation. In another approach, unidirectional insertion in the desired orientation was increased through immobilization of His-tagged protein on Ni-NTA-functionalized beads, followed by *de novo* formation of a lipid bilayer around the beads to achieve proteo-lipobeads [106,140,269]. However, it will not be possible to remove the beads after reconstitution which is likely to influence membrane properties such as tightness, an indispensable necessity for investigations on ion pumps. Alternatively, fusion of a soluble unit (GFP or mCherry) to the small protein proteorhodopsin (~ 25 kDa) resulted in successfully guided unidirectional insertion into liposomes since the more hydrophobic part of the protein enters the membrane first, rendering the hydrophilic fusion domain outside of the liposomes. Although the fusion of GFP or mCherry might be too small to guide unidirectional orientation with respect to the size of the multi-subunit complex bo_3 oxidase (~150 kDa), the general principle is expected to be applicable if a larger hydrophilic domain is used. However, fusion

of a sufficiently large domain to a multi-subunit protein with a delicate assembly process [270] is expected to affect protein expression and folding negatively. In addition, bacterial expression of very large proteins is rare [271]. Therefore, an approach in which the soluble domain could be added post-translationally or *in vitro* would be more elegant and promising. A former PhD student in our lab, Dr. Andrea Amati, approached coupling of a large soluble domain to membrane proteins by various strategies. One of the most promising approaches was coupling via SpyTag/SpyCatcher. Using this strategy, together with a former master student Stefan Moning, he was able to unidirectionally insert proteorhodopsin into liposomes. For this reason, we used the Spy system to couple *bo₃* oxidase with the soluble unit MBPx (consisting of two copies of MBP and a SpyCatcher domain, resulting in a soluble ~95 kDa protein). As shown in chapter 4.3, while we have not achieved unidirectional and lipid-independent orientation with this method, preliminary experiments indicated a strong effect of the soluble unit on membrane protein orientation. This approach will be improved in near future. When considering the sizes of *bo₃* oxidase and MBPx (~150 kDa vs ~100 kDa), the soluble fraction is less than 50 % of the coupled construct. It seems obvious and intuitive to get a correlation between the size of the hydrophilic domain and membrane protein orientation. For that reason, a further goal will be to increase the fraction, e.g. using hydrophilic $\alpha_3\beta_3\gamma\varepsilon$ from the F_1 part of ATP synthase (>300 kDa) which has around double the size of *bo₃* oxidase. In other words, the larger the soluble unit, the better the orientation we would expect.

Further approaches to guide more unidirectional orientation could involve reconstitution in presence of high salt concentrations in order to reduce electrostatic-mediated insertion. While this e.g. increased the inside-out orientation of *bo₃* oxidase in anionic liposomes (see Chapter 4.2), however, unidirectional orientation was not achieved. Furthermore, this approach is not suitable when reconstituting into uncharged liposomes. It might thus especially be useful when unidirectional orientation is not mandatory for an experiment, but rather the orientation needs to be comparable in different liposomes. In case the lipid composition does not matter for downstream experiments, but the orientation should be enhanced, the use of positively charged lipids (e.g. DOTAP or EPC) might provide a powerful approach. Protonable lipids (e.g. DODAP) which are positively charged only at low pH but neutral at pH 7 might be of particular interest as they avoid unnaturally positively charged membrane surfaces during measurements. Similarly, the positive charge of DOTAP liposomes could be neutralized when the liposomes are fused with negatively charge liposomes after reconstitution via charge-mediated fusion [236]. Moreover, Knol et al. [124] showed a clear difference in the orientation of LacS when they reconstituted with DDM compared to Triton X-100. The authors observed that the two nonionic detergents behaved completely differently during solubilization of liposomes. While Triton X-100 maintained the liposomal structure even at concentrations beyond the onset of solubilization, DDM disrupted liposomes already at the onset of solubilization. LacS ended up to be oriented more unidirectionally with Triton X-100 than

with DDM with the hydrophilic part of the protein exposed to the outside, which was assumed to arise from different lipid-detergent structures formed with the two different detergents. In other words, while the hydrophilic part of LacS is unfavorable to penetrate the membrane and predominantly stays outside liposomes treated with Triton X-100 (leading to more unidirectional insertion into liposomes), lost integrity of the liposomes after DDM treatment leads to the insertion of LacS into the lipid bilayer from both surfaces (resulting in random orientation). Although this does not provide a generally applicable method to unidirectionally insert membrane proteins in the desired orientation (e.g. bo_3 oxidase has a larger soluble fraction at the side to be inserted into liposomes) it is important to understand the impact detergents can have on reconstitution and orientation. This will be of particular interest when applying the above-mentioned method of coupling a large soluble unit to a membrane protein to guide unidirectional orientation (e.g. to avoid MBPs in the construct bo_3-MBPx to penetrate the membrane).

The effect of lipids on proton coupling

Nilsson et al. did not observe an effect of the lipid head group on the individual activities of bo_3 oxidase and ATP synthase if coreconstituted into liposomes [1]. However, the authors provided experimental evidence that proton coupling between the two enzymes is highly impaired by negative charges of the lipid head groups, indicating an effect of the lipid composition either on lateral proton transfer rate or on the lateral distance between bo_3 oxidase and ATP synthase. For the investigation of the latter, we intended to reversibly link the two enzymes mechanically fixing the lateral distance between them.

The Spy system is a powerful tool for coupling two proteins or protein complexes, as the reactive parts can be introduced genetically and a covalent bond is formed, but several parameters have to be taken into account. First, although coupling efficiency is typically high, it might be impeded by several factors (e.g. detergent or other buffer components, steric hindrance, or low accessibility of SpyTag). In order to evaluate the afore-mentioned parameters as well as to prove the reaction, a method to monitor coupling efficiency during experiments is desirable. While SDS-PAGE is the preferred method to choose when coupling small and single-subunit proteins, complex band patterns and overlapping bands of different subunits prevent detection of disappearing and appearing bands of coupling educts and products, respectively, via SDS-PAGE if multi-subunit protein complexes are coupled. Coupling of structurally sophisticated proteins like the respiratory complexes used in this thesis thus requests other methods, for instance Western Blotting or fluorescent labeling of the subunits to couple. While mass spectrometry might display another possibility to prove coupling efficiency, sample complexity might increase as well with increasing number of different subunits, leading to complicated data analysis.

Depending on the application in downstream experiments, it is further essential to separate products from unreacted educts. A common way to separate proteins is via gel filtration. However, the separation of large protein complexes via gel filtration usually is a finicky process due to low peak resolution,

often resulting in non-quantitative separation of large complexes. Alternatively, affinity tags could be employed for the separation of unreacted educts. In case the same tag is present in both educts, such as e.g. the widely-used His-tag, the strategy is only useful when the tag was removed from one of the educts before coupling. This process, however, increases the number of experimental steps, typically leading to reduced product yield. More elegantly, Irsyad et al. recently presented Spy&Go purification [202], in which the non-reactive but still SpyTag-affine SpyDock protein is coupled to agarose beads enabling quantitative elimination of unreacted SpyTag-fused protein. In case the coupling reaction was performed with an excess of SpyTag protein (assuming that all SpyCatcher had reacted), this approach illustrates a good method to achieve pure coupled product.

However, during the time frame of this thesis, it was not possible to achieve a pure stoichiometric coupling product of bo_3 oxidase and ATP synthase, and it remains a future goal to investigate the effect of the lateral enzyme distance on proton coupling. However, once achieved, the construct will not only fix the initial distance between the two proteins but is also likely to suppress lipid-dependent orientation of bo_3 oxidase due to the large soluble domain of the ATP synthase. This assumption, however, has to be proven experimentally based on orientation determination measurements. Nevertheless, we would expect that coupling with ATP synthase might have a positive influence on bo_3 oxidase orienting in desired inside-out orientation supported by the ATP synthase.

The covalent coupling of two (membrane) proteins via the SpyTag/Catcher technology is also interesting for the investigation of proteins beyond respiratory enzymes. The comparison of a coupled proton pump and a secondary transporter that is driven by the proton motive force with the free floating individual enzymes will yield powerful insights. Spatial proximity of V-ATPase and Na^+/H^+ antiporter has been described to be important e.g. for proper functioning of pH homeostasis in endosomes [272].

Cleavage of bo_3 oxidase-ATP synthase *in situ* will reveal the actual impact of the distance, both in the presence and absence of negatively charged lipids. Theoretically, a lipid-dependent change in proton coupling between bo_3 oxidase and ATP synthase displays a suitable mechanism by which a cell can regulate ATP production via oxidative phosphorylation by altering interactions between primary proton pumps and ATP synthase rather than by modulating the activity of the individual enzymes [1]. Given the high dynamics and rapid changes in membrane lipid composition, this mechanism might provide a convenient way of ATP synthesis regulation. On the other hand, our highly simplified respiratory mimicking system does not reflect physiological conditions well with regard to enzyme density and the consequent limitations have to be considered. The enzyme density in liposomes is very low (protein:lipid ratio ≈ 1:25) compared to living cells, where respiratory enzymes are tightly packed (protein:lipid ratio ≈ 1:0.25 in the inner mitochondrial membrane [273]). The chance of a proton ejected from a primary proton pump to reach an ATP synthase molecule *in vivo* is thus extremely high, especially when concerning the 80

nm distance, in which lateral proton transfer is deasible to occur [193]. Additionally, the requirement of negatively charged lipids like e.g. the special lipid cardiolipin for efficient respiratory coupling [274] counters the physiological role of the lipid dependency observed *in vitro*. Nevertheless, only such *in vitro* experiments are able to identify possible mechanistic details like lateral proton transfer, while observation is suppressed in *in vivo* systems by the high protein density. The necessity of negatively charged lipids as observed in all membranes but especially respiratory membranes was also reflected in our experiments with NDH-2 in Chapter 4.2, a membrane-associated NADH dehydrogenase, that requires negatively charged lipids to efficiently reduce ubiquinone.

So far, only effects by changing the lipid head groups were investigated. Perspective experiments should also focus on the impact of the acyl chain on proton coupling between the two enzymes as well as on other biological and artificial effects. Similarly, the influence of other physiochemical properties (e.g. membrane curvature or membrane fluidity) on proton coupling might be interesting.

Coupling of bo_3 oxidase and ATP synthase might provide further advantages irrespective of the above-mentioned application of investigating a possible link between enzyme distance and proton coupling. A special interest of our group is the bottom-up construction of a complete respiratory chain, where the individually purified enzymes are coreconstituted into the same mimicking membrane system (e.g. liposomes or GUVs). Reversible coupling of the enzymes would provide an efficient method to achieve stoichiometric reconstitution, which would be crucial for quantitative downstream investigations of respiratory processes. Furthermore, it will provide a possibility to achieve coreconstitution of the two enzymes in nanodiscs in a 1:1 ratio. This experimental setup would allow to investigate lateral proton transfer along the membrane surface as nanodiscs do not provide a closed compartment [92] and coupled ATP synthesis therefore is expected to occur only in case of an existing lateral proton transfer. Additionally, since the crosslink is chosen to be present on the outside of liposomes after reconstitution, it might also help to orient bo_3 oxidase in the desired inside-out orientation due to the high fraction of inside-out oriented ATP synthase.

6 Curriculum vitae

Personal information

Name	**Sabina Deutschmann**
Date of birth	**23.09.1992**
Nationality	**Swiss**
Email address	**sabina.deutschmann@gmx.ch**
Address	**Bahnhofstrasse 6, 3114 Wichtrach**

Education

02.2017-12.2021 **PhD of Science in Biochemistry and Molecular Biology**

University of Bern
Department of Chemistry, Biochemistry and Pharmaceutical Sciences

Supervisor: Prof. Dr. Christoph von Ballmoos

"The importance of lipids on oxidative phosphorylation"

09.2014-04.2016 **Master of Science in Molecular Life Sciences, Biochemistry**

University of Bern
Department of Chemistry and Biochemistry

Supervisor: Prof. Dr. Christoph von Ballmoos

"The ATP synthase from *Vibrio cholerae* – the missing link between proton and sodium bioenergetics?"

09.2011-08.2014 **Bachelor of Science in Biochemistry and Molecular Biology**

University of Bern
Department of Chemistry and Biochemistry

2007-2011 **Matura with specialization in Languages (Spanish)**

Kantonsschule Olten

2005-2007	**Secondary school** Schönenwerd
1999-2005	**Primary school** Gretzenbach

Experiences in teaching

- Supervision of basic chemistry practical course of first year bachelor students
- Repeated organization and supervision of biochemistry practical course II for third year bachelor students (purification and characterization of a membrane protein)
- Supervision of three bachelor and two master students
- Co-supervision of a first-year apprentice as chemical lab technician

List of publications

- Andrea Marco Amati, Simone Graf, **Sabina Deutschmann**, Nicolas Dolder, Christoph von Ballmoos. "Current problems and future avenues in proteoliposome research." *Biochemical Society transactions* **48**, 1473-1492 (2020). doi:10.1042/BST20190966
- **Sabina Deutschmann**, Lukas Rimle, Christoph von Ballmoos. "Rapid Estimation of Membrane Protein Orientation in Liposomes." *ChemBioChem* **22***, (2021)* doi:10.1002/cbic.202100543

7 Declaration of Originality

Last name, first name: Deutschmann Sabina

Matriculation number: 11-102-415

I hereby declare that this thesis represents my original work and that I have used no other sources except as noted by citations.

All data, tables, figures and text citations which have been reproduced from any other source, including the internet, have been explicitly acknowledged as such.

I am aware that in case of non-compliance, the Senate is entitled to withdraw the doctorate degree awarded to me on the basis of the present thesis, in accordance with the "Statut der Universität Bern (Universitätsstatut; UniSt)", Art. 69, of 7 June 2011

Place, date

Bern, 10.12.2021

Signature

S. Deutschmann

8 Literature

1. Nilsson, T. *et al.* Lipid-mediated Protein-protein Interactions Modulate Respiration-driven ATP Synthesis. *Sci. Rep.* **6**, 24113 (2016).
2. Nelson, D. L. & Cox, M. M. *Lehninger Principles of Biochemistry 6th Edition*. (2013).
3. Edidin, M. Lipids on the frontier: A century of cell-membrane bilayers. *Nat. Rev. Mol. Cell Biol.* **4**, 414–418 (2003).
4. Gupta, S. & Ashkar, R. The dynamic face of lipid membranes. *Soft Matter* **17**, 6910–6928 (2021).
5. Honigmann, A. & Pralle, A. Compartmentalization of the Cell Membrane. *J. Mol. Biol.* **428**, 4739–4748 (2016).
6. Singer, S. J. & Nicolson, G. L. The fluid mosaic model of the structure of cell membranes. *Science (80-.).* **175**, 720–731 (1972).
7. Regen, S. L. The Origin of Lipid Rafts. *Biochemistry* **59**, 4617–4621 (2020).
8. Cooper, G. The Cell: A Molecular Approach. 2nd edition. https://www.ncbi.nlm.nih.gov/books/NBK9896/ (2000).
9. Strasser, C., Grote, P., Schäuble, K., Ganz, M. & Ferrando-May, E. Regulation of nuclear envelope permeability in cell death and survival. *Nucl. (United States)* **3**, 540–551 (2012).
10. Mitchell, P. Coupling of phosphorylation to electron and hydrogen transfer by a chemi-osmotic type of mechanism. *Nature* **191**, 144–148 (1961).
11. Harayama, T. & Riezman, H. Understanding the diversity of membrane lipid composition. *Nat. Rev. Mol. Cell Biol.* **19**, 281–296 (2018).
12. Van Meer, G., Voelker, D. R. & Feigenson, G. W. Membrane lipids: Where they are and how they behave. *Nat. Rev. Mol. Cell Biol.* **9**, 112–124 (2008).
13. Uphoff, A., Hermansson, M., Haimi, P. & Somerharju, P. *Analysis of complex lipidomes*. *Medical Applications of Mass Spectrometry* (Elsevier B.V., 2008). doi:10.1016/B978-044451980-1.50013-6.
14. Paradies, G., Paradies, V., De Benedictis, V., Ruggiero, F. M. & Petrosillo, G. Functional role of cardiolipin in mitochondrial bioenergetics. *Biochim. Biophys. Acta - Bioenerg.* **1837**, 408–417 (2014).
15. Dowhan, W., Bogdanov, M. & Mileykovskaya, E. *Functional Roles of Lipids in Membranes*. *Biochemistry of Lipids, Lipoproteins and Membranes: Sixth Edition* (Elsevier, 2016). doi:10.1016/B978-0-444-63438-2.00001-8.
16. Zhang, Y. & Rock, C. O. Membrane lipid homeostasis in bacteria. **6**, 222–233 (2008).
17. Marr, A. G. & Ingraham, J. L. Effect of temperature on the composition of fatty acids in total lipids and phospholipids of entomopathogenic nematodes. *J. Bacteriol.* **84,6**, 1260–1267 (1962).
18. van 't Klooster, J. S. *et al.* Membrane Lipid Requirements of the Lysine Transporter Lyp1 from Saccharomyces cerevisiae. 4023–4031 (2020) doi:10.1016/j.jmb.2020.04.029.
19. Jouhet, J. Importance of the hexagonal lipid phase in biological membrane organization. *Front. Plant Sci.* **4**, 1–5 (2013).
20. Linke, D. *Detergents : An Overview*. *Methods in Enzymology* vol. 463 (Elsevier Inc., 2009).
21. Seddon, A. M., Curnow, P. & Booth, P. J. Membrane proteins, lipids and detergents: Not just a soap opera. *Biochim. Biophys. Acta - Biomembr.* **1666**, 105–117 (2004).
22. Privé, G. G. Detergents for the stabilization and crystallization of membrane proteins. *Methods* **41**, 388–397 (2007).
23. Orwick-Rydmark, M., Arnold, T. & Linke, D. *The use of detergents to purify membrane proteins*. *Current Protocols in Protein Science* vol. 2016 (2016).
24. Mooney, R. A. Use of Digitonin-Permeabilized Adipocytes for cAMP Studies. *Methods Enzymol.* **159**, 193–

202 (1988).

25. Birch, J. *et al.* The fine art of integral membrane protein crystallisation. **147**, 150–162 (2018).

26. Yeh, V., Goode, A. & Bonev, B. B. Membrane Protein Structure Determination and Characterisation by Solution and Solid-State NMR. 1–23 (2020).

27. Johnson, J. E. & Cornell, R. B. Amphitropic proteins : regulation by reversible membrane interactions. **16**, 217–235 (1999).

28. Cornell, R. B. & Ridgway, N. D. CTP:phosphocholine cytidylyltransferase: Function, regulation, and structure of an amphitropic enzyme required for membrane biogenesis. *Prog. Lipid Res.* **59**, 147–171 (2015).

29. Krogh, A., Larsson, B., Von Heijne, G. & Sonnhammer, E. L. L. Predicting transmembrane protein topology with a hidden Markov model: Application to complete genomes. *J. Mol. Biol.* **305**, 567–580 (2001).

30. Shimizu, K., Cao, W., Saad, G., Shoji, M. & Terada, T. Comparative analysis of membrane protein structure databases. *BBA - Biomembr.* **1860**, 1077–1091 (2018).

31. White, S. https://blanco.biomol.uci.edu/mpstruc/ (25.11.2021).

32. https://www.rcsb.org/stats/growth/growth-released-structures (25.11.2021).

33. Klöpfer, K. & Hagn, F. Beyond detergent micelles: The advantages and applications of non-micellar and lipid-based membrane mimetics for solution-state NMR. **115**, 271–283 (2019).

34. Yin, H. & Flynn, A. D. Drugging Membrane Protein Interactions. *Annu. Rev. Biomed. Eng.* **18**, 51–76 (2016).

35. Nicholls, D. G. & Ferguson, S. J. *Bioenergetics 4*. (2013).

36. Otrin, L. *et al.* Artificial Organelles for Energy Regeneration. *Adv. Biosyst.* **3**, 1800323 (2019).

37. Collins, M. D. & Jones, D. Distribution of isoprenoid quinone structural types in bacteria and their taxonomic implications. *Microbiol. Rev.* **45**, 316–354 (1981).

38. Unden, G. & Dünnwald, P. The Aerobic and Anaerobic Respiratory Chain of Escherichia coli and Salmonella enterica : Enzymes and Energetics. (2008) doi:10.1128/ecosalplus.3.2.2.

39. Erhardt, H. *et al.* Organization of the Escherichia coli aerobic enzyme complexes of oxidative phosphorylation in dynamic domains within the cytoplasmic membrane. *Microbiologyopen* **3**, 316–326 (2014).

40. Unden, G. & Bongaerts, J. Alternative respiratory pathways of Escherichia coli: energetics and transcriptional regulation in response to electron acceptors. *Biochim. Biophys. Acta* **1320**, 217–234 (1997).

41. Heikal, A. *et al.* Structure of the bacterial type II NADH dehydrogenase: A monotopic membrane protein with an essential role in energy generation. *Mol. Microbiol.* **91**, 950–964 (2014).

42. Krishna, K. V. & Mohan, S. V. Purification and characterization of NDH-2 protein and elucidating its role in extracellular electron transport and bioelectrogenic activity. *Front. Microbiol.* **10**, 1–12 (2019).

43. Lencina, A. M. *et al.* Type 2 NADH dehydrogenase is the only point of entry for electrons into the Streptococcus agalactiae respiratory chain and is a potential drug target. *MBio* **9**, e01034-18 (2018).

44. Villegas, J. M., Volentini, S. I., Rintoul, M. R. & Rapisarda, V. A. Amphipathic C-terminal region of Escherichia coli NADH dehydrogenase-2 mediates membrane localization. *Arch. Biochem. Biophys.* **505**, 155–159 (2011).

45. Kerscher, S., Dröse, S., Zickermann, V. & Brandt, U. *The Three Families of Respiratory NADH Dehydrogenases. In: Schäfer G., Penefsky H.S. (eds) Bioenergetics. Results and Problems in Cell Differentiation*. *Morskoy Sbornik* vol. 11 (2007).

46. Feng, Y. *et al.* Structural insight into the type-II mitochondrial NADH dehydrogenases. *Nature* **491**, 478–482 (2012).

47. Iwata, M. *et al.* The structure of the yeast NADH dehydrogenase (Ndi1) reveals overlapping binding sites for water- and lipid-soluble substrates. *Proc. Natl. Acad. Sci. U. S. A.* **109**, 15247–15252 (2012).

48. Petri, J. *et al.* Structure of the NDH-2 – HQNO inhibited complex provides molecular insight into quinone-binding site inhibitors. *Biochim. Biophys. Acta - Bioenerg.* **1859**, 482–490 (2018).

49. Sena, F. V. *et al.* Type-II NADH:Quinone oxidoreductase from Staphylococcus aureus has two distinct binding sites and is rate limited by quinone reduction. *Mol. Microbiol.* **98**, 272–288 (2015).

50. Yang, Y. *et al.* Target Elucidation by Cocrystal Structures of NADH-Ubiquinone Oxidoreductase of Plasmodium falciparum (PfNDH2) with Small Molecule To Eliminate Drug-Resistant Malaria. *J. Med. Chem.* **60**, 1994–2005 (2017).

51. Hanukoglu, I. Proteopedia: Rossmann fold: A beta-alpha-beta fold at dinucleotide binding sites. *Biochem. Mol. Biol. Educ.* **43**, 206–209 (2015).

52. Blaza, J. N. *et al.* The mechanism of catalysis by type-II NADH:quinone oxidoreductases. *Sci. Rep.* **7**, 1–11 (2017).

53. Rapisarda, V. A. *et al.* Evidence for Cu(I)-thiolate ligation and prediction of a putative copper-binding site in the Escherichia coli NADH dehydrogenase-2. *Arch. Biochem. Biophys.* **405**, 87–94 (2002).

54. Schmid, R. & Gerloff, D. L. Functional properties of the alternative NADH:ubiquinone oxidoreductase from E. coli through comparative 3-D modelling. *FEBS Lett.* **578**, 163–168 (2004).

55. Sousa, F. L. *et al.* The superfamily of heme – copper oxygen reductases: Types and evolutionary considerations. *BBA - Bioenerg.* **1817**, 629–637 (2012).

56. Lee, H. J., Reimann, J., Huang, Y. & Ädelroth, P. Functional proton transfer pathways in the heme – copper oxidase superfamily. *BBA - Bioenerg.* **1817**, 537–544 (2012).

57. Chepuri, V., Lemieux, L., Au, D. C. T. & Gennis, R. B. The sequence of the cyo operon indicates substantial structural similarities between the cytochrome o ubiquinol oxidase of Escherichia coli and the aa3-type family of cytochrome c oxidases. *J. Biol. Chem.* **265**, 11185–11192 (1990).

58. Musser, S. M., Stowell, M. H. B. & Chan, S. I. Comparison of ubiquinol and cytochrome c terminal oxidases. *FEBS Lett.* **327**, 131–136 (1993).

59. Abramson, J. *et al.* The structure of the ubiquinol oxidase from Escherichia coli and its ubiquinone binding site. *Nat. Struct. Biol.* **7**, 910–917 (2000).

60. Berg, J., Block, S., Höök, F. & Brzezinski, P. Single Proteoliposomes with E. coli Quinol Oxidase: Proton Pumping without Transmembrane Leaks. *Isr. J. Chem.* **57**, 437–445 (2017).

61. Iwata, S., Ostermeier, C., Ludwig, B. & Michel, H. Structure at 2.8 Å resolution of cytochrome c oxidase from paracoccus denitrificans. *Nature* **376**, 660–669 (1995).

62. Su, C.-C. *et al.* A 'Build and Retrieve' methodology to simultaneously solve cryo-EM structures of membrane proteins. *Nat. Methods* **18**, 69–75 (2021).

63. Choi, S. K., Lin, M. T., Ouyang, H. & Gennis, R. B. Searching for the low affinity ubiquinone binding site in cytochrome bo3 from Escherichia coli. *Biochim. Biophys. Acta - Bioenerg.* **1858**, 366–370 (2017).

64. Choi, S. K. *et al.* Location of the Substrate Binding Site of the Cytochrome bo3 Ubiquinol Oxidase from Escherichia coli. *J. Am. Chem. Soc.* **139**, 8346–8354 (2017).

65. Yap, L. L. *et al.* The quinone-binding sites of the cytochrome bo3 ubiquinol oxidase from Escherichia coli. *Biochim. Biophys. Acta - Bioenerg.* **1797**, 1924–1932 (2010).

66. Xu, J. *et al.* Structure of the cytochrome aa3-600 heme-copper menaquinol oxidase bound to inhibitor HQNO shows TM0 is part of the quinol binding site. *Proc. Natl. Acad. Sci. U. S. A.* **117**, 872–876 (2020).

67. Von Ballmoos, C., Wiedenmann, A. & Dimroth, P. Essentials for ATP synthesis by F1F0 ATP synthases. *Annu. Rev. Biochem.* **78**, 649–672 (2009).

68. Walker, J. E. ATP Synthesis by Rotary Catalysis. (1962).

69. Walker, J. E. The ATP synthase: The understood, the uncertain and the unknown. *Biochem. Soc. Trans.* **41**, 1–16 (2013).

70. Guo, H., Suzuki, T. & Rubinstein, J. L. Structure of a bacterial ATP synthase. *Elife* **8**, 1–17 (2019).

71. Watt, I. N., Montgomery, M. G., Runswick, M. J., Leslie, A. G. W. & Walker, J. E. Bioenergetic cost of making an adenosine triphosphate molecule in animal mitochondria. *Proc. Natl. Acad. Sci. U. S. A.* **107**, 16823–16827 (2010).

72. Sobti, M. *et al.* Cryo-EM structures provide insight into how E. coli F1Fo ATP synthase accommodates symmetry mismatch. *Nat. Commun.* **11**, 2615 (2020).

73. Kaila, V. R. I. & Wikström, M. Architecture of bacterial respiratory chains. *Nat. Rev. Microbiol.* **19**, 319–330 (2021).

74. Kühlbrandt, W. & Davies, K. M. Rotary ATPases: A New Twist to an Ancient Machine. *Trends Biochem. Sci.* **41**, 106–116 (2015).

75. Allegretti, M. *et al.* Horizontal membrane-intrinsic α-helices in the stator a-subunit of an F-type ATP synthase. (2015) doi:10.1038/nature14185.

76. Chu, A., Zirngibl, R. A. & Manolson, M. F. The V-ATPase a3 subunit: Structure, function and therapeutic potential of an essential biomolecule in osteoclastic bone resorption. *Int. J. Mol. Sci.* **22**, 6934 (2021).

77. Zhao, J., Benlekbir, S. & Rubinstein, J. L. Electron cryomicroscopy observation of rotational states in a eukaryotic V-ATPase. *Nature* **521**, 241–245 (2015).

78. Kühlbrandt, W. Structure and Mechanisms of F-type ATP synthases. *Annu Rev Biochem.* **88**, 515–549 (2019).

79. Jang, S. & Javadov, S. Current Challenges in Elucidating Respiratory Supercomplexes in Mitochondria: Methodological Obstacles. *Front. Physiol.* **9**, 238 (2018).

80. Stroh, A. *et al.* Assembly of Respiratory Complexes I, III, and IV into NADH Oxidase Supercomplex Stabilizes Complex I in Paracoccus denitrificans. *J. Biol. Chem.* **279**, 5000–5007 (2004).

81. Fedotovskaya, O. *et al.* Identification of a cytochrome bc1-aa3 supercomplex in Rhodobacter sphaeroides. *Biochim. Biophys. Acta - Bioenerg.* **1862**, 148433 (2021).

82. Magalon, A. & Alberge, F. Distribution and dynamics of OXPHOS complexes in the bacterial cytoplasmic membrane. *Biochim. Biophys. Acta - Bioenerg.* **1857**, 198–213 (2016).

83. Renner, L. D. & Weibel, D. B. Cardiolipin microdomains localize to negatively curved regions of Escherichia coli membranes. *Proc. Natl. Acad. Sci. U. S. A.* **108**, 6264–6269 (2011).

84. Llorente-Garcia, I. *et al.* Single-molecule in vivo imaging of bacterial respiratory complexes indicates delocalized oxidative phosphorylation. *Biochim. Biophys. Acta - Bioenerg.* **1837**, 811–824 (2014).

85. Amati, A. M., Graf, S., Deutschmann, S., Dolder, N. & von Ballmoos, C. Current problems and future avenues in proteoliposome research. *Biochem. Soc. Trans.* **48**, 1473–1492 (2020).

86. Racker, E. & Stoeckenius, W. Reconstitution of purple membrane vesicles catalyzing light-driven proton uptake and adenosine triphosphate formation. *J. Biol. Chem.* **249**, 662–3 (1974).

87. Rigaud, J. L., Pitard, B. & Levy, D. Reconstitution of membrane proteins into liposomes: application to energy-transducing membrane proteins. *BBA* **1231**, 223–246 (1995).

88. Laubinger, W. & Dimroth, P. Characterization of the ATP Synthase of Propionigenium modesturn as a Primary Sodium Pump. *Biochemistry* **27**, 7531–7537 (1988).

89. Etemadi, A. H. *Functional and orientational features of protein molecules in reconstituted lipid membranes. Advances in lipid research* vol. 21 (ACADEMIC PRESS, INC., 1985).

90. Skrzypek, R., Iqbal, S. & Callaghan, R. Methods of reconstitution to investigate membrane protein function. *Methods* **147**, 126–141 (2018).

91. Rigaud, J.-L. & Lévy, D. Reconstitution of Membrane Proteins into Liposomes. in *Methods Enzymol.* vol. 372 65–86 (2003).

92. Shen, H. H., Lithgow, T. & Martin, L. L. Reconstitution of membrane proteins into model membranes: Seeking better ways to retain protein activities. *Int. J. Mol. Sci.* **14**, 1589–1607 (2013).

93. Degrip, W. J., Vanoostrum, J. & Bovee-Geurts, P. H. M. Selective detergent-extraction from mixed

detergent/lipid/protein micelles, using cyclodextrin inclusion compounds: A novel generic approach for the preparation of proteoliposomes. *Biochem. J.* **330**, 667–674 (1998).

94. Geertsma, E. R., Nik Mahmood, N. A. B., Schuurman-Wolters, G. K. & Poolman, B. Membrane reconstitution of ABC transporters and assays of translocator function. *Nat. Protoc.* (2008) doi:10.1038/nprot.2007.519.

95. Hatzi, P., Mourtas, S., G. Klepetsanis, P. & Antimisiaris, S. G. Integrity of liposomes in presence of cyclodextrins: Effect of liposome type and lipid composition. *Int. J. Pharm.* **333**, 167–176 (2007).

96. Knol, J. PhD-Thesis - Membrane Reconstitution and Functional Analysis of a Sugar Transport System. (1999).

97. Tsai, M. F. & Miller, C. Substrate selectivity in arginine-dependent acid resistance in enteric bacteria. *Proc. Natl. Acad. Sci. U. S. A.* **110**, 5893–5897 (2013).

98. van 't Klooster, J. S. *et al.* Membrane Lipid Requirements of the Lysine Transporter Lyp1 from Saccharomyces cerevisiae. *J. Mol. Biol.* **432**, 4023–4031 (2020).

99. Harris, N. J., Charalambous, K., Findlay, H. E. & Booth, P. J. Lipids modulate the insertion and folding of the nascent chains of alpha helical membrane proteins. *Biochem. Soc. Trans.* **46**, 1355–1366 (2018).

100. Martens, C. *et al.* Direct protein-lipid interactions shape the conformational landscape of secondary transporters. *Nat. Commun.* **9**, (2018).

101. Mirandela, G. Di., Tamburrino, G., Hoskisson, P. A., Zachariae, U. & Javelle, A. The lipid environment determines the activity of the Escherichia coli ammonium transporter AmtB. *FASEB J.* **33**, 1989–1999 (2019).

102. Vitrac, H., Mallampalli, V. K. P. S., Bogdanov, M. & Dowhan, W. The lipid-dependent structure and function of LacY can be recapitulated and analyzed in phospholipid-containing detergent micelles. *Sci. Rep.* **9**, (2019).

103. Dowhan, W., Vitrac, H. & Bogdanov, M. Lipid-Assisted Membrane Protein Folding and Topogenesis. *Protein J.* **38**, 274–288 (2019).

104. Von Ballmoos, C., Biner, O., Nilsson, T. & Brzezinski, P. Mimicking respiratory phosphorylation using purified enzymes. *Biochim. Biophys. Acta - Bioenerg.* **1857**, 321–331 (2016).

105. Öjemyr, L. N., Von Ballmoos, C., Faxén, K., Svahn, E. & Brzezinski, P. The membrane modulates internal proton transfer in cytochrome c oxidase. *Biochemistry* **51**, 1092–1100 (2012).

106. Schadauer, F. *et al.* Silica nanoparticles for the oriented encapsulation of membrane proteins into artificial bilayer lipid membranes. *Langmuir* **31**, 2511–2516 (2015).

107. Geiss, A. F. *et al.* Proteo-lipobeads to encapsulate cytochrome c oxidase from Paracoccus denitrificans. *J. Colloid Interface Sci.* **500**, 119–125 (2017).

108. Pols, T. *et al.* A synthetic metabolic network for physicochemical homeostasis. *Nat. Commun.* **10**, (2019).

109. Seigneuret, M. & Rigaud, J. L. Partial separation of inwardly pumping and outwardly pumping bacteriorhodopsin reconstituted liposomes by gel filtration. *FEBS Lett.* **228**, 79–84 (1988).

110. Huang, H. *et al.* Using fluorescence quenching titration to determine the orientation of a model transmembrane protein in mimic membranes. *Materials (Basel).* **12**, (2019).

111. Young, H. S., Rigaud, J. L., Lacapère, J. J., Reddy, L. G. & Stokes, D. L. How to make tubular crystals by reconstitution of detergent-solubilized Ca2+-ATPase. *Biophys. J.* **72**, 2545–2558 (1997).

112. Biner, O., Schick, T., Müller, Y. & von Ballmoos, C. Delivery of membrane proteins into small and giant unilamellar vesicles by charge-mediated fusion. *FEBS Lett.* **590**, 2051–2062 (2016).

113. Ishmukhametov, R. R., Russell, A. N. & Berry, R. M. A modular platform for one-step assembly of multi-component membrane systems by fusion of charged proteoliposomes. *Nat Commun* **7**, 13025 (2016).

114. Nordlund, G., Brzezinski, P. & Von Ballmoos, C. SNARE-fusion mediated insertion of membrane proteins into native and artificial membranes. *Nat. Commun.* **5**, 1–8 (2014).

115. Berg, J., Block, S., Höök, F. & Brzezinski, P. Single Proteoliposomes with E. coli Quinol Oxidase: Proton Pumping without Transmembrane Leaks. *Isr. J. Chem.* **57**, 437–445 (2017).

116. Li, M. *et al.* Single Enzyme Experiments Reveal a Long-Lifetime Proton Leak State in a Heme-Copper Oxidase. *J. Am. Chem. Soc.* **137**, 16055–16063 (2015).

117. Verkhovskaya, M. L. *et al.* Glutamic acid 286 in subunit I of cytochrome bo3 is involved in proton translocation. *Proc. Natl. Acad. Sci. U. S. A.* **94**, 10128–10131 (1997).

118. Krenn, B. E., Koppenaal, F., Van Walraven, H. S., Krab, K. & Kraayenhof, R. Co-reconstitution of the H+-ATP synthase and cytochrome b-563 c-554 complex from a thermophilic cyanobacterium. High ATP yield and mutual effects on the enzymatic activities. *BBA - Bioenerg.* **1140**, 271–281 (1993).

119. Lee, C. *et al.* A two-domain elevator mechanism for sodium/proton antiport. *Nature* **501**, 573–577 (2013).

120. Juge, N., Yoshida, Y., Yatsushiro, S., Omote, H. & Moriyama, Y. Vesicular glutamate transporter contains two independent transport machineries. *J. Biol. Chem.* **281**, 39499–39506 (2006).

121. Biner, O., Fedor, J. G., Yin, Z. & Hirst, J. Bottom-Up Construction of a Minimal System for Cellular Respiration and Energy Regeneration. *ACS Synth. Biol.* **9**, 1450–1459 (2020).

122. Uzdavinys, P. *et al.* Dissecting the proton transport pathway in electrogenic Na+/H+ antiporters. *Proc. Natl. Acad. Sci. U. S. A.* **114**, E1101–E1110 (2017).

123. Wiedenmann, A., Dimroth, P. & von Ballmoos, C. Δψ and ΔpH are equivalent driving forces for proton transport through isolated F0 complexes of ATP synthases. *Biochim. Biophys. Acta - Bioenerg.* **1777**, 1301–1310 (2008).

124. Knol, J., Sjollema, K. & Poolman, B. Detergent-mediated reconstitution of membrane proteins. *Biochemistry* **37**, 16410–16415 (1998).

125. Knol, J. *et al.* Unidirectional reconstitution into detergent-destabilized liposomes of the purified lactose transport system of Streptococcus thermophilus. *J. Biol. Chem.* **271**, 15358–15366 (1996).

126. Wang, L. & Sigworth, F. J. Structure of the BK potassium channel in a lipid membrane from electron cryomicroscopy. *Nature* **461**, 292–295 (2009).

127. Nomura, T., Cox, C. D., Bavi, N., Sokabe, M. & Martinac, B. Unidirectional incorporation of a bacterial mechanosensitive channel into liposomal membranes. *FASEB J.* **29**, 4334–4345 (2015).

128. Dixon, J. F. & Hokin, L. E. The reconstituted (Na,K)-ATPase is electrogenic. *J. Biol. Chem.* **255**, 10681–10686 (1980).

129. Hokin, L. E. & Dixon, J. F. Reconstitution of the Na,K-Pump by Freeze—thaw Sonication: Estimation of Coupling Ratio and Electrogenicity. *Methods Enzymol.* **156**, 141–155 (1988).

130. Santos, H. de L., Lopes, M. L., Maggio, B. & Ciancaglini, P. Na,K-ATPase reconstituted in liposomes: effects of lipid composition on hydrolytic activity and enzyme orientation. *Colloids Surfaces B Biointerfaces* **41**, 239–248 (2005).

131. Lee, K. Y. K. A. *et al.* Photosynthetic artificial organelles sustain and control ATP-dependent reactions in a protocellular system. *Nat. Biotechnol.* **36**, 530–535 (2018).

132. Happe, M., Teather, R. M., Overath, P., Knobling, A. & Oesterhelt, D. Direction of proton translocation in proteoliposomes formed from purple membrane and acidic lipids depends on the pH during reconstitution. *Biochim. Biophys. Acta - Biomembr.* **465**, 415–420 (1977).

133. Tunuguntla, R. *et al.* Lipid Bilayer Composition Can Influence the Orientation of Proteorhodopsin in Artificial Membranes. *Biophys. J.* **105**, 1388–1396 (2013).

134. Pfleger, N. *et al.* Solid-state NMR and functional studies on proteorhodopsin. *Biochim. Biophys. Acta - Bioenerg.* **1787**, 697–705 (2009).

135. Ritzmann, N. *et al.* Fusion Domains Guide the Oriented Insertion of Light-Driven Proton Pumps into Liposomes. *Biophys. J.* **113**, 1181–1186 (2017).

136. Rigaud, J. L., Paternostre, M. T. & Bluzat, A. Mechanisms of membrane protein insertion into liposomes during reconstitution procedures involving the use of detergents. 2. Incorporation of the light-driven

proton pump bacteriorhodopsin. *Biochemistry* **27**, 2677–2688 (1988).

137. RICHARD, P., RIGAUD, J.-L. & GRABER, P. Reconstitution of CF0F1 into liposomes using a new reconstitution procedure. *Eur. J. Biochem.* **193**, 921–925 (1990).

138. Lévy, D., Gulik, A., Bluzat, A. & Rigaud, J. L. Reconstitution of the sarcoplasmic reticulum Ca2+-ATPase: mechanisms of membrane protein insertion into liposomes during reconstitution procedures involving the use of detergents. *BBA - Biomembr.* **1107**, 283–298 (1992).

139. Eytan, G. D. Use of liposomes for reconstitution of biological functions. *BBA - Rev. Biomembr.* **694**, 185–202 (1982).

140. Zheng, H., Lee, S., Llaguno, M. C. & Jiang, Q.-X. bSUM: A bead-supported unilamellar membrane system facilitating unidirectional insertion of membrane proteins into giant vesicles. *J. Gen. Physiol.* **147**, 77–93 (2016).

141. Serdiuk, T. *et al.* YidC assists the stepwise and stochastic folding of membrane proteins. *Nat. Chem. Biol.* **12**, 911–917 (2016).

142. Serdiuk, T. *et al.* Insertion and folding pathways of single membrane proteins guided by translocases and insertases. *Sci. Adv.* **5**, 1–11 (2019).

143. Zhang, M., Mileykovskaya, E. & Dowhan, W. Cardiolipin Is Essential for Organization of Complexes III and IV into a Supercomplex in Intact Yeast Mitochondria. *J. Biol. Chem.* **280**, 29403–29408 (2005).

144. Arnarez, C., Marrink, S. J. & Periole, X. Molecular mechanism of cardiolipin-mediated assembly of respiratory chain supercomplexes. *Chem. Sci.* **7**, 4435–4443 (2016).

145. Mohraz, M. Reconstitution of Detergent-Solubilized Na,K-ATPase and Formation of Two-Dimensional Crystals. *J. Struct. Biol.* **125**, 76–85 (1999).

146. Cornelius, F. Modulation of Na,K-ATPase and Na-ATPase Activity by Phospholipids and Cholesterol. I. Steady-State Kinetics †. *Biochemistry* **40**, 8842–8851 (2001).

147. Abeywardena, M. Y., Allen, T. M. & Charnock, J. S. Lipid-protein interactions of reconstituted membrane-associated adenosinetriphosphatases. Use of a gel-filtration procedure to examine phospholipid-activity relationships. *Biochim. Biophys. Acta - Biomembr.* **729**, 62–74 (1983).

148. Cornelius, F., Turner, N. & Christensen, H. R. Z. Modulation of Na,K-ATPase by Phospholipids and Cholesterol. II. Steady-State and Presteady-State Kinetics †. *Biochemistry* **42**, 8541–8549 (2003).

149. Yeagle, P. L. & University of Connecticut, Storrs, CT, U. *The Membranes of Cells*. (2016).

150. Lichtenberg, D., Ahyayauch, H. & Goñi, F. M. The mechanism of detergent solubilization of lipid bilayers. *Biophysical Journal* vol. 105 289–299 (2013).

151. Marquardt, D., Geier, B. & Pabst, G. Asymmetric lipid membranes: towards more realistic model systems. *Membr.* **5**, 180–196 (2015).

152. Furse, S. & Scott, D. J. Three-Dimensional Distribution of Phospholipids in Gram Negative Bacteria. *Biochemistry* **55**, 4742–7 (2016).

153. Bogdanov, M. *et al.* Phospholipid distribution in the cytoplasmic membrane of Gram-negative bacteria is highly asymmetric, dynamic, and cell shape-dependent. *Sci. Adv.* **6**, eaaz6333 (2020).

154. Doktorova, M. *et al.* Preparation of asymmetric phospholipid vesicles for use as cell membrane models. *Nat. Protoc.* **13**, 2086–2101 (2018).

155. Markones, M. *et al.* Stairway to Asymmetry: Five Steps to Lipid-Asymmetric Proteoliposomes. *Biophys. J.* **118**, 294–302 (2020).

156. Althoff, T., Davies, K. M., Schulze, S., Joos, F. & Kühlbrandt, W. GRecon: A method for the lipid reconstitution of membrane proteins. *Angew. Chemie - Int. Ed.* **51**, 8343–8347 (2012).

157. Blum, T. B., Hahn, A., Meier, T., Davies, K. M. & Kühlbrandt, W. Dimers of mitochondrial ATP synthase induce membrane curvature and self-assemble into rows. *Proc. Natl. Acad. Sci. U. S. A.* **116**, 4250–4255 (2019).

158. Denisov, I. G., Schuler, M. A. & Sligar, S. G. Nanodiscs as a New Tool to Examine Lipid–Protein Interactions. in *Methods in Molecular Biology* vol. 2003 645–671 (2019).

159. Kariyazono, H. *et al.* Formation of stable nanodiscs by bihelical apolipoprotein A-I mimetic peptide. *J. Pept. Sci.* **22**, 116–122 (2016).

160. Carlson, M. L. *et al.* The Peptidisc, a simple method for stabilizing membrane proteins in detergent-free solution. *Elife* **7**, 1–23 (2018).

161. Angiulli, G. *et al.* New approach for membrane protein reconstitution into peptidiscs and basis for their adaptability to different proteins. *Elife* **9**, 1–20 (2020).

162. Smirnova, I. A. *et al.* Isolation of yeast complex IV in native lipid nanodiscs. *Biochim. Biophys. Acta - Biomembr.* **1858**, 2984–2992 (2016).

163. Dörr, J. M. *et al.* The styrene–maleic acid copolymer: a versatile tool in membrane research. *Eur. Biophys. J.* **45**, 3–21 (2016).

164. Dörr, J. M. *et al.* Detergent-free isolation, characterization, and functional reconstitution of a tetrameric K+ channel: The power of native nanodiscs. *Proc. Natl. Acad. Sci. U. S. A.* **111**, 18607–18612 (2014).

165. Parmar, M. J., Lousa, C. D. M., Muench, S. P., Goldman, A. & Postis, V. L. G. Artificial membranes for membrane protein purification, functionality and structure studies. *Biochem. Soc. Trans.* **44**, 877–882 (2016).

166. Broecker, J., Eger, B. T. & Ernst, O. P. Crystallogenesis of Membrane Proteins Mediated by Polymer-Bounded Lipid Nanodiscs. *Structure* **25**, 384–392 (2017).

167. Smirnova, I. A., Ädelroth, P. & Brzezinski, P. Extraction and liposome reconstitution of membrane proteins with their native lipids without the use of detergents. *Sci. Rep.* **8**, 14950 (2018).

168. Dutta, D., Esmaili, M., Overduin, M. & Fliegel, L. Expression and detergent free purification and reconstitution of the plant plasma membrane Na+/H+ antiporter SOS1 overexpressed in Pichia pastoris. *Biochim. Biophys. Acta - Biomembr.* **1862**, 183111 (2020).

169. Scheidelaar, S. *et al.* Effect of Polymer Composition and pH on Membrane Solubilization by Styrene-Maleic Acid Copolymers. *Biophys. J.* **111**, 1974–1986 (2016).

170. Liu, F., Lössl, P., Rabbitts, B. M., Balaban, R. S. & Heck, A. J. R. The interactome of intact mitochondria by cross-linking mass spectrometry provides evidence for coexisting respiratory supercomplexes. *Mol. Cell. Proteomics* **17**, 216–232 (2018).

171. Enríquez, J. A. Supramolecular Organization of Respiratory Complexes. *Annu. Rev. Physiol.* **78**, 533–561 (2016).

172. Brzezinski, P. New Structures Reveal Interaction Dynamics in Respiratory Supercomplexes. *Trends Biochem. Sci.* **45**, 3–5 (2020).

173. Rabe, M., Schwieger, C., Zope, H. R., Versluis, F. & Kros, A. Membrane Interactions of Fusogenic Coiled-Coil Peptides: Implications for Lipopeptide Mediated Vesicle Fusion. *Langmuir* **30**, 7724–7735 (2014).

174. Stengel, G., Zahn, R. & Höök, F. DNA-Induced Programmable Fusion of Phospholipid Vesicles. *J. Am. Chem. Soc.* **129**, 9584–9585 (2007).

175. Chan, Y. H., van Lengerich, B. & Boxer, S. G. Lipid-anchored DNA mediates vesicle fusion as observed by lipid and content mixing. *Biointerphases* **3**, FA17 (2008).

176. Marsden, H. R., Tomatsu, I. & Kros, A. Model systems for membrane fusion. *Chem. Soc. Rev.* **40**, 1572–1585 (2011).

177. Raschle, T., Lin, C., Jungmann, R., Shih, W. M. & Wagner, G. Controlled Co-reconstitution of Multiple Membrane Proteins in Lipid Bilayer Nanodiscs Using DNA as a Scaffold. *ACS Chem Biol* **10**, 2448–2454 (2015).

178. Pitard, B., Richard, P., Duñach, M., Girault, G. & Rigaud, J. L. ATP synthesis by the F0F1 ATP synthase from thermophilic Bacillus PS3 reconstituted into liposomes with bacteriorhodopsin 1. FActors defining the optimal reconstitution of ATP synthases with bacteriorhodopsin. *Eur. J. Biochem.* **235**, 769–778 (1996).

179. Faxén, K., Gilderson, G., Ädelroth, P. & Brzezinski, P. A mechanistic principle for proton pumping by cytochrome c oxidase. *Nature* **437**, 286–289 (2005).

180. Toth, A. *et al.* Kinetic coupling of the respiratory chain with ATP synthase, but not proton gradients, drives ATP production in cristae membranes. *Proc. Natl. Acad. Sci. U. S. A.* **117**, 2412–2421 (2020).

181. Krulwich, T. A. Alkaliphiles: 'basic' molecular problems of pH tolerance and bioenergetics. *Mol. Microbiol.* **15**, 403–410 (1995).

182. Ädelroth, P. & Brzezinski, P. Surface-mediated proton-transfer reactions in membrane-bound proteins. *Biochim. Biophys. Acta - Bioenerg.* **1655**, 102–115 (2004).

183. Mulkidjanian, A. Y., Cherepanov, D. A., Heberle, J. & Junge, W. Proton transfer dynamics at membrane/water interface and mechanism of biological energy conversion. *Biochem.* **70**, 251–256 (2005).

184. Sandén, T., Salomonsson, L., Brzezinski, P. & Widengren, J. Surface-coupled proton exchange of a membrane-bound proton acceptor. *Proc. Natl. Acad. Sci. U. S. A.* **107**, 4129–4134 (2010).

185. Serowy, S. *et al.* Structural proton diffusion along lipid bilayers. *Biophys. J.* **84**, 1031–1037 (2003).

186. Agmon, N. *et al.* Protons and Hydroxide Ions in Aqueous Systems. *Chem. Rev.* **116**, 7642–7672 (2016).

187. Medvedev, E. S. & Stuchebrukhov, A. A. Mechanism of long-range proton translocation along biological membranes. *FEBS Lett.* **587**, 345–349 (2013).

188. Mulkidjanian, A. Y., Heberle, J. & Cherepanov, D. A. Protons @ interfaces: Implications for biological energy conversion. *Biochim. Biophys. Acta - Bioenerg.* **1757**, 913–930 (2006).

189. Springer, A., Hagen, V., Cherepanov, D. A., Antonenko, Y. N. & Pohl, P. Protons migrate along interfacial water without significant contributions from jumps between ionizable groups on the membrane surface. *Proc. Natl. Acad. Sci. U. S. A.* **108**, 14461–14466 (2011).

190. Cherepanov, D. A., Feniouk, B. A., Junge, W. & Mulkidjanian, A. Y. Low dielectric permittivity of water at the membrane interface: Effect on the energy coupling mechanism in biological membranes. *Biophys. J.* **85**, 1307–1316 (2003).

191. Smondyrev, A. M. & Voth, G. A. Molecular dynamics simulation of proton transport near the surface of a phospholipid membrane. *Biophys. J.* **82**, 1460–1468 (2002).

192. von Ballmoos, C., Biner, O., Nilsson, T. & Brzezinski, P. Mimicking respiratory phosphorylation using purified enzymes. *BBA - Bioenerg.* **1857**, 321–331 (2016).

193. Sjöholm, J. *et al.* The lateral distance between a proton pump and ATP synthase determines the ATP-synthesis rate. *Sci. Rep.* **7**, 2926 (2017).

194. Jarvik, J. W. & Telmer, C. A. Epitope tagging. *Annu. Rev. Genet.* **32**, 601–618 (1998).

195. Allen, K. N. & Imperiali, B. Lanthanide-tagged proteins - an illuminating partnership. *Curr. Opin. Chem. Biol.* **14**, 247–254 (2010).

196. Halo, T. L., Appelbaum, J., Hobert, E. M., Balkin, D. M. & Schepartz, A. Selective recognition of protein tetraserine motifs with a cell-permeable, pro-fluorescent bis-boronic acid. *J. Am. Chem. Soc.* **131**, 438–439 (2009).

197. Zakeri, B. *et al.* Peptide tag forming a rapid covalent bond to a protein, through engineering a bacterial adhesin. *Proc. Natl. Acad. Sci. U. S. A.* **109**, E690–E697 (2012).

198. Hagan, R. M. *et al.* NMR Spectroscopic and Theoretical Analysis of a Spontaneously Formed Lys–Asp Isopeptide Bond. *Angew Chem Int Ed Engl.* **122**, 8599–8603 (2010).

199. Keeble, A. H., Turkki, P., Stokes, S., Khairil, I. N. A. & Rahikainen, R. Approaching infinite affinity through engineering of peptide – protein interaction. *Proc Natl Acad Sci U S A.* **116**, 26523–26533 (2019).

200. Schreiber, G; Haran, G; Zhou, H. *Fundamental aspects of protein-protein association kinetics*. vol. 109 (2010).

201. Keeble, A. H. *et al.* Evolving Accelerated Amidation by SpyTag/SpyCatcher to Analyze Membrane

Dynamics. *Angew Chem Int ed* **56**, 16521–16525 (2017).

202. Khairil Anuar, I. N. A. *et al.* Spy&Go purification of SpyTag-proteins using pseudo-SpyCatcher to access an oligomerization toolbox. *Nat. Commun.* **10**, 1–13 (2019).

203. Fluman, N., Tobiasson, V. & von Heijne, G. Stable membrane orientations of small dual-topology membrane proteins. *Proc. Natl. Acad. Sci. U. S. A.* **114**, 7987–7992 (2017).

204. Hegde, R. S. & Keenan, R. J. Tail-anchored membrane protein insertion into the endoplasmic reticulum. *Nature Reviews Molecular Cell Biology* vol. 12 787–798 (2011).

205. Dröse, S., Galkin, A. & Brandt, U. Proton pumping by complex I (NADH:ubiquinone oxidoreductase) from Yarrowia lipolytica reconstituted into proteoliposomes. *Biochim. Biophys. Acta - Bioenerg.* **1710**, 87–95 (2005).

206. Gerber, G. E., Gray, C. P., Wildenauer, D. & Khorana, H. G. Orientation of bacteriorhodopsin in Halobacterium halobium as studied by selective proteolysis. *Proc. Natl. Acad. Sci. U. S. A.* **74**, 5426–5430 (1977).

207. Kalmbach, R. *et al.* Functional Cell-free Synthesis of a Seven Helix Membrane Protein: In situ Insertion of Bacteriorhodopsin into Liposomes. *J. Mol. Biol.* **371**, 639–648 (2007).

208. Fang, G. *et al.* Manipulation of activity and orientation of membrane-reconstituted di-tripeptide transport protein DtpT of Lactococcus lactis. *Mol. Membr. Biol.* **16**, 297–304 (1999).

209. Geest, M. van & Lolkema Juke S. Membrane Topology and Insertion of Membrane Proteins: Search for Topogenic Signals. *Microbiol. Mol. Biol. Rev.* **64**, 13–33 (2000).

210. Futai, M. Orientation of membrane vesicles from Escherichia coli prepared by different procedures. *J. Membr. Biol.* **15**, 15–28 (1974).

211. Pagano, A. & Spiess, M. Reconstitution of Rab4-dependent vesicle formation in vitro. *Methods Enzymol.* **403**, 81–92 (2005).

212. Bronder, A. M. *et al.* Oriented Membrane Protein Reconstitution into Tethered Lipid Membranes for AFM Force Spectroscopy. *Biophys. J.* **111**, 1925–1934 (2016).

213. Sumino, A., Uchihashi, T. & Oiki, S. Oriented Reconstitution of the Full-Length KcsA Potassium Channel in a Lipid Bilayer for AFM Imaging. *J. Phys. Chem. Lett.* 785–793 (2017) doi:10.1021/acs.jpclett.6b03058.

214. Knol, J. *et al.* Unidirectional reconstitution into detergent-destabilized liposomes of the purified lactose transport system of Streptococcus thermophilus. *J Biol Chem* **271**, 15358–15366 (1996).

215. Zhang, W., Bogdanov, M., Pi, J., Pittard, A. J. & Dowhan, W. Reversible Topological Organization within a Polytopic Membrane Protein is Governed by a Change in Membrane Phospholipid Composition. *J. Biol. Chem.* **278**, 50128–50135 (2003).

216. Vaughan, J. C., Dempsey, G. T., Sun, E. & Zhuang, X. Phosphine quenching of cyanine dyes as a versatile tool for fluorescence microscopy. *J. Am. Chem. Soc.* **135**, 1197–1200 (2013).

217. Li, J. *et al.* Cryo-EM structures of Escherichia coli cytochrome bo3 reveal bound phospholipids and ubiquinone-8 in a dynamic substrate binding site. *Proc. Natl. Acad. Sci. U. S. A.* **118**, (2021).

218. Cline, D. J. *et al.* New water-soluble phosphines as reductants of peptide and protein disulfide bonds: Reactivity and membrane permeability. *Biochemistry* **43**, 15195–15203 (2004).

219. Podlaha, J. & Podlahová, J. Compounds structurally related to complexone I. Tris(cabroxyethyl)phosphine. *Collect. Czechoslov. Chem. Commun.* **38**, 1730–1736 (1973).

220. Ma, J., Katsonouri, A. & Gennis, R. B. Subunit II of the cytochrome bo3 ubiquinol oxidase from Escherichia coli is a lipoprotein. *Biochemistry* **36**, 11298–11303 (1997).

221. Nanda, J. S. & Lorsch, J. R. *Labeling of a protein with fluorophores using maleimide derivitization*. *Methods in Enzymology* vol. 536 (Elsevier Inc., 2014).

222. Tronchere, H. & Boal, F. Liposome Flotation Assays for Phosphoinositide-protein Interaction. *Bio-Protocol* **7**, 3–8 (2017).

223. Bruggisser, J. *et al.* CD31 (PECAM-1) Serves as the Endothelial Cell- Specific Receptor of Clostridium perfringens b -Toxin ll ll Article CD31 (PECAM-1) Serves as the Endothelial Cell-Specific Receptor of Clostridium perfringens b -Toxin. **31**, 69–78 (2020).

224. Yue, T. *et al.* How transmembrane peptides insert and orientate in biomembranes: A combined experimental and simulation study. *Phys. Chem. Chem. Phys.* **18**, 17483–17494 (2016).

225. Huang, H. *et al.* Using Fluorescence Quenching Titration to Determine the Orientation of a Model Transmembrane Protein in Mimic Membranes. *Mater.* **12**, 349 (2019).

226. Warren, G. B. *et al.* Reconstitution of a calcium pump using defined membrane components. *Proc. Natl. Acad. Sci. U. S. A.* **71**, 622–626 (1974).

227. Pullman, M. E., Penefsky, H. S., Datta, A. & Racker, E. Partial resolution of the enzymes catalyzing oxidative phosphorylation. I. Purification and properties of soluble dinitrophenol-stimulated adenosine triphosphatase. *J. Biol. Chem.* **235**, 3322–3329 (1960).

228. Besch, H. R., Jones, L. R., Fleming, J. W. & Watanabe, A. M. Parallel unmasking of latent adenylate cyclase and (Na+,K+) ATPase activities in cardiac sarcolemmal vesicles. A new use of the channel forming ionophore alamethicin. *J. Biol. Chem.* **252**, 7905–7908 (1977).

229. Blackman, M. L., Royzen, M. & Fox, J. M. Tetrazine ligation: Fast bioconjugation based on inverse-electron-demand Diels-Alder reactivity. *J. Am. Chem. Soc.* **130**, 13518–13519 (2008).

230. Cook, G. M. *et al.* Purification and Biochemical Characterization of the F1Fo-ATP Synthase from Thermoalkaliphilic Bacillus sp. Strain TA2.A1. *J. Bacteriol.* **185**, 4442–4449 (2010).

231. Richard, P., Rigaud, J. -L & Gräber, P. Reconstitution of CF0F1 into liposomes using a new reconstitution procedure. *Eur. J. Biochem.* **193**, 921–925 (1990).

232. Ishmukhametov, R. R., Galkin, M. A. & Vik, S. B. Ultrafast purification and reconstitution of His-tagged cysteine-less Escherichia coli F 1Fo ATP synthase. *Biochim. Biophys. Acta - Bioenerg.* **1706**, 110–116 (2005).

233. Yap, L. L., Samoilova, R. I., Gennis, R. B. & Dikanov, S. A. Characterization of mutants that change the hydrogen bonding of the semiquinone radical at the QH site of the cytochrome bo3 from Escherichia coli. *J. Biol. Chem.* **282**, 8777–8785 (2007).

234. Rumbley, J. N., Nickels, E. F. & Gennis, R. B. One-step purification of histidine-tagged cytochrome bo3 from Escherichia coli and demonstration that associated quinone is not required for the structural integrity of the oxidase. *Biochim. Biophys. Acta - Protein Struct. Mol. Enzymol.* **1340**, 131–142 (1997).

235. Gaspard, G. J. & McMaster, C. R. Cardiolipin metabolism and its causal role in the etiology of the inherited cardiomyopathy Barth syndrome. *Chem. Phys. Lipids* **193**, 1–10 (2015).

236. Biner, O., Schick, T., Müller, Y. & von Ballmoos, C. Delivery of membrane proteins into small and giant unilamellar vesicles by charge-mediated fusion. *FEBS Lett.* **590**, 2051–2062 (2016).

237. Otrin, L. *et al.* Toward Artificial Mitochondrion: Mimicking Oxidative Phosphorylation in Polymer and Hybrid Membranes. *Nano Lett.* **17**, 6816–6821 (2017).

238. Lundgren, C. A. K. *et al.* Scavenging of superoxide by a membrane-bound superoxide oxidase. *Nat. Chem. Biol.* **14**, 788–793 (2018).

239. Graf, S. S., Hong, S., Müller, P., Gennis, R. & von Ballmoos, C. Energy transfer between the nicotinamide nucleotide transhydrogenase and ATP synthase of Escherichia coli. *Sci. Rep.* **11**, 21234 (2021).

240. Amati, A. M. Towards unidirectional reconstitution of membrane proteins into liposomes. (2020).

241. Eytan, G. D. Use of liposomes for reconstitution of biological functions. *Biochim Biophys Acta* **694**, 185–202 (1982).

242. Léger, C. *et al.* Enzyme electrokinetics: Energetics of succinate oxidation by fumarate reductase and succinate dehydrogenase. *Biochemistry* **40**, 11234–11245 (2001).

243. Björklöf, K., Zickermann, V. & Finel, M. Purification of the 45 kDa, membrane bound NADH dehydrogenase of Escherichia coli (NDH-2) and analysis of its interaction with ubiquinone analogues. *FEBS Lett.* **467**, 105–

110 (2000).

244. Battino, M., Fahmy, T. & Lenaz, G. Determination of the critical micelle concentration of short-chain ubiquinones in model systems. *Biochim. Biophys. Acta* **851**, 377–384 (1986).

245. Xie, J., Bogdanov, M., Heacock, P. & Dowhan, W. Phosphatidylethanolamine and monoglucosyldiacylglycerol are interchangeable in supporting topogenesis and function of the polytopic membrane protein lactose permease. *J. Biol. Chem.* **281**, 19172–19178 (2006).

246. Schleiff, E., Tien, R., Salomon, M. & Soll, J. Lipid composition of outer leaflet of chloroplast outer envelope determines topology of OEP7. *Mol. Biol. Cell* **12**, 4090–4102 (2001).

247. Baker, L. A., Watt, I. N., Runswick, M. J., Walker, J. E. & Rubinstein, J. L. Arrangement of subunits in intact mammalian mitochondrial ATP synthase determined by cryo-EM. *Proc. Natl. Acad. Sci. U. S. A.* **109**, 11675–11680 (2012).

248. Spikes, T. E., Montgomery, M. G. & Walker, J. E. Interface mobility between monomers in dimeric bovine ATP synthase participates in the ultrastructure of inner mitochondrial membranes. *Proc. Natl. Acad. Sci. U. S. A.* **118**, e2021012118 (2021).

249. Davies, K. M., Anselmi, C., Wittig, I., Faraldo-Gómez, J. D. & Kühlbrandt, W. Structure of the yeast F1Fo-ATP synthase dimer and its role in shaping the mitochondrial cristae. *Proc. Natl. Acad. Sci. U. S. A.* **109**, 13602–13607 (2012).

250. Cliff, L., Chadda, R. & Robertson, J. L. Occupancy distributions of membrane proteins in heterogeneous liposome populations. *Biochim. Biophys. Acta - Biomembr.* **1862**, 183033 (2020).

251. Preiss, L., Hicks, D. B., Suzuki, S., Meier, T. & Krulwich, T. A. Alkaliphilic bacteria with impact on industrial applications, concepts of early life forms, and bioenergetics of ATP synthesis. *Front. Bioeng. Biotechnol.* **3**, 1–16 (2015).

252. Rieger, B., Junge, W. & Busch, K. B. Lateral pH gradient between OXPHOS complex IV and F(0)F(1) ATP-synthase in folded mitochondrial membranes. *Nat. Commun.* **5**, 3103 (2014).

253. Brändén, M., Sandén, T., Brzezinski, P. & Widengren, J. Localized proton microcircuits at the biological membrane-water interface. *Proc. Natl. Acad. Sci. U. S. A.* **103**, 19766–19770 (2006).

254. Agasid, M. T. & Robinson, C. V. Probing membrane protein–lipid interactions. *Curr. Opin. Struct. Biol.* **69**, 78–85 (2021).

255. Deutschmann, S., Rimle, L. & von Ballmoos, C. Rapid estimation of membrane protein orientation in liposomes. *ChemBioChem* **22**, (2021).

256. Serowy, S. *et al.* Structural proton diffusion along lipid bilayers. *Biophys. J.* **84**, 1031–1037 (2003).

257. Medvedev, E. S. & Stuchebrukhov, A. A. Mechanism of long-range proton translocation along biological membranes. *FEBS Lett.* **587**, 345–349 (2013).

258. Cherepanov, D. A., Feniouk, B. A., Junge, W. & Mulkidjanian, A. Y. Low dielectric permittivity of water at the membrane interface: Effect on the energy coupling mechanism in biological membranes. *Biophys. J.* **85**, 1307–1316 (2003).

259. Smondyrev, A. M. & Voth, G. A. Molecular dynamics simulation of proton transport near the surface of a phospholipid membrane. *Biophys. J.* **82**, 1460–1468 (2002).

260. Dolder, N. & von Ballmoos, C. Bifunctional DNA duplexes permit efficient incorporation of pH probes into liposomes. *ChemBioChem* **21**, 2219–2224 (2020).

261. Stenberg, F., von Heijne, G. & Daley, D. O. Assembly of the Cytochrome bo3 Complex. *J. Mol. Biol.* **371**, 765–773 (2007).

262. Theßeling, A., Burschel, S., Wohlwend, D. & Friedrich, T. The long Q-loop of Escherichia coli cytochrome bd oxidase is required for assembly and structural integrity. *FEBS Lett.* **594**, 1577–1585 (2020).

263. Aggeler, R., Ogilvie, I. & Capaldi, R. A. Rotation of a γ-ε subunit domain in the Escherichia coli F1F0-ATP synthase complex. *J. Biol. Chem.* **272**, 19621–19624 (1997).

264. Keeble, A. H. *et al.* DogCatcher allows loop-friendly protein-protein ligation. *Cell Chem. Biol.* 1–12 (2021)

doi:10.1016/j.chembiol.2021.07.005.

265. Ernst, R., Ballweg, S. & Levental, I. Cellular mechanisms of physicochemical membrane homeostasis. *Curr. Opin. Cell Biol.* **53**, 44–51 (2018).

266. Ernst, R., Ejsing, C. S. & Antonny, B. Homeoviscous Adaptation and the Regulation of Membrane Lipids. *J. Mol. Biol.* **428**, 4776–4791 (2016).

267. Uchida, Y. & Holleran, W. M. Omega-O-acylceramide, a lipid essential for mammalian survival. *J. Dermatol. Sci.* **51**, 77–87 (2008).

268. Rawicz, W., Olbrich, K. C., McIntosh, T., Needham, D. & Evans, E. A. Effect of chain length and unsaturation on elasticity of lipid bilayers. *Biophys. J.* **79**, 328–339 (2000).

269. Geiss, A. F. *et al.* Proteo-lipobeads to encapsulate cytochrome c oxidase from Paracoccus denitrificans. *J Colloid Interface Sci* **500**, 119–125 (2017).

270. Sinclair, J. C., Davies, K. M., Vénien-Bryan, C. & Noble, M. E. M. Generation of protein lattices by fusing proteins with matching rotational symmetry. *Nat. Nanotechnol.* **6**, 558–562 (2011).

271. Ma, Y., Lee, C. J. & Park, J. S. Strategies for optimizing the production of proteins and peptides with multiple disulfide bonds. *Antibiotics* **9**, 541 (2020).

272. Kondapalli, K. C., Kallay, L. M., Muszelik, M. & Rao, R. Unconventional chemiosmotic coupling of NHA2, a mammalian Na+/H+ antiporter, to a plasma membrane H+ gradient. *J. Biol. Chem.* **287**, 36239–36250 (2012).

273. Jadiya, P. & Tomar, D. Mitochondrial protein quality control mechanisms. *Genes (Basel).* **11**, 563 (2020).

274. Prola, A. *et al.* Cardiolipin content controls mitochondrial coupling and energetic efficiency in muscle. *Sci. Adv.* **7**, (2021).

9 Appendix

9.1 Current problems and future avenues in proteoliposome research

Biochemical Society Transactions (2020) **48** 1473–1492
https://doi.org/10.1042/BST20190966

PORTLAND PRESS

Review Article

Current problems and future avenues in proteoliposome research

Andrea Marco Amati, Simone Graf, Sabina Deutschmann, Nicolas Dolder and Christoph von Ballmoos

Department of Chemistry and Biochemistry, University of Bern, Freiestrasse 3, 3012 Bern, Switzerland

Correspondence: Christoph von Ballmoos (christoph.vonballmoos@dcb.unibe.ch)

Membrane proteins (MPs) are the gatekeepers between different biological compartments separated by lipid bilayers. Being receptors, channels, transporters, or primary pumps, they fulfill a wide variety of cellular functions and their importance is reflected in the increasing number of drugs that target MPs. Functional studies of MPs within a native cellular context, however, is difficult due to the innate complexity of the densely packed membranes. Over the past decades, detergent-based extraction and purification of MPs and their reconstitution into lipid mimetic systems has been a very powerful tool to simplify the experimental system. In this review, we focus on proteoliposomes that have become an indispensable experimental system for enzymes with a vectorial function, including many of the here described energy transducing MPs. We first address long standing questions on the difficulty of successful reconstitution and controlled orientation of MPs into liposomes. A special emphasis is given on coreconstitution of several MPs into the same bilayer. Second, we discuss recent progress in the development of fluorescent dyes that offer sensitive detection with high temporal resolution. Finally, we briefly cover the use of giant unilamellar vesicles for the investigation of complex enzymatic cascades, a very promising experimental tool considering our increasing knowledge of the interplay of different cellular components.

Introduction

Lipid membranes are found in all living cells and provide several vital functions. Not only do they protect the organism from a potentially hostile environment, but they also allow chemical compartmentalization, e.g. reducing und oxidizing conditions in bacterial cytoplasm and periplasm, respectively. In eukaryotes, cellular organelles such as mitochondria, endoplasmic reticulum or endosomes are also surrounded by membranes. The chemical scaffold of these membranes is a bilayer of lipid molecules, that hosts small hydrophobic components such as vitamins, quinones, and pigments, as well as very large and complex membrane proteins (MPs). The mass percentage of proteins in natural membranes varies between 25% in the myelin sheath and 75% in energy transducing membranes such as the mitochondrial inner membrane [1–3]. This complexity makes the direct investigation of MP function in native membranes difficult. To circumvent this problem, MPs are purified and reinserted into membrane mimetic systems, such as protein wrapped lipid patches (nanodiscs), (supported) planar lipid bilayers or lipid vesicles [4]. Here, we focus on the use of small to giant unilamellar vesicles (GUVs) (diameter ranging from 30 nm to 50 μm), called liposomes, to study MPs with vectorial functions. Bordered by a single lipid bilayer, liposomes form spontaneously from dried lipids resuspended in aqueous solution.

The advent of proteoliposome studies is tightly coupled to the experimental verification of the chemiosmotic theory brought forward by Peter Mitchell in 1961 [5,6]. This hypothesis led to a controversy amongst research groups across continents that lasted for decades [7]. A crucial experiment, positively stimulating the debate, was the coreconstitution of purple membrane *Halobacterium salinarum* (i.e. essentially 2D-crystallized bacteriorhodopsin) and the F_1F_0 ATP synthase from

Received: 14 May 2020
Revised: 10 July 2020
Accepted: 14 July 2020

Version of Record published:
24 August 2020

Biochemical Society Transactions (2020) 48 1473–1492
https://doi.org/10.1042/BST20190966

mitochondria, showing ATP synthesis upon illumination, as described by Racker and Stoeckenius [8] along with other coreconstitutions [9–11]. It was the simplicity of these experiments which stood out and manifested the connection between an electrochemical gradient and ATP synthesis. The use of purified components inserted into an empty lipid bilayer ensured that no unknown factors had to be considered during the interpretation of results. Racker's method was readily picked up by many researchers to advance the mechanistic understanding of various MPs. A comprehensive overview of numerous pioneering experiments is given by Etemadi [12].

In general, proteins embedded in liposomes can be investigated employing the same techniques that are also used to study enzymes in solution, such as UV/VIS and fluorescence spectroscopy. Nevertheless, the signal-to-noise ratio of optical measurements is typically decreased in proteoliposomes due to light scattering. Importantly, proteoliposomes also allow for electrometric techniques to follow charge movements across the membranes, as initially developed by Drachev et al. [13,14] for light-inducible reactions and recently adapted by Fendler and colleagues [15,16] for slower reactions that require mixing techniques (SSM electrophysiology). Proteoliposomes can also be immobilized onto many different kinds of support further increasing their experimental value [17].

Besides examining transmembrane transport, liposomes have been used to investigate other membrane related biological phenomena, especially membrane fusion events. Fusion of lipid bilayers is vital during virus entry into their host cells, for instance, where it is either triggered by direct virus-membrane interaction or it is receptor-mediated. Liposome studies have successfully been used to investigate virus-target cell interactions and potential inhibitors [18], mechanistic studies of virus-membrane fusion [19–22], or interaction of viral protein, receptor and antibodies in HIV [23]. Furthermore, proteoliposomes have been used for NMR based structure determination of MPs, wherein the membrane ensures proper protein folding due to the near-native environment [24–26]. Finally, liposomes have been long-known as promising drug delivery systems for both hydrophobic and hydrophilic drugs alike [27–32], which is a very active field of research.

In this short review, we will highlight three different aspects of current proteoliposome research. In the first, main part, we will focus on the use of liposomes for the investigation of MPs, many of them being ion-translocating enzymes involved in cellular bioenergetics. As our knowledge of the interplay of cellular components vastly expanded in the last years, experimental setups of more complex systems are of increasing interest. This also involves the coreconstitution of several MPs in desired orientations into the same liposomal membrane. However, robust protocols to measure or guide orientation of reconstituted proteins or to coreconstitute MPs into the same membrane are still in development. We discuss current problems during reconstitution of MPs and their joining into more complex systems. In the second part, we will discuss recent progress in the development of fluorescent dyes that are suitable for proteoliposome studies. Using orthogonal chemistry and different linker techniques, such dyes can be tailored to meet specific requirements, ensuring high sensitivity and temporal resolution. Finally, we briefly describe the use of giant vesicles in the bottom-up construction of synthetic cells, highlighting recent projects, in which an impressive complexity of experimental systems was achieved.

Membrane protein reconstitution in a nutshell

In the seminal experiment of Racker and Stoeckenius described above, native purple bacteria were mixed with cholate-extracted mitochondrial particles (containing enriched F_1F_0 ATP synthase) with asolectin lipids that had been sonicated and solubilized by the bile salt sodium cholate. This mixture was then dialyzed to remove excess detergent allowing the formation of proteoliposomes capable of light-driven ATP synthesis [8]. Almost 50 years later, close variants of this very method are still powerful protocols to reconstitute MPs. Over the years, several other approaches to functionally reconstitute purified MPs into liposomes were developed. Some employ organic solvents, or mechanical means such as sonication, freeze-thawing, or French-press [33,34]. However, the most common methods are based on the use of detergents discussed in the next paragraphs. For an overview of different reconstitution techniques consider the pioneering reviews [33] and [12], for more recent perspectives refer to [4,35–37].

Generally, the process of detergent-mediated reconstitution can be divided into two main steps. First, a purified and detergent-solubilized MP is mixed with lipids. Second, the detergent is removed from the mixture, leading to the incorporation of the MP into liposomes. In the first step, the lipids are added to the solubilized MP either as fully solubilized mixed detergent-lipid micelles, or as preformed, detergent-destabilized vesicles. Detergent removal in the second step is achieved by various methods based on the critical micelle concentration (CMC) of the employed detergent [33]. For small sized micelles (<25 kDa, high CMC; e.g. sodium cholate,

octyl glucoside), rapid dilution, dialysis with an appropriately sized membrane or size exclusion chromatography can be used. For detergents forming large micelles (typically very low CMC), adsorption to polystyrene beads or complex formation with various cyclodextrins is used [35,38–40]. Especially the use of cyclodextrins holds promise as different ring sizes are available that offer some specificity for certain detergents [38], e.g. allowing the selective removal of one detergent from a detergent mixture. While the exact mechanism of reconstitution by detergent removal is still not fully understood [36,41], there is agreement that at a critical detergent concentration (which depends on a variety of factors), solubilized MPs cannot be kept in a soluble state any further and either precipitate or spontaneously integrate into the present phospholipid membrane [4,36]. The efficiency of the reconstitution process (fraction of the solubilized MP that incorporates into liposomes) depends on various factors, as e.g. the MP of interest itself, the type of detergent used, the initial detergent concentration, the composition of the lipid membrane, the choice of buffer and ionic strength and importantly, the method and rate of detergent removal [33,36].

A special role is assigned to the lipid composition in proteoliposomes. Critical aspects for a good lipid mixture are easy liposome formation, preservation of enzyme activity and tightness of the liposomes towards leakage of protons or other ions. For many MPs, a (rather crude) lecithin (phosphatidylcholine (PC)) extract of soybean has been successfully applied. In this extract, next to PC, phosphatidylethanolamine (PE), and the negative lipid phosphatidyl inositol (PI) are the other main components. Although both PC and PI are not found in bacteria, the extract has been successfully used for many prokaryotic MPs. In addition, natural extracts from bacteria, e.g. from *Escherichia coli* or mixtures from synthetic lipids are used. Tsai and Miller [42] have convincingly shown that mixtures of synthetic lipids are much tighter towards proton leakage compared with a polar extract of *E. coli* lipids. Although being outside of the scope of this review, it is noteworthy that the correct lipid composition can have a direct impact on the protein activity as briefly described in the following few examples. Non-bilayer lipids such as PE were shown to stimulate the activity of secondary transporters (e.g. Lyp1 of *Saccheromyces cerevisiae*) [43]. Furthermore, the head groups of lipids, especially of anionic lipids, are responsible for the topology and the regulation of conformational dynamics of transporters by interacting with the transport proteins [44–48]. The importance of negatively charged lipids, especially cardiolipin, for the activity and stability of bacterial and mitochondrial respiratory (super)complexes has also been described [49–51].

The impact of lipids on the reconstitution process has been studied for some proteins, e.g. Na^+/K^+-ATPase [52–56]. De Lima Santos et al. [52] proposed that the lipids surrounding the MP, as well as the physical state of the lipid environment as e.g. its fluidity, have a stabilizing effect on MPs. Longer saturated fatty acyl chains decreased membrane fluidity leading to activity loss of the MP. Thus, phospholipid mixtures that contribute to membrane fluidity (higher fractions of short-chain or unsaturated fatty acyl chains) can reduce activity loss [52,53,55,57]. Further excellent studies, in which many of these parameters have been described, were published for bacteriorhodopsin and ATP synthase by Paternostre and colleagues, as well as for LacS by Knol and colleagues (see Table 1 and references therein as well as Lichtenberg et al.) [58]. These studies show that the lipid composition can affect both the reconstitution yield and the orientation of the protein in the membrane (see below). A final complication is the natural asymmetry of lipid composition in the two leaflets of the bilayer as observed in eukaryotes and prokaryotes [59–61] and first protocols for the generation of asymmetric liposomes have been described [62,63].

In contrast with natural membranes, proteoliposomes contain much fewer proteins (<5% of lipid weight), as higher amounts of protein often negatively affect the reconstitution process. An interesting approach to tackle this problem is the GreCon method, in which the solubilized protein is placed onto a sucrose density gradient with increasing concentrations of cyclodextrin and detergent-destabilized liposomes. During centrifugation, the detergent is gradually replaced by lipids, yielding liposomes with very high protein content, even triggering 2D-cristallization [64]. In the density gradient, proteoliposomes and empty liposomes migrate differently and are visible as opaque bands allowing their facile separation. Such proteoliposomes have been successfully used for electron tomography imaging using large membrane complexes [65], but have not yet been tested for transport measurements.

In recent years, peptides mimicking the properties of nanodiscs [66], i.e. embedding the MP in small lipid bilayer discs surrounded by a scaffold protein, have been described [67–69]. While these have the advantage over traditional nanodiscs that their size can be modulated by varying the peptide to lipid ratio, they share the common drawback that they cannot be used to extract protein from native membranes, making the prior use of detergent necessary. A MP extraction method not requiring any detergent is based on the use of styrene maleic acid (SMA) lipid particles (SMALPs), which has been successfully employed to purify [70,71] and also

Biochemical Society Transactions (2020) **48** 1473–1492
https://doi.org/10.1042/BST20190966

Table 1. Non-exhaustive list of different studies with a focus on coreconstitution of MPs or orientation of MPs Part 1 of 3

Membrane protein	Organism	Study	Comments	References
aa_3 *CcO*	*Rhodobacter sphaeroides*	Coreconstitution	Coreconstitution of aa_3 *CcO* with F_1F_0 ATP synthase (*E. coli*) or spinach ATP synthase.	[112]
		Investigating orientation	70–80% CcO was found with soluble domain of subunit II carrying the cytochrome *c*-binding site towards the outside of the liposomes. Functional unidirectionality can be imposed over orientation of the MP in the liposomal membrane by providing cytochrome *c* and electrons only on one side of the membrane.	[93]
	Paracoccus denitrificans	Influencing orientation	MP was immobilized on Ni-NTA-functionalized silica nanoparticles for orientated encapsulation into liposomes (bead on outside of proteoliposome).	[97,98]
ArcD2	*Lactococcus lactis*	Coreconstitution	Coreconstitution with OpuA and soluble proteins ArcA, B and C (*L. lactis*)	[109]
Bacteriorhodopsin	*Halobacterium salinarum*	Coreconstitution	Coreconstitution with ATP synthase from bovine heart mitochondria.	[8]
		Investigating orientation	Only slight preference for inside-out was detected.	[205]
			Orientation in proteoliposomes was shown to depend on lipid composition of the liposomes, pH value, ionic strength, and membrane curvature (in order of decreasing influence on orientation).	[80]
Ca^{2+}-P-ATPase	Rabbit sarcoplasmic reticulum	Investigating orientation	Unidirectional orientation with 80–100% of the cytoplasmic domain facing outwards was observed, depending on the rate of detergent removal	[206]
Cytochrome bo_3 ubiquinol oxidase	*E. coli*	Coreconstitution	Coreconstitution of bo_3 oxidase with F_1F_0 ATP synthase (*E. coli*) via charge-mediated fusion of liposomes to GUVs	[114,115]
			Coreconstitution of bo_3 oxidase with F_1F_0 ATP synthase (*E. coli*) or spinach ATP synthase	[112]
			Coreconstitution of bo_3 oxidase with F_1F_0 ATP synthase (*E. coli*) via SNARE-mediated fusion	[113]
		Investigating orientation	72–77% to pump protons out of liposomes	[162,167]
			Unidirectional orientation is reported using a reconstitution method based on Rigaud et al. [33] However, no biochemical proof of unidirectionality is provided.	[207]
Cytochrome *b*-563/*c*-554 (*Qbc*)	*Synechococcus 6716*	Coreconstitution	Coreconstitution with H^+-ATP synthase from *Synechococcus 6716.*	[111]
F_1F_0 ATP synthase	*E. coli*	Coreconstitution	Refer to cytochrome bo_3 ubiquinol oxidase. Further coreconstitutions with Na^+/H^+ antiporters (*Thermus thermophilus* NapA and human NHA2), rat VGLUT2 as well as mitochondrial complex I from *Bos taurus* together with alternative oxidase from *Trypanosoma brucei brucei*.	[105–108]
		Investigating orientation	>97% of F_1 facing outwards was shown.	[86]
LacS	*Streptococcus thermophilus*	Investigating orientation	Different detergents and detergent concentrations were evaluated as well as different rates of detergent removal. Unidirectional inside-out orientation is reported	[87,208]

Continued

Table 1. Non-exhaustive list of different studies with a focus on coreconstitution of MPs or orientation of MPs Part 2 of 3

Membrane protein	Organism	Study	Comments	References
			for reconstitution with Triton X-100 and random orientation for reconstitution with *n*-Dodecyl β-D-maltoside.	
Large-conductance calcium- and voltage-activated potassium channel (BK)	*Homo sapiens*	Investigating orientation	70% inside-out orientation of MP is reported.	[209]
Mechanosensitive channel of small conductance (MscS)	*Bacterial* (no further statement made)	Investigating orientation	Unidirectional incorporation is reported based solely on electrophysiological results; no physical evidence is provided. Two ion channel reconstitution methods based on dehydration/rehydration of liposomes in presence of MP were tested.	[210]
Na^+/K^+-P-ATPase	*Electrophorus electricus* or *Squalus acanthias*	Investigating orientation	Functional unidirectionality was imposed over orientation of MP in membrane by selective inhibition of one of the two orientation populations with ouabain (exterior) or vanadate ions (interior).	[211,212]
	Dark red outer medulla of kidney of adult New Zealand white rabbits	Investigating orientation	Different protein-to-lipid ratios, different phospholipids and methods of detergent removal were investigated.	[52]
Proteorhodopsin	Uncultured *Gammaproteobacterium EBAC31A08*	Coreconstitution	Coreconstitution with *Spinacia oleracea* PSII and *Bacillus pseudofirmus* ATP synthase	[189]
		Influencing orientation	Interaction of MP with the surface of the liposomes was shown to dictate orientation. The surface charge of liposomes was modulated to prearrange orientation.	[85,94]
			MP was immobilized on Ni-NTA-functionalized silicate beads for orientated reconstitution (bead on outside of proteoliposome).	[213]
			Fusion domains were reported to guide the orientated insertion of proteorhodopsin into liposomes.	[95]
Various (Ca^{2+}-P-ATPase, H^+-F-ATPase, LacS)	Various	Investigating orientation	More uniform orientation of MPs was observed in the reconstituted liposomal bilayer when reconstituted into preformed, detergent-destabilized liposomes.	[81,87,90,91,214]
Voltage-dependent K^+ channel (K_VAP)	*Aeropyrum pernix*	Influencing orientation	Ni-NTA-functionalized beads were used as membrane organization centers during bilayer reconstitution (bead in proteoliposome; bSUM).	[96]
YidC	*Escherichia coli*	Coreconstitution	Coreconstitution with LacY and SecYEG as a fusion construct	[110,121]

For the latter, studies are further distinguished between simply investigating orientation under one or several different conditions and actively influencing orientation by different means. Studies are grouped according to the investigated MP and the origin of the MP and the studied parameter is indicated. A short summary of the study is provided in the comments row.

functionally reconstitute MPs into lipid bilayers [72–76]. Recent examples are the purification and reconstitution of cytochrome *c* oxidase from *S. cerevisiae* [75] and of a plant sodium/proton antiporter [76]. Although not without downside (the solubilization properties of SMAs are pH-dependent) [77], these novel molecules are valuable gadgets in the toolbox of MP biochemists.

The problem of protein orientation

In cells, insertion of MPs in membranes is thought to happen co-translationally and the final orientation of the protein is fixed during insertion and remains static (see [78] for a recent discussion on the topic).

Biochemical Society Transactions (2020) **48** 1473–1492
https://doi.org/10.1042/BST20190966

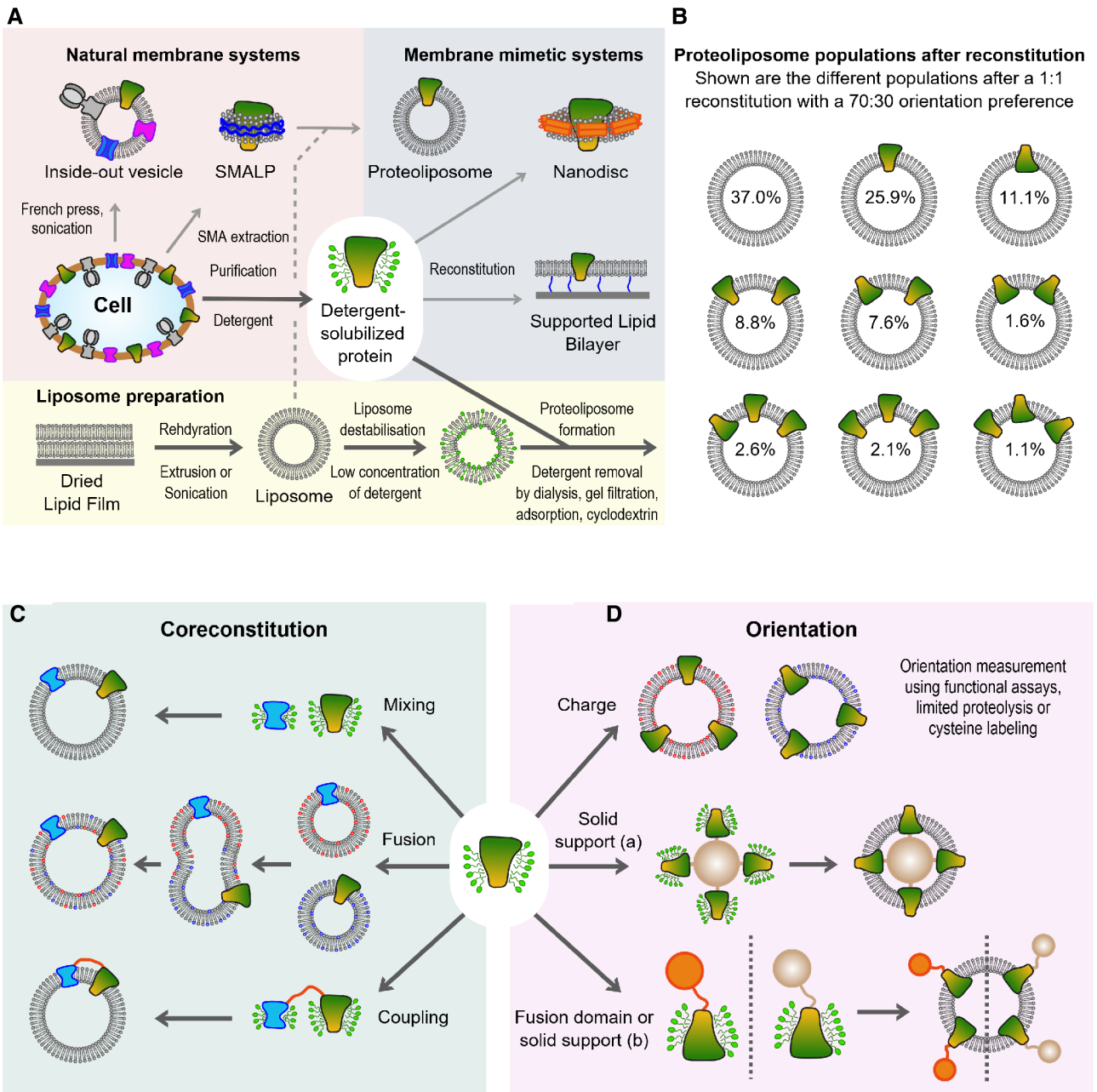

Figure 1. The ins and outs of membrane protein reconstitution Part 1 of 2

(**A**) The general procedure for the formation of proteoliposomes is shown as well as a few alternative approaches for the *in vitro* study of membrane protein (MP) function. In a first step, MPs are extracted and purified from the native cell environment using detergents. In parallel, liposomes are formed by rehydration of a dried lipid film and subsequent extrusion or sonication of the vesicles. These liposomes are partially solubilized by the

Unfortunately, this is not the case during MP reconstitution into liposomes as no translational machinery or chaperones are present that help to insert MPs into the liposomal bilayer [79,80].

The relative orientation of the inserted MP strongly affects functional studies. As liposomes typically contain many copies of the MP in a random orientation, hundreds of different proteoliposome populations are formed during a single reconstitution process, causing a strong heterogeneity in the experimental system (see Figure 1B). In some cases, functional unidirectionality can be imposed over random orientation of the MPs by using substrates which are unable to penetrate the membrane (e.g. ATP, NADH, cytochrome *c*), but in others,

Figure 1. The ins and outs of membrane protein reconstitution Part 2 of 2

addition of detergents and mixed with the detergent-solubilized MP to form proteoliposomes after removal of the detergent by a variety of methods. Detergent-free extraction of MPs from the cell can be achieved by generating inside-out vesicles [204] or using styrene maleic acid (SMA) copolymers to generate SMALPs. The latter can be used for the detergent-free reconstitution of MPs into liposomes [70–76]. If a closed compartment is not needed, detergent-solubilized MPs can also be reconstituted into planer supported lipid bilayers or nanodiscs [4]. (**B**) The calculated distribution of proteoliposome populations after reconstitution with a 1 : 1 liposome to protein stoichiometry and a 70% green-side out preference in orientation. Values were calculated assuming a Poisson distribution for reconstitution and a binomial distribution for orientation. Only populations >1% are shown. (**C**) Coreconstitution of more than one membrane protein. Shown are coreconstitutions by a combined incubation of both MPs with liposomes, via fusion of different proteoliposome populations (e.g. charge-mediated fusion, red lipids = negatively charged, blue lipids = positively charged) [114,115], or via covalent/transient coupling of the MPs prior to reconstitution [120]. (**D**) Methods for the guided orientation during reconstitutions. Shown are examples of charge-controlled insertion [85,94], by coupling the MP to a solid support (a) that will be encapsulated by the liposome [96] or by attaching a fusion domain [95] or coupling to a solid support (b) [97,98] that will be excluded from the vesicle interior.

the substrate binding site is located in the hydrophobic part of the membrane and, hence, both populations are stimulated (e.g. quinone-coupled enzymes). Alternatively, membrane impermeable inhibitors can be used, which selectively inhibit one enzyme population [81]. In a worst-case scenario, the reconstitution method yields unidirectional insertion, but in the non-preferred orientation (e.g. substrate binding site on the inside), complicating functional experiments. The orientation of MPs is not only important for primary ion pumps but has to be considered as well for secondary transport proteins. While these can often catalyze transport of their substrates in both directions, the affinities for the substrate might be different on either side of the membrane, a situation that severely complicates the quantitative interpretation of experimental results. The difficulties imposed by uncontrolled orientation are even more pronounced if the coupled activity of two or more MPs coreconstituted in the same liposomal membrane is investigated (see Table 1).

The orientation of reconstituted MPs is difficult to predict and even harder to influence, and it seems to be essentially unique for each protein and specific set of reconstitution technique [36]. Over the past decades, however, several studies have accumulated knowledge on protein orientation (see Table 1). Many reports describe the use of bacteriorhodopsin or proteorhodopsin, which are good models for monomeric MPs with no soluble domain, but inadequate as models for large multi-subunit MPs or MPs harboring large soluble domains. A prerequisite for the investigation of MP orientation in liposomal membranes is a reliable assay to determine the ratio of the two possible populations. If feasible, orientation can be assessed via a functional assay that is able to discriminate the relative contribution of both populations. As an example, the orientation of respiratory complex I in liposomes can be determined by measuring NADH:hexaammineruthenium oxidoreductase activity that can be spectroscopically followed at 340 nm. If NADH, which is membrane-impermeable, is added to liposomes, only the population with the NADH binding site oriented towards the outside will contribute to the activity. Upon solubilization of the proteoliposomes with detergent, all complex I molecules will contribute to the activity. Setting both activities in relation allows for estimation of the orientation of complex I in the liposomes [82]. However, care has to be taken in such approaches, as detergents often affect turnover activities of enzymes. Furthermore, if the measured activity is independent of the presence of the membrane, nonincorporated enzyme also contributes to the activity. A different method that has been used to determine orientation of proteo-/bacteriorhodopsin, is the use of proteases which will only digest MP domains accessible from the outside of the liposomes due to their inability to cross the lipid bilayer. The cleavage pattern can then be analyzed by SDS–PAGE, Western blot or mass spectrometry [83–85]. However, this cannot be considered as a general approach, since cleavage patterns are expected to become increasingly complex with larger proteins, and proteolysis might be incomplete. A special case is the F_1F_0 ATP synthase, in which those hydrophilic F_1 head groups that are located on the outside of the liposomes can be specifically stripped off using defined buffer conditions [86]. Yet another approach, often used for secondary antiporters, is based on the selective labeling of cysteine residues from the outside by a membrane impermeable thiol-reactive compound. This is followed by complete labelling with membrane permeable biotin-maleimide that can later be detected by Western-blot analysis [87–89]. Further attempts to determine orientation of MPs reconstituted into liposomes can be found in Table 1.

Biochemical Society Transactions (2020) 48 1473–1492
https://doi.org/10.1042/BST20190966

Over the years, it has been found that numerous parameters can affect enzyme orientation during reconstitution. De Lima Santos et al. [52] report that at a slow detergent removal rate, liposome formation precedes protein incorporation into liposomes (leading to a more unidirectional incorporation of the MP), while liposome formation and protein incorporation happen simultaneously with fast detergent removal (resulting in a random orientation of MPs). Knol et al. [87] found a similar behavior for LacS, including further differences depending on the detergent used for reconstitution. If unidirectional orientation is not desirable, repetitive freeze/thaw cycles were shown to randomize orientation [39].

In general, experiments have shown that orientation seems to be more uniform when the MPs are reconstituted into preformed, partially detergent-solubilized liposomes [41,90–92]. A rationale behind this observation is that the most hydrophilic domain will be least efficient in crossing the bilayer, and the protein will insert with its most hydrophobic side first [41]. However, experiments with cytochrome *c* oxidases show that the hydrophilic extramembraneous cytochrome *c*-binding domain (~25 kDa) of subunit II is not sufficient to promote more asymmetry than a 70 : 30 ratio [93]. F_1F_0 ATP synthase, on the other hand, with its soluble 350 kDa F_1 head group, has been reported to incorporate >95% with its head piece towards the outside with a similar reconstitution protocol [86]. In proteins such as bR and pR, where no large soluble domain is present, the interaction of the surface charge of the proteins and liposomes seems to play a role [85,94]. Tunuguntla et al. hold the asymmetry of charge distribution of pR, i.e. an overall positive charge at the C-terminus and a negative charge at the N-terminus, responsible for the lipid-charge dependent orientation of pR in liposomes. Through the use of either positively or negatively charged lipids in their liposomes, the N- or the C-terminus could be attracted towards the liposomal membrane, respectively, promoting a unidirectional orientation of pR [85].

In one of the very few attempts to actively influence orientation, Ritzmann et al. [95] recently showed that fusion domains can guide orientated insertion of pR into liposomes. By genetic engineering, GFP and mCherry were added to the C-terminus or to the N-terminus as fusion domains, respectively. The resulting fusion proteins pumped protons across the liposomal membrane in opposite directions upon reconstitution. This elegant method is unique in the sense that both orientations can be chosen by attaching a fusion domain on either end of the protein and is a promising approach for small proteins with no soluble domain. Whether the addition of a GFP is sufficient to orient larger MPs remains to be determined. Other approaches for guided orientation employed Ni-NTA-functionalized beads to immobilize His-tagged MPs prior to reconstitution [96–98], a method also used to form planar bilayers for AFM studies [99,100]. The liposomal membrane was formed *de novo* between the immobilized MPs either around the bead-support [96], or the beads were suggested to force unidirectional orientation because they were too big to be incorporated into the newly formed liposomes [97,98]. However, a more thorough characterization of these methods, e.g. regarding membrane leakiness, is required. Taken together, despite identification of several parameters that influence orientation of a MP in liposomes, there is still no general method to reconstitute MPs independently of all these parameters. The rather unpredictable effect of the lipid composition on the yield and on the orientation displays a major problem, as the effect of different lipid compositions on protein activity is a frequent aspect of research. A general method for guided orientation of MPs independent of the lipid composition is highly desirable. Approaches, in which orientation is guided by steric constraints might display a promising tool that has to be further developed in the future [95–98]. Robust and easy to implement methods for the quantitative determination of incorporation yield and relative protein orientation are required to compare established and develop new reconstitution protocols, e.g. only a small subset of detergents have been used in reconstitution.

Coreconstitution of membrane proteins

The incorporation of different MPs into the same liposomal membrane is called coreconstitution and is desirable for several reasons. The small interior volume of liposomes leads to quick accumulation or depletion of the transported substrate, which does not allow for long steady-state measurements and thus complicates quantitative interpretation of the data. For instance, if a membrane potential is required for the transport process, often a potassium/valinomycin diffusion potential is used that quickly exhausts due to the rapid change of the internal K^+ concentration. Furthermore, as our understanding of biological processes increases, the interplay of different proteins at the molecular level becomes an important field of research. An impressive example of cooperating enzymes are the members of the respiratory chain which have been shown to form different supercomplexes in mitochondria [101,102]. Functional measurements comparing kinetics and efficiencies between

individual complexes or multiple complexes arranged in a supercomplex are necessary to understand the functional relevance of such supramolecular arrangements [103,104].

There are relatively few reports on the coreconstitution of more than one type of MP in the same liposomal membrane. Most work has been published on the coreconstitution of ATP synthase together with proton pumps such as bacteriorhodopsin, cytochrome bo_3 ubiquinol oxidase and cytochrome *c* oxidase, which energize the liposomal membrane with an electrochemical potential. Such systems have been recently extended by the addition of peripheral MPs. Biner et al. [105] added trypanosomal alternative oxidase to proteoliposomes containing coreconstituted ATP synthase from *E. coli* and mitochondrial complex I to generate a minimal respiratory chain. Furthermore, ATP synthase has been used as a constant generator of proton motive force for several proton dependent secondary transporters, such as Na^+/H^+ antiporter [106,107] and glutamate transporter [108]. An alternative way to regenerate ATP from ADP and phosphate was recently shown in a synthetic metabolic network consisting of coreconstituted ArcD and OpuA as well as soluble proteins ArcA, B and C entrapped in the vesicle lumen. In this complex network, ArcA — D couple the breakdown of arginine to the regeneration of ATP which is then used by OpuA for glycine betaine transport which regulates the internal osmotic balance of the vesicles [109]. Non-transport related processes can also be studied by coreconstitution such as the chaperone activity of the MP YidC on the folding of LacY [110]. Further examples of coreconstitutions are given in Table 1. In all these examples, both types of integral MPs have been reconstituted in parallel. However, given the individual requirements of every MP for optimal reconstitution and orientation, it has to be assumed that these coreconstitutions were far from being optimal [8,111,112].

One way to resolve this problem is to split the coreconstitution into two steps. First, either protein of interest is reconstituted under optimal conditions individually, followed by fusion of the two populations. Successful functional coreconstitution of two MPs by fusion was first reported using a minimal SNARE machinery that fused liposome populations containing either F_1F_0 ATP synthase or bo_3 oxidase [113]. The same enzymes have also been successfully coreconstituted using fusion of oppositely charged proteoliposome populations [114,115]. However, the latter method requires the use of non-natural positively charged lipids, limiting the free choice of the lipid composition. Alternative techniques which have been used for 'pure' liposome fusion are coiled-coil forming peptides [116] as well as complementary DNA strands [117,118]. However, these methods have not yet been tested with MP containing liposomes [119].

From the above considerations on orientation and coreconstitution experiments, it is obvious that the relative number of MPs reconstituted (stoichiometry) and the distribution of orientation of these MPs is of high importance for quantitative interpretations. Given the various parameters influencing reconstitution efficiency and orientation, this seems an almost insuperable obstacle. A ray of hope was provided by Raschle et al. with a method that ensures a 1 : 1 reconstitution stoichiometry of MPs. Using maleimide chemistry, complementary DNA molecules were attached to a unique cysteine of individual VDAC populations [120]. Upon DNA hybridization, the two populations form a stable complex that can be purified and reconstituted. This technique should be applicable to any MP and using DNA linkers of appropriate lengths might not only ensure the correct stoichiometry, but also correct relative orientation of the reconstituted proteins. Alternatively, proteins can be genetically linked by creating a fusion construct that can be cleaved via proteases, as was used in the coreconstitution of SecYEG and YidC in a 1 : 1 stoichiometry [121].

Rational design of fluorescent dyes to follow enzyme function

As mentioned in the introduction, many different methods have been successfully used to follow chemical reactions in proteoliposomes, ranging from fast techniques such as absorption spectroscopy or electrometry, over luminescence (ATP detection) to slow methods such as micro electrodes, NMR, or uptake/release of isotope labeled substrates [122–125]. Probably the best combination of high sensitivity and high temporal resolution is found in fluorescent dyes which are able to detect a variety of reactions such as the change of proton or other ion concentrations or the presence of a membrane potential. Some of these dyes are membrane impermeable and have to be entrapped inside the liposomes (and the nonincorporated dye has to be removed) while others can be added from the outside, where they typically interact with the membrane. These latter, hydrophobic dyes are mainly used for the detection of proton gradients (e.g. ACMA, acridine orange) [112,126–129] or membrane potentials (e.g. oxonol VI, TMRE, VoltageFluors) [130–134] and do not directly report the translocated substrates.

Biochemical Society Transactions (2020) **48** 1473–1492
https://doi.org/10.1042/BST20190966

In the following, we focus on membrane-anchored fluorescent probes that offer several advantages over entrapped dyes. A prototype of such a lipid anchored dye is obtained by the reaction of an amine-reactive carboxyfluorescein derivative with PE, first reported in 1984 by Thelen et al. [135] Such lipophilic probes have been mostly used *in vivo* [136–141] or to characterize different membrane properties [142]. Recently, Kemmer et al. have coupled the ratiometric pH sensitive dyes pHrodo or SNARF to PE, which in contrast with fluorescein increase fluorescence upon acidification. Notably, they found a significant increase in the apparent pK_a of the lipid coupled dyes in comparison with their soluble counterparts, an effect that is likely related to the close proximity of the dye to the membrane [143,144]. To avoid this pK_a shift, a linker can be introduced between the fluorophore and the lipophilic moiety [137].

The main advantage of membrane-anchored sensors compared with soluble dyes is their efficient incorporation into the liposomes. The lipid moiety of the former ensures stable and efficient integration into the lipid bilayer which reduces the amount of potentially costly dyes that have to be used, as entrapment of freely soluble dye is an inherently inefficient procedure [145–150]. Even more importantly, membrane-anchored dyes do not leak from the membrane, a problem often encountered with soluble dyes containing carboxylic acids. On the other side, an obvious drawback of lipid coupled dyes is that they are randomly distributed in both leaflets and selective removal or quenching is impossible or connected to the use of harsh chemicals that are often incompatible with delicate MPs and their catalytic activities [151]. We have recently solved this limitation by using a DNA double strand between the lipophilic anchor (cholesterol) and fluorescent moiety. Incorporation efficiency of the dye was shown to be >90%, and the outer dye is conveniently removed by a short incubation of the liposomes with DNase I and an ultracentrifugation step. In addition, the use of a DNA linker suppressed the undesired pK_a shift, previously observed with dyes directly coupled to a lipid. The simple chemistry involved makes this method attractive for many different sensors and the use of DNA hybridization technology ensures a high versatility [152]. In addition to these simple examples, more advanced membrane-anchored sensors rely on structural changes of environmentally sensitive DNA motifs, such as the pH sensitive i-Motif [153,154], G-quadruplexes [141,155,156], aptamers [138], DNAzymes [157], nanotweezers [158,159], and nanoswitches [160]. In these, the structural changes are transformed into a fluorescent read-out by attaching fluorescence quencher or FRET pairs to the DNA, in order to detect protons, metal ions and even small solutes such as ATP. Although mostly used *in vivo* so far, such complex sensors could also be useful for liposomal studies.

The development of new fluorescent dyes that are photostable as well as progress in the sensitivity of microscope cameras has further stimulated the field of single molecule techniques. Here, instead of observing the readout of an ensemble of a large number of molecules, single enzymes are monitored by fluorescence microscopy which allows to classify them into populations with different enzymatic behaviors. While such techniques have been around for many years for soluble enzymes and MPs in detergent solution [161–164], their application with proteoliposomes is very limited so far. It is, however, thanks to single molecule experiments with soluble and liposome embedded F_1F_0 ATP synthase that we have such a detailed picture of the F_1 binding change mechanism [165]. Apart from the ATP synthase, the groups of Jeuken and Stamou have performed single molecule proton pumping measurements with the quinol oxidase of *E. coli* [162] and the plasmamembrane P-type ATPase [166], in which the pH change within the lumen of small unilamellar vesicles (SUVs) was followed by fluorescent pH sensors. Surprisingly, in both systems they have observed long phases of enzymatic inactivity or even passive proton leakage through the protein and have attributed their findings to a sensitive enzyme regulation by the local environment (but see Berg et al. for a different finding) [167]. In case of the bo_3 oxidase, Jeuken and colleagues combined single protein/liposome studies with electrochemical measurements by tethering the proteoliposome to a gold electrode. By applying a voltage to the electrode, electrons were directly donated via lipid embedded ubiquinone to the bo_3 enzyme [162].

The challenges of fluorescent detection is to find a probe with all desired properties, such as high incorporation into vesicles, resistance to bleaching, specificity for the substrate/product, and high signal-to-noise ratio. Rational design of fluorescent dyes using click-chemistry in combination with biomolecules such as DNA allow for optimization of these properties leading to improved probes for the investigation of enzyme function in proteoliposomes.

Towards a synthetic cell

In the last section, we would like to briefly touch the potential of GUVs to study MP function. In contrast with 'classical' liposomes, GUVs are much larger in size (1–100 μm) and can directly be observed by light microscopic techniques [168]. On the downside, GUVs are less robust and their preparation is less straightforward

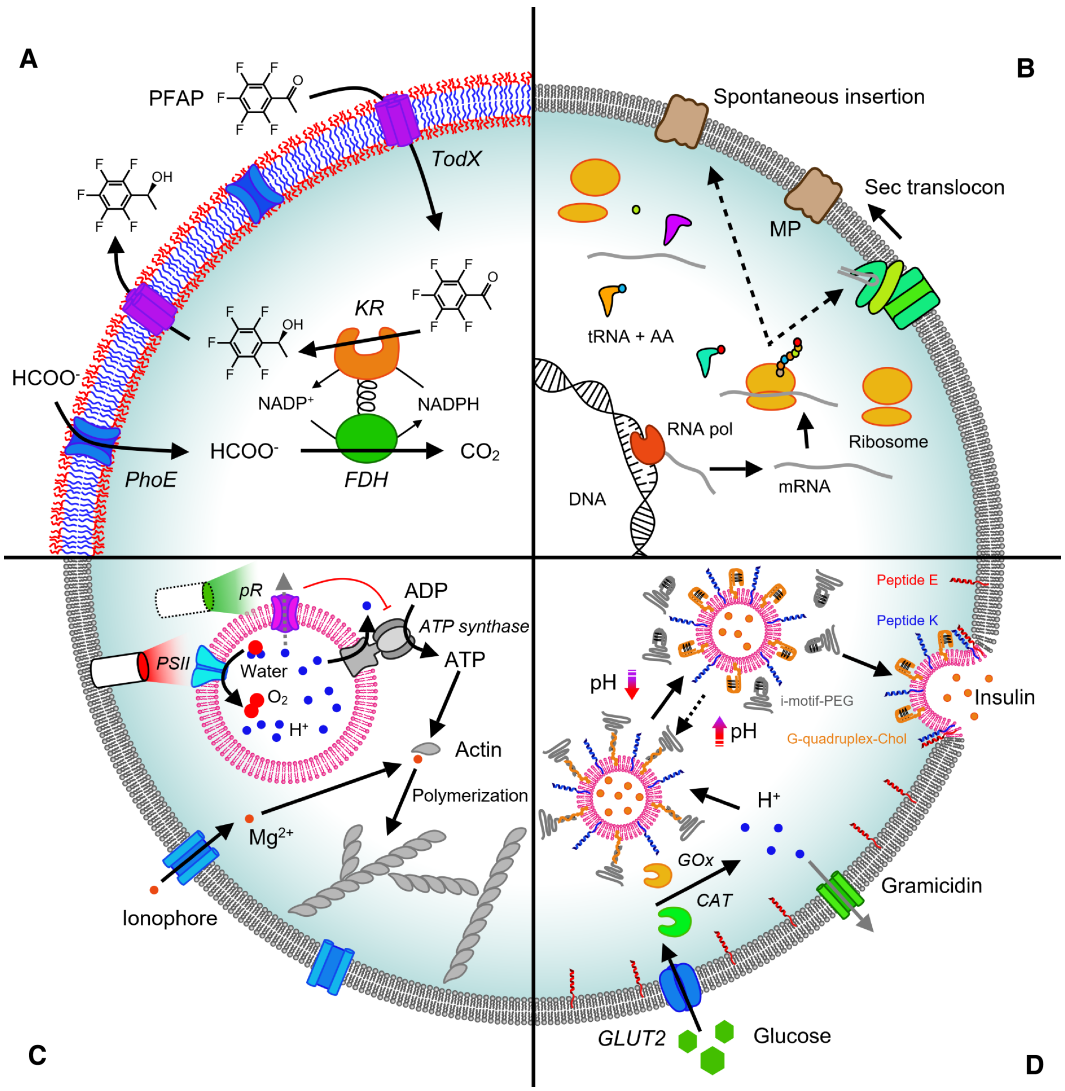

Figure 2. Applications of membrane proteins (MPs) in giant unilamellar vesicles (GUVs) and polymerosomes. Part 1 of 2 (**A**) MPs embedded in a polymerosome membrane enables import and export of substrates and products from a synthetic reaction cell. In that cell, pentafluoracetophenon (PFAP) is transformed to (S)-pentafluorophenyl ethanol ((S)-PFE) by ketoreductase (KR) inside of polymerosomes with NADPH as cofactor. NADPH is regenerated by formate dehydrogenase (FDH) which is fused to KR. As PFAP, (S)-PFE and formate do not readily diffuse across the polymerosome membrane, the selective channel protein TodX and the outer membrane pore PhoE were reconstituted in the membrane to alleviate the mass transport limitations [198]. (**B**) Membrane protein synthesis in GUVs by *in vitro* transcription and translation. Relevant components shown for these processes are DNA, RNA polymerase (RNA pol), the produced mRNA, ribosomes, tRNAs and amino acids (AA). After translation, the synthesized MP inserts either spontaneously [181] into the vesicle membrane, or requires the Sec translocon for correct insertion [182]. (**C**) Regulated ATP synthesis promoting actin polymerization in synthetic organelles. The membrane proteins F_1F_0 ATP synthase, photosystem II (PSII) and proteorhodopsin (pR) are coreconstituted in SUVs that are entrapped in GUVs. Red light stimulates PSII leading to oxidation of water and thus acidification of the SUV interior. Acidification leads to a proton gradient across the SUV membrane energizing ATP synthesis in the GUV lumen that is used to polymerize actin. On the other hand, green light stimulates proton export from the SUV lumen by proteorhodopsin, abolishing the proton gradient. Consequently, synthesis of ATP is stopped and actin polymerization is interrupted [189]. (**D**) Design of minimal pancreatic beta cell. The glucose transporter GLUT2 is reconstituted into the membrane of GUVs containing SUVs with encapsulated insulin. After uptake by GLUT2, glucose is oxidized by glucose oxidase (GOx) and catalase (CAT), leading to an acidification of the GUV lumen. This pH drop leads to the dehybridization of DNA double strand anchored to the SUV outer membrane by the formation of a pH sensitive motif, exposing the fusogenic peptide K on the outer SUV membrane.

Biochemical Society Transactions (2020) **48** 1473–1492
https://doi.org/10.1042/BST20190966

Figure 2. Applications of membrane proteins (MPs) in giant unilamellar vesicles (GUVs) and polymerosomes. Part 2 of 2
This allows fusion of the SUV with the GUV membrane via peptide E/K interaction, leading to the release of the encapsulated insulin. Gramicidin present in the GUV membrane modulates the pH response and allows to discern between normal and hyperglycemic conditions [191]. Figure 2A–D is adapted from the respective publications.

(see [169–178] for literature on GUV formation). Compared with SUVs, GUVs have a vastly increased surface and inner volume that allows for the encapsulation of entire protein machineries, small vesicles or even whole bacteria, in order to mimic increasingly complex functions of living cells [179]. Already in 2004, Noireaux and Libchaber [180] demonstrated the successful *in vitro* transcription and translation (IVTT) of GFP within GUVs, and recently similar systems were used to produce MPs directly inside GUVs, with either spontaneous [181] or assisted insertion [182] into the membrane. Very few examples describe the use of GUVs as replacement for SUVs in traditional vectorial transport experiments with MPs. A reason for this lack of transport experiments is the less than straightforward insertion of MPs into the fragile GUV membrane which is an ongoing field of research [114,115,168,183]. Levy and colleagues [184] showed successful detergent-mediated (using very small amounts of detergent) incorporation of bacteriorhodopsin which acidified the GUV lumen upon illumination and was followed by the pH sensitive dye pyranine. Biner et al. applied charge-mediated fusion to insert up to three different MPs reconstituted in positively charged SUV into a negatively charged GUV membrane [119]. Hansen et al. [185] finally reconstituted glucose transporter GLUT1 into GUVs using hydrogel-assisted swelling. Passive uptake of glucose into the GUV lumen was detected with a glucose oxidase coupled fluorescence system that was entrapped during GUV formation.

Given their size, GUVs are also of interest in the research on synthetic or artificial cells [183,186,187]. A recent example is the light-induced energization of IVTT in GUVs after entrapment of SUVs containing bacteriorhodopsin and ATP synthase [188], mimicking a cellular organelle. Lee et al. used photosystem II (PSII) and proteorhodopsin coreconstituted with ATP synthase in SUVs that can individually be stimulated by red and green light, respectively. PSII generates a pH gradient by oxidation of water on the inside of the vesicles and pR dissipates the gradient by outward proton pumping. These liposomes were entrapped in GUVs and, depending on the used light, ATP synthesis is either stimulated or abolished [189].

Another impressive example to use GUVs as a cell-mimicking system was demonstrated by Ces and colleagues by creating a non-natural signal cascade. Passive calcium influx into the GUV lumen via α-hemolysin activates phospholipase A2 that triggered liposome embedded mechanosensitive channels. The successful signal cascade was demonstrated by the release of calcein from the liposomes which can be detected as a fluorescence increase [190]. Finally, Chen et al. demonstrated the bottom-up synthesis of pancreatic beta cells using GUVs. The uptake of glucose via the glucose transporter GLUT2 into the GUV lumen triggered a cascade that mediated controlled insulin release by fusion of insulin containing vesicles with the GUV membrane. Most impressively, the system was able to discriminate between normal and hyperglycemic glucose concentrations [191].

As mentioned above, GUVs are not very stable and have also been shown to be susceptible for leakage [192,193]. Cell-sized vesicles produced from synthetic block copolymers, so called polymerosomes [194] or hybrids thereof with liposomes are improved in this regard [186,195] and have successfully been used to mimic compartmentalization of the eukaryotic cell [196] or to achieve spatial separation of otherwise incompatible multienzyme synthesis reactions [197,198]. However, initial experiments on polymersome embedded MPs have shown that enzymatic activity was decreased compared with pure lipid vesicles [199,200]. Nevertheless, proton pumping by bo_3 oxidase was recently demonstrated in hybrid polymer–lipid GUVs [201]. Some of these examples discussed above are depicted in Figure 2, see legend for further details.

These cell-mimetic applications greatly demonstrate the potential of giant vesicles. Importantly, a wise choice of detection method is crucial that allows high temporal resolution combined with sufficient sensitivity. To this end, photostable fluorophores are required to minimize bleaching during observation of single vesicles. To allow for prolonged observation and addition of substrates, vesicles have to be immobilized, which might have adverse effects on membrane properties such as the tightness of the membrane. Recently, experiments using microfluidics have shown formation and entrapment of GUVs in a nano-factory on a chip [202,203], which in the future might allow to create automated systems. However, many of the current approaches (single molecule measurements, microfluidics) require technical expertize and specialized equipment which limits the use of the

techniques in other laboratories. In the future, robust methods with a broad application and high reproducibility are critical for the success of GUVs in the field of MP research. Equivalently important is a detailed description of the data treatment. As microscopy experiments produce a large amount of data, user-friendly yet powerful analytical software is a necessary support during data analysis.

Perspectives

- *Importance of the field*: Proteoliposome research continues to be an indispensable tool for the mechanistic understanding of MPs. With the advent of structure determination by cryo electron microscopy, functional measurements are becoming the rate-limiting step.
- *Current thinking*: Development of improved methods for the precise orientation and coreconstitution of MPs into membranes are required. This is especially relevant for the bottom-up construction of artificial cells. Using fluorescent dyes with precisely tailored properties will ensure high sensitivity and temporal resolution.
- *Future directions*: Microscopy based measuring techniques applied on liposomes will further minimize the required amount of MPs, enabling the investigation of eukaryotic enzymes. The use of microfluidics for the generation and manipulation of GUVs might allow a higher level of control in lab-on-a-chip type experiments.

Competing Interests
The authors declare that there are no competing interests associated with the manuscript.

Funding
Research in the author's laboratory is funded by the Swiss National Science Foundation [grant no.176154].

Author Contribution
All authors contributed to the writing and editing of the manuscript.

Acknowledgements
We thank the members of the group for helpful discussions.

Abbreviations
CMC, critical micelle concentration; GUVs, giant unilamellar vesicles; IVTT, *in vitro* transcription and translation; MP, membrane proteins; PC, phosphatidylcholine; PE, phosphatidylethanolamine; PFAP, pentafluoracetophenon; PI, phosphatidyl inositol; PSII, photosystem II; SMA, styrene maleic acid; SUVs, small unilamellar vesicles.

References
1 Stillwell, W. (2016) Chapter 1 - Introduction to biological membranes. An Introd. to Biol. Membr. (Second Edition), Elsevier, ISBN 9780444637727, 3–15 https://doi.org/10.1016/B978-0-444-63772-7.00001-4
2 Alberts, B., Johnson, A., Lewis, J., Raff, M., Roberts, K. and Walter, P. (2017) *Molecular Biology of the Cell*, Garland Science, New York, NY
3 Nelson, D.L., Lehninger, A.L. and Cox, M.M. (2008) *Lehninger Principles of Biochemistry.* W. H. Freeman, New York
4 Shen, H.H., Lithgow, T. and Martin, L.L. (2013) Reconstitution of membrane proteins into model membranes: seeking better ways to retain protein activities. *Int. J. Mol. Sci.* **14**, 1589–1607 https://doi.org/10.3390/ijms14011589
5 Mitchell, P. (1966) Chemiosmotic coupling in oxidative and photosynthetic phosphorylation. *Biol. Rev.* **41**, 445–502 https://doi.org/10.1111/j.1469-185X.1966.tb01501.x
6 Mitchell, P. (1961) Coupling of phosphorylation to electron and hydrogen transfer by a chemi-osmotic type of mechanism. *Nature* **191**, 144–191 https://doi.org/10.1038/191144a0
7 Prebble, J. (2002) Peter Mitchell and the ox phos wars. *Trends Biochem. Sci.* **27**, 209–212 https://doi.org/10.1016/S0968-0004(02)02059-5
8 Racker, E. and Stoeckenius, W. (1974) Reconstitution of purple membrane vesicles catalyzing light-driven proton uptake and adenosine triphosphate formation. *J. Biol. Chem.* **249**, 662–663 PMID: 4272126
9 Hinkle, P.C., Kim, J.J. and Racker, E. (1972) Ion transport and respiratory control in vesicles formed from cytochrome oxidase and phospholipids. *J. Biol. Chem.* **247**, 1338–1339 PMID: 4334497

10 Racker, E. (1972) Reconstitution of a calcium pump with phospholipids and a purified Ca ++ - adenosine triphosphatase from sacroplasmic reticulum. *J. Biol. Chem.* **247**, 8198–8200 PMID: 4264487
11 Eytan, G.D., Persson, B., Ekebacke, A. and Rydström, J. (1987) Energy-linked nicotinamide-nucleotide transhydrogenase. Characterization of reconstituted ATP-driven transhydrogenase from beef heart mitochondria. *J. Biol. Chem.* **262**, 5008–5014 PMID: 3558383
12 Etemadi, A.H. (1985) Functional and orientational features of protein molecules in reconstituted lipid membranes. *Adv. Lipid Res.* **21**, 281–428 https://doi.org/10.1016/B978-0-12-024921-3.50014-9
13 Drachev, L.A., Kaulen, A.D., Ostroumov, S.A. and Skulachev, V.P. (1974) Electrogenesis by bacteriorhodopsin incorporated in a planar phospholipid membrane. *FEBS Lett.* **39**, 43–45 https://doi.org/10.1016/0014-5793(74)80012-8
14 Drachev, L.A., Jasaitis, A.A., Kaulen, A.D., Kondrashin, A.A., Liberman, E.A., Nemecek, I.B. et al. (1974) Direct measurement of electric current generation by cytochrome oxidase, H+-ATPase and bacteriorhodopsin. *Nature* **249**, 321–324 https://doi.org/10.1038/249321a0
15 Bazzone, A., Barthmes, M. and Fendler, K. (2017) SSM-based electrophysiology for transporter research. *Methods Enzymol.* **594**, 31–83 https://doi.org/10.1016/bs.mie.2017.05.008
16 Schulz, P., Garcia-Celma, J.J. and Fendler, K. (2008) SSM-based electrophysiology. *Methods* **46**, 97–103 https://doi.org/10.1016/j.ymeth.2008.07.002
17 Früh, V., IJzerman, Ad P. and Siegal, G. (2011) How to catch a membrane protein in action: a review of functional membrane protein immobilization strategies and their applications. *Chem. Rev.* **111**, 640–656 https://doi.org/10.1021/cr900088s
18 Smit, J.M., Waarts, B.L., Bittman, R. and Wilschut, J. (2003) Liposomes as target membranes in the study of virus receptor interaction and membrane fusion. *Methods Enzymol.* **372**, 374–392 https://doi.org/10.1016/S0076-6879(03)72022-9
19 Hoekstra, D. and Klappe, K. (1993) Fluorescence assays to monitor fusion of enveloped viruses. *Methods in enzymology*, **220**, 261 -276. https://doi.org/10.1016/0076-6879(93)20088-k
20 Tuthill, T.J., Bubeck, D., Rowlands, D.J. and Hogle, J.M. (2006) Characterization of early steps in the poliovirus infection process: receptor-decorated liposomes induce conversion of the virus to membrane-anchored entry-intermediate particles. *Journal of virology* **80**, 172–180
21 Whitbeck, J.C., Zuo, Y., Milne, R.S.B., Cohen, G.H. and Eisenberg, R.J. (2006) Stable association of herpes simplex virus with target membranes is triggered by low pH in the presence of the gD receptor, HVEM. *J. Virol.* **80**, 3773–3780 https://doi.org/10.1128/JVI.80.8.3773-3780.2006
22 Vallbracht, M., Brun, D., Tassinari, M., Vaney, M.C., Pehau-Arnaudet, G., Guardado-Calvo, P. et al. (2017) Structure-function dissection of pseudorabies virus glycoprotein B fusion loops. *J. Virol.* **92**, 1–26 https://doi.org/10.1128/JVI.01203-17
23 Zhukovsky, M.A., Basmaciogullari, S., Pacheco, B., Wang, L., Madani, N., Haim, H. et al. (2010) Thermal stability of the human immunodeficiency virus type 1 (HIV-1) receptors, CD4 and CXCR4, reconstituted in proteoliposomes. *PLoS One* **5**, e13249 https://doi.org/10.1371/journal.pone.0013249
24 Yeliseev, A. (2019) Expression and preparation of a G-protein-coupled cannabinoid receptor CB2 for NMR structural studies. *Curr. Protoc. Protein Sci.* **96**, 1–21 https://doi.org/10.1002/cpps.83
25 Shi, C., Öetster, C., Bohg, C., Li, L., Lange, S., Chevelkov, V. et al. (2019) Structure and dynamics of the rhomboid protease GlpG in liposomes studied by solid-state NMR. *J. Am. Chem. Soc.* **141**, 17314–17321 https://doi.org/10.1021/jacs.9b08952
26 Zhou, S., Pettersson, P., Huang, J., Sjöholm, J., Sjöstrand, D., Pomès, R. et al. (2018) Solution NMR structure of yeast Rcf1, a protein involved in respiratory supercomplex formation. *Proc. Natl. Acad. Sci. U.S.A.* **115**, 3048–3053 https://doi.org/10.1073/pnas.1712061115
27 Patel, M.M. and Patel, B.M. (2017) Crossing the blood-brain barrier: recent advances in drug delivery to the brain. *CNS Drugs* **31**, 109–133 https://doi.org/10.1007/s40263-016-0405-9
28 Li, X., Tsibouklis, J., Weng, T., Zhang, B., Yin, G., Feng, G. et al. (2017) Nano carriers for drug transport across the blood-brain barrier. *J. Drug Target.* **25**, 17–28 https://doi.org/10.1080/1061186X.2016.1184272
29 Mittal, S., Chaudhary, A., Chaudhary, A. and Kumar, A. (2020) Proniosomes: the effective and efficient drug-carrier system. *Ther. Deliv.* **11**, 125–137 https://doi.org/10.4155/tde-2019-0065
30 Zylberberg, C. and Matosevic, S. (2016) Pharmaceutical liposomal drug delivery: a review of new delivery systems and a look at the regulatory landscape. *Drug Deliv.* **23**, 3319–3329 https://doi.org/10.1080/10717544.2016.1177136
31 Abu Lila, A.S. and Ishida, T. (2017) Liposomal delivery systems: design optimization and current applications. *Biol. Pharm. Bull.* **40**, 1–10 https://doi.org/10.1248/bpb.b16-00624
32 Lee, Y. and Thompson, D.H. (2017) Stimuli-responsive liposomes for drug delivery. *Wiley Interdiscip. Rev. Nanomed. Nanobiotechnol.* **9** https://doi.org/10.1002/wnan.1450
33 Rigaud, J.L., Pitard, B. and Levy, D. (1995) Reconstitution of membrane proteins into liposomes: application to energy-transducing membrane proteins. *Biochim. Biophys. Acta* **1231**, 223–246 https://doi.org/10.1016/0005-2728(95)00091-V
34 Laubinger, W. and Dimroth, P. (1988) Characterization of the ATP synthase of Propionigenium modestum as a primary sodium pump. *Biochemistry* **27**, 7531–7537 https://doi.org/10.1021/bi00419a053
35 Rigaud, J.-L. and Lévy, D. (2003) Reconstitution of membrane proteins into liposomes. *Methods Mol. Biol.* **1635**, 65–86 https://doi.org/10.1016/S0076-6879(03)72004-7
36 Skrzypek, R., Iqbal, S. and Callaghan, R. (2018) Methods of reconstitution to investigate membrane protein function. *Methods* **147**, 126–141 https://doi.org/10.1016/j.ymeth.2018.02.012
37 Seddon, A.M., Curnow, P. and Booth, P.J. (2004) Membrane proteins, lipids and detergents: not just a soap opera. *Biochim. Biophys. Acta* **1666**, 105–117 https://doi.org/10.1016/j.bbamem.2004.04.011
38 Degrip, W.J., Vanoostrum, J. and Bovee-Geurts, P.H. (1998) Selective detergent-extraction from mixed detergent/lipid/protein micelles, using cyclodextrin inclusion compounds: a novel generic approach for the preparation of proteoliposomes. *Biochem. J.* **330**(Pt 2), 667–674 https://doi.org/10.1042/bj3300667
39 Geertsma, E.R., Nik Mahmood, N.A.B., Schuurman-Wolters, G.K. and Poolman, B. (2008) Membrane reconstitution of ABC transporters and assays of translocator function. *Nat. Protoc.* **3**, 256–266 https://doi.org/10.1038/nprot.2007.519
40 Hatzi, P., Mourtas, S., Klepetsanis, P.G. and Antimisiaris, S.G. (2007) Integrity of liposomes in presence of cyclodextrins: effect of liposome type and lipid composition. *Int. J. Pharm.* **333**, 167–176 https://doi.org/10.1016/j.ijpharm.2006.09.059
41 Knol, J. (1999) PhD-Thesis - Membrane Reconstitution and Functional Analysis of a Sugar Transport System
42 Tsai, M.F. and Miller, C. (2013) Substrate selectivity in arginine-dependent acid resistance in enteric bacteria. *Proc. Natl. Acad. Sci. U.S.A.* **110**, 5893–5897 https://doi.org/10.1073/pnas.1301442110

43 Van Klooster, J.S., Cheng, T., Sikkema, H.R. and Jeucken, A. (2020) Membrane lipid requirements of the lysine transporter Lyp1 from *Saccharomyces cerevisiae*. *J. Mol. Biol.* **432**, 4023–4031 https://doi.org/10.1016/j.jmb.2020.04.029
44 Harris, N.J., Charalambous, K., Findlay, H.E. and Booth, P.J. (2018) Lipids modulate the insertion and folding of the nascent chains of alpha helical membrane proteins. *Biochem. Soc. Trans.* **46**, 1355–1366 https://doi.org/10.1042/BST20170424
45 Martens, C., Shekhar, M., Borysik, A., Lau, A.M., Reading, E., Tajkhorshid, E. et al. (2018) Direct protein–lipid interactions shape the conformational landscape of secondary transporters. *Nat. Commun.* **9**, 4151 https://doi.org/10.1038/s41467-018-06704-1
46 Mirandela, G.D., Tamburrino, G., Hoskisson, P.A., Zachariae, U. and Javelle, A. (2019) The lipid environment determines the activity of the *Escherichia coli* ammonium transporter AmtB. *FASEB J.* **33**, 1989–1999 https://doi.org/10.1096/fj.201800782R
47 Vitrac, H., Mallampalli, V.K.P.S., Bogdanov, M. and Dowhan, W. (2019) The lipid-dependent structure and function of LacY can be recapitulated and analyzed in phospholipid-containing detergent micelles. *Sci. Rep.* **9**, 11338 https://doi.org/10.1038/s41598-019-47824-y
48 Dowhan, W., Vitrac, H. and Bogdanov, M. (2019) Lipid-assisted membrane protein folding and topogenesis. *Protein J.* **38**, 274–288 https://doi.org/10.1007/s10930-019-09826-7
49 Zhang, M., Mileykovskaya, E. and Dowhan, W. (2005) Cardiolipin is essential for organization of complexes III and IV into a supercomplex in intact yeast mitochondria. *J. Biol. Chem.* **280**, 29403–29408 https://doi.org/10.1074/jbc.M504955200
50 Paradies, G., Paradies, V., De Benedictis, V., Ruggiero, F.M. and Petrosillo, G. (2014) Functional role of cardiolipin in mitochondrial bioenergetics. *Biochim. Biophys. Acta* **1837**, 408–417 https://doi.org/10.1016/j.bbabio.2013.10.006
51 Arnarez, C., Marrink, S.J. and Periole, X. (2016) Molecular mechanism of cardiolipin-mediated assembly of respiratory chain supercomplexes. *Chem. Sci.* **7**, 4435–4443 https://doi.org/10.1039/C5SC04664E
52 de Lima Santos, H., Lopes, M.L., Maggio, B. and Ciancaglini, P. (2005) Na,K-ATPase reconstituted in liposomes: effects of lipid composition on hydrolytic activity and enzyme orientation. *Colloids Surf. B Biointerfaces* **41**, 239–248 https://doi.org/10.1016/j.colsurfb.2004.12.013
53 Mohraz, M. (1999) Reconstitution of detergent-solubilized Na,K-ATPase and formation of two-dimensional crystals. *J. Struct. Biol.* **125**, 76–85 https://doi.org/10.1006/jsbi.1998.4067
54 Cornelius, F. (2001) Modulation of Na,K-ATPase and Na-ATPase activity by phospholipids and cholesterol. I. Steady-state kinetics. *Biochemistry* **40**, 8842–8851 https://doi.org/10.1021/bi010541g
55 Abeywardena, M.Y., Allen, T.M. and Charnock, J.S. (1983) Lipid–protein interactions of reconstituted membrane-associated adenosinetriphosphatases. Use of a gel-filtration procedure to examine phospholipid-activity relationships. *Biochim. Biophys. Acta* **729**, 62–74 https://doi.org/10.1016/0005-2736(83)90456-X
56 Cornelius, F., Turner, N. and Christensen, H.R.Z. (2003) Modulation of Na,K-ATPase by phospholipids and cholesterol. II. Steady-state and presteady-state kinetics. *Biochemistry* **42**, 8541–8549 https://doi.org/10.1021/bi034532e
57 Yeagle, P.L. (1993) *The Membrane of Cells* (2nd edition), Academic Press
58 Lichtenberg, D., Ahyayauch, H. and Goni, F.M. (2013) The mechanism of detergent solubilization of lipid bilayers. *Biophys. J.* **105**, 289–299 https://doi.org/10.1016/j.bpj.2013.06.007
59 Marquardt, D., Geier, B. and Pabst, G. (2015) Asymmetric lipid membranes: towards more realistic model systems. *Membranes* **5**, 180–196 https://doi.org/10.3390/membranes5020180
60 Furse, S. and Scott, D.J. (2016) Three-dimensional distribution of phospholipids in gram negative bacteria. *Biochemistry* **55**, 4742–4747 https://doi.org/10.1021/acs.biochem.6b00541
61 Bogdanov, M., Pyrshev, K., Yesylevskyy, S., Ryabichko, S., Boiko, V., Ivanchenko, P. et al. (2020) Phospholipid distribution in the cytoplasmic membrane of Gram-negative bacteria is highly asymmetric, dynamic, and cell shape-dependent. *Sci. Adv.* **6**, eaaz6333 https://doi.org/10.1126/sciadv.aaz6333
62 Doktorova, M., Heberle, F.A., Eicher, B., Standaert, R.F., Katsaras, J., London, E. et al. (2018) Preparation of asymmetric phospholipid vesicles for use as cell membrane models. *Nat. Protoc.* **13**, 2086–2101 https://doi.org/10.1038/s41596-018-0033-6
63 Markones, M., Fippel, A., Kaiser, M., Drechsler, C., Hunte, C. and Heerklotz, H. (2020) Stairway to asymmetry: five steps to lipid-asymmetric proteoliposomes. *Biophys. J.* **118**, 294–302 https://doi.org/10.1016/j.bpj.2019.10.043
64 Althoff, T., Davies, K.M., Schulze, S., Joos, F. and Kühlbrandt, W. (2012) GRecon: a method for the lipid reconstitution of membrane proteins. *Angew. Chem. Int. Ed. Engl.* **51**, 8343–8347 https://doi.org/10.1002/anie.201202094
65 Blum, T.B., Hahn, A., Meier, T., Davies, K.M. and Kühlbrandt, W. (2019) Dimers of mitochondrial ATP synthase induce membrane curvature and self-assemble into rows. *Proc. Natl. Acad. Sci. U.S.A.* **116**, 4250–4255 https://doi.org/10.1073/pnas.1816556116
66 Denisov, I.G., Schuler, M.A. and Sligar, S.G. (2019) Nanodiscs as a new tool to examine lipid–protein interactions. *Methods Mol. Biol.* **2003**, 645–671 https://doi.org/10.1007/978-1-4939-9512-7_25
67 Kariyazono, H., Nadai, R., Miyajima, R., Takechi-Haraya, Y., Baba, T., Shigenaga, A. et al. (2016) Formation of stable nanodiscs by bihelical apolipoprotein A-I mimetic peptide. *J. Pept. Sci.* **22**, 116–122 https://doi.org/10.1002/psc.2847
68 Carlson, M.L., Young, J.W., Zhao, Z., Fabre, L., Jun, D., Li, J. et al. (2018) The Peptidisc, a simple method for stabilizing membrane proteins in detergent-free solution. *eLife* **7**, 1–23 https://doi.org/10.7554/eLife.34085
69 Angiulli, G., Dhupar, H.S., Suzuki, H., Wason, I.S., Duong Van Hoa F. and Walz, T. (2020) New approach for membrane protein reconstitution into peptidiscs and basis for their adaptability to different proteins. *eLife* **9**, 1–20 https://doi.org/10.7554/eLife.53530
70 Smirnova, I.A., Sjöstrand, D., Li, F., Björck, M., Schäfer, J., Östbye, H. et al. (2016) Isolation of yeast complex IV in native lipid nanodiscs. *Biochim. Biophys. Acta* **1858**, 2984–2992 https://doi.org/10.1016/j.bbamem.2016.09.004
71 Dörr, J.M., Scheidelaar, S., Koorengevel, M.C., Dominguez, J.J., Schäfer, M., van Walree, C.A. et al. (2016) The styrene–maleic acid copolymer: a versatile tool in membrane research. *Eur. Biophys. J.* **45**, 3–21 https://doi.org/10.1007/s00249-015-1093-y
72 Dörr, J.M., Koorengevel, M.C., Schäfer, M., Prokofyev, A.V., Scheidelaar, S., van der Cruijsen, E.A. et al. (2014) Detergent-free isolation, characterization, and functional reconstitution of a tetrameric K+ channel: The power of native nanodiscs. *Proc. Natl. Acad. Sci. U.S.A.* **111**, 18607–18612 https://doi.org/10.1073/pnas.1416205112

73 Parmar, M.J., Lousa, C.D.M., Muench, S.P., Goldman, A. and Postis, V.L.G. (2016) Artificial membranes for membrane protein purification, functionality and structure studies. *Biochem. Soc. Trans.* **44**, 877–882 https://doi.org/10.1042/BST20160054
74 Broecker, J., Eger, B.T. and Ernst, O.P. (2017) Crystallogenesis of membrane proteins mediated by polymer-bounded lipid nanodiscs. *Structure* **25**, 384–392 https://doi.org/10.1016/j.str.2016.12.004
75 Smirnova, I.A., Ädelroth, P. and Brzezinski, P. (2018) Extraction and liposome reconstitution of membrane proteins with their native lipids without the use of detergents. *Sci. Rep.* **8**, 14950 https://doi.org/10.1038/s41598-018-33208-1
76 Dutta, D., Esmaili, M., Overduin, M. and Fliegel, L. (2020) Expression and detergent free purification and reconstitution of the plant plasma membrane Na^+/H^+ antiporter SOS1 overexpressed in *Pichia pastoris*. *Biochim. Biophys. Acta* **1862**, 183111 https://doi.org/10.1016/j.bbamem.2019.183111
77 Scheidelaar, S., Koorengevel, M.C., van Walree, C.A., Dominguez, J.J., Dörr, J.M. and Killian J.A. (2016) Effect of polymer composition and pH on membrane solubilization by styrene-maleic acid copolymers. *Biophys. J.* **111**, 1974–1986 https://doi.org/10.1016/j.bpj.2016.09.025
78 Fluman, N., Tobiasson, V. and Von Heijne, G. (2017) Stable membrane orientations of small dual-topology membrane proteins. *Proc. Natl. Acad. Sci. U.S.A.* **114**, 7987–7992 https://doi.org/10.1073/pnas.1706905114
79 Hegde, R.S. and Keenan, R.J. (2011) Tail-anchored membrane protein insertion into the endoplasmic reticulum. *Nat. Rev. Mol. Cell Biol.* **12**, 787–798 https://doi.org/10.1038/nrm3226
80 Huang, H., Ge, B., Zhang, S., Li, J., Sun, C., Yue, T. et al. (2019) Using fluorescence quenching titration to determine the orientation of a model transmembrane protein in mimic membranes. *Materials* **12**, 349 https://doi.org/10.3390/ma12030349
81 Eytan, G.D. (1982) Use of liposomes for reconstitution of biological functions. *Biochim. Biophys. Acta* **694**, 185–202 https://doi.org/10.1016/0304-4157(82)90024-7
82 Dröse, S., Galkin, A. and Brandt, U. (2005) Proton pumping by complex I (NADH:ubiquinone oxidoreductase) from *Yarrowia lipolytica* reconstituted into proteoliposomes. *Biochim. Biophys. Acta* **1710**, 87–95 https://doi.org/10.1016/j.bbabio.2005.10.001
83 Gerber, G.E., Gray, C.P., Wildenauer, D. and Khorana, H.G. (1977) Orientation of bacteriorhodopsin in *Halobacterium halobium* as studied by selective proteolysis. *Proc. Natl. Acad. Sci. U.S.A.* **74**, 5426–5430 https://doi.org/10.1073/pnas.74.12.5426
84 Kalmbach, R., Chizhov, I., Schumacher, M.C., Friedrich, T., Bamberg, E. and Engelhard M. (2007) Functional cell-free synthesis of a seven helix membrane protein: in situ insertion of bacteriorhodopsin into liposomes. *J. Mol. Biol.* **371**, 639–648 https://doi.org/10.1016/j.jmb.2007.05.087
85 Tunuguntla, R., Bangar, M., Kim, K., Stroeve, P., Ajo-Franklin, C.M. and Noy, A. (2013) Lipid bilayer composition can influence the orientation of proteorhodopsin in artificial membranes. *Biophys. J.* **105**, 1388–1396 https://doi.org/10.1016/j.bpj.2013.07.043
86 Wiedenmann, A., Dimroth, P. and von Ballmoos, C. (2008) $\Delta\psi$ and ΔpH are equivalent driving forces for proton transport through isolated F0 complexes of ATP synthases. *Biochim. Biophys. Acta* **1777**, 1301–1310 https://doi.org/10.1016/j.bbabio.2008.06.008
87 Knol, J., Veenhoff, L., Liang, W.J., Henderson, P.J., Leblanc, G. and Poolman, B. (1996) Unidirectional reconstitution into detergent-destabilized liposomes of the purified lactose transport system of *Streptococcus thermophilus*. *J. Biol. Chem.* **271**, 15358–15366 https://doi.org/10.1074/jbc.271.26.15358
88 Fang, G., Friesen, R., Lanfermeijer, F., Hagting, A., Poolman, B. and Konings, W.N. (1999) Manipulation of activity and orientation of membrane-reconstituted di-tripeptide transport protein DtpT of *Lactococcus lactis*. *Mol. Membr. Biol.* **16**, 297–304 https://doi.org/10.1080/096876899294517
89 van Geest, M. and Lolkema, J.S. (2000) Membrane topology and insertion of membrane proteins: search for topogenic signals. *Microbiol. Mol. Biol. Rev.* **64**, 13–33 https://doi.org/10.1128/MMBR.64.1.13-33.2000
90 Richard, P., Rigaud, J.L. and Graber, P. (1990) Reconstitution of CF0F1 into liposomes using a new reconstitution procedure. *Eur. J. Biochem.* **193**, 921–925 https://doi.org/10.1111/j.1432-1033.1990.tb19418.x
91 Levy, D., Gulik, A., Bluzat, A. and Rigaud, J.L. (1992) Reconstitution of the sarcoplasmic reticulum Ca(2+)-ATPase: mechanisms of membrane protein insertion into liposomes during reconstitution procedures involving the use of detergents. *Biochim. Biophys. Acta* **1107**, 283–298 https://doi.org/10.1016/0005-2736(92)90415-I
92 Pagano, A. and Spiess, M. (2005) Reconstitution of Rab4-dependent vesicle formation in vitro. *Methods Enzymol.* **403**, 81–92 https://doi.org/10.1016/S0076-6879(05)03008-9
93 Öjemyr, L.N., Von Ballmoos, C., Faxén, K., Svahn, E. and Brzezinski, P. (2012) The membrane modulates internal proton transfer in cytochrome c oxidase. *Biochemistry* **51**, 1092–1100 https://doi.org/10.1021/bi201795c
94 Happe, M., Teather, R.M., Overath, P., Knobling, A. and Oesterhelt, D. (1977) Direction of proton translocation in proteoliposomes formed from purple membrane and acidic lipids depends on the pH during reconstitution. *Biochim. Biophys. Acta* **465**, 415–420 https://doi.org/10.1016/0005-2736(77)90092-X
95 Ritzmann, N., Thoma, J., Hirschi, S., Kalbermatter, D., Fotiadis, D. and Müller, D.J. (2017) Fusion domains guide the oriented insertion of light-driven proton pumps into liposomes. *Biophys. J.* **113**, 1181–1186 https://doi.org/10.1016/j.bpj.2017.06.022
96 Zheng, H., Lee, S., Llaguno, M.C. and Jiang, Q.-X. (2016) bSUM: A bead-supported unilamellar membrane system facilitating unidirectional insertion of membrane proteins into giant vesicles. *J. Gen. Physiol.* **147**, 77–93 https://doi.org/10.1085/jgp.201511448
97 Schadauer, F., Geiss, A. F., Srajer, J., Siebenhofer, B., Frank, P., Reiner-Rozman, C. et al. (2015) Silica nanoparticles for the oriented encapsulation of membrane proteins into artificial bilayer lipid membranes. *Langmuir* **31**, 2511–2516 https://doi.org/10.1021/la504417j
98 Geiss, A. F., Bliem, C., Frank, P., Reiner-Rozman, C., Kewney, J., Boersch, M. et al. (2017) Proteo-lipobeads to encapsulate cytochrome c oxidase from *Paracoccus denitrificans*. *J. Colloid Interface Sci.* **500**, 119–125 https://doi.org/10.1016/j.jcis.2017.04.009
99 Bronder, A. M., Bieker, A., Elter, S., Etzkorn, M., Häussinger, D. and Oesterhelt, F. (2016) Oriented membrane protein reconstitution into tethered lipid membranes for AFM force spectroscopy. *Biophys. J.* **111**, 1925–1934 https://doi.org/10.1016/j.bpj.2016.08.051
100 Sumino, A., Uchihashi, T. and Oiki, S. (2017) Oriented reconstitution of the full-length KcsA potassium channel in a lipid bilayer for AFM imaging. *J. Phys. Chem. Lett.* 785–793 https://doi.org/10.1021/acs.jpclett.6b03058
101 Jang, S. and Javadov, S. (2018) Current challenges in elucidating respiratory supercomplexes in mitochondria: methodological obstacles. *Front. Physiol.* **9**, 238 https://doi.org/10.3389/fphys.2018.00238
102 Liu, F., Lössl, P., Rabbitts, B.M., Balaban, R.S. and Heck, A.J.R. (2018) The interactome of intact mitochondria by cross-linking mass spectrometry provides evidence for coexisting respiratory supercomplexes. *Mol. Cell. Proteomics* **17**, 216–232 https://doi.org/10.1074/mcp.RA117.000470

103 Enríquez, J.A. (2016) Supramolecular organization of respiratory complexes. *Annu. Rev. Physiol.* **78**, 533–561 https://doi.org/10.1146/annurev-physiol-021115-105031
104 Brzezinski, P. (2020) New structures reveal interaction dynamics in respiratory supercomplexes. *Trends Biochem. Sci.* **45**, 3–5 https://doi.org/10.1016/j.tibs.2019.10.011
105 Biner, O., Fedor, J.G., Yin, Z. and Hirst, J. (2020) Bottom-up construction of a minimal system for cellular respiration and energy regeneration. *ACS Synth. Biol.* **9**, 1450–1459
106 Lee, C., Kang, H.J., von Ballmoos, C., Newstead, S., Uzdavinys, P., Dotson, D.L. et al. (2013) A two-domain elevator mechanism for sodium/proton antiport. *Nature* **501**, 573–577 https://doi.org/10.1038/nature12484
107 Uzdavinys, P., Coinçon, M., Nji, E., Ndi, M., Winkelmann, I., von Ballmoos, C. et al. (2017) Dissecting the proton transport pathway in electrogenic Na+/H+ antiporters. *Proc. Natl. Acad. Sci. U.S.A.* **114**, E1101–E1110 https://doi.org/10.1073/pnas.1614521114
108 Juge, N., Yoshida, Y., Yatsushiro, S., Omote, H. and Moriyama, Y. (2006) Vesicular glutamate transporter contains two independent transport machineries. *J. Biol. Chem.* **281**, 39499–39506 https://doi.org/10.1074/jbc.M607670200
109 Pols, T., Sikkema, H. R., Gaastra, B. F., Frallicciardi, J., Śmigiel, W. M., Singh, S. et al. (2019) A synthetic metabolic network for physicochemical homeostasis. *Nat. Commun.* **10**, 4239 https://doi.org/10.1038/s41467-019-12287-2
110 Serdiuk, T., Balasubramaniam, D., Sugihara, J., Mari, S.A., Kaback, H.R. and Müller, D.J. (2016) YidC assists the stepwise and stochastic folding of membrane proteins. *Nat. Chem. Biol.* **12**, 911–917 https://doi.org/10.1038/nchembio.2169
111 Krenn, B.E., Koppenaal, F., Van Walraven, H.S., Krab, K. and Kraayenhof, R. (1993) Co-reconstitution of the H+-ATP synthase and cytochrome b-563c-554 complex from a thermophilic cyanobacterium. *Biochim. Biophys. Acta* **1140**, 271–281 https://doi.org/10.1016/0005-2728(93)90066-O
112 Von Ballmoos, C., Biner, O., Nilsson, T. and Brzezinski, P. (2016) Mimicking respiratory phosphorylation using purified enzymes. *Biochim. Biophys. Acta* **1857**, 321–331 https://doi.org/10.1016/j.bbabio.2015.12.007
113 Nordlund, G., Brzezinski, P. and Von Ballmoos, C. (2014) SNARE-fusion mediated insertion of membrane proteins into native and artificial membranes. *Nat. Commun.* **5**, 1–8 https://doi.org/10.1038/ncomms5303
114 Biner, O., Schick, T., Muller, Y. and von Ballmoos, C. (2016) Delivery of membrane proteins into small and giant unilamellar vesicles by charge-mediated fusion. *FEBS Lett.* **590**, 2051–2062 https://doi.org/10.1002/1873-3468.12233
115 Ishmukhametov, R.R., Russell, A.N. and Berry, R.M. (2016) A modular platform for one-step assembly of multi-component membrane systems by fusion of charged proteoliposomes. *Nat. Commun.* **7**, 13025 https://doi.org/10.1038/ncomms13025
116 Rabe, M., Schwieger, C., Zope, H.R., Versluis, F. and Kros, A. (2014) Membrane interactions of fusogenic coiled-coil peptides: implications for lipopeptide mediated vesicle fusion. *Langmuir* **30**, 7724–7735 https://doi.org/10.1021/la500987c
117 Stengel, G., Zahn, R. and Höök, F. (2007) DNA-induced programmable fusion of phospholipid vesicles. *J. Am. Chem. Soc.* **129**, 9584–9585 https://doi.org/10.1021/ja073200k
118 Chan, Y.H., van Lengerich, B. and Boxer, S.G. (2008) Lipid-anchored DNA mediates vesicle fusion as observed by lipid and content mixing. *Biointerphases* **3**, FA17 https://doi.org/10.1116/1.2889062
119 Marsden, H.R., Tomatsu, I. and Kros, A. (2011) Model systems for membrane fusion. *Chem. Soc. Rev.* **40**, 1572–1585 https://doi.org/10.1039/C0CS00115E
120 Raschle, T., Lin, C., Jungmann, R., Shih, W. M. and Wagner, G. (2015) Controlled Co-reconstitution of Multiple Membrane Proteins in Lipid Bilayer Nanodiscs Using DNA as a Scaffold. *ACS chemical biology*, **10**, 2448–2454. https://doi.org/10.1021/acschembio.5b00627
121 Serdiuk, T., Steudle, A., Mari, S. A., Manioglu, S., Kaback, H. R., Kuhn, A. et al. (2019) Insertion and folding pathways of single membrane proteins guided by translocases and insertases. *Sci. Adv.* **5**, 1–11 https://doi.org/10.1126/sciadv.aau6824
122 Tsien, R.Y. (1980) New calcium indicators and buffers with high selectivity against magnesium and protons: design, synthesis, and properties of prototype structures. *Biochemistry* **19**, 2396–2404 https://doi.org/10.1021/bi00552a018
123 Minta, A. and Tsien, R.Y. (1989) Fluorescent indicators for cytosolic sodium. *J. Biol. Chem.* **264**, 19449–19457 PMID: 2808435
124 Verkman, A.S. (1990) Development and biological applications of chloride-sensitive fluorescent indicators. *Am. J. Physiol.* C375–CC88, **259** https://doi.org/10.1152/ajpcell.1990.259.3.C375
125 Berendes, R., Burger, A., Voges, D., Demange, P. and Huber, R. (1993) Calcium influx through annexin V ion channels into large unilamellar vesicles measured with fura-2. *FEBS Lett.* **317**, 131–134 https://doi.org/10.1016/0014-5793(93)81507-V
126 Rydström, J. (1979) Energy-linked nicotinamide nucleotide transhydrogenase. Properties of proton-translocating and ATP-driven transhydrogenase reconstituted from synthetic phospholipids and purified transhydrogenase from beef heart mitochondria. *J. Biol. Chem.* **254**, 8611–8619 PMID: 38254
127 Dufour, J.P., Goffeau, A. and Tsong, T.Y. (1982) Active proton uptake in lipid vesicles reconstituted with the purified yeast plasma membrane ATPase. Fluorescence quenching of 9-amino-6-chloro-2-methoxyacridine. *J. Biol. Chem.* **257**, 9365–9371 PMID: 6213606
128 Wielandt, A.G., Palmgren, M.G., Fuglsang, A.T., Günther-Pomorski, T. and Justesen, B.H. (2016) Measuring H+ pumping and membrane potential formation in sealed membrane vesicle systems. *Methods Mol. Biol.* **1377**, 171–180 https://doi.org/10.1007/978-1-4939-3179-8_17
129 Graf, S., Brzezinski, P. and von Ballmoos, C. (2019) The proton pumping bo oxidase from Vitreoscilla. *Sci. Rep.* **9**, 1–10 https://doi.org/10.1038/s41598-019-40723-2
130 Waggoner, A.S. (1979) Dye indicators of membrane potential. *Annu. Rev. Biophys. Bioeng.* **8**, 47–68 https://doi.org/10.1146/annurev.bb.08.060179.000403
131 Loew, L.M. (2015) Design and use of organic voltage sensitive dyes. *Adv. Exp. Med. Biol.* **859**, 27–53 https://doi.org/10.1007/978-3-319-17641-3_2
132 Miller, E.W. (2016) Small molecule fluorescent voltage indicators for studying membrane potential. *Curr. Opin. Chem. Biol.* **33**, 74–80 https://doi.org/10.1016/j.cbpa.2016.06.003
133 Liu, P. and Miller, E.W. (2020) Electrophysiology, unplugged: imaging membrane potential with fluorescent indicators. *Acc. Chem. Res.* **53**, 11–19 https://doi.org/10.1021/acs.accounts.9b00514
134 Vetter, I., Carter, D., Bassett, J., Deuis, J. R., Tay, B., Jami, S. et al. (2020) High-Throughput fluorescence assays for ion channels and GPCRs. *Adv. Exp. Med. Biol.* **1131**, 27–72 https://doi.org/10.1007/978-3-030-12457-1_3
135 Thelen, M., Petrone, G., O'Shea, P.S. and Azzi, A. (1984) The use of fluorescein-dipalmitoylphosphatidylethanolamine for measuring pH-changes in the internal compartment of phospholipid vesicles. *Biochim. Biophys. Acta* **766**, 161–168 https://doi.org/10.1016/0005-2728(84)90228-7

136 Etter, E.F., Minta, A., Poenie, M. and Fay, F.S. (1996) Near-membrane [Ca2+] transients resolved using the Ca^{2+} indicator FFP18. *Proc. Natl. Acad. Sci. U.S.A.* **93**, 5368–5373 https://doi.org/10.1073/pnas.93.11.5368
137 Ke, G., Zhu, Z., Wang, W., Zou, Y., Guan, Z., Jia, S. et al. (2014) A cell-surface-anchored ratiometric fluorescent probe for extracellular pH sensing. *ACS Appl. Mater. Interfaces* **6**, 15329–15334 https://doi.org/10.1021/am503818n
138 Xiong, M., Zhu, H., Rong, Q., Yang, C., Qiu, L., Zhang, X. B. et al. (2016) A membrane-anchored fluorescent probe for detecting K+ in the cell microenvironment. *Chem. Commun.* **52**, 4679–4682 https://doi.org/10.1039/C6CC00192K
139 Yao, H.W., Zhu, X.Y., Guo, X.F. and Wang, H. (2016) An amphiphilic fluorescent probe designed for extracellular visualization of nitric oxide released from living cells. *Anal. Chem.* **88**, 9014–9021 https://doi.org/10.1021/acs.analchem.6b01532
140 Ohgaki, R., Teramura, Y., Hayashi, D., Quan, L., Okuda, S., Nagamori, S. et al. (2017) Ratiometric fluorescence imaging of cell surface pH by poly (ethylene glycol)-phospholipid conjugated with fluorescein isothiocyanate. *Sci. Rep.* **7**, 1–9 https://doi.org/10.1038/s41598-017-17459-y
141 Świtalska, A., Dembska, A., Fedoruk-Wyszomirska, A. and Juskowiak, B. (2018) Cholesterol-bearing fluorescent g-quadruplex potassium probes for anchoring at the langmuir monolayer and cell membrane. *Sensors (Switzerland)* **18**, 2201 https://doi.org/10.3390/s18072201
142 Cebecauer, M. and Šachl, R. (2016) Lipophilic fluorescent probes: guides to the complexity of lipid membranes. In *Fluorescent Analogs of Biomolecular Building Blocks: Design and Applications* (Wilhelmsson, M. and Tor, Y. eds.), pp. 367–392, John Wiley & Sons
143 Kemmer, G.C., Bogh, S.A., Urban, M., Palmgren, M.G., Vosch, T., Schiller, J. et al. (2015) Lipid-conjugated fluorescent pH sensors for monitoring pH changes in reconstituted membrane systems. *Analyst* **140**, 6313–6320 https://doi.org/10.1039/C5AN01180A
144 Schwamborn, M., Schumacher, J., Sibold, J., Teiwes, N.K. and Steinem, C. (2017) Monitoring ATPase induced pH changes in single proteoliposomes with the lipid-coupled fluorophore Oregon Green 488. *Analyst* **142**, 2670–2677 https://doi.org/10.1039/C7AN00215G
145 Nichols, J.W. and Deamer, D.W. (1976) Catecholamine uptake and concentration by liposomes maintaining pH gradients. *Biochim. Biophys. Acta* **455**, 269–271 https://doi.org/10.1016/0005-2736(76)90169-3
146 Bally, M.B., Hope, M.J., Van Echteld, C.J.A. and Cullis, P.R. (1985) Uptake of safranine and other lipophilic cations into model membrane systems in response to a membrane potential. *Biochim. Biophys. Acta* **812**, 66–76 https://doi.org/10.1016/0005-2736(85)90522-X
147 Schubert, R., Wolburg, H., Schmidt, K.H. and Roth, H.J. (1991) Loading of preformed liposomes with high trapping efficiency by detergent-induced formation of transient membrane holes. *Chem. Phys. Lipids* **58**, 121–129 https://doi.org/10.1016/0009-3084(91)90118-U
148 Leiding, T., Górecki, K., Kjellman, T., Vinogradov, S.A., Hägerhäll, C. and Arsköld, S. P. (2009) Precise detection of pH inside large unilamellar vesicles using membrane-impermeable dendritic porphyrin-based nanoprobes. *Anal. Biochem.* **388**, 296–305 https://doi.org/10.1016/j.ab.2009.02.023
149 Xu, X., Khan, M.A. and Burgess, D.J. (2012) Predicting hydrophilic drug encapsulation inside unilamellar liposomes. *Int. J. Pharm.* **423**, 410–418 https://doi.org/10.1016/j.ijpharm.2011.12.019
150 Eloy, J.O., Claro de Souza, M., Petrilli, R., Barcellos, J.P., Lee, R.J. and Marchetti, J.M. (2014) Liposomes as carriers of hydrophilic small molecule drugs: Strategies to enhance encapsulation and delivery. *Colloids Surf. B Biointerfaces* **123**, 345–363 https://doi.org/10.1016/j.colsurfb.2014.09.029
151 Chiantia, S., Klymchenko, A.S. and London, E. (2012) A novel leaflet-selective fluorescence labeling technique reveals differences between inner and outer leaflets at high bilayer curvature. *Biochim. Biophys. Acta* **1818**, 1284–1290 https://doi.org/10.1016/j.bbamem.2012.02.005
152 Dolder, N. and von Ballmoos, C. (2020) Bifunctional DNA duplexes permit efficient incorporation of pH probes into liposomes. *ChemBioChem* **21**, 202000146 https://doi.org/10.1002/cbic.202000146
153 Ying, L., Xie, N., Yang, Y., Yang, X., Zhou, Q., Yin, B. et al. (2016) A cell-surface-anchored ratiometric i-motif sensor for extracellular pH detection. *Chem. Commun.* **52**, 7818–7821 https://doi.org/10.1039/C6CC03163C
154 Dembska, A., Bielecka, P. and Juskowiak, B. (2017) pH-Sensing fluorescence oligonucleotide probes based on an i-motif scaffold: a review. *Anal. Methods* **9**, 6092–6106 https://doi.org/10.1039/C7AY01942D
155 Swiatkowska, A. and Juskowiak, B. (2014) Effect of cholesterol anchoring group on the properties of G-quadruplex-based FRET probes for potassium ion. *Chemosensors* **2**, 267–286 https://doi.org/10.3390/chemosensors2040267
156 Feng, G., Luo, X., Lu, X., Xie, S., Deng, L., Kang, W. et al. (2019) Engineering of nucleic acids and synthetic cofactors as holo sensors for probing signaling molecules in the cellular membrane microenvironment. *Angew. Chem. Int. Ed.* **58**, 6590–6594 https://doi.org/10.1002/anie.201901320
157 Qiu, L., Zhang, T., Jiang, J., Wu, C., Zhu, G., You, M. et al. (2014) Cell membrane-anchored biosensors for real-time monitoring of the cellular microenvironment. *J. Am. Chem. Soc.* **136**, 13090–13093 https://doi.org/10.1021/ja5047389
158 Liu, L., Dou, C. X., Liu, J. W., Wang, X. N., Ying, Z. M. and Jiang, J. H. (2018) Cell surface-anchored DNA nanomachine for dynamically tunable sensing and imaging of extracellular pH. *Anal. Chem.* **90**, 11198–11202 https://doi.org/10.1021/acs.analchem.8b03589
159 Zeng, S., Liu, D., Li, C., Yu, F., Fan, L., Lei, C. et al. (2018) Cell-surface-anchored ratiometric DNA tweezer for real-time monitoring of extracellular and apoplastic pH. *Anal. Chem.* **90**, 13459–13466 https://doi.org/10.1021/acs.analchem.8b03299
160 Yuan, J., Deng, Z., Liu, H., Li, X., Li, J., He, Y. et al. (2019) Cell-surface-anchored ratiometric DNA nanoswitch for extracellular ATP imaging. *ACS Sensors* **4**, 1648–1653 https://doi.org/10.1021/acssensors.9b00482
161 Zhao, Y., Terry, D., Shi, L., Weinstein, H., Blanchard, S. C. and Javitch, J. A. (2010) Single-molecule dynamics of gating in a neurotransmitter transporter homologue. *Nature* **465**, 188–193 https://doi.org/10.1038/nature09057
162 Li, M., Jørgensen, S.K., McMillan, D.G., Krzemiński, Ł., Daskalakis, N.N., Partanen, R. et al. (2015) Single enzyme experiments reveal a long-lifetime proton leak state in a heme-copper oxidase. *J. Am. Chem. Soc.* **137**, 16055–16063 https://doi.org/10.1021/jacs.5b08798
163 Nishizaka, T., Hasimoto, Y. and Masaike, T. (2011) *Single Molecule Enzymology*, vol. **778**, Humana Press, New York
164 English, B. P., Min, W., van Oijen, A. M., Lee, K. T., Luo, G., Sun, H. et al. (2006) Ever-fluctuating single enzyme molecules: Michaelis–Menten equation revisited. *Nat. Chem. Biol.* **2**, 87–94 https://doi.org/10.1038/nchembio759
165 Volkán-Kacso, S. and Marcus, R.A. (2017) What can be learned about the enzyme ATPase from single-molecule studies of its subunit F1? *Q. Rev. Biophys.* **50**, e14 https://doi.org/10.1017/S0033583517000129
166 Veshaguri, S., Christensen, S. M., Kemmer, G. C., Ghale, G., Møller, M. P., Lohr, C. et al. (2016) Direct observation of proton pumping by a eukaryotic P-type ATPase. *Science* **351**, 1469–1473 https://doi.org/10.1126/science.aad6429
167 Berg, J., Block, S., Höök, F. and Brzezinski, P. (2017) Single proteoliposomes with *E. coli* quinol oxidase: proton pumping without transmembrane leaks. *Isr. J. Chem.* **57**, 437–445 https://doi.org/10.1002/ijch.201600138

168 Jorgensen, I.L., Kemmer, G.C. and Pomorski, T.G. (2017) Membrane protein reconstitution into giant unilamellar vesicles: a review on current techniques. *Eur. Biophys. J.* **46**, 103–119 https://doi.org/10.1007/s00249-016-1155-9
169 Pautot, S., Frisken, B.J. and Weitz, D.A. (2003) Production of unilamellar vesicles using an inverted emulsion. *Langmuir* **19**, 2870–2879 https://doi.org/10.1021/la026100v
170 Funakoshi, K., Suzuki, H. and Takeuchi, S. (2007) Formation of giant lipid vesiclelike compartments from a planar lipid membrane by a pulsed jet flow. *J. Am. Chem. Soc.* **129**, 12608–12609 https://doi.org/10.1021/ja074029f
171 Walde, P., Cosentino, K., Engel, H. and Stano, P. (2010) Giant vesicles: preparations and applications. *Chembiochem* **11**, 848–865 https://doi.org/10.1002/cbic.201000010
172 Matosevic, S. and Paegel, B.M. (2013) Layer-by-layer cell membrane assembly. *Nat. Chem.* **5**, 958–963 https://doi.org/10.1038/nchem.1765
173 Deshpande, S., Caspi, Y., Meijering, A.E.C. and Dekker, C. (2016) Octanol-assisted liposome assembly on chip. *Nat. Commun.* **7**, 10447 https://doi.org/10.1038/ncomms10447
174 Stein, H., Spindler, S., Bonakdar, N., Wang, C. and Sandoghdar, V. (2017) Production of isolated giant unilamellar vesicles under high salt concentrations. *Front. Physiol.* **8**, 63 https://doi.org/10.3389/fphys.2017.00063
175 Bellon, J.A., Pino, M.J. and Wilke, N. (2018) Low-cost equipment for electroformation of Giant Unilamellar Vesicles. *HardwareX* **4**, e00037 https://doi.org/10.1016/j.ohx.2018.e00037
176 Rideau, E., Wurm, F.R. and Landfester, K. (2019) Self-assembly of giant unilamellar vesicles by film hydration methodologies. *Adv. Biosyst.* **3**, 1800324 https://doi.org/10.1002/adbi.201800324
177 Girish, V., Pazzi, J., Li, A. and Subramaniam, A.B. (2019) Fabrics of diverse chemistries promote the formation of giant vesicles from phospholipids and amphiphilic block copolymers. *Langmuir* **35**, 9264–9273 https://doi.org/10.1021/acs.langmuir.9b01621
178 Matsushita-Ishiodori, Y., Hanczyc, M.M., Wang, A., Szostak, J.W. and Yomo, T. (2019) Using imaging flow cytometry to quantify and optimize giant vesicle production by water-in-oil emulsion transfer methods. *Langmuir* **35**, 2375–2382 https://doi.org/10.1021/acs.langmuir.8b03635
179 Göpfrich, K., Haller, B., Staufer, O., Dreher, Y., Mersdorf, U., Platzman, I. et al. (2019) One-pot assembly of complex giant unilamellar vesicle-based synthetic cells. *ACS Synth. Biol.* **8**, 937–947 https://doi.org/10.1021/acssynbio.9b00034
180 Noireaux, V. and Libchaber, A. (2004) A vesicle bioreactor as a step toward an artificial cell assembly. *Proc. Natl. Acad. Sci. U.S.A.* **101**, 17669–17674 https://doi.org/10.1073/pnas.0408236101
181 Gessesse, B., Nagaike, T., Nagata, K., Shimizu, Y. and Ueda, T. (2018) G-protein coupled receptor protein synthesis on a lipid bilayer using a reconstituted cell-free protein synthesis system. *Life* **8**, 54 https://doi.org/10.3390/life8040054
182 Ohta, N., Kato, Y., Watanabe, H., Mori, H. and Matsuura, T. (2016) In vitro membrane protein synthesis inside Sec translocon-reconstituted cell-sized liposomes. *Sci. Rep.* **6**, 1–9 https://doi.org/10.1038/s41598-016-0001-8
183 Biner, O., Schick, T., Ganguin, A.A. and von Ballmoos, C. (2018) Towards a synthetic mitochondrion. *Chim. Int. J. Chem.* **72**, 291–296 https://doi.org/10.2533/chimia.2018.291
184 Dezi, M., Di Cicco, A., Bassereau, P. and Levy, D. (2013) Detergent-mediated incorporation of transmembrane proteins in giant unilamellar vesicles with controlled physiological contents. *Proc. Natl. Acad. Sci. U.S.A.* **110**, 7276–7281 https://doi.org/10.1073/pnas.1303857110
185 Hansen, J.S., Elbing, K., Thompson, J.R., Malmstadt, N. and Lindkvist-Petersson, K. (2015) Glucose transport machinery reconstituted in cell models. *Chem. Commun.* **51**, 2316–2319 https://doi.org/10.1039/C4CC08838G
186 Spoelstra, W.K., Deshpande, S. and Dekker, C. (2018) Tailoring the appearance: what will synthetic cells look like? *Curr. Opin. Biotechnol.* **51**, 47–56 https://doi.org/10.1016/j.copbio.2017.11.005
187 Stano, P. (2018) Is research on "Synthetic Cells" moving to the next level? *Life* **9**, 3 https://doi.org/10.3390/life9010003
188 Berhanu, S., Ueda, T. and Kuruma, Y. (2019) Artificial photosynthetic cell producing energy for protein synthesis. *Nat. Commun.* **10**, 1325 https://doi.org/10.1038/s41467-019-09147-4
189 Lee, K.Y., Park, S.J., Lee, K. A., Kim, S.H., Kim, H., Meroz, Y. et al. (2018) Photosynthetic artificial organelles sustain and control ATP-dependent reactions in a protocellular system. *Nat. Biotechnol.* **36**, 530–535 https://doi.org/10.1038/nbt.4140
190 Hindley, J.W., Zheleva, D.G., Elani, Y., Charalambous, K., Barter, L., Booth, P.J. et al. (2019) Building a synthetic mechanosensitive signaling pathway in compartmentalized artificial cells. *Proc. Natl. Acad. Sci. U.S.A.* **116**, 16711–16716 https://doi.org/10.1073/pnas.1903500116
191 Chen, Z., Wang, J., Sun, W., Archibong, E., Kahkoska, A.R., Zhang, X. et al. (2018) Synthetic beta cells for fusion-mediated dynamic insulin secretion. *Nat. Chem. Biol.* **14**, 86–93 https://doi.org/10.1038/nchembio.2511
192 Fischer, A., Oberholzer, T. and Luisi, P.L. (2000) Giant vesicles as models to study the interactions between membranes and proteins. *Biochim. Biophys. Acta* **1467**, 177–188 https://doi.org/10.1016/S0005-2736(00)00217-0
193 Nishimura, K., Matsuura, T., Sunami, T., Fujii, S., Nishimura, K., Suzuki, H. et al. (2014) Identification of giant unilamellar vesicles with permeability to small charged molecules. *RSC Adv.* **4**, 35224–35232 https://doi.org/10.1039/C4RA05332J
194 Beales, P.A., Khan, S., Muench, S.P. and Jeuken, L.J.C. (2017) Durable vesicles for reconstitution of membrane proteins in biotechnology. *Biochem. Soc. Trans.* **45**, 15–26 https://doi.org/10.1042/BST20160019
195 Rideau, E., Dimova, R., Schwille, P., Wurm, F.R. and Landfester, K. (2018) Liposomes and polymersomes: a comparative review towards cell mimicking. *Chem. Soc. Rev.* **47**, 8572–8610 https://doi.org/10.1039/C8CS00162F
196 Schmitt, C., Lippert, A.H., Bonakdar, N., Sandoghdar, V. and Voll, L.M. (2016) Compartmentalization and transport in synthetic vesicles. *Front. Bioeng. Biotechnol.* **4**, 1–12 https://doi.org/10.3389/fbioe.2016.00019
197 Klermund, L., Poschenrieder, S.T. and Castiglione, K. (2017) Biocatalysis in polymersomes: improving multienzyme cascades with incompatible reaction steps by compartmentalization. *ACS Catal.* **7**, 3900–3904 https://doi.org/10.1021/acscatal.7b00776
198 Schwarzer, T.S., Klermund, L., Wang, G. and Castiglione, K. (2018) Membrane functionalization of polymersomes: alleviating mass transport limitations by integrating multiple selective membrane transporters for the diffusion of chemically diverse molecules. *Nanotechnology* **29**, 44 https://doi.org/10.1088/1361-6528/aadb7e
199 Khan, S., Li, M., Muench, S.P., Jeuken, L.J.C.C. and Beales, P.A. (2016) Durable proteo-hybrid vesicles for the extended functional lifetime of membrane proteins in bionanotechnology. *Chem. Commun.* **52**, 11020–11023 https://doi.org/10.1039/C6CC04207D

Biochemical Society Transactions (2020) **48** 1473–1492
https://doi.org/10.1042/BST20190966

200 Otrin, L., Marušič, N., Bednarz, C., Vidaković-Koch, T., Lieberwirth, I., Landfester, K. et al. (2017) Toward artificial mitochondrion: mimicking oxidative phosphorylation in polymer and hybrid membranes. *Nano Lett.* **17**, 6816–6821 https://doi.org/10.1021/acs.nanolett.7b03093
201 Marušič, N., Otrin, L., Zhao, Z., Lira, R.B., Kyrilis, F.L., Hamdi, F. et al. (2020) Constructing artificial respiratory chain in polymer compartments: insights into the interplay between bo3 oxidase and the membrane. *Proc. Natl. Acad. Sci. U.S.A.* **117**, 15006–15017 https://doi.org/10.1073/pnas.1919306117
202 Al Nahas, K., Cama, J., Schaich, M., Hammond, K., Deshpande, S., Dekker, C. et al. (2019) A microfluidic platform for the characterisation of membrane active antimicrobials. *Lab Chip* **19**, 837–844 https://doi.org/10.1039/C8LC00932E
203 Schaich, M., Cama, J., Al Nahas, K., Sobota, D., Sleath, H., Jahnke, K. et al. (2019) An integrated microfluidic platform for quantifying drug permeation across biomimetic vesicle membranes. *Mol. Pharm.* **16**, 2494–2501 https://doi.org/10.1021/acs.molpharmaceut.9b00086
204 Futai, M. (1974) Orientation of membrane vesicles from *Escherichia coli* prepared by different procedures. *J. Membr. Biol.* **15**, 15–28 https://doi.org/10.1007/BF01870079
205 Seigneuret, M. and Rigaud, J.L. (1988) Partial separation of inwardly pumping and outwardly pumping bacteriorhodopsin reconstituted liposomes by gel filtration. *FEBS Lett.* **228**, 79–84 https://doi.org/10.1016/0014-5793(88)80589-1
206 Young, H.S., Rigaud, J.L., Lacapère, J.J., Reddy, L.G. and Stokes, D.L. (1997) How to make tubular crystals by reconstitution of detergent-solubilized Ca2(+)-ATPase. *Biophys. J.* **72**, 2545–2558 https://doi.org/10.1016/S0006-3495(97)78898-2
207 Verkhovskaya, M.L., Garcìa-Horsman, A., Puustinen, A., Rigaud, J.L., Morgan, J.E., Verkhovsky, M.I. et al. (1997) Glutamic acid 286 in subunit I of cytochrome bo_3 is involved in proton translocation. *Proc. Natl. Acad. Sci. U.S.A.* **94**, 10128–10131 https://doi.org/10.1073/pnas.94.19.10128
208 Knol, J., Sjollema, K. and Poolman, B. (1998) Detergent-mediated reconstitution of membrane proteins. *Biochemistry* **37**, 16410–16415 https://doi.org/10.1021/bi981596u
209 Wang, L. and Sigworth, F.J. (2009) Structure of the BK potassium channel in a lipid membrane from electron cryomicroscopy. *Nature* **461**, 292–295 https://doi.org/10.1038/nature08291
210 Nomura, T., Cox, C.D., Bavi, N., Sokabe, M. and Martinac, B. (2015) Unidirectional incorporation of a bacterial mechanosensitive channel into liposomal membranes. *FASEB J.* **29**, 4334–4345 https://doi.org/10.1096/fj.15-275198
211 Dixon, J.F. and Hokin, L.E. (1980) The reconstituted (Na,K)-ATPase is electrogenic. *J. Biol. Chem.* **255**, 10681–10686 PMID: 6253484
212 Hokin, L.E. and Dixon, J.F. (1988) Reconstitution of the Na,K-pump by freeze—thaw sonication: estimation of coupling ratio and electrogenicity. *Methods Enzymol.* **156**, 141–155 https://doi.org/10.1016/0076-6879(88)56017-2
213 Pfleger, N., Wörner, A. C., Yang, J., Shastri, S., Hellmich, U.A., Aslimovska, L. et al. (2009) Solid-state NMR and functional studies on proteorhodopsin. *Biochim. Biophys. Acta* **1787**, 697–705 https://doi.org/10.1016/j.bbabio.2009.02.022
214 Rigaud, J.L., Paternostre, M.T. and Bluzat, A. (1988) Mechanisms of membrane protein insertion into liposomes during reconstitution procedures involving the use of detergents. 2. Incorporation of the light-driven proton pump bacteriorhodopsin. *Biochemistry* **27**, 2677–2688 https://doi.org/10.1021/bi00408a007